Designing and evaluating the technical, economic and environmental performance of an adsorption cooling system operating using bioresources from waste streams of mango processing

by

Aaron Dzigbor

Dissertation presented for the Degree

of

DOCTOR OF PHILOSOPHY
(CHEMICAL ENGINEERING)

in the Faculty of Engineering
at Stellenbosch University

The financial assistance of the National Research Foundation (NRF) towards this research is hereby acknowledged. Opinions expressed and conclusions arrived at, are those of the author and are not necessarily to be attributed to the NRF.

Supervisor
(Prof. Annie Chimphango)

December 2019

Stellenbosch University https://scholar.sun.ac.za

DECLARATION

By submitting this thesis electronically, I declare that the entirety of the work contained therein is my own, original work, that I am the sole author thereof (save to the extent explicitly otherwise stated), that reproduction and publication thereof by Stellenbosch University will not infringe any third party rights and that I have not previously in its entirety or in part submitted it for obtaining any qualification.

This dissertation includes [three] original papers published in peer-reviewed journals or books and [zero] unpublished publications. The development and writing of the papers (published and unpublished) were the principal responsibility of myself and, for each of the cases where this is not the case, a declaration is included in the dissertation indicating the nature and extent of the contributions of co-authors.

Date: *[December 2019]*

Copyright © 2019 Stellenbosch University

All rights reserved

Stellenbosch University https://scholar.sun.ac.za

PLAGIARISM DECLARATION

1. Plagiarism is the use of ideas, material and other intellectual property of another's work and to present is as my own.

2. I agree that plagiarism is a punishable offence because it constitutes theft.

3. I also understand that direct translations are plagiarism.

4. Accordingly all quotations and contributions from any source whatsoever (including the internet) have been cited fully. I understand that the reproduction of text without quotation marks (even when the source is cited) is plagiarism.

5. I declare that the work contained in this dissertation, except where otherwise stated, and is my original work and that I have not previously (in its entirety or in part) submitted it for obtaining any qualification.

Student number:

Initials and surname: A. Dzigbor

Signature:……..

Date:……..

Stellenbosch University https://scholar.sun.ac.za

ABSTRACT

This study sought to improve the technical performance (coefficient of performance (COP) and specific cooling power (SCP)), environmental impacts and economic viability of employing the adsorption working pairs produced from waste streams of mango processing in the adsorption cooling system (ACS). The specific objectives were: to produce and characterize mango seed husk activated carbon (AC) using NaCl as the activation agent and compared with commercial AC; assess the performance (in terms of COP and SCP) of the mango seed husk AC (with commercial AC as the control) paired with both high-grade and low-grade ethanol as refrigerants; improve the heat and mass transfer performance of commercial AC paired with both high-grade and low-grade ethanol as refrigerants through composite formation; and evaluate the environmental and economic impacts of integrating adsorption cooling system (ACS) in dried mango chips processing in both grid and off-grid power conditions.

Mango seed husk AC was produced through slow pyrolysis method using NaCl as the activation agent. About 100 g of dried mango seed husk was soaked in 250 ml of NaCl solution of concentrations (10 w/v%, 20 w/v%, and 30 w/v%) to obtain impregnation ratios of 0.25, 0.5 and 0.75 at 25 ˚C. The carbonization temperatures were 400 ˚C, 450 ˚C, and 500 ˚C. The experimental design was based on a 3^3 (impregnation ration, soaking time, and carbonization time) Box-Behnken fractional factorial optimization method with three center runs, giving total runs of 15. The responses analyzed were bulk density, ash content, and surface area. The optimized mango seed husk AC produced was tested in an ACS constructed in-house and its performance compared with commercial AC. The composite AC were also formed by soaking commercial AC in NaCl solution at varying concentrations of 10 w/v %, 15 w/v %, 20 w/v %, 25 w/v %, 30 w/v % and 35.7 w/v %, for 24 hours at 25 ˚C, dried at 105 ˚C for 24 hours and then

Stellenbosch University https://scholar.sun.ac.za

tested in ACS constructed in-house with high purity (99.7%) and low-grade (60%) ethanol to evaluate the effect of ethanol grade on the performance of the composite formed. Finally, three scenarios for each power setting (on-grid and off-grid) were studied, on-grid: coal as boiler fuel and conventional chiller for cooling (Scenario 1), mango seed as boiler fuel and adsorption chiller for cooling (Scenario 2) and mango seed as boiler fuel and ACS for cooling (Scenario 3). Off-grid scenarios 4, 5 and 6 corresponded to on-grid scenarios 1, 2 and 3, respectively. Environmental impacts and economic viability for each scenario were based on material and energy balances and South African economic conditions, respectively.

The results showed that mango seed husk AC had comparable ash content (6.92%) to the commercial AC. The SCP, COP and temperature drop recorded in ACS for mango seed husk AC when paired with high purity (99.7%) ethanol reduced from 40 W/kg, 0.050 and 4.46 ˚C to 37.3 Wkg^{-1}, 0.048, and 4.5 ˚C, respectively, when paired with low-grade ethanol (60%). Moreover, the COP and SCP of commercial AC paired with high purity ethanol were 0.099 and 84.5 Wkg^{-1}, which reduced to 0.091 and 75.5 W/kg, respectively, when paired with low-grade ethanol. In addition, the COP of the composite AC containing 20%, 25% and 30% NaCl paired with low-grade ethanol were 0.121, 0.160 and 0.146, respectively, which were higher than when paired with high purity ethanol, thus 0.082, 0.080, and 0.076, respectively. In terms of environmental and economic impacts, on-grid scenario 3 showed the greatest potential for reducing emissions and improving economic viability by emitting 7.10×10^5 $kgCO_2eq/yr$ and internal rate of return (IRR) of 25.33% compared to scenario 1 that had the GHG emission of 7.89×10^5 $kgCO_2eq/yr$ and IRR of 17.48%. In off-grid, scenario 6 had the least GHG emission of 6.90×10^5 $kgCO_2eq/yr$ and IRR of 24.84%

Stellenbosch University https://scholar.sun.ac.za

while scenarios 4 had the highest GHG emission of 7.67×10^5 $kgCO_2eq/yr$ and IRR of 16.09%.

Overall, it is possible to improve the heat and mass transfer of activated carbon paired with low-grade ethanol. The improvement in heat and mass transfer when AC + NaCl was paired with low-grade ethanol suggests that low-grade ethanol can be used as an alternative refrigerant. However, in areas where silica gel is accessible, forming composite with silica gel + NaCl paired with pure water as refrigerant would eliminate the mass transfer challenges associated with using AC+NaCl composites paired with ethanol. Furthermore, the replacement of vapour compression cooling technology with ACS and boiler fuel with mango seed has led to the reduction in GHG emission and improvement in the economic viability of dried mango chip processing. Thus, the study has improved the technical, economic and environmental performance of ACS in terms of temperature maintenance, resource consumption, and emissions.

Stellenbosch University https://scholar.sun.ac.za

ABSTRAK

Hierdie studie het beoog om die tegniese werkverrigting (koëffisiënt van werkverrigting (KVW) en spesifieke verkoelingskrag (SVK)), omgewingsimpak en ekonomiese lewensvatbaarheid te verbeter deur die aanwending van adsorpsiepare geproduseer uit die afvalstrome van mango-prosessering in die adsorpsie verkoelingstelsel. Die spesifieke doelstellings was: om mangosaaddop geaktiveerde koolstof (GK) te produseer deur NaCl as die aktiveringsmiddel te gebruik, dit te karakteriseer en met kommersiële GK te vergelyk; die werkverrigting (in terme van KVW en SVK) van die mangosaaddop GK (met kommersiële GK as die kontrole) gekombineer met beide hoë suiwerheid en lae-graad etanol as koelmiddels, te assesseer; die hitte- en massa-oordrag werkverrigting van kommersiële GK gekombineerd met beide hoë suiwerheid en lae-graad etanol as koelmiddels te verbeter deur samestelling vorming; en die assessering van die omgewings- en ekonomiese impak wanneer adsorpsie verkoelingstelsel (AVS) in gedroogde mangoskyfie-prosessering geïntegreer word in beide netwerk en buite-netwerk krag kondisies

Mangosaaddop GK is geproduseer deur ’n stadige pirolise metode deur gebruik te maak van NaCl as die aktiveringsmiddel. Ongeveer 100 g gedroogde mangosaaddop is in 250 ml NaCl oplossing geweek met konsentrasies (10 % w/v, 20 % w/v, en 30 % w/v) om impregneringsverhoudings van 0.25, 0.5 en 0.75 by 25 °C te verkry. Die verkolingstemperature was 400 °C, 450 °C, en 500 °C. Die eksperimentele ontwerp is gebaseer op ’n 3^3 (impregneringsverhouding, weektyd, en verkolingstyd) Box-Behnken fraksionele faktoriaal optimeringsmetode met drie middellope, vir ’n totaal van 15 lope. Die response geanaliseer was massadigtheid, as-inhoud, en oppervlakarea. Die geoptimiseerde mangosaaddop GK geproduseer is getoets in ’n

Stellenbosch University https://scholar.sun.ac.za

binne-huis geboude AVS en sy werkverrigting is vergelyk met kommersiële GK. Die saamgestelde GK is ook gevorm deur kommersiële GK in NaCl oplossing by verskeie konsentrasies van 10 % w/v, 15 % w/v, 20 % w/v, 25 % w/v, 30 % w/v en 35.7 % w/v, vir 24 uur by 25 °C te week, te droog by 105 °C vir 24 uur, en dan te toets in ’n binne-huis geboude AVS met hoë suiwerheid (99.7 %) en lae-graad (60 %) etanol om die effek van etanol graad op die werkverrigting van die samestelling gevorm, te evalueer. Laastens, drie scenario’s vir elke kragstelsel (binne-netwerk en buite-netwerk) is bestudeer: steenkool as ketelbrandstof en konvensionele afkoeler vir verkoeling (Scenario 1), mangosaad as ketelbrandstof en konvensionele afkoeler vir verkoeling (Scenario 2), en mangosaad as ketelbrandstof en AVS vir verkoeling (Scenario 3). Buite-netwerk scenario’s 4, 5 en 6 stem ooreen met binne-netwerk scenario’s 1, 2 en 3, onderskeidelik. Omgewingsimpak en ekonomiese lewensvatbaarheid vir elke scenario is gebaseer op materiaal- en energiebalanse en Suid-Afrikaanse ekonomiese kondisies, onderskeidelik.

Die resultate het gewys dat mangosaaddop GK vergelykbare as-inhoud (6.92 %) het as die kommersiële GK. Die SVK, KVW en temperatuurval aangeteken in AVS vir mangosaaddop GK wanneer dit met hoë suiwerheid (99.7 %) etanol gekombineer is, was 77.3 W/kg, 0.048 en 4.5 °C – ’n afname van 87.5 W/kg, 0.050 en 4.46 °C wanneer dit gekombineer word met lae-graad etanol (60 %). Verder, die KVW en SVK van kommersiële GK gekombineer met hoë suiwerheid etanol was 0.098 en 122 W/kg, wat afgeneem het na 0.091 en 111 W/kg, onderskeidelik, wanneer gekombineer is met lae-graad etanol. Daarby was die KVW van die saamgestelde GK wat 20 %, 25 %, en 30 % NaCl bevat, gekombineer met lae-graad etanol 0.121, 0.160 en 0.146, onderskeidelik. Dit was hoër as toe dit gekombineer is met hoë suiwerheid etanol – 0.082, 0.080, en 0.076, onderskeidelik. In terme van omgewings- en

Stellenbosch University https://scholar.sun.ac.za

ekonomiese impak, het binne-netwerk scenario 3 die grootste potensiaal gewys vir die vermindering van emissies en verbetering van ekonomiese lewensvatbaarheid deur uitstorting van 7.10×10^5 $kgCO_2$ ekw/jr en interne opbrengskoers (IOK) van 25.33 %, vergelyk met scenario 1 wat KHG emissies van 7.89×10^5 $kgCO_2$ ekw/jr en IOK van 17.48 % gehad het. In buite-netwerk, het scenario 6 die minste KHG emissies gehad - 6.90×10^5 $kgCO_2$ ekw/jr en IOK van 24.84 %, terwyl scenario 4 die hoogste KHG emissies van 7.67×10^5 $kgCO_2$ ekw/jr gehad het en IOK van 16.09 %.

Alles in ag geneem, is dit moontlik om die hitte- en massa-oordrag van geaktiveerde koolstof gekombineer met lae-graad etanol te verbeter. Die verbetering in hitte- en massa-oordrag wanneer GK + NaCl met lae-graad etanol gekombineer is, stel voor dat lae-graad etanol gebruik kan word as ’n alternatiewe verkoeler. In areas waar silika jel bereikbaar is, sal die vorming van ’n samestelling met silika jel + NaCl gekombineer met suiwer water as verkoeler, die massa-oordrag uitdagings geassosieer met die gebruik van GK + NaCl samestellings gekombineer met etanol, elimineer. Verder, die vervanging van damp kompressie verkoelingstegnologie met AVS, en ketelbrandstof met mangosaad, het tot die vermindering in KHG emissies gelei en die verbetering in ekonomiese lewensvatbaarheid van gedroogde mangoskyfie-prosessering. Dus het hierdie studie die tegniese, ekonomiese en omgewingswerkverrigting van AVS in terme van temperatuur handhawing, hulpbron verbruik en emissies, verbeter.

Stellenbosch University https://scholar.sun.ac.za

DEDICATION

Dedicated to my family for their encouragement and support.

Stellenbosch University https://scholar.sun.ac.za

ACKNOWLEDGEMENT

First of all, I would like to express my gratitude to the Almighty God for protecting me during my study period. I would like to express my appreciation to my supervisor, Prof Annie Chimphango, for her support and encouragement during the study period. I am indebted to my siblings for their continued encouragement and well wishes. I would also like to express my gratitude to colleagues, friends and other well-meaning persons at the Department of Process Engineering, Stellenbosch University. I would like to thank the following persons for the assistance I received from them: Prof Gorgens' group for providing me with the pyrolysis and analytical facilities needed to complete this study, and Mr. Jos Weerdenburg, Mr Anton Cordier, and Mr Brent Gideons at Process Engineering workshop for assistance provided during construction of my experimental rings. Finally, my sincere gratitude goes to The National Research Fund (NRF) for the financial support.

Stellenbosch University https://scholar.sun.ac.za

TABLE OF CONTENTS

Stellenbosch University https://scholar.sun.ac.za

Stellenbosch University https://scholar.sun.ac.za

Stellenbosch University https://scholar.sun.ac.za

Stellenbosch University https://scholar.sun.ac.za

Stellenbosch University https://scholar.sun.ac.za

TABLES

Stellenbosch University https://scholar.sun.ac.za

Stellenbosch University https://scholar.sun.ac.za

FIGURES

Stellenbosch University https://scholar.sun.ac.za

Stellenbosch University https://scholar.sun.ac.za

Stellenbosch University https://scholar.sun.ac.za

Stellenbosch University https://scholar.sun.ac.za

ABBREVIATIONS

AC	Activated carbon
ACS	Adsorption cooling system/chiller
C	Equipment cost at the current year
C_O	Equipment cost at some time in the past
CEPCI	Chemical engineering plant cost index
CVCC	Conventional vapour compression cooler/chiller
GWP	Global warming potential
IRR	Internal rate of return
LCAC	Low cost adsorption chiller/cooler
M	Scaled-up equipment capacity
M_O	Original equipment capacity
NPV	Net present value
TCI	Total capital investment
TS	Total solid
LHV	Lower heating value
COP	coefficient of performance
SCP	specific cooling power

Stellenbosch University https://scholar.sun.ac.za

SYMBOLS

n Scaling index or exponential parameter

A pre-exponential factor (or prefactor) (s^{-1})

Q Energy (J)

P Pressure (kPa)

T Temperature (K)

A Area (m^2)

h Enthalpy (Jkg^{-1})

R Gas constant ($Jmol^{-1}K^{-1}$ or Jkg^{-1})

$\dot{Q}$ Rate of heat transfer (Js^{-1} or W)

m mass (kg)

$\dot{m}$ Mass flow rate (kgs^{-1})

η_{th} Combustion efficiency (%)

η Truck engine efficiency (%)

C_p Specific heat of water ($kJkg^{-1}K^{-1}$)

$\dot{W}$ Work input (Js^{-1} or W)

E Characteristic energy of adsorption $(\mathrm{kJkg^{-1}})$

W Equilibrium adsorption capacity $(\mathrm{kgkg^{-1}})$

W_o Maximum possible adsorption capacity $(\mathrm{kgkg^{-1}})$

τ_{cycle} Cycle time (s)

x mass fraction

Subscripts

comb Combustion

ref refrigerant

1, 2,3…..process stages

Stellenbosch University https://scholar.sun.ac.za

eva	evaporator
abs	absorber
con	condenser
ads	adsorbent
trans	transportation
elect	electrical
gen	generator
s	saturation
f	liquid
g	vapour

Stellenbosch University https://scholar.sun.ac.za

Stellenbosch University https://scholar.sun.ac.za

Chapter 1 Introduction

1.1 Cooling technologies and their role in food security

Lack of cooling technologies is a major cause of postharvest losses of perishable crops, causing food insecurity and loss of income for communities that rely heavily on agriculture for their livelihoods [1,2]. There are many cooling technologies available such as conventional vapour compression cooling system (CVCC), vacuum cooling, hydro-cooling, evaporative cooling, etc. but most of these require electricity to operate while some such as evaporative cooling technologies are weather dependent. Therefore, providing agricultural communities with reliable cooling technologies throughout the season can impact positively on their food security and economic well-being.

Alternative postharvest cooling technologies include adsorption cooling systems (ACSs) that have been used in the postharvest handling of perishable produce to minimize the consumption of electricity and reduce greenhouse gas emissions [3]. ACS employs a solid material called adsorbent to take up a refrigerant gas at low pressure and temperature followed by desorption by heat [4]. The heat can be obtained from solar, geothermal, waste heat from factories, combustion of fuels [4–6] and many other sources. The independence of ACS on electricity and environmental conditions such as relative humidity makes this cooling system an ideal choice for use in off-grid communities.

The performance of the ACS is assessed by specific cooling power (SCP) in addition to the coefficient of performance (COP). The SCP is affected by the cycle time which is the time between the adsorption of the refrigerant, pre-heating of the adsorber bed and its content, desorption of the refrigerant, cooling of the adsorber bed and the start

Stellenbosch University https://scholar.sun.ac.za

of the next adsorption. Furthermore, the cooling performance of ACSs is also affected by the type of adsorbent/refrigerant pairing used. The frequently used adsorbent/refrigerant pairings are AC/ethanol, AC/methanol, AC/ammonia, silica gel/water, and zeolite/water [6,7]. These adsorbent/refrigerant pairings are either associated with global warming, toxicity or poor performance due to inefficient heat and mass transfer [8,9].

This study seeks to introduce sustainable innovations in ACS operations in the form of introducing novel composite adsorbent and refrigerant pairs and utilization of bioenergy from waste streams of mango processing, to make AC more eco-friendly and low cost. In particular, the innovations are expected to improve the technical, economic and environmental performance of ACS in terms of temperature maintenance, resource consumption, and emissions. In the study, mango seed husk, a bioresource generated from the mango processing waste stream, served both as the source of heat and an adsorbent. The mango seed husk was processed into AC using sodium chloride as an activation agent, which subsequently was used to produce composite AC-sodium chloride adsorbent for the cooling system. The other portion of the mango husk is combusted for energy generation to run the cooling system.

1.2 Mango waste from mango processing as feedstocks for bioenergy and bio-sorbents in low cost refrigeration system

During the processing of mango into various products, a huge amount of wastes are generated [10,11]. Mango seeds and peels are the main wastes generated, each representing 17-22% and 10-20% of the weight of fruit respectively depending on the variety [12]. Even though some processors processed the whole mango fruit into value-added products such as mango atchar, most processors dispose of the mango

Stellenbosch University https://scholar.sun.ac.za

waste streams into the environment [10] which causes environmental hazards such as emission of methane gas during decomposition of the mango waste. Exploring the suitability of and subsequent use of mango waste to replace commercial adsorbents and as a source of energy in the area of adsorption refrigeration will reduce waste handling and food insecurity issues and be a source of income.

Stellenbosch University https://scholar.sun.ac.za

Stellenbosch University https://scholar.sun.ac.za

Chapter 2 Literature review

2.1 Overview of cooling systems

Cooling technologies play a critical role in slowing down senescence, maintaining product quality and extending shelf life, which is the postharvest period a product remains acceptable [13]. The rate of deterioration of horticultural produce is influenced by temperature [13] according to Arrhenius' equation as follows

$$K = Ae^{-E_a/(RT)} \qquad 2.1$$

Where: K is the rate constant (s^{-1}), T is the temperature(K), A is the pre-exponential factor (or prefactor) (s^{-1}), E_a is the activation energy ($kJmol^{-1}$), R is the universal gas constant ($kJmol^{-1}K^{-1}$). Thus, storing horticultural produce at relatively high temperature increases the rate of chemical, biochemical and physiological processes, which result in faster deterioration. The choice and design of cooling technologies depend on factors such as physiological properties of the fresh produce, power consumption and supply, source and availability of materials, ambient conditions, cost and environmental impacts. A detailed discussion of these factors for each cooling technology has been provided below. Classification of the available cooling technologies is shown in Figure 2.1.

2.1.1 Conventional vapour compression cooling system

A conventional vapour compression cooling (CVCC) system comprises four basic components: evaporator, condenser, expansion valve and compressor. The flow chart of the operation of the conventional vapour compression cooling system is shown in Figure 2.2.

Stellenbosch University https://scholar.sun.ac.za

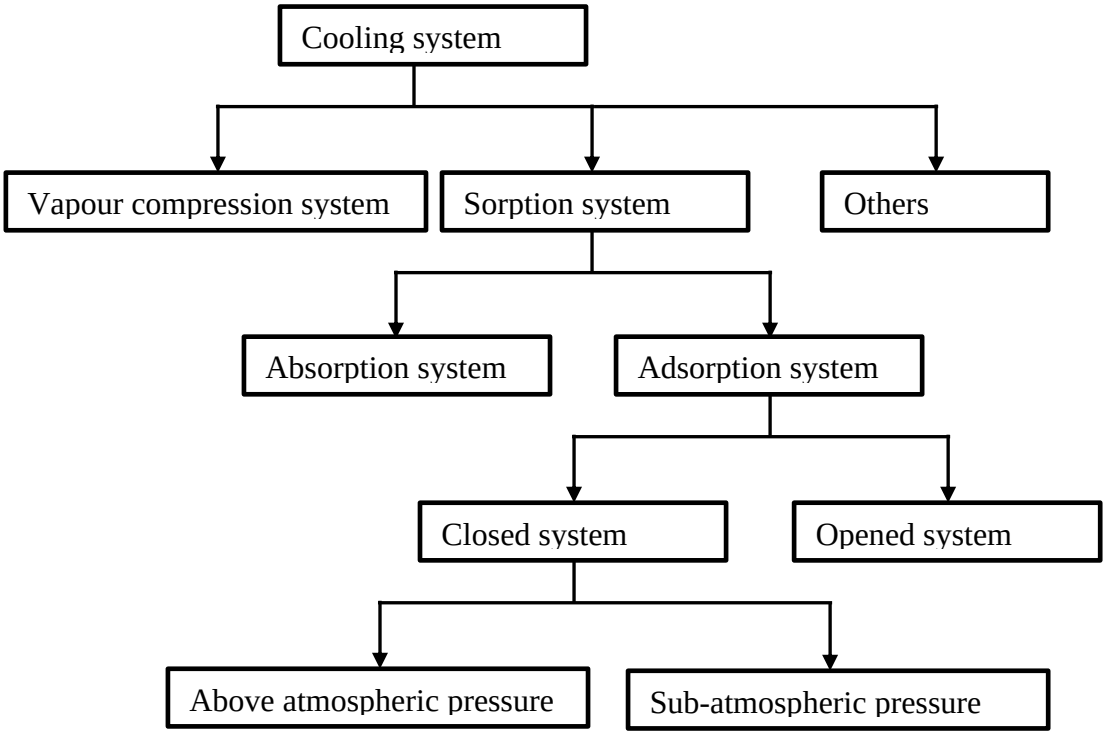

Figure 2.1 Classification of cooling systems [adapted from [14,15]]

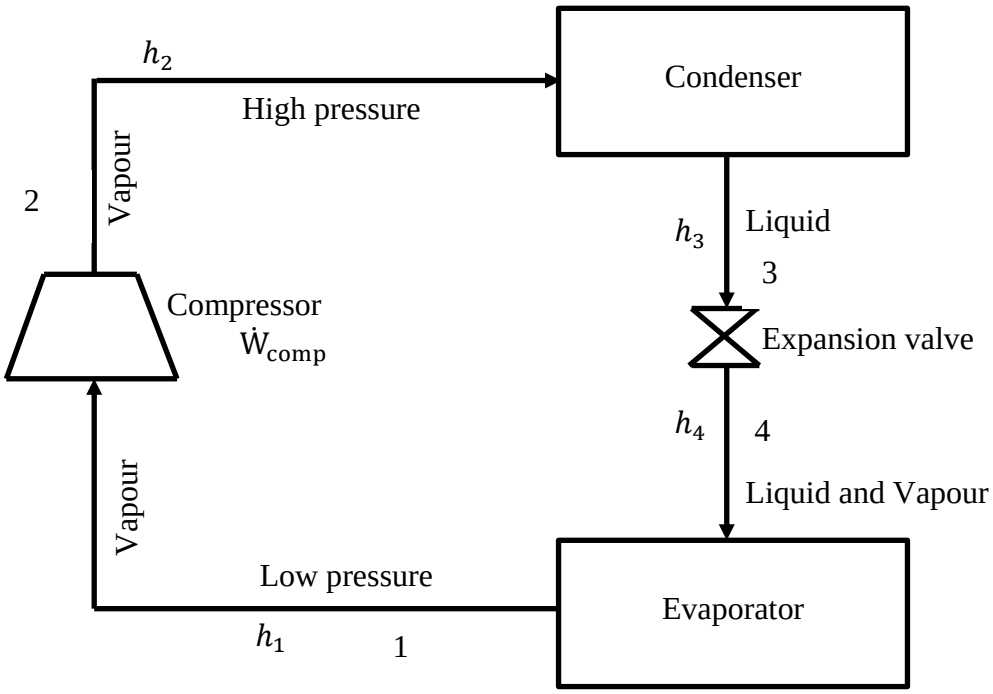

Figure 2.2 Flow chart for the conventional vapour compression cooling cycle. Note: 1, 2, 3 and 4 are the states of the refrigerant during the process

Stellenbosch University https://scholar.sun.ac.za

Heat transfer fluid (refrigerant) undergoes evaporation, compression, condensation, and expansion processes, respectively, as it enters and exits these components. Liquefied refrigerant goes into the evaporator and it is converted into vapour by addition of latent heat of vaporization from the evaporator compartment. This results in cooling the evaporator compartment. The cooling effect in the evaporator can be calculated using Equation 2.2.

$$\frac{\dot{Q}_{eva}}{\dot{m}_{ref}} = h_1 - h_4 = h_{fg} \qquad 2.2$$

Where: $\dot{Q}_{eva}$ is the cooling rate in the evaporator (kJs^{-1}), h_1 and h_4 are the specific enthalpies of the refrigerant exiting and entering the evaporator ($kJkg^{-1}$), and $\dot{m}_{ref}$ is the refrigerant mass flow rate (kgs^{-1}), h_{fg} is specific the latent heat of vaporization of the refrigerant ($kJkg^{-1}$). The refrigerant vapour then enters the compressor where it is pressurized to relatively high pressure and temperature. Assuming the compression is adiabatic, the energy input during the compression process can be determined using Equation 2.3.

$$\frac{\dot{W}_{comp}}{\dot{m}_{ref}} = h_2 - h_1 \qquad 2.3$$

Where: $\dot{W}_{comp}$ is the compressor work input rate (kJs^{-1}), h_2 and h_1 are the enthalpies of the refrigerant exiting and entering the compressor ($kJkg^{-1}$). When the pressure approaches that of the condenser, the vapour enters the condenser where it is cooled to the liquid and there is heat transfer from the refrigerant to the surroundings. The energy rejected during the condensation of the refrigerant can be determined using Equation 2.4.

$$\frac{\dot{Q}_{con}}{\dot{m}_{ref}} = h_2 - h_3 \qquad 2.4$$

Stellenbosch University https://scholar.sun.ac.za

Where: $\dot{Q}_{con}$ is the rate of heat rejection by the condenser (kJs^{-1}), h_2 and h_3 are the enthalpies of the refrigerant exiting and entering the condenser ($kJkg^{-1}$), and $\dot{m}_{ref}$ is the refrigerant mass flow rate (kgs^{-1}). After exiting the condenser, the liquid refrigerant enters the expansion valve where the depressurization of the refrigerant vapour takes place before re-entering the evaporator. There is no heat transfer during the throttling process. The refrigerant leaves the expansion valve as a two-phase liquid-vapor mixture.

$$h_3 = h_4 = h_{f4} + x_{ref}\left(h_{g4} - h_{f4}\right) \qquad 2.5$$

Where: h_3 and h_4 are the specific enthalpies of the refrigerant entering and exiting the expansion valve ($kJkg^{-1}$), h_{f4} and h_{g4} are specific enthalpies of the liquid and vapour component of the two-phase liquid-vapor mixture leaving the expansion valve ($kJkg^{-1}$), and x_{ref} is the fraction of the two-phase liquid-vapor mixture that in the vapour phase. The cycle then repeats itself. The coefficient of performance of the process can be determined by Equation 2.6.

$$COP = \frac{\frac{\dot{Q_{eva}}}{\dot{m_{ref}}}}{\frac{\dot{W}_{comp}}{\dot{m}_{ref}}} = \frac{h_1 - h_4}{h_2 - h_1} \qquad 2.6$$

The CVCC systems have limitations of electricity dependency and utilization of environmentally unfriendly refrigerants. The power input of 412.5 kW was reportedly required to operate a conventional vapour compression chiller with the cooling capacity of 597 kW [16] while CO_2 emission of 75 ton/year was reported for a conventional vapour compression chiller that used 750 kg of refrigerant R134a with 7% leakage of the refrigerant [17]. Furthermore, about 1.25 kg CO_2 is emitted per kWh of power produced from coal to operate this cooling

Stellenbosch University https://scholar.sun.ac.za

technology [18]. As a result of these limitations, sorption cooling systems have been proposed and studied as a suitable substitute for vapour compression cooling systems.

2.1.2 Other cooling systems

There are other cooling technologies that are also employed for postharvest handling of fresh horticultural produce. Some of these cooling technologies are forced-air cooling, hydro-cooling, vacuum cooling, and evaporative cooling.

Forced-air precooling

Forced-air cooling usually uses a conventional compression system. A forced-air system is a precooling method that manages the air flow (using a blower) around the produce [13,19]. The amount of power consumed depends on the amount of cooling desired and the type of fresh produce to be cooled. To reduce the temperature of 5 kg of cauliflower head from 24 ˚C to 1 ˚C requires 0.3684 kW (blower and the conventional cooling system) of power consumption [20]. This technology also resulted in a loss of 2.89% weight of the cauliflower head due to evaporation of water from its surface [20]. This weight loss is undesirable for both farmers and processors because the economic benefit of the product is related to the weight. Loss of water also affects the quality attributes of the produce. In addition to weight loss and electricity dependence, the high cost of construction and installation is hampering the use of this technology in rural communities. A 3.5 kW of forced air built by USDA (United States Department of Agriculture) team in Maryland, United States costs US $1,200 USD [21].

Stellenbosch University https://scholar.sun.ac.za

Hydro-cooling

In the case of fast cooling of produce, hydro-cooling is employed, which involves showering or dipping the product in chilled water [21]. The produce and the packaging material have to be water tolerant in order to apply this cooling method [13,21]. The amount of water and electricity consumption to cool four ton of broccoli from 30 ˚C to 6 ˚C by showering with water at 0 ˚C was estimated by Thorpe [22]. It was reported that hydro-cooling with water recycling requires 20 kWh of electricity consumption and water consumption of 75 liters per ton of broccoli whereas, without any recycling, the power and water consumption are 300 kWh and 60,000 liters per ton of broccoli respectively [22].

Vacuum cooling

A highly sensitive product might require cooling at lower pressure. For vacuum cooling, the pressure in the cooling chamber is reduced to a point where water boils at a low temperature. The produce is cooled as water evaporate from its surface [13]. Vacuum cooling could be applied to fresh produce with a large surface to volume ratio such as spinach, parsley, lettuce, broccoli, etc. [13,23,24]. The operation of vacuum cooling is dependent on electricity consumption, which may not be readily available in every agricultural community, to create the vacuum needed to effect the evaporation of the water. For example, 5 kg of cauliflower head was cooled from 24 ˚C to 1 ˚C for about an hour by consuming 0.8516 kW of electricity to reduce the pressure from atmospheric to 2.9 kPa [20]. As a result of evaporation of the water, a weight loss of 4.55% was recorded for the cauliflower head [20], which is undesirable since it is related to the profit that farmers and processors can make. Apart from the vacuum pump to create the

Stellenbosch University https://scholar.sun.ac.za

vacuum, other expensive components such as condenser also required to condense the water vapour to be discharged through the drain [25]. Thus, the electricity consumed, and expensive equipment needed for vacuum cooling prohibits its application in rural communities.

Evaporative cooling

Evaporative cooling is the most economical way of reducing the temperature by moisturizing the air. It has some benefits over mechanical refrigeration system. It is friendly to the environment (reduces CO_2 emission) as it does not use refrigerant [26]. It does not make noise as there is no moving part. It uses little or no electricity. Energy consumption by evaporative cooling is about 4-10 times lower than that for conventional vapour especially in dry and hot climatic conditions [27,28]. It does not require high initial capital investment, as well as the operational cost is negligible. The operating cost is about 20 times lower than that for CVCC [27,29]. It can be quickly and easily installed [26]. Its maintenance is easy and can be constructed with locally available materials in remote areas [21,26,30]. However, its cooling efficiency depends on the prevailing weather condition [21,26,30]. Evaporative cooling can reduce weight loss and quality defects, such as wilting since air is humidified and cooled by the system [27]. However, the high relative humidity achieved in the evaporative cooling could encourage the growth of microorganisms since the recommended storage relative humidity for most fresh produce is about 85-95% [27] that can cause deterioration of the fresh produce. There is also a high risk of contracting Legionnaire's disease if the recycled water for cooling is not monitored and treated [27]. There have been attempts to improve the performance of

Stellenbosch University https://scholar.sun.ac.za

evaporative cooling by introducing a desiccant wheel to adsorb water in the process air and fan to induce forced convection [31–33]. To make the system suitable for areas with the limited supply of electricity, the thermoelectric generator could be used to generate power the fan and the desiccant wheel [34]. Regardless of the source of power to drive the desiccant wheel and the fan, the performance of the system depends heavily on changing humidity in the atmosphere thereby making it unreliable and not an ideal choice for cooling.

More so, since evaporative cooling depends on the prevailing weather conditions, the temperature difference between the dry-bulb temperature and wet-bulb temperatures of the ambient air which is the driving force is normally very small leading to low cooling capacity. Despite this, the COP of evaporative cooling is very high compared with other cooling technologies due to less energy consumption by the evaporative cooler. COP of evaporative cooling is reported to be in the range of 15-20 while that for CVCC is between 2 to 4 [35].

2.1.3 Sorption cooling system

Sorption cooling systems can be categorized into absorption (liquid-gas system) or adsorption system (solid-gas system). Absorption is a reversible volumetric occurrence where the substance in a gaseous phase (absorbate) is taken in and combines with another substance in the liquid phase (absorbent) to form a solution, followed by subsequent separation by heat [14,36]. A conventional absorption cooling system is made up of an absorber, a pump, a generator, a condenser and an evaporator [36] which works in a cyclical fashion to achieve the cooling effect. The flow process of the conventional absorption cooling system

Stellenbosch University https://scholar.sun.ac.za

is shown in Figure 2.3. Condenser and evaporator perform a similar function as in the conventional vapour compression system. Absorption cooling system, however, differs from the CVCC regarding the number of heat transfer fluid used. While only one suitable heat transfer fluid (refrigerant) is used in a vapour compression system, the absorption cooling system employs two heat transfer fluid (the absorbent solution and refrigerant) [36]. The cyclical process begins in the absorber where the absorbent (e.g. LiBr solution) takes in the refrigerant vapour (e.g. water vapour) which exits the evaporator at reduced temperature and pressure. The liquid absorbent-refrigerant solution is transported to the generator by a pump through a heat exchanger where it is preheated by the hot concentrated absorbent solution (e.g. LiBr solution) returning from the generator. Reaching the generator, the liquid absorbent-refrigerant solution is heated to relatively high temperature and pressure to evaporate the refrigerant (e.g. water) from the mixture of a liquid absorbent and refrigerant vapour. The refrigerant vapour then enters the condenser to be condensed and liquid absorbent (e.g. LiBr solution) returns to the absorber. The condensed refrigerant then passes through an expansion valve without any heat transfer nor work done on the refrigerant and enters the evaporator. When the refrigerant enters the evaporator, it takes up heat from the evaporator compartment and the refrigerant is vaporized and goes to the absorber to be absorbed by the absorbent. The process repeats itself [36].

Stellenbosch University https://scholar.sun.ac.za

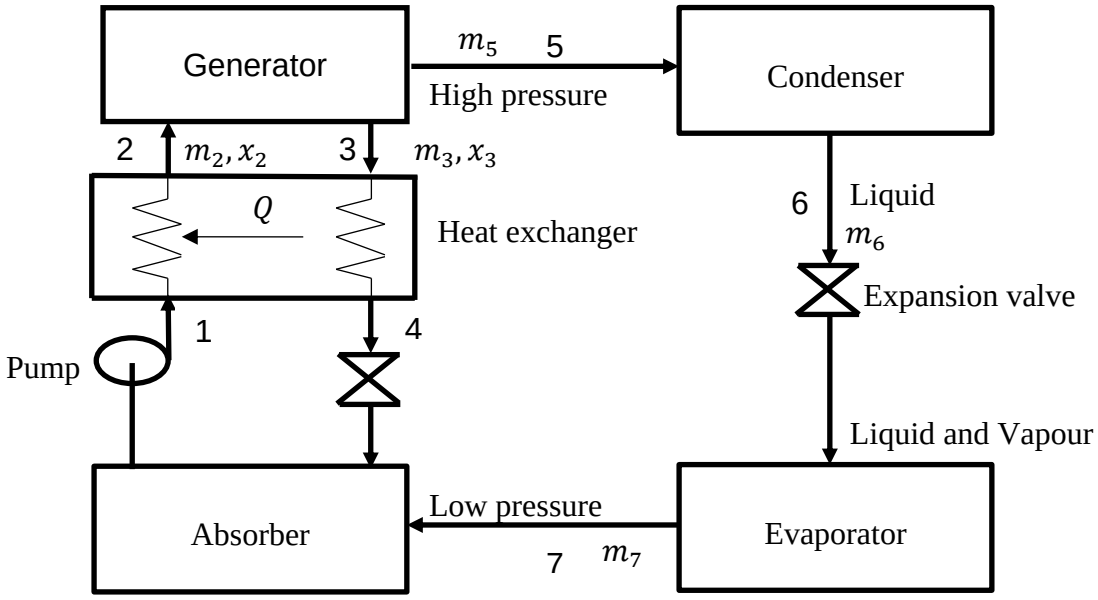

Figure 2.3 Flow chart of a typical absorption cooling system [redrawn from [36]]
Note: 1, 2, 3, 4, 5 & 6 are the stages of the process

The mass and energy balance equations for the entire process is as presented in Equation 2.7.

$$\dot{m}_{ref} = \dot{m}_5 = \dot{m}_6 = \dot{m}_7 \qquad 2.7$$

Where: $\dot{m}_{ref}$ is the mass flow rate of the refrigerant (kgs^{-1}), $\dot{m}_5$, $\dot{m}_6$ and $\dot{m}_7$ are the mass flow rates (kgs^{-1}) of the stream at stages 5, 6, and 7, respectively.

Mass balance in the generator is presented in Equation 2.8

$$\dot{m}_2 = \dot{m}_3 + \dot{m}_5 \qquad 2.8$$

Where: $\dot{m}_2$, $\dot{m}_3$ and $\dot{m}_5$ are the mass flow rates (kgs^{-1}) of the stream at stages 2, 3, and 5, respectively.

The mass balance in the absorbent solution is as given in Equation 2.9.

$$\dot{m}_3 x_3 = \dot{m}_2 x_2 \qquad 2.9$$

Where: $\dot{m}_2$ and $\dot{m}_3$ are the mass flow rates (kgs^{-1}) defined in Equation 2.7, x_2 and x_3 are the concentrations of the stream at stage 2 and 3, respectively. It follows that the amount of heat added to the absorbent solution-refrigerant mixture in the generator is as given in Equation 2.10.

Stellenbosch University https://scholar.sun.ac.za

$$\dot{Q}_{gen} = \dot{m}_5 h_5 + \dot{m}_3 h_3 - \dot{m}_2 h_2 \qquad 2.10$$

Where: $\dot{m}_2$, $\dot{m}_3$ and $\dot{m}_5$are the mass flow rates (kgs^{-1}) defined in Equations 2.6 and 2.7; h_2, h_3 and h_5 are the specific enthalpies (kJkg^{-1}) at stages 2, 3, and 5, respectively, $\dot{Q}_{gen}$ is rate of heat addition in the generator (kJs^{-1}).

Amount of heat liberated through the absorber is presented in Equation 2.11

$$\dot{Q}_{abs} = \dot{m}_7 h_7 + \dot{m}_4 h_4 - \dot{m}_1 h_1 \qquad 2.11$$

Where: $\dot{m}_1$, $\dot{m}_4$ and $\dot{m}_7$ are the mass flow rates (kgs^{-1}) of streams at stages 1, 4, and 7, respectively; h_1, h_4, and h_7 are the specific enthalpies (kJkg^{-1}) at stages 1, 4, and 7, respectively; $\dot{\mathrm{Q}}_{\mathrm{abs}}$ is the rate of heat rejection through the absorber (kJs^{-1}). Amount of heat liberated through the condenser is presented in Equation 2.12.

$$\dot{Q}_{con} = \dot{m}_6 h_6 - \dot{m}_5 h_5 \qquad 2.12$$

Where $\dot{m}_5$ and $\dot{m}_6$are the mass flow rates (kJs^{-1}) defined in Equation 2.6; h_5 and h_6 are the specific enthalpies (kJkg^{-1}) at stages 5 and 6, respectively. The cooling rate in the evaporator compartment is then calculated using Equation 2.13

$$\dot{Q}_{eva} = \dot{m}_{ref}(h_1 - h_7) \qquad 2.13$$

Where: $\dot{m}_{ref}$ is the refrigerant mass flow rates (kJs^{-1}) defined in Equation 2.6; h_1 and h_7 are the specific enthalpies (kJkg^{-1}) defined in Equation 2.11.

Absorption cooling system has some operational and costs limitations that hinder its application. The absorption system requires electricity to run one or more pumps, which are critical components of the system [37], and therefore may not be suitable for communities with limited access to electricity or cannot afford the electricity. About 107.5 kW of electricity was reportedly required to operate an absorption cooling system with a cooling capacity of 2395 kW [16]. Regardless

Stellenbosch University https://scholar.sun.ac.za

of the electricity consumption by pumps, the high capital cost of absorption cooling systems is a major drawback for this technology. An absorption cooling system with a cooling capacity 2395 kW was reported to cost about US $314,348 while the conventional vapour compression cooling technology of the same cooling capacity was also reported to cost about US $178, 137 [16,38]. Due to the high capital cost, the absorption cooling systems have found little application for small-scale cooling systems.

An adsorption cooling system comprises four main components: an adsorber (or desorber), evaporator, condenser, and valve. A typical flow diagram and Clapeyron diagram of an ACS are shown in Fig 2.4. The adsorption cooling cycle proceeded through four cyclical processes (Fig 2.4): isosteric pre-heating process, isobaric desorption process, isosteric pre-cooling process, and isobaric adsorption process. The process begins by allowing the mode of the valve between hot adsorbent B (adsorbent that is already charged with the refrigerant and about to be heated) and evaporator to be closed but opened to cold adsorbent A which allows vaporized refrigerant gas from the evaporator to be adsorbed into the pores of cold adsorbent A where the refrigerant gas condenses into liquid (process 4-1: Isobaric cooling). During the adsorption process, heat of adsorption is generated resulting in rise in temperature (below the boiling point of the refrigerant) and pressure of the adsorbent and its content. As more refrigerant is adsorbed, more heat of adsorption is generated, and temperature and pressure increase. Since rise in temperature has negative effect on adsorption [39], this heat is quickly removed into the environment. While this process is ongoing, the adsorbent B (that was already charged with the refrigerant to its maximum

Stellenbosch University https://scholar.sun.ac.za

adsorption capacity) is preheated (Process 1-2: isosteric heating) which raises its temperature and pressure (but below its boiling point) similar to the effect created by compressor in the conventional vapour compression system (Section 2.1.1). This compressor effect is dependent on the type of adsorbent/refrigerant pair involved. The heating of the adsorbent B continues (Process 2-3: isobaric heating) and the refrigerant vaporizes and begins to leave the adsorbent B to desorb its adsorbed the refrigerant gas and the valve between adsorbent B and condenser is opened (while it is closed to adsorbent A) to allow refrigerant vapour (gas) to flow to the condenser to be condensed into liquid and heat of condensation is rejected into the environment. After the desorption of the refrigerants, the hot adsorbent B is cooled down (process 3-4: isobaric cooling). The condensed refrigerant then passes through an expansion valve without any heat transfer nor work done on the refrigerant and enters the evaporator. When the refrigerant enters the evaporator, it takes up heat from the evaporator compartment and the refrigerant is vaporized. The mode of the valve between hot adsorbent B is now opened to allow the vaporized refrigerant goes to the adsorbent B to be adsorbed by the absorbent while the valve is closed to adsorbent A. As the adsorption continues, adsorbent A is heated, and the process repeats itself. The time lapse between the beginning of adsorption of refrigerant in adsorber A, the desorption of refrigerant from adsorber B, the cooling of adsorber B, and the start of the next adsorption in adsorber A is termed cycle time.

Stellenbosch University https://scholar.sun.ac.za

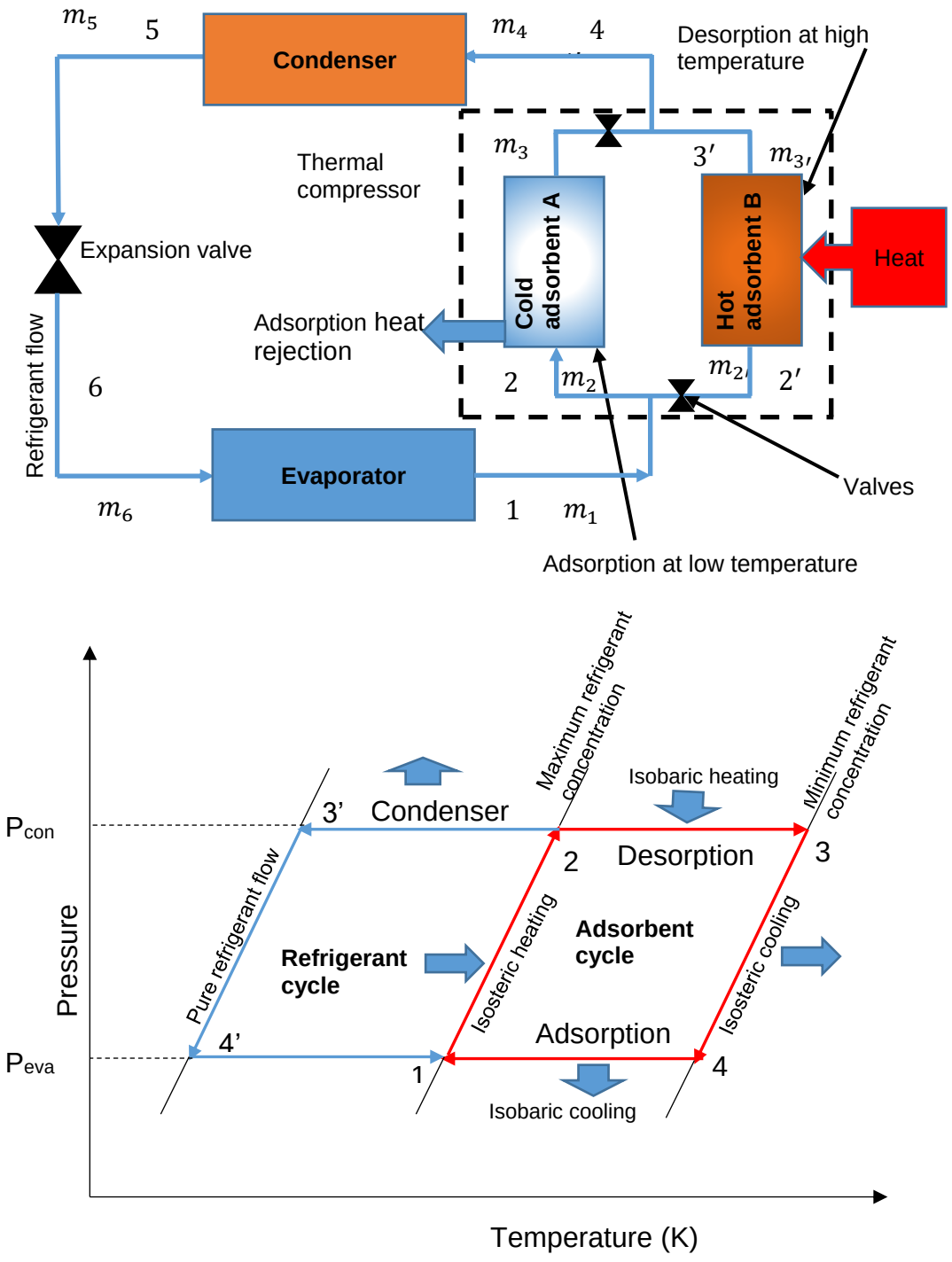

Figure 2.4: a. Flow chart of a typical single-stage two-bed adsorption cooling systems; b. Clapeyron diagram for the conventional single-stage two-bed adsorption cooling system. Note: 1, 2, 3, 4, 5 & 6 are the stages of the process

Stellenbosch University https://scholar.sun.ac.za

For an ideal ACS, the material balance in Fig 2.4a can be written as follows:

$$\dot{m}_2 = \dot{m}_3 \qquad 2.14$$

$$\dot{m}_{2'} = \dot{m}_{3'} \qquad 2.15$$

$$\dot{m}_{ref} = \dot{m}_1 = \dot{m}_4 = \dot{m}_5 = \dot{m}_6 = \dot{m}_2 + \dot{m}_{2'} \qquad 2.16$$

Where: $\dot{m}_1$, $\dot{m}_2$, $\dot{m}_3$, $\dot{m}_4$, $\dot{m}_5$, $\dot{m}_6$are the mass flow rates (kgs^{-1}) of the stream at stages 1,2, 3, 4, 5, and 6, respectively.

The ACS energy balance could be determined by considering Fig 2.4b for the adsorbent bed, the condenser and the evaporator as follows:

Adsorbent bed

Four processes occur in the adsorbent bed. The energy balance for each of these processes are provided below

1. Process 1-2: Isosteric heating

In this process, the adsorbent bed is preheated. The total sensible heat input during this process is the sum of the sensible heats of the adsorbent container, porous adsorbent, and the refrigerant (liquid and vapour phase) at the constant highest adsorption capacity. These are given by the following Equation 2.17 [40,41]

$$Q_{isosteric\ heating} = \int_{T_1}^{T_2} m_{mc} C_{mc} dT + \int_{T_1}^{T_2} m_{ads} C_{ads} dT + \int_{T_1}^{T_2} m_{ref} C_{ref} dT \qquad 2.17$$

Where: m_{mc} is the mass of the adsorbent container (kg), C_{mc} is the specific heat capacity of the adsorbent container ($Jkg^{-1}K^{-1}$), m_{ads} is the mass of the adsorbent (kg), C_{ads} is the specific heat capacity of the adsorbent ($Jkg^{-1}K^{-1}$), m_{ref} is the mass of the refrigerant (kg), C_{ref} is the specific heat capacity of the refrigerant ($Jkg^{-1}K^{-1}$), T_1 and T_2 are the temperatures (K) at states 1 and 2 respectively.

Stellenbosch University https://scholar.sun.ac.za

2. Process 2-3: Isobaric heating

The total energy required to drive this process has two main effects. Firstly, it causes a sensible heating of all the adsorbent bed constituents and increases their internal energy. Secondly, it initiates the desorption of the refrigerant from the adsorbent and produces the gas phase. Therefore, the total input heat is the sum of the sensible heats (of the adsorbent container, the adsorbent, and the refrigerant) and the total latent heat of desorption (Equations 2.18 & 2.19) [40,41]

$$Q_{isobaric\ heating} = \int_{T_2}^{T_3} m_{mc} C_{mc} dT + \int_{T_2}^{T_3} m_{ads} C_{ads} dT + \int_{T_2}^{T_3} m_{ref} C_{ref} dT \qquad 2.18$$

$$Q_{desorption} = -m_{ads} \int_{T_2}^{T_3} q_{st} \left[\frac{\partial W}{\partial T}\right]_{P=Pcon} dT \qquad 2.19$$

Where m_{mc}, C_{mc}, m_{ads}, C_{ads}, m_{ref}, C_{ref} are defined in Equation 2.20, $\frac{\partial W}{\partial T}$ is the change in refrigerant uptake or concentration (kgkg^{-1}) with respect to temperature, q_{st} is the isosteric heat adsorption of the adsorbent/refrigerant pair (Jkg^{-1}), T_2 and T_3 are the temperatures (K) at states 2 and 3 respectively.

3. Process 3-4: Isosteric cooling

During the cooling process, the refrigerant concentration (kg adsorbed refrigerant per kg of adsorbent) is at its minimum and sensible heat is transferred to the ambient. The total heat transferred from the adsorbent bed during this process is computed by [40,41]:

$$Q_{isosteric\ cooling} = \int_{T_4}^{T_3} m_{mc} C_{mc} dT + \int_{T_4}^{T_3} m_{ads} C_{ads} dT + \int_{T_4}^{T_3} m_{ref} C_{ref} dT \qquad 2.20$$

Where: m_{mc}, C_{mc}, m_{ads}, C_{ads}, m_{ref}, C_{ref} are defined in Equation 2.20, T_3 and T_4 are the temperatures (K) at states 3 and 4, respectively.

Stellenbosch University https://scholar.sun.ac.za

4. Process 4-1: Isobaric cooling

Once the pressure of the adsorbent container and its content reach that of the adsorption pressure, the refrigerant is adsorbed onto the adsorbent and heat of adsorption is generated which raise the temperature of the adsorbent container and its content (which is normally removed by cooling the adsorbent container and its content). The total heat generated during isobaric adsorption is the sum of sensible heats (Equation 2.21) and internally generated the heat of adsorption (Equation 2.22) [40,41]

$$Q_{isobaric\ adsorption} = \int_{T_1}^{T_4} m_{mc} C_{mc} dT + \int_{T_1}^{T_4} m_{ads} C_{ads} dT + \int_{T_1}^{T_4} m_{ref} C_{ref} dT \qquad 2.21$$

$$Q_{adsorption} = -m_{ads} \int_{T_1}^{T_4} q_{st} \left[\frac{\partial W}{\partial T}\right]_{P=Pads} dT \qquad 2.22$$

Where m_{mc}, C_{mc}, m_{ads}, C_{ads}, m_{ref}, C_{ref} are defined in Equation 2.20, $\frac{\partial W}{\partial T}$ is the change in refrigerant uptake (kgkg^{-1}) with respect to temperature, q_{st} is the isosteric (latent) heat of adsorption of the adsorbent/refrigerant pair (Jkg^{-1}), T_1 and T_4 are the temperatures (K) at states 1 and 4 respectively. The effect of changes in composition of the refrigerant and the adsorbent on isosteric (latent) heat of adsorption was discussed further in Chapter 6.

Condenser

The refrigerant vapour enters the condenser as soon as it desorbs from the adsorbent bed. In the condenser, the thermal energy of the refrigerant gas is removed first by rejection of sensible energy from the superheated vapour at the condenser pressure and temperature. When the refrigerant vapor reaches the saturated vapour state, it starts to condense, and the latent energy of

Stellenbosch University https://scholar.sun.ac.za

condensation is rejected to the ambient. The total heat rejected can be calculated as

$$Q_{con} = m_{ref}\left[h_{g\ (Pcon,T)} - h_{f(Tamb)}\right] \qquad 2.23$$

Where: Q_{con} is the condenser energy rejected; $h_{g\ (Pcon,T)}$ is specific heat of the refrigerant vapour at the condenser temperature and pressure (kJkg^{-1}); $h_{f(Tamb)}$ is specific heat of the liquid refrigerant at the ambient temperature and pressure (kJkg^{-1}); m_{ref} is the mass of the condensed refrigerant (kg).

Evaporator

As the refrigerant vapour is being adsorbed from the evaporator by the adsorbent, the useful cooling in the evaporator can be calculated using Equation 2.24 [3,41]

$$Q_{eva} = m_{ref}h_{fg} \qquad 2.24$$

Despite the similar thermodynamic principles underlining the operation of both adsorption and absorption cooling system, there are some differences in terms of component and performance. Pump is not a component of adsorption cooling system and therefore does not depend on electricity to function. However, the performance of adsorption system is inferior compare to that of absorption system [6,36,42]. The COP of absorption cooling system could be up to 1.2 whereas that for ACS is normally less than 0.6 [35] Absorption cycle requires a higher temperature heat source to run its operation in comparison with adsorption cooling system. The mechanism of adsorption system is described in detail in Section 2 3.

Stellenbosch University https://scholar.sun.ac.za

2.2 Adsorption cooling system

Adsorption cooling systems rely on the adsorption of a refrigerant gas into an adsorbent at low pressure followed by removal of heat of adsorption, and subsequent desorption of the refrigerant by heating the adsorbent [43]. During the adsorption of the refrigerant onto the adsorbent, the refrigerant absorbs heat from the evaporator compartment in the form of latent heat of vaporization. This leaves a cooling effect in the refrigerant container [4]. The amount of heat absorbs from the refrigerant container depends on the latent heat of vaporization of the refrigerant, the amount of refrigerant adsorbent, the adsorbent/refrigerant pair involved and the strength of attraction. A refrigerant with a high latent heat of vaporization paired with an appropriate adsorbent is generally preferred. Latent heat of vaporization of ethanol is about 40% less than that of water and AC has a weak affinity for water. Therefore, low-grade ethanol (60% ethanol, 40% water) paired with composite AC+NaCl was used as the adsorbent/refrigerant pair in this study. Since water and ethanol are miscible and therefore some water also evaporates during the adsorption process, the latent heat of vaporization of the low-grade ethanol would be higher than that for the high-grade ethanol. The detailed operation of the continuous ACS is explained in Section 2.1.2

2.2.1 Development of adsorption cooling systems

The ACSs are categorized into a single-stage, two-stage, and three-stage system depending on the temperature of the heat source [15,44–46]. Single-stage adsorption system requires the highest heat source temperature, followed by that for two-stage and three-stage system.

Stellenbosch University https://scholar.sun.ac.za

2.2.2 Single-stage adsorption cooling systems (ACSs)

The most common and basic ACSs are single-stage adsorption systems. The basic conventional single-stage ACS is the two-bed adsorption system (Figure 2.4a). The Clapeyron diagram for the conventional two-bed single-stage ACS is shown in Figure 2.4b. The two-bed single-stage ACS undergoes four processes per cycle [40] and the energy balance for each of the processes is as described in Section 2.1.2. Modifications have been done to the basic conventional single-stage adsorption systems to enhance performance. This is done by heat and mass transfer intensification as well as by better heat management schemes [47]. The modifications introduced to enhance the performance of the single-stage adsorption systems include thermal wave cycle, forced convection cycles and cascading cycles [48–50], as well as mass recovery and heat recovery or increased adsorber beds [51,52]. Examples of the advanced single-stage systems include two-bed mass recovery [51,52], three-bed [53,54] three-bed mass recovery/heat recovery [55,56], four-bed [57], four-bed mass recovery/heat recovery [58] and six-bed adsorption system. The experimental COP value of 0.90 at 5 ˚C evaporator temperature, the condenser temperature of 40 ˚C and 200 ˚C desorption temperature was obtained for forced convective thermal wave cycle [59].

However, most of these systems are complex and the actual equipment is yet to be built and tested to evaluate the COP in practice [59]. Despite these modifications, single-stage adsorption system used heat source at a higher temperature than the other stage systems, and therefore, has the limitation of not being able to function when the heat source temperature is below 50 ˚C along

Stellenbosch University https://scholar.sun.ac.za

with a condenser temperature of 30 ˚C or higher [44,54,60]. Additional equipment such as a pump may be required to run thermal wave cycles [59].

2.2.3 Multi-stage adsorption cooling system

Despite several heat management schemes to improve COP in adsorption cooling systems using advanced single-stage systems, the challenge remains that the systems cannot be used when the temperature difference between the heat source and the heat sink is less than 25 ˚C [44]. Therefore, two-stage and three-stage cycles have been proposed to utilize unexploited near-ambient temperature waste heat [59] which is impossible with the basic cycles [44,61,62]. The two-stage cycle is made up of six heat exchangers: a condenser, an evaporator and two pairs of adsorbers [44,54]. A two-stage system, which involved introducing two additional adsorbers, utilizing a heat source temperature below 50 ˚C in combination with a 30 ˚C condenser temperature (thus, the temperature difference between the heat source and the sink known as desorption temperature lift $(T_{des} - T_{con})$ is < 25 ˚C and cannot be used by single-stage adsorption systems) was proposed [44]. The two-stage system works on the concept of reducing the regenerating or desorption temperature lift $(T_{des} - T_{con})$ of the adsorbent by dividing the evaporator temperature lift $(T_{con} - T_{eva})$ into two smaller stages [44] (Figure 2.5). This reduces the final desorption temperature from $T_{des}{}'$ for single-stage adsorption systems to T_{des} for two-stage adsorption systems (Figure 2.5). Therefore, the refrigerant pressure increases through two successive stages of pressurization from the evaporator to the condenser pressure level [44]. The Dühring diagram for the conventional two-bed single-stage ACS is shown in Figure 2.5.

Stellenbosch University https://scholar.sun.ac.za

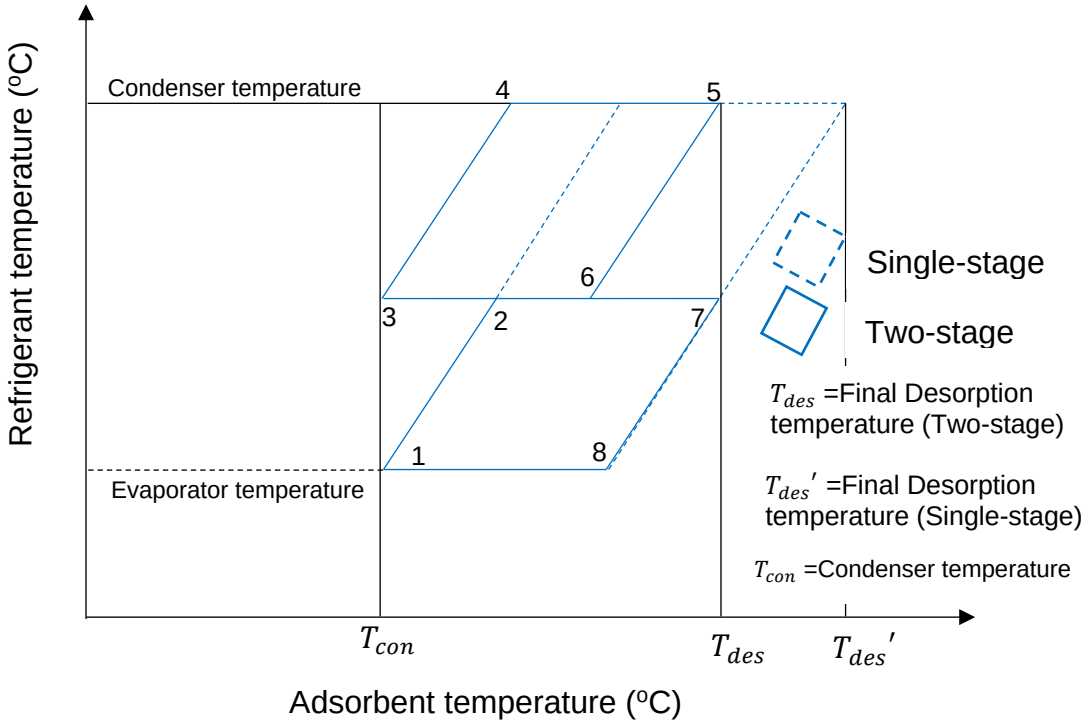

Figure 2.5 Comparison of the Dühring diagram for the conventional two-stage adsorption cooling system [Re-drawn from [[44]] Note: T_{con} is condenser temperature, T_{des} is final desorption temperature (two-stage), $T_{des'}$ is final desorption temperature (single-stage)

The first stage of pressurization increases the refrigerant pressure from the pressure level of the evaporator to an intermediary pressure level, which is lower than the pressure in the condenser. In the second stage, the refrigerant pressure is raised from the intermediary pressure level to the condenser pressure level (Figure 2.5).

Despite the advantage of low-temperature utilization, multi-stage systems are bulkier than the single-stage due to the increase in the number of adsorbent beds from two in the conventional single-stage system to four or six in multi-stage systems. Furthermore, as the number of adsorbent beds increases the amount of construction material and cost also increase. Therefore, the conventional

Stellenbosch University https://scholar.sun.ac.za

single-stage adsorption system was chosen, designed and constructed in this study. As long as there is enough supply of heat source, single-stage would be cheaper in terms of material cost, easier to construct and operate compared with multi-stage systems. The heat source in this study is the mango seed waste which is abundantly available in mango growing communities.

2.2.4 Performance measurements of adsorption cooling systems

Performance measurements are important to assess the system and to improve its performance. It also helps in comparing the system to what has already be done. There are many ways to assess the technical performance of a cooling technology such as energy efficiency ratio (EER), the coefficient of performance (COP [63,64]) and the specific cooling power (SCP [65,66]). EER is the ratio of net cooling capacity - or heat removed (in Btu) to the total input rate of electric energy applied [67]. EER can be converted to COP and provides similar information (amount of latent heat removed, and power supplied) compared to COP and therefore has not been used often to describe the performance of ACS. In the adsorption cooling system, the commonly used methods to assess the performance of adsorption cooling systems are by COP and SCP (Equations 2.25, 2.26 and 2.27). COP is the ratio of the heat removed (which as product mass of refrigerant and its latent heat of evaporation) in the evaporator to the heat supplied to the ACS.

$$Coefficient\ of\ performance\ (COP) = \frac{Q_{eva}}{Q_{supplied}} \qquad 2.25$$

$$Q_{eva} = m_{ref} h_{fg} \qquad 2.26$$

Stellenbosch University https://scholar.sun.ac.za

$$Specific\ cooling\ power\ (SCP) = \frac{Q_{eva}}{m_{ads}\tau_{cycle}}(W/kg\ adsorbent) \qquad 2.27$$

Where $Q_{supplied}$ is the total heat supplied (J), m_{ads} is the mass of the adsorbent (kg), τ_{cycle} is the cycle time (s), m_{ref} is the mass of the refrigerant (kg), h_{fg} is the specific latent heat of evaporation ($kJkg^{-1}$), Q_{eva} is the heat extracted in the evaporator (J).

2.3 Principle mechanism in an adsorption process

ACS works based on the principle of adsorption. Adsorption is a surface phenomenon (the higher the surface area the higher the adsorption) whereby molecules are attracted and deposited onto a surface. The surface is known as the adsorbent and the molecule is known as the adsorbate (or refrigerant). Adsorption can be categorized into physisorption (physical adsorption) or chemisorption (chemical adsorption). The adsorption dynamics of each type of adsorption process is different depending on the type of adsorbent/refrigerant pair involved. The physisorption and chemisorption would occur simultaneously in composite adsorbents such as activated carbon impregnated with salts such as $CaCl_2$, NaCl and water-based refrigerants as the water-ethanol mixture (60% ethanol: 40% water) being proposed in this study.

Physisorption

Physisorption, also known as physical adsorption, refers to the phenomenon in which gas molecules are adhere to a porous surface through van der Waals forces at a pressure less than the vapor pressure of the gas molecules [68,69]. Studies have shown that in cases where water-based refrigerants such as the water-ethanol mixture refrigerants, paired with AC, the water is less readily

Stellenbosch University https://scholar.sun.ac.za

adsorbed due to the non-polar nature of both ethanol and AC [70,71]. Therefore, the use of composite adsorbent (AC+ NaCl) as being proposed in this study would enhance the performance of the refrigerant. The AC component of the composite adsorbent would adsorb the refrigerant molecules (mostly the ethanol because e AC is a poor adsorbent for water [70,72]) to the pores of the adsorbent through van der Waals forces and liberate a latent heat of adsorption [69]. The rate of liberation of the heat of adsorption is usually different for different refrigerants and their mixtures (thus, whether the refrigerant is pure or a mixture as is the case with the use of water-ethanol mixture [71]) (Figure 2.5). The heat of adsorption for physisorption is, however, usually lower than 80 $kJmol^{-1}$ [69,73].

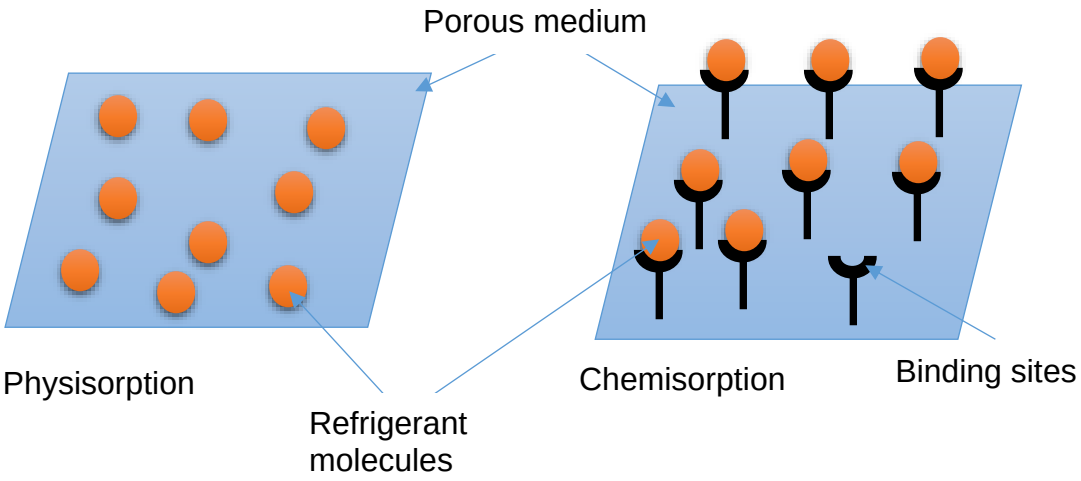

Figure 2.6 Schematic diagram of physisorption and chemisorption [redrawn from [69]]

Due to the exothermic nature of physisorption, the rate of adsorption normally reduces with increase in temperature because of the increases in the kinetic energy of the refrigerant molecules, thereby, reducing the van der Waals forces, which leads to the reduction in the adsorption rate.

Stellenbosch University https://scholar.sun.ac.za

Chemisorption

Unlike physisorption, the chemisorption depends on the existence of chemical bonds (binding sites) between the adsorbent and the refrigerant (adsorbate) (Figure 2.5). Salts like NaCl have a strong affinity for water than refrigerants such as ethanol [70], the NaCl component of the composite adsorbent would attract refrigerant molecules (mostly water molecules from the low-grade ethanol) leading to the formation of covalent bonding or hydrogen bonding and therefore liberate high heat of adsorption (generally greater than 80 $kJmol^{-1}$) in comparison with physisorption [69,73]. Chemisorption occurs slowly at low temperature and then increases with temperature after certain activation energy (normally greater than 40 $kJmol^{-1}$) is attained [73]. The adsorption rate in chemisorption continues to increase up to a certain temperature where the chemical bonds between the adsorbent and the refrigerant (adsorbate) are overcome and then decreases [73]. The chemical bond between the adsorbent and the refrigerant in chemisorption are, however, broken down using thermal energy during desorption at high temperature depending on the refrigerant and adsorbent pairing under consideration [69]. In contrast to adsorption, the desorption rate (the rate of removal of refrigerant (adsorbate) from the adsorbent) increases with increase in temperature.

2.3.1 Adsorption equilibrium isotherm models

Adsorption equilibrium data is one of the important data needed for the sizing of ACS [74]. These data are generally different for different adsorbent/refrigerant pairs and are therefore generated through experimental studies [74].There are several models used to describe the adsorption equilibrium data of an

Stellenbosch University https://scholar.sun.ac.za

adsorbent/refrigerant pair. These models are applied to the adsorption and desorption stages of the ACS. The commonly used models are the Freundlich equation, the Langmuir equation, BET equation, and Dubinin equations. Each of these models has its own limitations. Due to the nature of the adsorbent/refrigerant used in this study, the suitable model must describe both physisorption and chemisorption adsorption processes.

Freundlich Equation

Freundlich model is usually applied to adsorption processes that occur on heterogeneous surfaces (physisorption) [75] such as activated carbon and molecular sieves [76] and homogenous surfaces (chemisorption). It gives an isotherm expression that explains the distribution of active adsorption sites on the adsorbent and its surface heterogeneity [75,76]. The Freundlich equation can be written as shown below [14]:

$$W = W_o \left(\frac{P}{P_S(T)}\right)^{1/n} \qquad 2.28$$

Where W is the equilibrium adsorption uptake (kgkg^{-1}) is, W_o is the equilibrium adsorption uptake (kgkg^{-1}), $P_S\ (T)$ is the saturation pressure (kPa) at temperature T, P is the adsorption pressure (kPa), n is the exponential parameter. The slope of the isotherm ranges between 0 and 1 and this is used to measure the adsorption intensity or surface heterogeneity of the adsorbent. A slope approaching zero implies the surface is more heterogeneous, whereas uniform surfaces (chemisorption) have the slope below unity but greater than zero [76]. Despite its application for both chemisorption and physisorption, Freundlich isotherm model is not suitable to describe the equilibrium data in this study since

Stellenbosch University https://scholar.sun.ac.za

it is not consistent thermodynamically as it does not obey Henry's law at low refrigerant (adsorbate) concentration or pressure [75,76].

Langmuir Equation

Langmuir model is used to describe monolayer adsorption on a homogeneous surface (chemisorption) [75] and it is based on the principle that the rate of adsorption equals the rate of desorption [15]. Langmuir model assumes that the molecules of the refrigerant are adsorbed onto a fixed localized site, one site can accommodate one refrigerant molecule, refrigerant molecules adsorbed onto the nearby sites do no interact and all adsorption sites have same adsorption energy [15,77]. The Langmuir equation model can be represented by Equation below.

$$\theta = \frac{BP}{1 + BP} \qquad 2.29$$

Where P is the adsorption pressure(kPa), θ is the number of sites on the adsorbent occupied by the gaseous refrigerant, B is the equilibrium constant.

Since the adsorbent in this study (composite AC+NaCl) has both heterogeneous and homogenous surface, Langmuir model is not suitable to describe the equilibrium data in this study.

BET Equation

Brunauer–Emmett–Teller (BET) model, like Langmuir's model, is based on adsorption to a localized adsorption site where there is no interaction between the refrigerant on adjacent adsorption sites. However, the BET theory applies to multilayer adsorption while the Langmuir adsorption model applies to monolayer adsorption. BET theory usually used to calculate the specific surface area for porous media. The BET model could be represented by

Stellenbosch University https://scholar.sun.ac.za

$$\frac{q}{q_s} = \frac{B(P/P_S)}{(1 - P/P_S)(1 - P/P_S) + B(P/P_S)} \qquad 2.30$$

Where P is the adsorption pressure(kPa), B is the equilibrium constant, P_S is the refrigerant saturation pressure(kPa), q is the refrigerant concentration. BET model is appropriate for adsorption onto solid surfaces with homogeneous chemical properties [78]. The surface of composite adsorbent used in this study is, however, not chemically homogenous since the NaCl is not covering all the pores of the AC (NaCl is impregnated only in the micropore of AC [79]). Thus, BET model may not be appropriate in this case.

Dubinin Equations

The model is a semi-empirical equation used to describe the adsorption of gases on microporous adsorbents through the pore-filling mechanism [75,78]. It has also been used to study the adsorption behavior of cadmium on nano zero-valent iron particles (chemisorption) [75]. Thus, this model is suitable to fit the adsorption equilibrium data in this study. There are two variations of the Dubinin equation: Dubinin–Radushkevich (D-R) and Dubinin–Astakhov (D–A) equations. The Dubinin–Radushkevich (D-R) equation is given by [80]

$$W = W_o \, exp\left\{\left[-\frac{RT}{E} ln \frac{P_S(T)}{P}\right]^2\right\} \qquad 2.31$$

A modification of the Dubinin–Radushkevich (D-R) equation was done to develop the Dubinin–Astakhov (D–A) equation [14,80]

$$W = W_o \, exp\left\{-D \left[T ln \frac{P_s(T)}{P}\right]^n\right\} \qquad 2.32$$

Where D is the affinity coefficient. Both D and n depend on the brand and the type of adsorbent/refrigerant pair [14].

Stellenbosch University https://scholar.sun.ac.za

2.3.2 Adsorption kinetics

Another important parameter in the design of ACS is the adsorption kinetics. This parameter controls the cycle time of the adsorption process (fast kinetics implies shorter cycle time) [74] and sizing of the ACS. Kinetics data is different for different adsorbent/refrigerant pair. Adsorbent/refrigerant pairs with a strong affinity for each other generally result in fast diffusion [74] of the refrigerant to the adsorbent and fast kinetics. Fast kinetics are generally preferred as it leads to a reduction in the cycle time and size of the adsorber. Slow kinetics may be overcome by increasing the amount of adsorbent [74] which consequently increase the size of the adsorber and bulkiness of the ACS. Another way to overcome slow kinetics is through composite formation. AC is known to have weak attraction (affinity) for water [70,71] and therefore low-grade ethanol may not be a good refrigerant pairing for AC and would lead to slow kinetics and long cycle time. To increase this attraction for water fraction in low-grade ethanol, composite AC+NaCl was formed and the kinetics of this composite need to be measured and used in the sizing of the ACS. One of the well-known adsorption kinetic models is the linear driving force model which is used to understand the dynamics of adsorption and to predict the system performance. The adsorption or desorption rate of the adsorbent/refrigerant pair is estimated using the linear driving force model below [79]:

$$\frac{dW}{dt} = K\left(W_{eq} - W\right) \qquad 2.33$$

Stellenbosch University https://scholar.sun.ac.za

Where: W is the equilibrium uptake (kgkg^{-1}), W_{eq} is the equilibrium adsorption uptake (kgkg^{-1}), K is the equilibrium constant, $\frac{dW}{dt}$ is the rate of adsorption uptake at any particular time.

2.4 Selection of adsorbent and refrigerant

A choice of a suitable adsorbent/refrigerant pair is critical to the performance of the ACS. The amount of heat (latent heat) removed from the refrigeration compartment depends on latent heat of vaporization of the refrigerant at the temperature and pressure in the ACS, as well as a suitable adsorbent to adsorb a large quantity of the refrigerant. The evaporation temperature is determined by the temperature at which desired refrigeration is to be achieved/maintained while the pressure is a requirement to achieve evaporation at this temperature which can be achieved through compressor effect (as discussed in section 2.1.2). In addition, changes in the adsorbent-refrigerant pair also affects the performance of ACS due to change in heat of adsorption associated with different adsorbent/refrigerant pairs. High heat of adsorption limits the rate of adsorption of refrigerant by the adsorbent [39] and this affects the performance of the ACS. A good refrigerant with a high latent heat of vaporization paired with an unsuitable adsorbent with a large surface area translates into poor adsorption of the refrigerant and poor performance of the system. Similarly, a good adsorbent with a large surface area paired with an unsuitable refrigerant with a high latent heat of vaporization also translates into poor system performance. Examples of unsuitable pairing are AC/water [71] and silica gel/ethanol while examples of suitable pairing are silica gel/water [44], AC/ethanol [81]. There are certain criteria

Stellenbosch University https://scholar.sun.ac.za

used in selecting the desirable adsorbent and refrigerant to be used. These criteria have been described below.

2.4.1 Choice of adsorbent

The adsorbents can be classified as physical, chemical and composite adsorbents. Figure 2.7 shows the classification of adsorbents used in the adsorption cooling system.

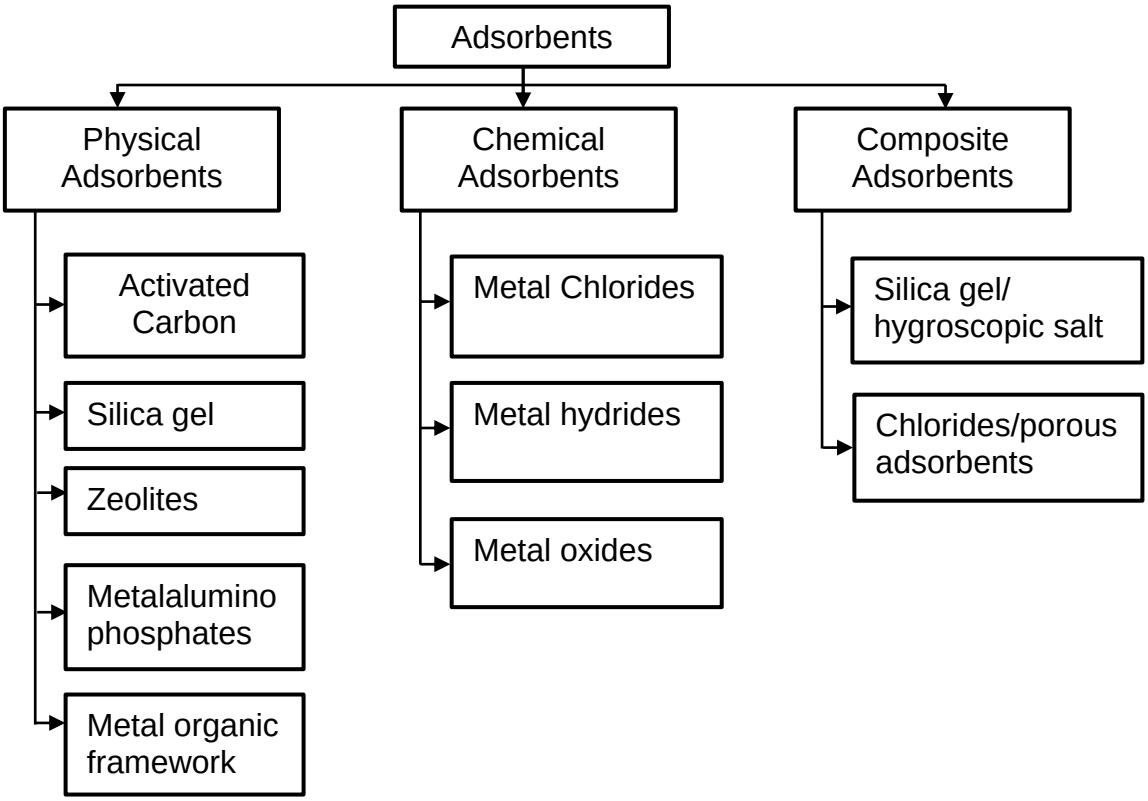

Figure 2.7 Classification of adsorbents [adopted from [82]]

Adsorbents are solid materials onto which refrigerants/adsorbates are adsorbed. A suitable adsorbent for adsorption cooling should have the following characteristics [83]: These characteristics of the adsorbent are to be considered with reference to the possible adsorbents and refrigerants as each of these

Stellenbosch University https://scholar.sun.ac.za

properties are dependent on the type of refrigerant and adsorbent under consideration and the operation conditions of the ACS.

1. Adsorption of a large quantity of the refrigerant at low temperature
2. Desorption of most of the refrigerant when the heat is applied
3. Have a large concentration difference with a small change in desorption temperature.
4. Ability to adsorb and desorb the refrigerant for many cycles.
5. Must have a high heat of adsorption relative to sensible heat.
6. High thermal conductivity and be thermally and chemically stable.
7. Non-toxic and non-corrosive.
8. Low cost and widely available.

In reality, there is no ideal adsorbent that has all of the above characteristics.

2.4.2 Choice of refrigerant

Table 2.1 shows some refrigerants used in ACS and their global warming potential. There are many factors that must be considered when selecting the best refrigerant. As with the adsorbent, the characteristics of the refrigerant are to be considered with reference to the possible adsorbents and refrigerants pairs as each of these properties are dependent on the type of refrigerant and adsorbent under consideration and the operation conditions of the ACS. Some of these factors are [84]:

1. High latent heat of evaporation to minimize the circulation rate of the refrigerant and reduce the amount of adsorbent to use.

Stellenbosch University https://scholar.sun.ac.za

2. The molecular size of the refrigerant should be small to facilitate faster adsorption onto the adsorbent.

3. Refrigerant with a strong affinity with the adsorbent to reduce the amount of adsorbent to be used thereby minimizing the size of the heat exchangers

4. The refrigerant/adsorbent pair should not solidify over the expected range of concentration and temperature conditions to which it is subjected.

5. The refrigerant should be very volatile than the adsorbent to facilitate the separation of the refrigerant from the adsorbent.

6. The refrigerant should be thermally stable with the adsorbent at the operating temperature conditions.

7. The refrigerant should be non-toxic, non-corrosive and non-flammable.

8. The production process of the refrigerant should have low global warming potential (GWP)

Stellenbosch University https://scholar.sun.ac.za

Table 2.1 Types of refrigerants used in adsorption cooling system and their global warming potential [9].

Refrigerant	**Chemical formula**	**GWP**
R134a	$C_2H_2F_4$	1300
R507	$50\%C_2HF_5+50\%C_2H_3F_3$	3300
Methanol	CH_3OH	2.8
Water	H_2O	NA
Ethanol	C_2H_5OH	NA
R113	$C_2F_3Cl_3$	5000
R141b	$C_2H_3FCl_2$	630
Ammonia	NH_3	0
R114	$C_2F_4Cl_2$	9300
R115	C_2F_5Cl	9300
R11	CCl_3F	4000
R12	CCl_3F_2	8500
R13	$CClF_3$	11700
R21	$CHFCl_2$	210
R23	CHF_3	1700
n-Butane	C_4H_{10}	4

Stellenbosch University https://scholar.sun.ac.za

2.5 Problems with adsorption cooling systems

2.5.1 Poor thermal conductivity of the adsorbents

One of the causes of the low coefficient of performance of the current ACSs is the low thermal conductivity of the adsorbent [85]. The thermal conductivity of AC falls between 0.15 $Wm^{-1}K^{-1}$ to 0.50 $Wm^{-1}K^{-1}$ [86–89]. For instance, the COP obtained for AC/ammonia, AC/ethanol, and AC/methanol working pairs are 0.67 [6], 0.8, and 0.78 [81,90,91], respectively.

Many studies have been done to produce a composite adsorbent to increase the performance of AC adsorption systems by using chloride salts which affected the heat of adsorption, adsorption kinetics and thermodynamic equilibrium of the composites formed [6,92]. Chloride salts used are calcium chloride, magnesium chloride, barium chloride, strontium chloride [6], manganese II chloride, nickel chloride and cobalt II chloride [93] and lithium chloride [94]. The thermal conductivity of some of these chloride salts is 0.57-0.598 $Wm^{-1}K^{-1}$ for magnesium chloride [95], 1.09 $Wm^{-1}K^{-1}$ for calcium chloride [96]. The introduction of these chloride salts has led to an increase in the amount of refrigerant adsorbed and specific cooling performance. For example, specific cooling performance increased from 557 Wkg^{-1} of the adsorbent for AC/ammonia to 731 Wkg^{-1} of adsorbent obtained for AC-calcium chloride composite/ammonia pair [6]. Hence improving the heat transfer performance of the AC could have positive effect on the amount of refrigerant adsorbed and specific cooling performance.

One method is to increase the thermal conductivity of the granular fixed beds consists of decreasing the inter-granular porosity by mixing together AC granules

Stellenbosch University https://scholar.sun.ac.za

of different sizes [97]. The approach resulted in a 35% improvement in thermal conductivity of the AC [97]. This approach could have negative effect on the kinetics of adsorption and desorption, thus affecting mass transfer. Another method is to use a consolidated adsorbent (formed by mixing adsorbents with a binder and the mixture is compressed) to increase internal heat transfer within the adsorber. However, consolidated adsorbents have the problem of low mass transfer which could result in very low adsorption rates, particularly sub-atmospheric pressure refrigerants such as water, methanol, and ethanol [42,59,98,99]. Therefore, it was proposed to perform experiments to determine the thermal conductivity and wall coefficients of performance of consolidated adsorbents, as well as their permeability (which is a measurement of mass transfer performance) to enhance and to optimize the heat and mass transfer performance of the consolidated adsorbents [47].

2.5.2 Design of adsorber beds

The adsorbent bed plays a critical role in adsorption cooling. Its performance affects the performance of the entire system. Shmroukh et al. [100] noted that poor adsorber bed designs lead to the production of thermal dead zones within the adsorber, thus, creating areas without efficient and adequate heat and mass transfer. Experiments with adsorber bed have produced high values for adsorption capacity and coefficient of performance, which deviate from the real adsorption refrigeration systems. Li et al. [99] classified resistance to heat transfer inside the adsorber bed into:

1. Convective heat transfer resistance between the heat transfer fluid and the adsorbent tube wall

Stellenbosch University https://scholar.sun.ac.za

2. The thermal conduction resistance through the metal wall of the adsorber bed
3. The thermal contact resistance between the metallic wall and the adsorbent particulate
4. Thermal conduction resistance within the adsorbent

According to Li et al. [99], resistances 1 and 2 contribute very little to the thermal resistance and can be reduced by increasing the heat transfer fluid velocity and reducing the wall thickness respectively while 3 and 4 are the main causes of thermal resistances. The thermal contact resistance between the metallic wall and the adsorbent could be minimized by using coated adsorber or increasing the heat transfer area by using heat exchangers [7,99]. Coated adsorbers are used to decrease thermal contact resistance between the metallic wall and the adsorbent. This is done by using binders that stick the adsorbent onto the metallic wall. In doing so, the mass of the adsorber is also increased. This innovation increased the metal-adsorbent heat transfer coefficient [7,42]. The main drawback of this innovation is that the ratio of the inert mass and adsorbent mass is increased thereby decreasing the COP [47]. However, effective heat management is required to overcome this challenge.

Another method to reduce heat transfer resistance is the use of heat exchangers including finned tubes, plate fins, plate heat exchangers, and plate-fin heat exchangers [99] if the wall heat transfer coefficient is not high and if no swelling and shrinking effect of occurs in the adsorbent. The shortcoming of this technique is that it increases the thermal capacity of the adsorber [47].

Stellenbosch University https://scholar.sun.ac.za

2.5.3 Adsorbent/refrigerant pairing

The choice of adsorbent and refrigerant (adsorbate) pair used in adsorption cooling is essential to its performance [5,83]. The working pairs such as AC/ethanol, AC/methanol, AC/ammonia, silica gel/water, and zeolite/water [5,6,93] have limitations in their performance. Water has low saturation pressure which limits its evaporation resulting in poor mass transfer performance [5,6,82], methanol and ammonia are both toxic [5,6]. Ethanol has a low latent heat of vaporization [5,82] but is environmentally benign and not poisonous [8].

Some studies have been done to outline the challenges of some working pairs. For instance, a review was presented by Askalany et al.[101] on ACSs with adsorption pairs of AC with ammonia, ethanol, methanol, hydrogen, nitrogen, and diethyl, pitch-based AC (Maxsorb III) with R134a, R507A, and n-butane and AC with CO_2 respectively. It was noted from their work that the refrigerants R134a and R507a are not eco-friendly due to their high global warming potential (GWP) (due to the environmental impacts of producing the refrigerant) of 1300 kg CO_2 per kg refrigerant [9]. Also, n-butane, hydrogen, methanol, ethanol, and diethyl ether are not suitable because of their high flammability while ammonia is a highly poisonous refrigerant [101].

A review was done by Shmroukh et al. [93] to compare a range of adsorption refrigeration working pairs such as AC/methanol, AC/ethanol, and AC. Maximum equilibrium adsorption capacity for AC/methanol, AC/ethanol, and AC (maxsorb III)/R-134a were reported as 0.259 $kgkg^{-1}$, 1.2 $kgkg^{-1}$ and 2 $kgkg^{-1}$ respectively. The conclusion reached from this further study was needed to develop adsorption

Stellenbosch University https://scholar.sun.ac.za

pairs having higher adsorption capacity with little or no environmental impact, as well as to build reliable, efficient, and durable adsorption systems [93].

A novel adsorbent was produced from AC, silica-gel, and $CaCl_2$ for use in solar adsorption cooling and dehumidification systems to increase the coefficient of performance of AC [79]. The silica gel and $CaCl_2$ were introduced into the pores of the raw AC. Investigations revealed that the maximum adsorption capacity of the new adsorbent was 0.23 kg water per kg adsorbent at 27 ˚C and a water vapour pressure of 900 Pa. It was further reported that the maximum adsorption capacity of the raw AC and pure $CaCl_2$ were 0.02 kg water per kg of AC and 0.9 g water vapour per gram of $CaCl_2$ respectively under the same conditions [79]. The results of this study reveal that the synthesized adsorbent (silica gel AC/$CaCl_2$) performed better than both raw AC and pure $CaCl_2$ [79]. Moreover, the thermal conductivity of the adsorbent was also improved by the introduction of $CaCl_2$ [79].

2.5.4 Source and availability of adsorbent and refrigerant

Commercially, AC is produced by using high-cost raw materials such as petroleum coke [102] and coal [103]. The price of coal and petroleum cokes are US$72.5/ton and US$110.5/ton [104] respectively. Furthermore, these materials, coal and petroleum coke, are non-renewable, their reserves are being depleted [105], and also contribute to pollution of the environment as a result of the presence of sulphur and greenhouse gas emissions during the production and activation of AC due to the energy supply needed for activation [106] as one constituent of these materials. In addition, these materials are also not available in most communities. Besides, both commercial AC and chloride salts used are

Stellenbosch University https://scholar.sun.ac.za

expensive [107,108] resulting in a high cost of ACSs. Besides, zeolite and silica gel are not readily available in rural communities while AC could be made from many carbonaceous materials including agricultural residues such as mango kernel, and solid wastes from processing which are readily available in rural communities [41]. Furthermore, AC can be made to suit a specific application by varying the process parameters such as activation time, activation temperature, the concentration of the activation chemical, etc [41].

Despite being readily available, water performs poorly with AC [109]. Ammonia is not readily available in rural communities and it is expensive. Ethanol can be produced locally available agricultural materials such as fruits and vegetables due to the availability of fermentable substrates [110,111]. For example, ethanol could be produced from blemished mangoes and peels as a means of reducing challenges of mango waste handling. The sugar content of mango and mango peels are 16-18% w/v and 11-13% w/v respectively, making them suitable for ethanol production through fermentation [112,113].

2.5.5 Source of energy for adsorption cooling in food processing

Finding a suitable heat source to power the ACS is critical not only to the performance of the ACS but also to the environment. Fossil fuel sources of heat are not suitable for powering adsorption systems because of depletion of reserves, fluctuating market prices and greenhouse gas emission, and low coefficient of performance of the adsorption cycle [105]. Renewable energy options such as solar and wind are intermittent and unpredictable [114], the capital cost for geothermal energy production is high (it ranges between US$1,500 to US$3,000 per kW) [115], and cannot be afforded by small-scale

Stellenbosch University https://scholar.sun.ac.za

farmers and processors. Hydro energy is dependent on the availability of a river which is not available in all communities as well as regular rainfall or snowfall which is unpredictable [114].

Biomass is another source of energy which is readily available in the form of agricultural and forestry residues and these could be used as a source of heat to power the adsorption system. For example, the energy content of sun-dried mango kernel (10-15% moisture content) is 21.74 $MJkg^{-1}$ [116,117] which is comparable to low-grade coal (heating value of 18.0-25.5 $MJkg^{-1}$) [117]. The utilization of mango kernel as a heat source may be a cost-effective way to minimize the problem of waste disposal along the mango supply chain [12].

A large amount of waste heat is also available in the food industry. During the primary utilization of energy, large quantities of waste heat are discarded into the environment in the form of hot water and hot exhaust air (Table 2.2). The discharge of waste heat reduces the efficient utilization of the primary energy but causes thermal pollution [59]. Waste heat may include thermal energy stored in hot water, hot exhaust air, combustion flue gas, and hot liquid foods. For example, refrigerated trucks are generally powered by diesel engines. The energy efficiency of diesel engines is about 35% and the temperature of exhaust gas from a diesel engine is 500 ˚C. Therefore the employment of these waste exhaust gas in adsorption refrigeration could reduce fuel consumption and improve the overall efficiency of the engine [47,118–123]. Table 2.2 shows quantities of some waste heat available in the food industry [124].

Stellenbosch University https://scholar.sun.ac.za

Table 2.2 Quantities of waste heat in a canned fruit and vegetable processing facility(adapted from [124])

Unit operations	**Product**	**Quantity (m^3/ton of product)**	**Temperature (°C)**	**Heat content (MJ/ton of product)***
Water blanching	Snap beans	0.124-0.350	90	33.6-94.9
	Lima beans	0.822	90	222.9
	Peas	0.240-0.385	90	65.1-104.4
Steam blanching	Snap beans	0.125-0.150	90	33.9-40.7
	Lima beans	0.113-0.238	90	30.7-64.6
	Peas	0.191-0.313	90	51.8-84.9
Vibratory spiral blancher	Snap beans	0.027	90	7.3
	Lima beans	0.025	90	6.8
	Brussels sprouts	0.015	90	4.1
	Broccoli	0.011	90	2.9
	Cauliflower	0.003	90	0.8
Steam blanching with water recovery	Snap beans	4.937	90	1339.3
	Lima beans	4.967	90	1347.4
	Peas	4.967	90	1347.4
Cooker condensate		0.117-0.210	120	31.7-56.9
Cooling water		0.250-0.415	55	67.8-112.6
Can topping water overflow		0.165-0.210	95	44.8-56.9

* 25 °C was used as the reference temperature

Stellenbosch University https://scholar.sun.ac.za

2.6 Economic and environmental impacts of an adsorption cooling system

2.6.1 Economic impacts analysis

Adsorption cooling systems have been reported to be more expensive in comparison with the conventional vapour compression chiller. For instance, the capital cost of 10 kW nominal cooling power adsorption cooling system for room cooling was reported to cost € 13000 [125]. The adsorption cooler was to be driven by solar energy. The installed cost (the sum of the cost of the solar field, the solar circuit, the adsorption chiller itself) of this adsorption cooling system was reported to be between € 26323 - € 29733, while the installed cost of the conventional vapour compression chiller of the same cooling power was € 4260 [125]. The annual operating cost of this adsorption cooling system was reported to be between € 435 - € 728 per annum compared with €1489 per annum for the conventional vapour compression chiller of the same cooling power [125]. As a result of the utilization of solar energy to power the adsorption cooling system, the estimated annual savings was between € 761-1054 while the annual electrical energy savings 2668-3631 kW [125]. The payback period for the adsorption cooling system ranges from 13-15 years [125]. Thus, ACS are expensive than the conventional vapour compression chiller of the same cooling capacity.

2.6.2 Environmental impacts analysis adsorption cooling system

The contribution of adsorption cooling systems to global warming stems from the type of refrigerants used [9,126] and the greenhouse gas emission associated with the source of desorption energy supply [126]. Greenhouse has emission resulting from the production of both refrigerant and adsorbent, and the leakage

Stellenbosch University https://scholar.sun.ac.za

of refrigerants [126] are the main causes of environmental degradation of of refrigerants and adsorbents. Table 2.1 (Section 2.4.2) shows the types of refrigerants used in the adsorption cooling system and their global warming potential. As a result of the high global warming potential of chlorine, bromine, and fluorine-containing refrigerants such as R134a, R507, R141, R11, R12, R13, R21, R23, R113, R114, and R115 (Table 2.1), attention has now been focused on environmentally benign refrigerants such as ethanol and water. Apart from the contribution to global warming potential, some refrigerants like methanol are toxic and can, therefore, destroy living organisms in the environment is not handled properly. Furthermore, both methanol and ethanol also pose fire risks and should be handled properly to avoid the destruction of properties through a fire outbreak. The source of desorption energy supply to the adsorption cooling system has been discussed in Section 2.6.5. A 10 kW cooling capacity solar powered adsorption cooling system was used to cool a room. It was reported that there was between 890.7-1251.8 [125] reduction in emissions compared with the conventional vapour compression cooling system of the same cooling capacity.

Adsorption system is relatively an environmentally friendly system in comparison with the vapour compression system [8]. The utilization of adsorption cooling technology was reported to have resulted in the reduction of CO_2 emission by conventional vapour compression chiller of the same cooling capacity from 50 kg CO_2/ kWh to 14.9 kg CO_2/ kWh [127]. Furthermore, ACS can be driven by waste heat at a temperature as low as 50 $^{\circ}$C [53] which is readily available in the food industry (Table 2.1 in Section 2.3.5) while absorption cooling system is driven by heat source temperature at least 110 $^{\circ}$C [128]. Adsorber/desorber bed in the ACS

Stellenbosch University https://scholar.sun.ac.za

functions like the compressor in the vapour compression system but in this case, the compression takes place by application of heat instead of electric power to change the mode from adsorber to desorber. The absence of an electrically powered mechanical compressor has led to a reduction in electrical energy consumption. For instance, the driving energy of 90 kW for conventional vapour compression cooling was reduced to 26.8 kW in an industrial adsorption chiller to cool water from the initial temperature of 31 ˚C to 9 ˚C [127]. The energy consumption by ACS can be reduced further in a small ACS due to the absence of a pump which makes this technology possible to use in off-grid communities [3].

2.7 Production of bio-based sorbents

There are different types of bio-based sorbents such as aerogels, foam membranes, inorganic meshes, and surface modified fabrics [129]. Others are natural products such as cotton, rice straw, coconut husk, banana peels [129], etc. that have been used extensively during separation processes. Each of these sorbents has a different production method for a particular application. For instance, glucose aerosol could be produced through the process of hydrothermal carbonization, freeze-drying, and pyrolysis while cellulose nanofibers could also be produced following hydrophobic modification and freeze-drying [129]. Activated carbon is one of the bio-based sorbents widely used. This study is focused on activated carbon production and its application in adsorption cooling systems. Production of AC can either be through physical or chemical activation or physicochemical activation [10,130–132]. Prior to the activated carbon production, the feedstock undergoes some pre-treatment steps

Stellenbosch University https://scholar.sun.ac.za

such as washing, drying, size reduction, and sieving. Washing is necessary to remove for loose compounds including sand, dust and mineral impurities that may have been attached to the feedstock through contact with the sand during harvesting of the biomass or transportation process [132,133]. The presence of these impurities on the feedstock, if not removed, may contribute to the high ash content of the resultant activated carbon resulting in low adsorption capacity and mechanical strength of the activated [132,134]. Sulaiman et al [132,135] investigated the reduction of ash component of oil palm shell, fronds, and trunk through washing. It was found that the ash component reduced by 43.16%, 52.18%, and 7.42% respectively for palm shell, frond, and trunk in comparison with the unwashed biomass [132,135]. The removal of the impurities on the feedstock through washing is influenced by (i) type of mixing (agitation or non-agitation), (ii) size of feedstock, (iii) amount of water, and (iv) soaking time [136]. Drying of the feedstock after washing is necessary to reduce the mechanical energy spent during size reduction [137]. Drying normally takes place in an air-oven drier at 80 ^{0}C or sun drying for two consecutive days [132] prior to size reduction (crushing, grinding, and milling). Despite the cost incur during drying and size reduction due to the energy consumption, Bamaga et al [138] noted that these pre-treatment steps may reduce for the cost associated with from poor waste disposal through landfilling or other methods. Besides, size reduction is critical in classification and suitability of the activated carbon produced. Activated carbon is categorized into powder, granular and pellet forms and each has its unique application [132].

Stellenbosch University https://scholar.sun.ac.za

Generally, feedstock pre-treatment steps for activated carbon production should be [132]:

1. affordable and consumes less energy and feedstock
2. Consume less water and chemical to reduce liquid waste discharge
3. Have a low operational risk

Table 2.3 Table Classification and application of activated carbon [132]

Type activated carbon	**Description**	**Application**
Powder	Particle size <0.18 mm, average diameter of 01.15-0.25 mm	Suitable for a batch experiment followed by filtration. Applied in liquid phase applications
Granular	Particle size of 0.2–5 mm. Irregular in shape	Used in an adsorption application such as adsorption cooling and vapour phase applications
Pellet	A powdered activated carbon mixed with a binder, and fused and shaped into a pellet. Diameter ranging from 0.8 to 5.0 mm	Applied mainly in gas phase application

2.7.1 Physical activation method

The material is carbonized under an inert atmosphere and then activated at a high temperature ranging from 800 ˚C -1000 ˚C [139] using either steam or carbon dioxide as the activating reagent to convert portion of the carbon into AC. The physical activation method can be represented by the reaction below [132]:

$$C + CO_2 \rightarrow 2CO \qquad \Delta H = +173\ kJmol^{-1}$$

Stellenbosch University https://scholar.sun.ac.za

$$C + H_2O \rightarrow CO + H_2 \quad \Delta H = +132\, kJmol^{-1}$$

The carbonization increases the carbon contents of the char produced with increased surface area compared with the biomass from which it is produced [132]. The carbonization process proceeds through four stages [132]:

1. Stage 1 refers to the dehydration stage where moisture is removed from the feedstock at a temperature below 200 ˚C.
2. Stage 2 refers to the onset of feedstock decomposition leading to the discharge of tar and organic acids and this occurs at 170 ˚C -270 ˚C.
3. Stage 3 the decomposition of the feedstock occurs at 270 ˚C –350 ˚C and liquid and gas are discharged.
4. Stage 4 occurs at a temperature greater than 350 ˚C where there is an increase in carbon content through the removal of remaining volatiles.

Physical activation, however, results in high energy consumption, low carbon yield [132], and expensive and dangerous (especially steam activation) for small-scale systems [139].

2.7.2 Chemical activation method

In chemical activation, the material is treated with activating chemical prior to carbonization at a temperature between 400 ˚C-500 ˚C [10,140]. Activation chemicals used are $CaCl_2$, $ZnCl_2$, H_3PO_4, K_2CO_3, and KOH to produce activated carbon with different properties depending on the activation chemical used [141]. Chemical activation is preferred to physical activation as the former results in higher yields and uses less operating energy, and is particularly suitable for biomass materials [10,131,140]. There are two chemical activation procedures: 1. Physical mixing of the dried feedstock and the solid chemical followed by

Stellenbosch University https://scholar.sun.ac.za

carbonization process and 2. Wet impregnation method where the biochar or the raw feedstock are soaked in an activating chemical solution and dried prior to carbonization process [142]. Rashidi and Yusup [132] stated that dehydrating agents used as chemical activation such as $CaCl_2$ and $ZnCl_2$ prevent the formation unwanted products such as tar and other liquid products that have the ability to block the pores and improves the volatile material evolution from the carbon leading to the pore development.

2.7.3 Physiochemical activation

This involves the chemical impregnation of the feedstock, followed by the physical activation using CO_2 or steam [143]. According to Chowdhury et al [144], physicochemical activation could be applied when the chemical agent is not completely removed during the washing stage of the chemical activation method, leading to pore blockage. Thus, an additional step of physical activation is required to improve the pore formation. This combination of physical and chemical activation method produces activated carbon having unique properties [132].

2.7.4 Overview of technologies for activated carbon production

The type of technology for activated carbon production impacts on the characteristics of the final product [132].

Furnace/Pyrolysis carbonization

Conventionally, AC is produced through carbonization in a furnace [145,146]. Heat is transferred to the feedstock through conduction, convection, and radiation from the outer surface where the heat source is located to the inner where the

Stellenbosch University https://scholar.sun.ac.za

feedstock is located. As a result of the slow heat transfer from the heat source to the material partly due to the low heat transfer of the feedstock, a thermal gradient is established in the furnace, leading to long carbonization times and high energy consumption and operating cost. Examples of feedstocks that were carbonized using pyrolysis are shown in Table 2.4

Microwave carbonization

Microwave heating is another technology employed in the production of activated carbon. Microwave heating provides electromagnetic energy at 0.3 GHz to 300 GHz that is absorbed by the feedstock and converted into energy and uniformly distributed throughout the feedstock [132,147]. Since microwave heating is able to transmit at an extremely faster speed (speed of light) [148], activated carbon production using the microwave heating method is faster, resulting in reduced processing time, and low energy cost compared with the conventional method of heating [132]. Examples of feedstocks that were carbonized in a microwave carbonization are shown in Table 2.4

Hydrothermal carbonization

Hydrothermal carbonization improves the carbon content of the feedstock prior to activation, a feature that is also shared by the conventional carbonization method. Unlike the conventional carbonization method, hydrothermal carbonization takes place in water (liquid phase) [149]. The hydrothermal is a smokeless operation [132] which takes occurs in water suspension at 180 ˚C-280 ˚C and in some cases at 300 ˚C -390 ˚C for a few hours in an autoclave [132,150] and at a slightly greater pressure than the saturated pressure of water, to ensure the water remains in a liquid phase and to achieve an inert

Stellenbosch University https://scholar.sun.ac.za

condition [132]. The product from the hydrothermal carbonization is called hydro-char [150].

Table 2.4 Overview of technology and feedstock for activated carbon production

Feedstock	**Activation type**	**Carbonization technology**	**Maximum Surface area (m^2g^{-1})**	**Reference**
Palm shell	Chemical (H_3PO_4)	Furnace	615	[143]
Palm shell	Physicochemical (CO_2)	Furnace	614	[143]
Empty palm fruit bunch fibers	Physical (steam)	Furnace (pyrolysis)	603.76	[145]
Waste tea	Chemical (K_2CO_3)	Furnace (Nabertherm S27)	1722	[146]
Waste tea	Physicochemical (H_3PO_4)+ carbonization at 350˚C	Microwave furnace	1157	[151]
Palm empty fruit bunch	Chemical ($ZnCl_2$)	Furnace	86.62	[152]
Palm shell	Chemical H_3PO^4/KOH	Furnace	490/810	[153]
Lignin	Chemical KOH	Hydrothermal	3235	[149]
Palm date seed	Chemical NaOH	hydrothermal	1282.89	[154]
Coconut shell	Chemical NaOH	Hydrothermal	876.14	[155]

It has been reported that most of the reaction in the hydrothermal carbonization occurs with the first 20 minutes [132]. The reaction that takes place during the hydrothermal method of lignocellulosic material is shown below

$$C_6H_{10}O_{5(s)} \rightarrow C_6H_2O_{(s)} + 5H_2O_{(l)} \qquad \Delta H = -2.52\ MJkg^{-1}$$

Stellenbosch University https://scholar.sun.ac.za

Hydrothermal carbonization can be applied feedstocks high in moisture content since the product takes place in a liquid state. Thus, pre-drying of the feedstock is eliminated. This would result in time, cost and energy saving to dry the feedstock which is a requirement in conventional carbonization method. Furthermore, it eliminates air pollution resulting from hazardous gas emissions (CO_2, nitrogen oxide, sulphur oxide) from conventional carbonization method as these gasses dissolve in the water [132]. The hydro-char produced normally has a very low surface area [156,157] as it is yet to be activated. The activation of the hydro-char is done either by chemically or physically to improve the surface area [154,155,157]. Examples of feedstocks used for hydrothermal carbonization followed by activation are shown in Table 2.4.

2.8 Production of composite activated carbon adsorbent

Composite adsorbents are produced to improve the heat and mass transfer properties, as well as adsorption properties (e.g. equilibrium adsorption capacity, and heat of adsorption) of a physical adsorbent such as activated carbon. Composite adsorbents can be produced by simple mixtures of physical adsorbents such as activated carbon and chloride salts in a defined mass or volume ratio. This method is used particularly for granular activated carbon [6,85]. Impregnation is another method of producing a composite adsorbent where chloride salt is dissolved in water or other solution. Activated carbon is then put in the salt solution and dried to remove the water [6]. This can improve thermal conductivity by up to 10 times, which is larger than that of the composite beds produced using simple mixture method [85,119]. To further enhance the thermal

Stellenbosch University https://scholar.sun.ac.za

conductivity, consolidated beds can be formed by compressing impregnated beds [6,85,119]. In some cases, binders are used [85].

Stellenbosch University https://scholar.sun.ac.za

Chapter 3 Problem statement and research objectives

3.1 Problem statement

Cooling plays a critical role in the preservation of fresh produce from deterioration [13]. Several cooling technologies have been designed for the preservation of agricultural produce. The current cooling technologies have an inherent problem of rising electricity cost, limited water availability, weather dependent and negative environmental effects and therefore are not effectively used by farmers and processors in both grid and off-grid agricultural communities [34]. Furthermore, to avoid failure of adoption, the impacts of introducing new technological innovation must be assessed in terms of technical performance (COP, SCP), economic performance (IRR, NPV), and environmental performance (GWP) to ensure that it is economically and environmentally sustainable. In this study, processing and preservation of mangoes would be used as a case study. Mango was chosen because it can be processed into a stable product by employing cooling and drying unit operations which can be integrated by using an adsorption cooling system.

Adsorption cooling is driven by heat from sources such as solar, geothermal, waste heat from factories, combustion of fuels, etc. [5,6,158]. The existing ACSs have adsorber bed packed with low thermal conductivity adsorbent, as well as expensive and poor performance working pairs. This makes ACSs not affordable in rural agricultural communities. Therefore, it is essential to enhance the performance of the ACS by developing adsorption pairs which are environmentally benign with improved properties (sorption capacity, heat and

Stellenbosch University https://scholar.sun.ac.za

mass transfer) to build adsorption refrigeration systems that are compact, efficient, reliable, and durable. Furthermore, mango seed wastes are abundantly available in mango growing communities and it has the potential of being used as AC because of its lignocellulose content [10,116]. Sodium chloride (NaCl) which has higher thermal conductivity than commonly used salts [96,159] is also accessible [139]. The heating value of mango seed is comparable to coal [116,117] and therefore would serve as a suitable renewable energy source.

In this study, both high-grade (99.7%) and low-grade (60%) ethanol would be used as the refrigerant. A composite AC+NaCl would be formed to improve the thermal and adsorption performance of AC. The utilization of NaCl is expected to improve the properties (sorption capacity, heat and mass transfer, and compressor effect) of the composite AC+NaCl of when paired with ethanol/water mixture due to the high water affinity of NaCl compared with untreated AC. Secondly, mango seed AC would be synthesized and used as an adsorbent. NaCl would be the activation chemical used to produce the mango seed AC. In addition, the economic and environmental impacts of integrating ACS along with the replacement of coal with mango seed as the boiler fuel in dried mango chips processing in both grid and off-grid communities would be assessed.

3.2 Research questions

To achieve the overall objective of improving performance and making ACSs affordable, the following research questions will be answered:

(1) What are the physical and functional properties of AC produced from mango seed using pyrolysis activated with NaCl?

Stellenbosch University https://scholar.sun.ac.za

(2) At what conditions can AC from mango seed be produced in a pyrolysis method to have functional properties that are close to or better than conventional AC?

(3) How do sodium chloride concentration, soaking time and carbonization time impact on AC characteristics?

(4) How and why changes in changes in AC properties through composite formation affect the performance of ACS?

(5) How does the adsorption cooling performance of water-ethanol mixture improve by formation of composite AC+NaCl adsorbent?

(6) What are the economic and environmental benefits of integrating the ACS and replacement of boiler in a fruit processing plant, using mango processing as a case study?

3.3 Research objectives

The main objective of this study is to improve the technical, environmental and economic performance of ACS for storing perishable horticultural produce in rural agricultural communities without access to electricity, using mangoes as a case study.

3.3.1 Specific objectives

(i) Produce and characterize AC from mango seed husk and sodium chloride.

(ii) Assess the performance of the NaCl activated mango seed husk carbon with both high-grade ethanol and low-grade ethanol as refrigerants.

Stellenbosch University https://scholar.sun.ac.za

(iii) Explain the fundamental mechanisms by which changes to AC (through composite formation) and refrigerant (ethanol) grade affect the system performance

(iv) Evaluate the economic impacts and environmental impacts of integrating ACS and replacing the boiler fuel in mango food processing.

3.4 Novelty statement

Heat transfer and adsorption performance of AC have been improved by using several chloride salts to form composite adsorbents [160–162]. The introduction of these chloride salts gives the resultant adsorbent its unique thermal and adsorption characteristics. The thermal conductivity of the adsorbents is reported to have increased through the composite formation with chloride salts [94,160,161]. The salts used to form the composite adsorbents have low thermal conductivity compared with sodium chloride (NaCl). For example, the thermal conductivity of $CaCl_2$ is 1.09 $Wm^{-1}K^{-1}$ [96] while that of NaCl is 7 $Wm^{-1}K^{-1}$ [159]. Moreover, most of these studies employed high-grade (pure) refrigerants such as ethanol paired with the composite adsorbent formed. However, studies involving low-grade ethanol (the mixture of water and ethanol) as the refrigerant have not been reported. Understandably, water/ethanol mixtures would affect the mass transfer in the adsorption bed unless the functional properties of the adsorbent are modified to aid both heat and mass transfer. NaCl has not been used to form a composite with AC despite its higher thermal conductivity than the other chloride salts used in previous studies. Therefore, in this study, NaCl was used to form a composite with AC to pair with low-grade ethanol. The utilization of NaCl is expected to improve simultaneously both the heat and mass transfer

Stellenbosch University https://scholar.sun.ac.za

properties, sorption capacity and the compressor effect when paired with ethanol/water mixture due to the high water affinity of NaCl.

Drying and cooling are the most energy-intensive unit operations in a dried mango chips processing plant. Currently, in South Africa, energy for the drying unit is obtained from steam generated by the combustion of coal. Coal as fossil fuel contributes to greenhouse gas (GHG) emission, it is costly and not renewable. Moreover, the exhaust from the boiler which contains substantial energy is rejected into the environment. Furthermore, the conventional vapour compression technology is used as the cooling technology. This technology also contributes further to the degradation of the environment due to its dependence on electricity produced from coal and the type of refrigerant used. Therefore, this study used an integrated approach to study the economic and environmental impacts of replacing both the conventional vapour compression technology and boiler fuel with ACS and mango seed generated during the mango processing. The energy from the boiler exhaust was used to power the ACS. This was to lead to zero-waste generation, reduce greenhouse gas (GHG) emission, and improve the economic viability of the dried mango chips processing.

3.5 Scientific contributions

The results from this study have been published in three peer-reviewed journals and are presented here with permission from the publishers (Appendix A1, A2 & A3).

The following are the contributions of myself and my supervisor (co-authors) contributed to Chapters 5, 6 &7 in the dissertation:

Stellenbosch University https://scholar.sun.ac.za

Chapter	Authors	Nature of contribution	Extent of contribution
Chapter 5:Production and optimization of NaCl-activated carbon from mango seed using surface response methodology	Myself	Organized and reviewed literature. Performed experiment and analyzed data. Conceptualized and wrote the paper	85%
	Prof Annie Chimphango	Provided advice as the supervisor Contributed to editing of paper	15%
Chapter 6: Evaluating the potential of using ethanol /water mixture as a refrigerant in an adsorption cooling system by using activated carbon-sodium chloride composite adsorbent and mango seed activated carbon	Myself	Organized and reviewed literature Performed experiment and analyzed data Conceptualized and wrote the paper	80%
	Prof Annie Chimphango	Provided advice as the supervisor Contributed to editing of paper	20%
Chapter 7:An integrated strategy targeting drying and cooling unit operations to improve economic viability and reduce environmental impacts in a mango processing plant	Myself	Organized and reviewed literature Gathered and modelled the data Conceptualized and wrote the paper	80%
	Prof Annie Chimphango	Provided advice as the supervisor Contributed to editing of paper	20%

Stellenbosch University https://scholar.sun.ac.za

1. Production and optimization of NaCl-activated carbon from mango seed using response surface methodology. This published in *Biomass Conversion and Biorefinery* (https://doi.org/10.1007/s13399-018-0361-3). This can be found in Chapter 5.

The study has investigated the production and optimization of granular mango husk AC for gas phase applications, particularly adsorption cooling. The optimization was done by varying the soaking time, carbonization temperature, and impregnation ratio of the dry weight of mango seed husk to NaCl. The optimized granular AC produced has a comparable surface area to AC produced from agro-residues but has the advantage of lower ash content compared to AC produced from agro-residues.

2. Evaluating the potential of using ethanol/water mixture as a refrigerant in the adsorption cooling system by using commercial activated carbon - sodium chloride composite adsorbent and mango seed activated carbon. This is presented in Chapter 6. Part of this Chapter has been published in *International Journal of Refrigeration* (https://doi.org/10.1016/j.ijrefrig.2018.09.025).

The study has provided information on the possibility of improving the properties of AC+ NaCl composite paired with high purity and low-grade ethanol in an ACS. The presence of NaCl in the AC has increased the COP and SCP when paired with low-grade ethanol.

3. An integrated strategy targeting drying and cooling unit operations to improve economic viability and reduce environmental impacts in a mango processing plant. This is presented in Chapter 7 and has been published in *Clean*

Stellenbosch University https://scholar.sun.ac.za

Technologies and Environmental Policy (https://doi.org/10.1007/s10098-018-1623-2)

This study has investigated the economic and environmental impacts of replacing boiler fuel and vapour compression cooling technology in dried mango chips processing plant powered on-grid and off-grid were investigated using an integrated approach based on zero-waste generation. The replacement of vapour compression cooling technology with ACS and boiler fuel with mango seed has led to the reduction in GHG emission and improvement in the economic viability of dried mango chip processing.

Stellenbosch University https://scholar.sun.ac.za

Chapter 4 Research approach

4.1 Research methodology

This study was done through a multidisciplinary technique involving harnessing skills, knowledge and expertise to perform various tasks. The mango seed husk was used in this study because it is a lignocellulosic material, thus making it suitable for AC production [132]. The mango seed was opened to separate the husk from the seed. The de-husked mango seed, on the other hand, was not used to produce the AC due to its high-value bioactive contents such as oil, nutrients, and other essential elements which could be extracted to add economic value to the mango seed [163]. The mango seed husk was subjected to size reduction prior to chemical characterization to determine the amount of lignin, cellulose, and hemicellulose it contains. The mango seed husk was then used to produce AC. There are two ways to produce AC: physical method and chemical method. The physical method involves a two-step method of carbonization and activation. The activation is done by using steam at high temperature or carbon dioxide on a carbonized material. However, due to the danger of using steam at high pressure at the small-scale level, steam activation was not used. Moreover, carbon dioxide is not environmentally friendly and contribute to global warming. In the chemical method of AC production, the activation and the carbonization steps take place simultaneously. The chemicals used could be acids, bases, or salts. The type of chemical used affects the properties and application of the AC formed. In this study, NaCl was used as the activation chemical due to its ability to increase the amount of carbon yield [164], and its accessibility for small scale

Stellenbosch University https://scholar.sun.ac.za

production of activated carbon. The mango seed husk was prepared for AC production by steeping the mango seed husk in various concentration of sodium chloride at various lengths of time. The steeping time and NaCl concentration affect the properties of AC produced. The treated mango seed husk was then carbonized using slow pyrolysis method. The type of pyrolysis method used determines the carbonization temperature range, yield, and properties of the carbon. Fast pyrolysis is known to take place at high temperature, resulting in the production of more bio-oil and less carbon [136]. On the other hand, slow pyrolysis is known to occur at a relatively lower temperature than the fast pyrolysis to produce more carbon and less bio-oil. Since the focus is to produce AC, slow pyrolysis method was used in this study. Characterization and optimization of the AC were done to determine the best factors that give the best properties (Details of the AC production from mango seed husk could be found in Chapter 5).

It was expected to produce enough AC from the mango seed husk to use for composite formation with NaCl. The purpose of the composite formation is to enhance the properties (sorption capacity, compressor, heat and mass transfer) of the refrigerant and adsorbents pairing during adsorption cooling. However, due to the small production capacity of the laboratory scale pyrolysis equipment available, the mango seed husk AC produced was not enough for the composite formation. Therefore, commercial AC was used for composite formation. The composites formed, the mango seed husk AC, and untreated commercial AC was used as the adsorbents for testing in ACS (details of these tests can be found in Chapter 6).

Stellenbosch University https://scholar.sun.ac.za

The next activity was the design and construction of the adsorption cooling system. Two-bed, single-stage ACS model was chosen because of its simplicity and it is less difficult to construct and operate and uses less material to construct when compared with two-stage models. Factors considered in the design were the properties of the refrigerant (e.g. latent heat of vaporization, mass transfer of the refrigerant) and the adsorbent (e.g. surface area, heat transfer properties, affinity to attract the refrigerant, adsorption equilibrium data) as well as the operating condition and the physiological properties (e.g. respiratory heat) of the mango fruit (Details can be found in Section 4.2). Both high-grade (99.7%) and low-grade (60%) ethanol were used as the refrigerants. Based on the above, the construction materials were selected to ensure minimal heat transfer between the storage chamber and the environment. The double wall of stainless steel and the polystyrene was constructed as the storage chamber. Polystyrene was used as insulation material because of its ease of accessibility and it is less costly.

Finally, the ACS was integrated into a mango dried chips processing by replacing CVCC with ACS (powered by boiler waste heat). The knowledge in GHG emission and plant design and economics was used in assessing the environmental and economic impacts of integrating ACS in dried chips processing in order to develop sustainable dried mango chips processing that is profitable and more eco-friendly (Chapter 7).

4.2 Design of the adsorption cooling system

Two-bed, single-stage ACS was designed in-house to be used for adsorption cooling testing of various adsorbents in Chapter 6. Two-bed, single-stage ACS model was chosen because of its simplicity and it is less difficult to construct and

Stellenbosch University https://scholar.sun.ac.za

operate and uses less material to construct when compared with two-stage models. Properties of the refrigerant, and the adsorbent (activated carbon), as well as the operating condition and the physiological properties of the mango fruit, were considered in the sizing of the components of the ACS. The properties of the refrigerants considered were its latent heat of vaporization, saturation pressure, and the specific heat capacity. The adsorbent properties considered were the BET surface area, adsorption equilibrium, and isotherm data and kinetics data [74] (more information on these data can be found in Chapter 6). The design of the ACS was based on the northern South African climate as that is where mango is cultivated. The average environmental temperature during the harvesting period (from January to April) of the mango was taken as 30 ˚C. In addition, the physiological properties of the mango fruit were considered in choosing the storage temperature of the mango fruit. The recommended storage temperature of the mango was assumed to be 12 ˚C [165] (Table 4.1). Transient factors such as the opening of the door to remove stored mango fruit could affect the heat transfer and cooling rates in the storage chamber. Estimation of heat infiltration during storage through door opening depends on several factors such as the frequency of opening, and the velocity of air flow into the storage chamber when the door is opened. The velocity of air flow into the storage chamber when the door is opened depends on the prevailing ambient air condition around the storage chamber. However, since door opening increases the heat load and reduces the cooling rate of the mango fruit, frequent opening of the door could have undesirable consequences such as weight loss of the mango fruit, increase spoilage, and attendant economic and environmental impacts. Hence the ACS

Stellenbosch University https://scholar.sun.ac.za

was designed on the assumption that there would be no door opening during storage. Using these initial data and the above assumptions, the refrigerator cabinet heat transfer, the evaporator coils, and the condenser coil were analyzed, designed and constructed. The components were then connected to each other through valves and sealed.

Table 4.1 Parameters considered in the design of the adsorption cooling system

Parameter	**Value**
Field/ambient temperature, T_{field}	30 ˚C
Recommended cooling temperature, T_{ref}	12 ˚C
Evaporator temperature, T_{eva}	12 ˚C
Condenser temperature, T_{con}	30 ˚C

Prior to performance testing for commissioning, the entire system was checked for leaks by subjecting it to a 2 MPa hydrostatic pressure to ensure that the system was sealed since the system operates under vacuum condition and any leakage of air from the environment into the system would affect the system performance. Details design of each component is shown below

Refrigerator storage cabinet analysis

The purpose of the refrigerator storage cabinet is to prevent heat transfer from the surroundings to the inside of the cabinet. The amount of heat transferred to the storage cabinet determines the amount of work a refrigerator will need to do and this, in turn, affects the size of the parts of the whole refrigerator. Heat is transferred by conduction, convection, and radiation. In order to allow minimum heat transfer into the storage cabinet, it is important to choose an insulation

Stellenbosch University https://scholar.sun.ac.za

material that has low thermal conductivity. In this study, polystyrene (thermal conductivity of 3.84 $\times 10^{-5}$ kWm^{-1} k^{-1}) was chosen because of its ease of use, availability, cost and low thermal conductivity. A 0.4 m × 0.4 m× 0.3 m stainless steel container which was readily available in the Process Engineering department workshop was fitted with polystyrene (Insulpro CC) and evaporator (copper) coils for used as the storage cabinet in this design. The refrigeration heat load was based on the full mango fruit storage capacity. During the storage of the mango in the storage cabinet, the heat load would consist of heat gain through the wall of the refrigerator cabinet, field heat of mango, respiratory heat of mango, and heat infiltration through the opening of the storage area. The detailed calculation of these heat loads is shown in Appendix B.

Heat gain through the refrigerator wall

The refrigerator cabinet had an inner wall made of stainless steel and an outer wall of polystyrene as shown in Appendix B. There is parallel convection and radiation (from the ambient) heat transfer occurring at the outside of the storage chamber, while heat transfer through the walls of the storage chamber occurs in series. The thermal resistance network and the heat load calculation is shown in Appendix B.

Product field heat load

The air in the refrigerator cabinet surrounding the mangoes has to be cooled. The heat content of the air is affected by the field heat of the mangoes. In the case of the field heat, the rate of heat transfer from the mango to the air would be by natural convection as there is no fan. Natural convection is governed by the geometry, the orientation of the mango in the refrigeration compartment, as well

Stellenbosch University https://scholar.sun.ac.za

as the temperature difference between the mango surface and surrounding refrigerator air. It was assumed that the mangoes are spherical in shape. The diameter of the mango was assumed to be 0.086 m [166]. Therefore, Equations 4.1 to 4.5 could be used to estimate the heat transfer coefficient [167]

$$Nu = 2 + \frac{0.589\, {Ra_D}^{1/4}}{[1 + (0.469/Pr)^{9/16}]^{4/9}} \quad 4.1$$

$$Ra_D = \frac{g\beta\left(T_{field} - T_{ref}\right)D^3}{\nu^2} Pr \quad 4.2$$

$$h = \frac{k}{D} Nu \quad 4.3$$

$$T_f = \frac{T_{amb} + T_{eva}}{2} \quad 4.4$$

$$\beta = \frac{1}{T_f} \quad 4.5$$

Where: Nu is the Nusselt number, D is the diameter (characteristic length) of the mango (m). β is the coefficient of volume expansion (K^{-1}), g is the gravitational acceleration (ms^{-2}), T_{field} and T_{eva} are ambient and evaporator temperature respectively defined in Table 4.1, T_f represents the temperature of film of air (K), v is the kinematic viscosity of the air (m^2s^{-1}), h is the heat transfer coefficient ($Wm^{-2}K^{-1}$), Pr is Prandtl number.

By using Equation 4.1 to 4.5, the heat transfer coefficient could be calculated which was then used to calculate the field heat transfer rate

$$\dot{Q} = hA\left(T_{field} - T_{ref}\right) \times N_{mango} \quad 4.6$$

Where: A is the heat transfer area of the mango fruit, and N_{mango} is the number of mango fruit in the storage chamber.

The respiration heat load of mango

Stellenbosch University https://scholar.sun.ac.za

Mangoes continue their metabolic activity in the form of respiration, after harvest. During the respiration process, heat is generated. The amount of respiratory heat produced by mango is 133.4×10^{-3} Wkg^{-1} at 15 ˚C [165] which is close to the storage temperature. Therefore, the total amount of respiratory heat produced in during storage of the mango is calculated as

$$\dot{Q}_{respiration} = m_{mango} \times 133.4 \times 10^{-3}\, Wkg^{-1} \qquad 4.7$$

Where: m_{mango} is the mass of mango stored in the storage chamber.

Evaporator analysis

The evaporator is at a pressure of 5 kPa lower temperature while the air in the storage chamber is at atmospheric pressure. Since temperature and pressure are directly related, the evaporator temperature is also lower than the air inside the storage chamber. Therefore, the thin layer of warm air in the storage chamber surrounds the evaporator and heat of transfer (by conduction) from the thin warm air to the evaporator coils leading to the evaporation of the refrigerant (at the saturation temperature of the evaporator operating pressure). Consequently, the temperature thin layer of air close to the evaporator coil drops and its density increases since at constant pressure density of a gas and its temperature are inversely related [167]. Thus, the denser air goes down and it is replaced by another thin warm layer of air which also transfer heat to the evaporator to cause the refrigerant to evaporate, leading to temperature drop and increase in density of this thin layer of air. This air also goes down and it is replaced by another. Thus, the temperature in the storage chamber reduces from the top close to the evaporator to the bottom of the storage chamber. Thus, the continuous replacement of denser and colder air by lighter and warmer air creates a natural

Stellenbosch University https://scholar.sun.ac.za

convection current [167] in the storage chamber leading to the overall temperature drop in the storage chamber. In order to estimate the heat transfer between the evaporator and the air inside the storage chamber, the following correlation is used

$$\dot{Q}_{total} = hA(T_{amb} - T_{eva}) \qquad 4.8$$

Where: T_{amb} is the ambient temperature (K), T_{eva} is the evaporator saturation temperature (K) (Table 4.1), $\dot{Q}_{total}$ is the sum of heat transfer through the six faces of the storage chamber, the field heat from the mango fruit, and the respiratory heat (W), (details in Appendix B), A is the heat transfer area (m^2), h is the heat transfer coefficient ($Wm^{-2}K^{-1}$).

In order to find the heat transfer area, the heat transfer the natural heat transfer coefficient must be known. This can be computed using the correlation below [167,168]

$$Nu = 0.59 \times {Ra_L}^{1/4} \qquad 4.9$$

Where: Nu is Nusselt number, Ra_L is the Rayleigh number

The Rayleigh number was also estimated using Equation 4.10 [167]

$$Ra_L = \frac{g\beta(T_{amb} - T_{eva}){L_c}^3}{\nu^2} Pr \qquad 4.10$$

Where: g is the gravitational acceleration (ms^{-2}), β and T_f could be estimated using Equations 4.4 and 4.5, T_{amb} and T_{eva} are defined in Table 4.1, L_c is the characteristic length which represents the height of the storage chamber (m), ν is the kinematic viscosity of the air (m^2s^{-1}), h is the heat transfer coefficient ($Wm^{-2}K^{-1}$), Pr is Prandtl number.

Stellenbosch University https://scholar.sun.ac.za

Thus, the Nusselt number obtained in Equation 4.7 could be used to estimate the heat transfer coefficient using Equation 4.11 [167]

$$Nu = \frac{h\,L_c}{k} \qquad 4.11$$

The parameters in Equation 4.11 are as defined above. Substituting the heat transfer coefficient obtained in Equation 4.11 into Equation 4.8, the heat transfer area could be calculated. With the heat transfer area obtained, the length of the copper pipe (evaporator) could be calculated using Equations 4.12

$$A = 2\pi rL \qquad 4.12$$

Where: A is the heat transfer area (m^2), r is the radius of the copper pipe (m), L is the length of the copper pipe (m).

Condenser analysis

During desorption of the refrigerant, the refrigerant is heated until it evaporates from the adsorbent. When the refrigerant vapour comes into contact with a condenser which is at a lower temperature than the saturation temperature of the refrigerant vapour at condenser pressure, the refrigerant vapour condenses. During the condensation, the refrigerant gives out its latent heat of vaporization and this leads to phase change from vapour to liquid. However, the condensed liquid refrigerant is still at high temperature. Thus, it needs to be cooled down further by giving out its sensible energy prior to flowing into the evaporator. Thus, the total energy rejected during condensation is the sum of the latent heat and the sensible heat. The following parameters were used in the condenser sizing

1. The condenser is wire-and-tube type condenser.
2. Condenser temperature (T_{con}) = Ambient temperature ($T_{amb,1}$) = 30 ^{o}C

Stellenbosch University https://scholar.sun.ac.za

3. Temperature of ambient air after coming in contact with hot condenser $T_{amb,2}$ surface goes up by about 3 ^{o}C above local ambient temperature [169].
4. The mass flow rate of the refrigerant, $\dot{m}_{ref} = 2.174 \times 10^{-4}\ \mathrm{kgs}^{-1}$ (Table 6.5 Chapter 6).
5. Saturated temperature of hot ethanol (T_1) = 80 ^{o}C
6. Final temperature of ethanol after cooling (T_2) = 35 ^{o}C
7. Latent heat of vaporization of ethanol (h_{fg}) = 840 kJkg^{-1}
8. External diameter of copper pipe (d_o) = 9.375 × 10^{-3} m
9. Internal diameter of copper pipe (d_i) = 6.25 × 10^{-3} m

Therefore, the energy balance for the condenser could be determined using Equation 4.13

$$\dot{Q}_{con} = \dot{m}_{ref}\, h_{fg} + \dot{m}_{ref} C_{p,ref} (T_{sat} - T_{con}) \qquad 4.13$$

The heat transfer area of the condenser could be estimated using Equation 4.14.

$$\dot{Q}_{con} = UA\Delta T_{lm} \qquad 4.14$$

However, U and ΔT_m are not known and needs to be calculated. ΔT_{lm} could be calculated using Equation 4.15

$$\Delta T_{lm} = \frac{(T_1 - T_{amb,2}) - (T_2 - T_{amb,1})}{ln\left(\frac{T_1 - T_{amb,2}}{T_2 - T_{amb,1}}\right)} \qquad 4.15$$

The parameters in Equation 4.15 are defined above.

The overall heat transfer coefficient could also be calculated using Equation 4.16

$$\frac{1}{U_O} = \frac{1}{h_o} + \frac{1}{h_{od}} + \frac{d_o \ln(d_o/d_i)}{2k_w} + \frac{d_o}{d_i} \times \frac{1}{h_{id}} + \frac{d_o}{d_i} \times \frac{1}{h_i} \qquad 4.16$$

Where:

Stellenbosch University https://scholar.sun.ac.za

U_O is the overall heat transfer coefficient based on the outside area of the tube ($Wm^{-2}K^{-1}$)

h_o is the outside fluid heat transfer coefficient ($Wm^{-2}K^{-1}$),

h_i is the inside fluid heat transfer coefficient ($Wm^{-2}K^{-1}$)

h_{od} is the outside dirt coefficient (fouling factor) ($Wm^{-2}K^{-1}$)taken to be 5000 $Wm^{-2}K^{-1}$ [170],

h_{id} is the inside dirt coefficient (fouling factor) which is assumed to be 5000 $Wm^{-2}K^{-1}$ [170],

k_w is the thermal conductivity of copper tube wall taken to be 378 $Wm^{-1}K^{-1}$ [170]

d_i is the tube inside diameter (m)

d_o is the tube outside diameter (m)

In order to estimate the overall heat transfer coefficient, the outside air heat transfer coefficient, h_o, and the inside refrigerant heat transfer coefficient, h_i need to be determined. The outside air heat transfer coefficient, h_o could be calculated by using the simple correlation between h_i and h_o proposed by Chaddock and Chato which is as follows that heat transfer coefficient inside tubes (h_i) is 0.77 times that of heat transfer coefficient outside the tubes (h_o) if the vapour Reynolds number Re < 35000 [171].Thus,

$$h_i = 0.77\, h_o \qquad 4.16$$

The inside refrigerant heat transfer coefficient, h_i was estimated using the relation as follows [171,172]

$$h_i = 0.555 \left[g\rho_l \frac{(\rho_l - \rho_v)\, {k_l}^3\, h_{fg}}{\mu_l \times (T_{sat} - T_{con}) \times d_i} \right]^{\frac{1}{4}} \qquad 4.17$$

Stellenbosch University https://scholar.sun.ac.za

Where:

ρ_l is the density of liquid ethanol (kgm^{-3})

ρ_v is the density of ethanol vapour (kgm^{-3})

μ_l is the dynamic viscosity of liquid ethanol ($kgm^{-1}s^{-1)}$

μ_v is the dynamic viscosity of ethanol vapour ($kgm^{-1}s^{-1)}$

k_l is the thermal conductivity of liquid ethanol ($Wm^{-1}K^{-1}$)

h_{fg} is the latent heat of vaporization(Jkg^{-1})

Thus, the heat transfer area and length of the pipe could be calculated using Equation 4.18 and 4.19 respectively.

$$A = \frac{\dot{Q}_{con}}{U\Delta T_{lm}}$$

$$L = \frac{A}{\pi d_o}$$

Where: L is the length of the copper pipe (m), d_o and A are defined above.

Adsorber sizing

The size of the adsorbent container was estimated by taking into account the adsorption equilibrium data and adsorption kinetics [74] of the adsorbent/ refrigerant pair (activated carbon/ethanol in this case) Details of these parameters could be found in Chapter 6 of this dissertation. With this information, the amount of refrigerant (ethanol) to be used, the amount of activated carbon needed and therefore the volume of the adsorbent container (adsorber) is calculated as follows

The total amount of ethanol to be used is

$$m_{ref} = \dot{m}_{ref} \times \tau_{cycle} \qquad 4.18$$

Stellenbosch University https://scholar.sun.ac.za

Where: $\dot{m}_{ref}$ is the refrigerant flow rate (kgs^{-1}), τ_{cycle} is the cycle time (s), m_{ref} is the mass of ethanol (kg).

Now, the quantity of activated carbon (AC) needed is estimated as follows

$$m_{ads} = W_o \times m_{ref} \qquad 4.19$$

Where: m_{ads} is the mass of adsorbent (kg), W_o is the maximum equilibrium uptake (kgkg^{-1}), m_{ref} is the mass of ethanol (kg).

The volume of the adsorbent container could be calculated by taking into consideration the amount of activated carbon needed, and the bulk density of activated carbon by using the relation

$$V_{ads} = \frac{m_{ads}}{\rho_{ads}} \qquad 4.20$$

Where: m_{ads} is the mass of adsorbent (kg), ρ_{ads} is the bulk density of the adsorbent (kgm^{-3}), V_{ads} is the volume of the adsorbent (m^3).

Energy analysis of the adsorption process

As explained in Section 2.3.2, an adsorption cooling system undergoes four processes: isosteric heating, isobaric desorption heating, isosteric cooling, and isobaric adsorption processes. The energy balance equation for each of the processes (Equations 2.20 to 2.25) has been presented in Section 2.3.2. Therefore, the total energy input is the sum of isosteric heating (Equation 2.20), isobaric desorption heating (Equation 2.21) and heat of adsorption/desorption (Equation 2.22). This could be expressed as [81]

$$Q_{total} = Q_{sensible} + Q_{latent} \qquad 4.21$$

Where: $Q_{sensible}$ is the sum of isosteric heating, isobaric desorption heating (J), Q_{latent} is the heat desorption/adsorption (J), Q_{total} is the total energy input (J). The heat of desorption/adsorption is an internally generated heat which is

Stellenbosch University https://scholar.sun.ac.za

dependent on the adsorbent/refrigerant pair (details could be found in Chapter 6). Mango seed is combusted to serve as the source of energy in this study, the sensible energy ($Q_{sensible}$) could be estimated as the useful energy supplied ($Q_{supplied}$) to the ACS. Therefore, in terms of external heat supplied (desorption energy is excluded) Equation 4.21 could be expressed as follows [173–175].

$$Q_{supplied} = \eta_1 \times \eta_2 \times m_{mango} \times LHV \qquad 4.22$$

Where: η_1 is the combustion efficiency, η_2 is the fraction of combustion energy, m_{mango} is the mass of mango seed combusted, LHV is the lower heating value of mango seed (MJkg^{-1}) (details could be found in Chapter 6).

Furthermore, during the isosteric cooling stage, the condensed refrigerant is at a higher temperature and pressure than the evaporator (Figure 2.6). The refrigerant enters the evaporator where it absorbs heat from the storage chamber (as explained above) and evaporates to be adsorbed onto the adsorbent. Thus, the useful cooling rate could be expressed as

$$\dot{Q}_{eva} = \dot{m}_{ref}(h_g - h_f) = \dot{m}_{ref} h_{fg} \qquad 4.23$$

Where: $\dot{Q}_{eva}$ is the evaporator useful cooling rate (Js^{-1}), h_g is the specific enthalpy of the refrigerant as it leaves the evaporator (Jkg^{-1}), h_f is the specific enthalpy of the refrigerant leaving the condenser (Jkg^{-1}), h_{fg} is the specific latent heat of evaporation (Jkg^{-1}), $\dot{m}_{ref}$ is the refrigerant mass transfer rate (kgs^{-1}).

Therefore, the useful evaporator cooling is the product of evaporator useful cooling rate and cycle time. This is presented as follows

$$Q_{eva} = \tau_{cycle} \times \dot{Q}_{eva} = \tau_{cycle} \times \dot{m}_{ref} h_{fg} \qquad 4.24$$

Stellenbosch University https://scholar.sun.ac.za

Where: τ_{cycle} is the cycle time (s), Q_{eva} is the useful evaporator cooling (J), $\dot{Q}_{eva}$, $\dot{m}_{ref}$, h_{fg} are defined in Equation 4.23.

Therefore, the COP and SCP of the ACS is estimated as

$$COP = \frac{Q_{eva}}{Q_{supplied}} \qquad 4.25$$

$$SCP = \frac{Q_{eva}}{m_{ads}\tau_{cycle}} \qquad 4.26$$

Where: SCP is the specific cooling power (Wkg^{-1}), COP is the coefficient of performance, $Q_{supplied}$, m_{ads}, τ_{cycle}, and Q_{eva} are defined in Equations 2.22 and 2.24.

4.3 Production of activated carbon

A slow pyrolysis method was used to produce the mango seed husk AC because of the thermal and chemical properties of the mango seed husk under inert conditions. Slow pyrolysis is the thermal decomposition of biomass (e.g. mango seed husk) in the absence of oxygen and between 350 ˚C - 550 ˚C. The thermal degradation process consists of both simultaneous and successive reactions leading to the breakdown of long chains of carbon, hydrogen, and oxygen in the biomass (mango seed husk) into smaller molecules such as gases, oils, and char. Due to the low heating rate, slow pyrolysis takes several hours to complete. Mango seed husk is made up of hemicellulose, cellulose, and lignin and is known to decompose at temperatures between 220 ˚C - 315 ˚C, 315 ˚C - 400 ˚C, 160 ˚C-900 ˚C, respectively [176]. Slow pyrolysis was chosen because the decomposition temperature of the hemicellulose, cellulose, and lignin present in mango seed husk is comparable to the operating temperature range of slow

Stellenbosch University https://scholar.sun.ac.za

pyrolysis. NaCl was chosen as the activation chemical because it is easily accessible and affordable and has high thermal conductivity. The pyrolysis method was used because the required carbonization temperature of the mango seed husk could be reached in the pyrolysis equipment. The parameters considered for the production of the activated carbon (AC) from mango seed husk were: soaking time, NaCl impregnation ratio and carbonization temperature. The mango seeds were opened up to separate the kernel from the husk. The kernel could be used as an energy source to drive the adsorption cooling system (ACS). The size of the mango seeds was reduced and soaked in NaCl solution at different concentrations and soaking times. The treated mango seeds were then dried in an oven. The dried mango seed husk was taken through a slow pyrolysis process by varying the pyrolysis temperature and held for about 1 hour upon attaining the desired pyrolysis temperature. The final pyrolysis product was washed, dried and analyzed to determine its surface area, the ash content and bulk density. Details of the activated carbon production process could be found in Chapter 6.

4.4 Assessing the economic viability

The economic evaluation of the scenarios was conducted based on the South African economic condition such as the tax rate, interest rate, insurance, and inflation rate. The cost of equipment was obtained from equipment suppliers contacted or extracted from technical reports. Where necessary, some equipment costs were estimated based on cost data from different years using chemical engineering plant cost index (CEPCI) following Equation 4.28 and the capacities adjusted using Equations 4.27 [177,178].

Stellenbosch University https://scholar.sun.ac.za

$$C = C_O \left(\frac{M}{M_O}\right)^n \qquad 4.27$$

Where $C\ and\ C_O$ are the equipment costs at capacities $M\ and\ M_O$, respectively and n is the scale index.

$$Present\ cost = Original\ cost\ \left(\frac{CECPI_1}{CECPI_o}\right) \qquad 4.28$$

Where $CEPCI_1$ is the plant cost index at present time and $CEPCI_o$ is the plant cost index of the time original cost was obtained. The variable operating costs were calculated based on the raw material and flow rates of utilities resulted from material and energy balance calculations and their market prices. The operating costs were also calculated based on the South African economic condition. Since profit is expected at the end of the project after initial investment has been made, some economic indicators such as net present value (NPV) and internal rate of return (IRR) takes into account time value of money [177,178] were evaluated based the calculated capital costs and operating costs, on the basis of real values in the cumulative cash-flow calculation. The NPV provides an indication of the returns on investment of a project over the project life in the present monetary value terms. In addition, a sensitivity analysis was carried out in this study by varying the selling price of the dried mango chips to see its effect on the NPV and the internal rate of return (IRR).

4.5 Assessing the environmental impacts

The amount of energy expended by various unit operations, the fuel type used to supply energy under various scenarios and their respective emission factors were considered in the estimation of carbon dioxide (CO_2), methane (CH_4), and nitrous oxide (N_2O) emissions based on IPCC (Intergovernmental Panel on Climate

Stellenbosch University https://scholar.sun.ac.za

Change) standards or procedures. Furthermore, the amount of CH_4 and N_2O emitted were converted to their equivalent CO_2 by using their respective global warming potential (GWP) values. The GWP for CO_2, CH_4, and N_2O are 1, 25 and 310, respectively [179,180].

Stellenbosch University https://scholar.sun.ac.za

Stellenbosch University https://scholar.sun.ac.za

Chapter 5 Production and optimization of NaCl-activated carbon from mango seed using response surface methodology

ABSTRACT

Granular activated carbon (AC) produced from mango seed husk through chemical activation with NaCl has potential application in adsorption cooling system. The study investigated the relationship among process parameters and effects on physicochemical and functional properties of AC. Production conditions were optimized using response surface methodology for impregnation ratio (0.25, 0.5 and 0.75), soaking time (2 h, 4 h, and 6 h), and activation temperature (400 ˚C, 450 ˚C, and 500 ˚C). Surface area, ash content and bulk density were response variables. The AC was produced with comparable quality to commercial AC. Impregnation ratio, soaking time and carbonization temperature but not their interaction, had significant effects ($p< 0.05$) on AC surface area, ash content and bulk density. Optimum production conditions for soaking time, impregnation ratio and carbonization temperature were 4 h, 0.25 and 500 ˚C, respectively, which gave BET surface area, ash content and bulk density of 415 m^2g^{-1}, 6.92%, and 243 kgm^{-3}, respectively.

Key words: activated carbon; chemical activation; optimization; response surface methodology

5.1 Introduction

Mango processing generates a variety of residues including the seed, which consists of a husk and a kernel. The mango seed kernel contains carbohydrates

Stellenbosch University https://scholar.sun.ac.za

(58-80%), protein (6-13%) and essential amino acids and lipids (6-16%) [181] and it is a good source phenolics, carotenoids, vitamin C, and dietary fiber that improve human health and nutrition [163,181]. As a result, there is a potential for biorefining of the mango seed kernel into such low volume but high value-added products. The mango seed husk, on the other hand, has less commercial value compared with the mango seed kernel and it is therefore disposed of into the environment, which causes pollution or used as compost [181]. One of the ways to add economic value to the mango seed husk is through the production of activated carbon. Therefore, together with biorefining of the mango seed kernel, it can potentially increase the economic value of the mango seed as a feedstock in a biorefinery. Activated carbon is one of the commonly used adsorbents [182] in several applications including removal of dyes, odours, and contaminants, in water purification processes as well as in adsorption cooling processes [183–185]. The functional properties of activated carbon are among other factors influenced by the production method. Activated carbon can be produced through physical and chemical means. The physical activation method, which is generally applied to non-renewable feedstocks such as coke, pitch, and coal [132] involves carbonization in an inert atmosphere [130,186–188] followed by activation using steam (800˚C-1000˚C) or carbon dioxide [139]. Such physical activation method is costly due to its high carbonization temperature, high processing time, low carbon yield [132] and has high safety risks for small-scale applications. Unlike the physical activation method, the chemical activation method which is applied to biomass materials is economically feasible due to its shorter processing time,

Stellenbosch University https://scholar.sun.ac.za

higher activated carbon yield [132] and lower activation temperature (400˚C-500˚C [140,185,189,190]).

Activated carbon from biomass materials such as the mango seed husk is produced through chemical means where carbonization and activation occur simultaneously [107,108,139,186,188,191]. The activation chemicals are added before reaching the carbonization temperature of 400 ˚C-500 ˚C [140,185,189,190]. Many chemicals such as $CaCl_2$, $ZnCl_2$, H_3PO_4, K_2CO_3, and KOH have been used for the production of activated carbon [139,141,185,192]. Each of these chemicals affects pore formation differently and have different safety concerns that affect the application of the activated carbon produced. For example, H_3PO_4 restricts the escape of the tar from the carbon during carbonization, thus, affecting the development of pore structures [193]. The KOH, on the other hand, is normally applied to already carbonized materials because lower activated carbon yield when virgin biomass is used than other activating chemicals such as H_3PO_4 and $ZnCl_2$ [132]. Similar to $ZnCl_2$, the NaCl is a strong dehydrating agent, which prevents the formation of tars, which enhances the release of volatile matters from the carbon, which enhances the formation of well-developed pore structure in the carbon [132]. Furthermore, NaCl is not as toxic as other chemicals. The NaCl has a boiling point of 1465 ˚C, which is higher than the carbonization temperature, thus, does not decompose during carbonization to produce hazardous fumes [194,195]. On the other hand, the H_3PO_4 and $ZnCl_2$ with boiling points of 213 ˚C and 732 ˚C, respectively, may decompose at the carbonization temperature to produce toxic fumes [194,195]. Arguably, KOH has a boiling point of 1327 ˚C, which is equally higher than the typical carbonization

Stellenbosch University https://scholar.sun.ac.za

temperatures [132]. However, the presence of KOH in the effluent during the washing stage may be hazardous to the environment and humans [132]. Consequently, activated carbon produced using NaCl activation may be suitable for application in pharmaceutical and food industries unlike that from KOH and $ZnCl_2$ activation due to safety and contamination issues [132]. The time-weighted average recommended airborne exposure limit for NaCl of 5-10 mgm^{-3} [196] while that of $ZnCl_2$ and H_3PO_4 are 1-2 mgm^{-3} [194,195].

The NaCl is considered to be an effective catalyst for activated carbon production from wood sources [164]. Besides, NaCl has a high thermal conductivity than most of the chemicals used [159], which can increase the rate of heating of the mango seed husk during carbonization, and thus, becomes superior to other activation chemicals. Furthermore, most of these activation chemicals are not readily available for small-scale production. NaCl can be easily accessed at a small-scale level. The use of NaCl as an activating agent in the production of activated carbon from non-wood sources has been reported for the production of powdered activated carbon from mango seed husk [197] but not for granular activated carbon. Powdered activated (<0.045 mm) carbon is normally suited as an adsorbent in wastewater treatment whereas, granular activated carbon is suited for applications such as adsorption cooling because of high diffusion rate through the adsorbent bed and for not being easily sucked out of the adsorber during vacuum creation [198].

The physical and functional properties of activated carbon apart from the type of activation chemical, are affected by, soaking time, carbonization temperature and

Stellenbosch University https://scholar.sun.ac.za

particle size [140,187]. Therefore, it is important to understand the effects of the impregnation ratio, soaking time, carbonization temperature would have on the properties of the activated carbon. This study aimed to investigate the production of granular activated carbon from mango seed, targeting specifically the husk, through NaCl activation, as a potential adsorbent in the adsorption cooling system. The husk is targeted instead of the whole mango seed to produce the activated carbon in order to allow potential integration with mango seed biorefinery, which would produce low volume but high value-added bioproducts. Specifically, the study assessed the optimum production conditions for making the granular activated carbon from the mango seed husk by simultaneously considering the effects of NaCl impregnation ratio, soaking time, carbonization temperature and the interaction of these parameters on the physicochemical and functional properties, including surface area, ash content and bulk density using response surface methodology (RSM) [199].

5.2 Materials and methodology

5.2.1 Materials

The NaCl (99.5% in purity) was purchased from (Kimix chemical and laboratory suppliers' cc. Tommy Atkins mango kernels were kindly donated by Hoedspruit fruit processors (South Africa). Nitrogen gas (technical grade; 99.5% purity) 5.0 (Afrox Ltd) was used for the pyrolysis of the mango husk, while carbon dioxide and liquid nitrogen baseline 5.0 (Afrox Ltd) were used in the characterization of the activated carbon.

Stellenbosch University https://scholar.sun.ac.za

5.2.2 Mango husk preparation and characterization

Pre-dried Tommy Atkins mango kernels were obtained from Hoedspruit fruit processors (South Africa). The mango kernels were opened to separate the seeds from the husk. The mango husks were reduced into sizes ranging from 1 cm to 2 cm using a pair of scissors. The resulting mango husks were dried in an oven at 105˚C for 24 h until a constant weight was reached. A sample of the mango husks was milled in a Condux-Werkbei Hanau mill. The resulting particles were then sieved using a Vibratory Shaker Retsch AS200. The fractions that retained on 425 µm and 625 µm were used for chemical analysis. The samples were subjected to a proximate analysis based on ASTM standards: moisture [200], ash content [201], volatile matter [202] and fixed carbon. The lignocellulosic composition of the material was determined by NREL method [203].

5.2.3 Proximate analysis

The fractions (425 µm and 625 µm) were subjected to proximate analysis to determine the moisture, ash, fixed carbon, and volatile contents, based on ASTM-E-1131 [200] method using a Metler Toledo TGA/DSC 1 thermogravimetric analyzer. About 24 ± 3 mg of each lignin sample was loaded onto a 600 µl alumina crucible and placed on the TGA pan. The heat was supplied in a sequential manner to remove moisture removal at 110 ˚C, volatile content removal at 900 ˚C under nitrogen, fixed carbon combustion with oxygen at 900 °C.

Stellenbosch University https://scholar.sun.ac.za

5.2.4 Activated carbon production

The procedure for the production of the activated carbon from mango husk is shown in Fig. 5.1. NaCl solutions were prepared to the required impregnation ratios of 0.25, 0.50 and 0.75 defined as the ratio of the dry weight of NaCl to the weight of the mango husk based on the similar study [197]. Dried mango seed husk sample (100 g) containing sizes ranging from 1 cm to 2 cm, were mixed in a beaker with 250 mL of NaCl solution of a specified concentration (10% w/v, 20% w/v, and 30% w/v). The size of the mango seed husk was chosen by taking into account the requirement for producing granular activated carbon, which is suited for application in adsorption cooling systems that involve vacuum creation. Notably, activated carbon produced from smaller sized mango seed would likely be close to a powdered form, which could easily be sucked out during vacuum creation. Mango husks were soaked in NaCl solution for a period of 2, 4 and 6 h to obtain impregnation ratios of 0.25, 0.5 and 0.75 at room temperature (25 ˚C). The impregnated husks samples were dried in an oven at 50°C for 72 h. The moisture content at the end of the oven drying was about 25%. Approximately 50 g of the impregnated sample was placed in a stainless steel container, which was inserted into the reactor tube of the pyrolysis furnace for carbonization under nitrogen atmosphere, at a flow rate of 1 L/min and a heating rate of 10 ˚C per minute (Fig. 5.2). The carbonization temperatures were 400 ˚C, 450 ˚C, 500 ˚C, which was chosen based on previous studies. The optimum carbonization temperature for most biomass materials generally falls between 400 ˚C and 500 ˚C [140,183,187,204]. Once the carbonization temperature was reached, the samples were kept constant at the carbonization temperature for 1 h. At the end

Stellenbosch University https://scholar.sun.ac.za

of this process, the flow of the nitrogen gas continued to avoid carbon reacting with oxygen at high temperature to produce CO_2 which could lead to loss of carbon. After carbonization, the sample was cooled down outside the furnace at room temperature.

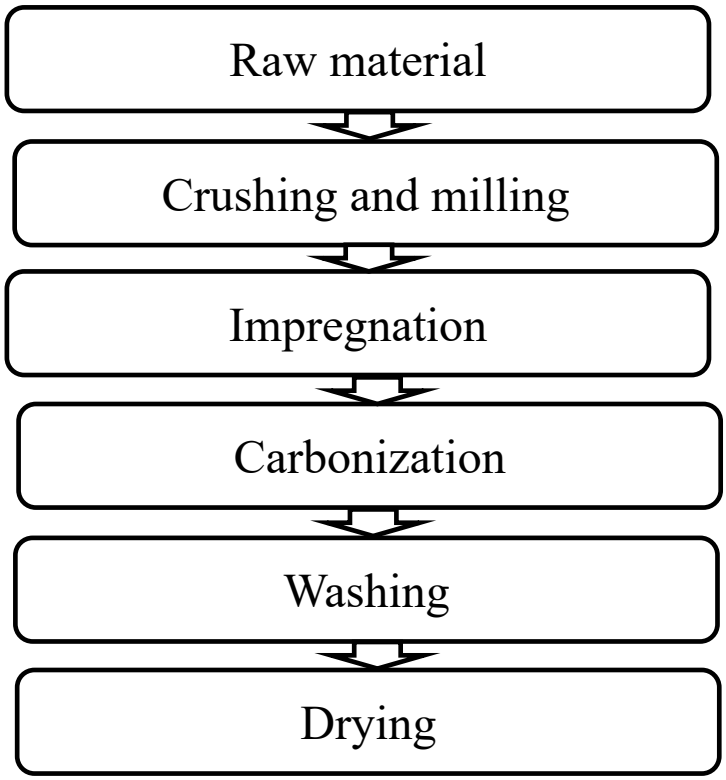

Figure 5.1 Process flow for the production of mango seed husk activated carbon using NaCl

The activated carbons produced were rinsed with demineralized water several times to remove any excess NaCl that did not react. The activated carbon was dried in an oven at 105 ˚C for 24 h to evaporate the water until constant weight was reached. The dried activated carbon was placed in a sealed container and stored in a desiccator.

Stellenbosch University https://scholar.sun.ac.za

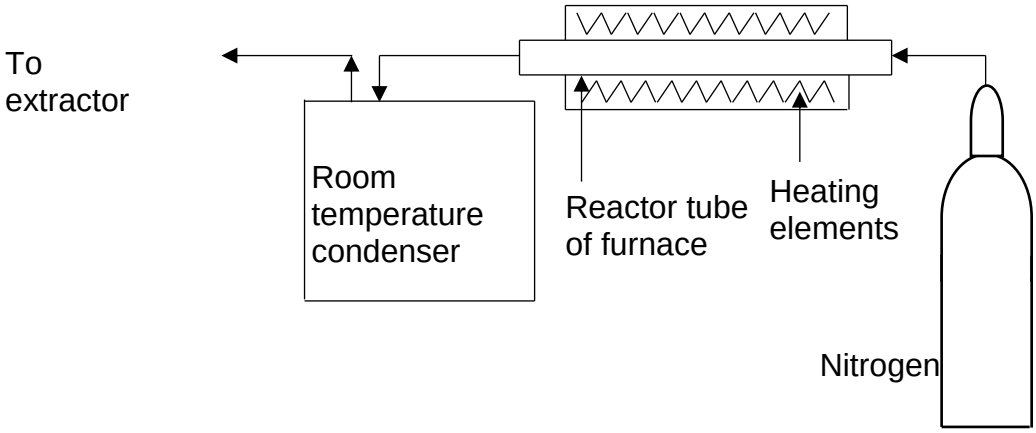

Figure 5.2 Set up for pyrolysis of treated mango husk for production of activated carbon.

5.2.5 Experimental design and statistical analysis

The experiments for the production of the activated carbon were carried in a 3^3 Box-Behnken fractional factorial [199] designed experiment with three center runs for impregnation ratio, soaking time, and carbonization temperature to give a total of 15 runs. The Box-Behnken fractional factorial was used because the optimum values were expected to be within the limits set for each variable [140]. The dependent variables (responses) analyzed are bulk density, ash content, and surface area. Commercial activated carbon was used as the benchmark in this study.

5.2.6 Activated carbon characterization

The bulk density of the AC produced was determined by the standard method [103,204,205]. Samples of activated carbon were weighed into a known volume graduated cylinder and tapped gently until the volume of activated carbon remained constant in the cylinder. The bulk density was calculated as the ratio of the weight of the activated carbon to the known volume of the closely packed sample. Ash content was also determined by the standard method [205]. Since

Stellenbosch University https://scholar.sun.ac.za

chemical activation normally produce narrow pores [188,206,207] and nitrogen has the problem of diffusion of the molecules inside the narrow pores (<0.7 nm) [208], it was suggested to use CO_2 for the characterization of micropores to complement to N_2 characterization [207]. Therefore, CO_2 was used for the characterization of the activated carbon to be used in the optimization process. After that, N_2 characterization was performed on the optimized product. The CO_2 characterization of the activated carbon was done using a 3Flex Surface Characterization Instrument from Micromeritics Instrument Corporation (Micromeritics ASAP 2020). About 0.3-0.6 g of each activated carbon samples were first freed of moisture and atmospheric vapour by application of electrically induced heat and evacuation in a VacPrep 061 degasser (Micromeritics Instrument Corporation). The sample was heated to 90 ˚C with vacuum pump running and held for 1 h and thereafter heated to 250 ˚C and kept at this temperature for 20 h while the vacuum was still running. Thereafter the sample was transferred to the 3Flex instrument (Accelerated Surface Area and Porosimetry System, Micromeritics Instrument Corporation) where in-situ degassing was done at a temperature of 175 ˚C with vacuum pump running for 1 hour. The sample temperature was then reduced to that of CO_2 (273 K) at a relative pressure range (P/Po) of 0.00005 – 0.025. The CO_2 gas was then admitted in an incremental dosage of 3.0 cm^3g^{-1}. Surface area and pore volume were determined on CO_2 adsorption isotherms measured at 273 K and the accumulated gas quantity adsorbed and CO_2 gas pressure data at that temperature (273 K) were then graphed to generate an adsorption isotherm. The isotherm data were then treated in accordance with BET theory [209] to arrive at

Stellenbosch University https://scholar.sun.ac.za

a specific surface area. These results were used for the optimization process through desirability analysis. The characterization of the activated carbon was done using N_2 by following similar steps. However, in this case, the sample temperature was then reduced to that of liquid nitrogen (77 K) after degassing. Nitrogen gas was then admitted in an incremental dosage of 3.0 cm^3g^{-1}. Surface area and pore volume were determined on N_2 adsorption isotherms measured at 77 K at a relative pressure range (P/Po) of 0.0000002-0.1026. The accumulated gas quantity adsorbed and N_2 gas pressure data at that temperature (77 K) were then graphed to generate an adsorption isotherm. The isotherm data were then treated in accordance with BET theory [209] to arrive at a specific surface area.

5.2.7 Regression analysis and optimization

Regression analysis was performed on data in order to derive the appropriate equation for each response. All variable parameters and their interactions were considered for a model for each response. Statistical analysis software (STATISTICA 13) was used to solve the coefficients of the second-order model with three variables for each response as shown below:

$$Y = \beta_0 + \beta_1 X_1 + \beta_2 X_2 + \beta_3 X_3 + \beta_{11} {X_1}^2 + \beta_{22} {X_2}^2 + \beta_{33} {X_3}^2 + \beta_{12} X_1 X_2 + \beta_{13} X_1 X_3 + \beta_{23} X_2 X_3 \quad 5.1$$

where β_0, β_1, β_2, β_3, β_{11}, β_{22}, β_{33}, β_{12}, β_{13} and β_{23} are the regression coefficients; X_1, X_2, and X_3 are the coded independent variables/regressor for soaking time, impregnation ratio and carbonization temperature; and Y is the particular response evaluated. Predicted values were solved from the derived equations for each of the response. The relationship of each response variable to the input variable was evaluated for its significance at a probability value of lower than 0.05

Stellenbosch University https://scholar.sun.ac.za

($p< 0.05$), and the strength of the relationship was evaluated using regression coefficient (R^2). Subsequently, a “lack of fit test” was performed to show the adequacy of the model at $p > 0.05$. In addition, normal distributions of the residuals were checked to validate the assumptions made in the ANOVA analysis [199]. Identification of the optimal production conditions involved surface plots (contour plots) of the effect on two variables while holding one at a set target. In addition, the desirability function approach has been used to obtain the production conditions at which the responses exhibit the ideal optimal value (maximum).

5.2.8 Fourier transform infrared spectroscopy (FTIR) analysis of surface functional groups on the activated carbon

The changes in surface functional groups on the activated carbon were analyzed surface using Fourier transform infrared spectroscopy (FTIR) in a Thermo Scientific Nicolet iS10 apparatus equipped with smart ITR diamond attenuated total reflectance (ATR). The experiments were carried out in the wavelength range of 250 cm^{-1} to 4500 cm^{-1} with the resolution of 4 cm^{-1} and total scans of 64 for each sample. This analysis was done to analyze the changes in the functional groups of the raw mango seed husk at different carbonization temperatures.

5.3 Results and Discussion

5.3.1 Mango seed husk characterization

Characterization of feedstock is important for determining the functional properties and quality of the activated carbon that can be formed [189,210]. The chemical composition analysis (Table 5.1) indicates that the mango husk

Stellenbosch University https://scholar.sun.ac.za

contains about 4.24% moisture, 19.56% fixed carbon 74.43% volatile matter and 2.73% ash (Table 5.1).

Table 5.1 Proximate analysis and lignocellulosic composition of mango seed husk.

Proximate analysis (wet basis)	**Composition (%)**
Moisture	4.24 ±0.04
Fixed carbon	19.56 ± 0.07
Volatile matter	73.43 ± 0.34
Ashes	2.73 ± 0.50
Lignocellulose analysis	
Cellulose	37.28 ± 2.58
Hemicellulose	19.03 ±1.11
Lignin	23.92 ±0.05

The percentage of lignin, hemicellulose, and cellulose are comparable to what is reported in the literature of 5%-20.71%, 15.6%-16.63%, and 34.68%-39.4%, respectively [116,131]. Furthermore, the higher the content of volatile matter, the greater the porosity and subsequently higher surface area of the activated carbon produced [188]. According to Suhas et al. [189], materials with a greater content of lignin produces activated carbon with a predominantly macroporous structure, while raw materials with a higher content of cellulose produce activated carbon with a predominantly microporous structure.

5.3.2 Effect of production conditions on characteristics of the activated carbon

Varying the impregnation ratio, soaking time, and carbonization temperature resulted in the production of activated carbon with different characteristics in

Stellenbosch University https://scholar.sun.ac.za

terms of surface area, ash content and bulk density (Table 5.2). High carbonization temperature provided activated carbon with high surface area, low ash content and bulk density (Table 5.2). The contour plots (Figs. 5.3a-c) show the trends for the effects of each parameter and interactions of the parameters on the specified responses for the activated carbon. The surface area of the activated carbon increased with increase soaking time and carbonization temperature (Figs. 5.3a (i & iii)). The surface area is a measure of the porosity of activated carbons on which adsorption can take place. The relationship between the surface area and the impregnation ratio was different from that of carbonization temperature. The surface area decreased with impregnation ratio up to a value of 0.45, thereafter the surface area increased (Figs. 5.3a (ii & iii)). Thus, the greater the impregnation ratio (beyond 0.45), coupled with either longer soaking times or high carbonization temperature, the higher the surface area for adsorption (Figs. 5.3a (i-iii)). The impregnation ratio and carbonization temperature were the two parameters that showed significant effects ($p<0.05$) on the surface area (Fig. 5.4a). However, the carbonization temperature had the greatest positive impact on the surface area of the activated carbon, whereas the impregnation ratio had the most negative effect (Fig. 5.4a). Increase in carbonization temperature increased the surface area (Fig. 5. 3a (i & ii), which can be attributed to the degradation of the hemicellulose, cellulose, and lignin that produces volatile compounds, bio-oil and carbon [189]. The degradation of these compounds, similar to dissolution by NaCl, leads to further opening of pores in the seed husk structure. However, the degradation of these components does not occur at the same temperature [176].

Stellenbosch University https://scholar.sun.ac.za

Table 5.2 Characteristics of activated carbon produced using pyrolysis method at different process conditions

Soaking time(h)	Impregnation ratio	Temperature (˚C)	Bulk density (kgm^{-3})	Ash content (%)	Surface area (m^2g^{-1})
6	0.75	450	242	9.59	223
4	0.50	450	212	8.20	173
4	0.50	450	207	6.47	160
4	0.75	400	257	11.70	177
4	0.75	500	192	9.23	215
2	0.75	450	252	10.07	195
4	0.25	500	232	5.94	205
6	0.50	500	203	7.78	215
2	0.25	450	269	5.93	158
4	0.25	400	251	6.00	155
4	0.50	450	238	7.57	202
6	0.50	400	242	8.93	125
6	0.25	450	262	7.52	201
2	0.50	400	272	8.87	116
2	0.50	500	208	6.38	172

For example, thermal degradation of hemicellulose, cellulose, and lignin would occur between 220 ˚C – 315 ˚C, 315 ˚C – 400 ˚C, 160 ˚C – 900 ˚C, respectively [176]. Therefore, the higher carbonization temperature of 400 ˚C – 500 ˚C applied (Table 5.2) most likely degraded hemicelluloses as well as the cellulose and lignin. The results are similar to Adinata et al [190] where activated carbon

Stellenbosch University https://scholar.sun.ac.za

produced with both KOH and K_2CO_3 as activation agents, showed similar trends for such temperature ranges.

The increase in soaking time increased the surface area of the activated carbon alone and also in interaction with the impregnation ratio and carbonization temperature. The effect suggests that during the manufacturing of activated carbon, these parameters may have to be monitored and controlled simultaneously for optimal surface area. However, since only the temperature (linear) and the impregnation ratio (quadratic) showed significant effects ($p< 0.05$) on the surface area (Fig. 5.4a), the desired surface area for the activated carbon can be tailored made by controlling the two parameters independently.

Presence of ash in the activated carbon indicates the presence of inorganic content, which reduces its quality [211]. Similar to the surface area, the carbonization temperature and impregnation ratio were the most important factors to consider when high quality activated carbon is desirable from the mango seed husks. The results show that the effects of these two parameters were significant at $p< 0.05$ on the ash content (Figs. 5.3b (i-iii)). On the other hand, a combination of high impregnation ratio and longer soaking time is not desirable for high quality activated carbon because of increased ash content (Figs. 5.3 b (ii)) unless it is accompanied by high carbonization temperature above 450 °C. At the stated temperature, the ash content is less than 8% for soaking times and impregnation ratio of less than 6 h and 0.6, respectively (Fig. 5.3b (i & iii)). The effect of carbonization temperature on ash content could be

Stellenbosch University https://scholar.sun.ac.za

because the sodium absorbed in the husk is reduced to metallic sodium at elevated temperatures and is subsequently lost during the washing stage [188]. Similar to the surface area, the impregnation ratio (linear) has the most negative effect on the quality of the activated carbon because the positive relationship with the ash content (Fig. 4b) whereas, the temperature has a negative relationship with the ash content.

Bulk density is an important parameter mainly for handling of the activated carbon in the adsorption cooling system, in particular, the adsorbent unit. The bulk density affects the volume that can be handled in the adsorbent unit per unit time. The bulk density was largely affected by all the three parameters, carbonization temperature, soaking time as well as impregnation ratio (Fig. 5.3c (i-iii)). The effects of carbonization temperature (linear), impregnation ratio (quadratic) and soaking time (quadratic) on the bulk density were significant ($p< 0.05$) (Fig. 5.4c). Activated carbon of low bulk density from the seed husks can be obtained if the production is done using impregnation ratios between 0.5 and 0.6 at temperatures above 500°C and soaking times between 3.5 h and 5.5 h (Fig. 5.3c (i & iii)). The increase in bulk density at reduced carbonization temperature may be related to the limited breakdown of the structural components, thus hemicellulose, cellulose and lignin [176], which leads to reduced porosity.

Stellenbosch University https://scholar.sun.ac.za

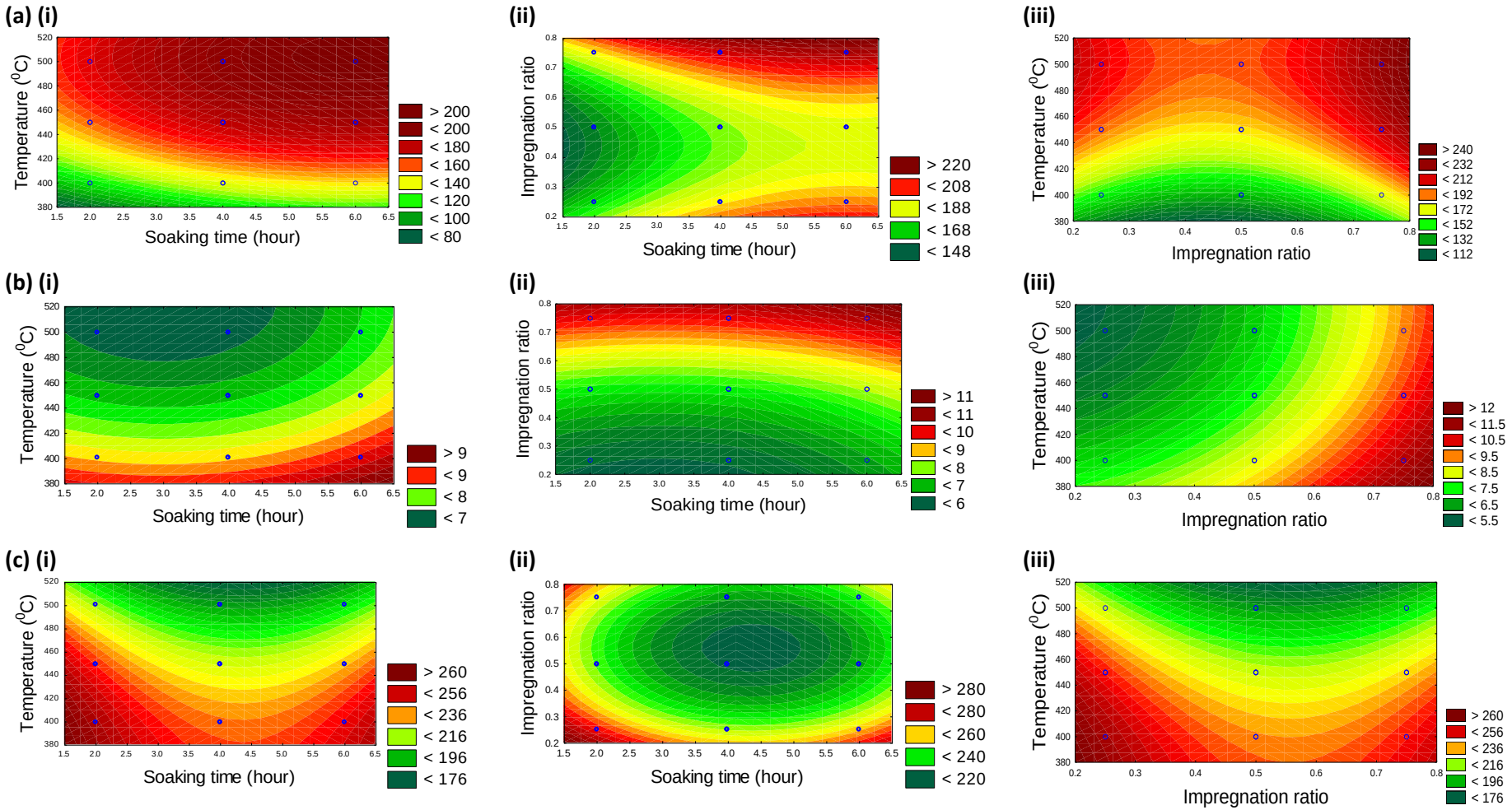

Figure 5.3 Effects (a) on surface area of (i) temperature vs soaking time at 0.50 impregnation ratio, (ii) impregnation ratio vs soaking time at 450°C & (iii) temperature vs impregnation ratio at 4 h soaking time; (b) on ash content of (i) temperature vs soaking at 0.50 impregnation ratio, (ii) impregnation ratio vs soaking time at 450°C & (iii) temperature vs impregnation ratio at 4 h soaking time; (c) on bulk density of (i) temperature vs soaking time at 0.50 impregnation ratio; (ii) impregnation ratio vs soaking time at 450°C & (iii) temperature vs impregnation ratio at 4 h soaking time

Stellenbosch University https://scholar.sun.ac.za

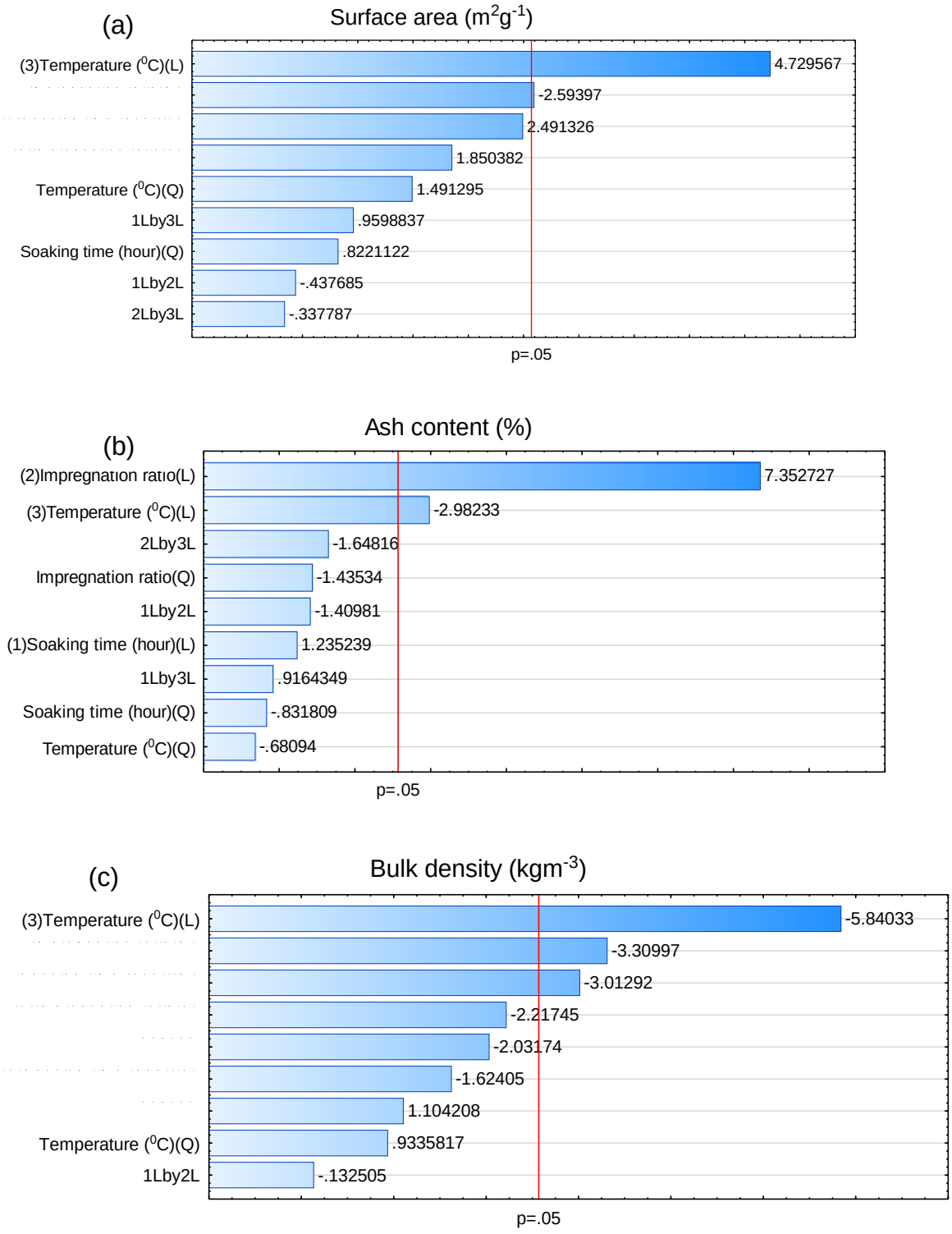

Figure 5.4 Pareto charts showing size and significance of effects of activation, temperature, soaking time and activation temperature on properties of mango seed husk activated carbon produced using NaCl as an activation agent

Stellenbosch University https://scholar.sun.ac.za

5.3.3 Optimal conditions for production of activated carbon from mango seed husk.

The non-linear regression coefficients for the model (Equation 5.1) are shown in Table 5.3a. The positive relationship between carbonization temperature and surface area is reflected by the positive coefficient whereas as the negative relationship with bulk density is reflected by the negative regression coefficient (Table 5.3a). The experimental data fitted the model for all the three outputs (surface area, ash content and bulk density) with adjusted R^2 of at least 0.8 (Table 5.3 (b)). The *p*-value from the lack of fit test showed that the data fitted the model at $p > 0.05$ (Table 5.3b). The optimum production conditions were identified to be 5.8 h for the soaking time, 0.25 impregnation ratio and 500 ˚C carbonization temperature (Table 5.4). The optimum carbonization temperature is comparable to the optimum temperature of 456 ˚C obtained when $ZnCl_2$ was used as activating chemical with optimum impregnation ratio of 1.08, to produce activated carbon from agave bagasse [187]. At the optimized conditions, the mango seed husk activated carbon had BET surface area of 415 m^2g^{-1}, ash content of 6.92% and bulk density of 243 kgm^{-3} (Table 5.4). The BET surface area falls within the range of 3 m^2g^{-1} to 1718 m^2g^{-1} reported for activated carbon produced from agricultural residues [185]. However, it is lower than the surface area of 618 m^2g^{-1}- 661 m^2g^{-1} for mango seed husk, which used NaCl as activation agent mainly because the activated carbon produced was in powder form whereas in this study it was in the granular form [197]. Similarly, activated carbon powder from coal, wood, and coconut, reported higher surface area of 750 m^2g^{-1}- 850 m^2g^{-1}, 900 m^2g^{-1}-1200 m^2g^{-1}, and 590 m^2g^{-1}-1500 m^2g^{-1}, respectively [212] than the activated carbon from the mango seed husk produced in this study. The activated carbon for the

Stellenbosch University https://scholar.sun.ac.za

commercial activated carbon had a particle size of 3 mm compared to10 mm for this study.

Table 5.3 Final regression coefficients, after discarding insignificant terms and values of the statistical test parameters that validate the model

a. Final regression coefficients, after discarding insignificant terms

	Surface area(m^2g^{-1})	**Ash content (%)**	**Bulk density(kgm^{-3})**
β_0	173.69	7.74	219.00
β_1	15.37	0.32	- 6.50
β_2	11.37	1.90	- 8.88
β_3	29.25	- 0.77	- 23.38
β_{11}	-	-	17.75
β_{22}	24.04	0.50	19.50
β_{33}	-13.21	-	- 5.50
β_{12}	-	- 0.52	-
β_{13}	8.50	-	6.25
β_{23}	-	- 0.60	-11.50

b. Values of the statistical test parameters that validate the model.

	Surface area(m^2g^{-1})	**Ash content (%)**	**Bulk density(kgm^{-3})**
Lack of fit	0.8883	0.7998	0.9808
R^2	0.8797	0.9113	0.9309
R^2 adjusted	0.7894	0.8447	0.8387

Stellenbosch University https://scholar.sun.ac.za

Table 5.4 Optimized conditions and predicted values of responses

Parameters	Predicted value	Responses	Optimum value
Soaking time	5.8 h	Surface area[a]	
		BET $_{CO2}$	223 m^2g^{-1}
Impregnation ratio	0.25	Ash content	6.92%
Temperature	500 °C	Bulk density	243 kgm^{-3}

[a] BET $_{N2}$ = 415 m^2g^{-1}

The ash content and bulk density of the mango seed husk activated carbon produced in this study was 6.92% and 243 kgm^{-3}, respectively, which shows improved quality when compared with the ash content of 13.55% - 14.75% for the activated carbon produced by Mise & Patil [197], but is close to about 6% reported for commercial activated carbon [212]. The bulk density of the mango seed husk activated carbon produced is higher than the 204 kgm^{-3} - 232 kgm^{-3} bulk density reported by Mise & Patil [197]. The relatively high bulk density of the activated carbon produced in this study makes it a better choice for use in vapour phase applications such as adsorption cooling since it would not be easily sucked out during vacuum creation process.

5.3.4 Validation of model production conditions for mango husk activated carbon

Using the predicted optimum production conditions in Table 5.4 to produce activated carbon, the surface area, ash content and the bulk density of the activated carbon produced were measured to validate the model (Table 5.5). The results (Table 5.5) showed that the values for surface area (BET $_{CO2}$), ash content and the bulk density of the activated carbon produced at the optimal conditions were very close to the predicted values deviating by 2.69%, 1.01%, and 2.06%, respectively [213].

Stellenbosch University https://scholar.sun.ac.za

Table 5.5 Validated model production conditions for mango husk activated carbon

Response	Optimized Model Value	Experimental value	Percentage error
Surface area, m^2g^{-1} (BET CO_2)	223	229	2.69
Ash content,%	6.92	6.99	1.01
Bulk density, kgm^{-3}	243	248	2.06

Furthermore, the surface area (BET N_2) obtained when nitrogen gas was used to estimate the BET surface area of the activated carbon produced was found to be 415 m^2g^{-1} (Table 5.4), which falls within the surface area of 300 m^2g^{-1} -2500 m^2g^{-1} reported by Campbell et al [214] for activated carbon.

5.3.5 Changes in surface functional groups on the activated carbon as determined by Fourier transform infrared spectroscopy (FTIR) analysis

The infra-red spectral bands (Fig. 5.5) depicted the changing structure of the various mango seed husk activated carbon samples. The infra-red spectrum of the raw mango seed husk shows the presence of several functional groups such as alkene, aromatic, ketone, hydroxyl, and carboxyl functional groups (Fig. 5.5). These kinds of functional groups are typical of many lignocellulose raw materials. The absorbance for the hydroxyl stretching vibrations of the water in the raw mango seed husk is correlated to the band at 3281 cm^{-1} [188,215,216]. Other bands detected in the raw mango seed husk are C=C (alkene functional group) at 1617 cm^{-1}, C=O (carbonyl functional group) with spectra band at 1732 cm^{-1}, organic acid (carboxyl functional group) at 2934 cm^{-1}, aromatic group (benzene) at 1443 cm^{-1}, and C-O (ether functional group) at 1038 cm^{-1} [188,217]. Several of the spectral bands in the raw mango seed husk disappeared with

Stellenbosch University https://scholar.sun.ac.za

increasing carbonization temperature due to thermal degradation of bonds of the lignocellulosic compounds present. The activated carbon produced at 400 ˚C and 450 ˚C showed a small peak at 1617 cm^{-1} suggesting that there could be cellulose and lignin present. However, the activated carbon produced at 500 ˚C showed fewer remnants of lignin because the lignin is totally broken down at such high temperatures [176]. The result supports the optimum carbonization temperature obtained (500 ˚C) evident from the absence or reduced absorbance from volatiles initially present in the sample.

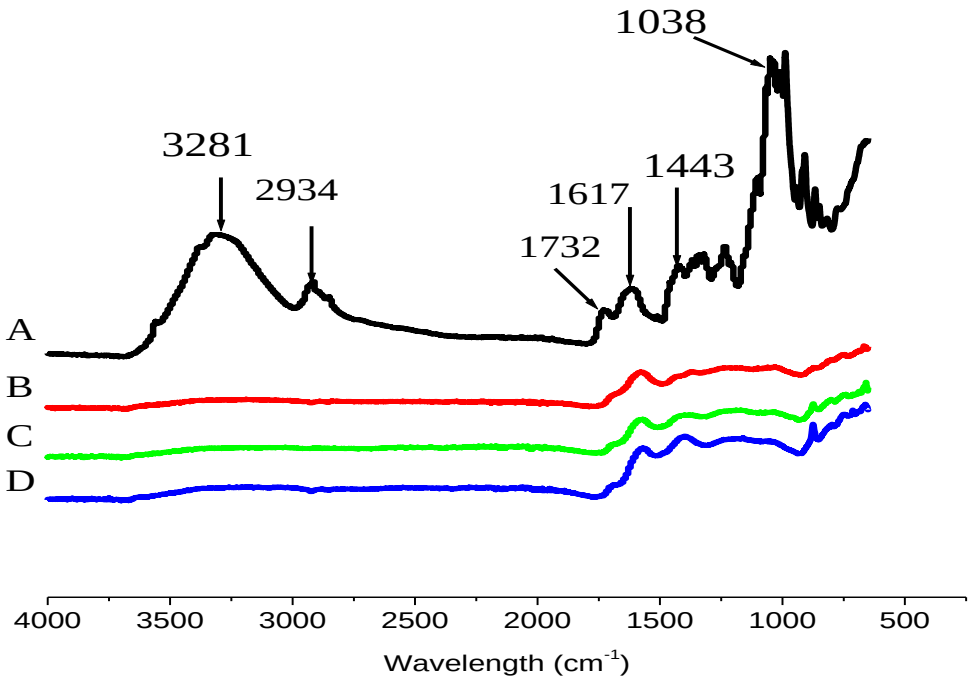

Figure 5.5 Comparison of FTIR spectra of raw mango seed husk (A); mango seed husk activated carbon produced at 500°C (B); mango seed husk activated carbon produced at 450°C (C); mango seed husk activated carbon produced at 400°C (D)

Therefore, activated carbon was produced from mango seed husk through simultaneous carbonization and activation with NaCl as the activation agent, which falls within the quality range (in terms of BET surface area and ash content) of commercial activated carbon. There are some precautions to be considered when using NaCl. Although it is a relatively safer activation agent than most activating

Stellenbosch University https://scholar.sun.ac.za

chemicals, NaCl has some challenges because of the corrosive effect to most metals, therefore anti-corrosive materials should be used to protect the equipment to use for soaking the biomass material and for the adsorber construction. Secondly, the discharged NaCl water need special disposal procedures to avoid damage to the environment.

5.4 Conclusion

The optimum mango husk activated carbon production conditions determined using response surface methodology for impregnation ratio, soaking time, carbonization temperature were 0.25, 5.8 h and 500 ˚C, respectively, which resulted in activated carbon with ash content of 6.92%, bulk density of 243 kgm^{-3} and surface area (BET $_{CO2}$) of 223 m^2g^{-1}, which was 415 m^2g^{-1} (BET $_{N2}$). These optimal activated carbon production conditions were within the surface area ranges of 300 m^2g^{-1} -2500 m^2g^{-1} found in the literature for similar materials [214]. At the validated production conditions, the ash content (6.69%), the bulk density (248 kgm^{-3}) and surface area (229 m^2g^{-1} (BET $_{CO2}$)) were within 2% error (1.01, 2.06 and 2.6%, respectively) of the predicted values, which suggests the possibility of using the model to predict and control the activated carbon production process. Furthermore, the lack of interaction among the production conditions suggests that the production of the activated carbon from mango seed husks can be controlled by varying each parameter independently to tailor make the quality of the activated carbon in terms of surface area, bulk density and ash content for different applications. Notably, the NaCl is a relatively safe and potentially an environmentally friendly alternative activation agent for the production of granular activated carbon from mango seed husk of comparable quality to commercial activated carbon as well as to activated carbon from biomass sources. Therefore, the study has provided an optimized process that is not only effective in producing functional

Stellenbosch University https://scholar.sun.ac.za

activated carbon but a process that has potential to reduce the environmental impact of activated carbon production and at the same time provide an opportunity for the development of an integrated biorefinery.

Stellenbosch University https://scholar.sun.ac.za

Chapter 6 Evaluating the potential of using ethanol /water mixture as a refrigerant in an adsorption cooling system by using activated carbon- sodium chloride composite adsorbent and mango seed activated carbon

ABSTRACT

Thermal properties and adsorbent - refrigerants compatibility, influence heat and mass transfer dynamics in adsorption cooling systems (ACS). Activated carbon (AC) +NaCl (10-35.7% w/v) composite adsorbents were paired with either high purity (99.7%) or low-grade ethanol (60% ethanol/ 40% water) refrigerants to assess the potential of ethanol/water mixture as a refrigerant. The adsorption cooling system (ACS) with activated carbon-sodium chloride (AC+ NaCl) composites adsorbent had coefficient of performance and specific cooling power in the range of 0.075-0.091 and 39 Wkg^{-1}-79 Wkg^{-1}, respectively, when paired with high purity ethanol, which increased to between 0.121-0.146 and 113-150 Wkg^{-1}, respectively, when paired with low-grade ethanol. Between 21 MJ-25 MJ per cycle was needed for the desorption of refrigerants in AC+NaCl composites adsorbent when paired with the low-grade ethanol, whereas more energy, 27 MJ per cycle, was required to desorb low-grade ethanol when paired with unmodified activated carbon (AC) in ACS. The study has shown that the thermal and mass transfer performances of AC+NaCl composites adsorbents superseded that of unmodified AC providing the potential for low-grade ethanol to be used as a potential alternative refrigerant in ACS especially in areas where pure ethanol is limited.

Stellenbosch University https://scholar.sun.ac.za

6.1 Introduction

Adsorption cooling system (ACS) has the potential for use in areas with limited or no electricity, water, and high-grade ethanol on condition that alternative sources of energy and refrigerants are made available. However, the ACS experience low specific cooling power (SCP), coefficient of performance (COP) and poor adsorbent heat and mass transfer. Table 6.1 shows COP and SCP reported for ACS. For improved performance, adsorbents physical properties have to enhance mass and heat transfer in the system. An adsorbent with high porosity has poor heat transfer and long cycle time, resulting in high energy consumption hence reduced SCP [6,218,219]. In addition, the adsorbent/refrigerant pairs used in ACS is critical to system performance[5,83] thus, their applicability in ACS targeting off-grid communities, water scarce and poor communities should be evaluated. Common adsorbent/refrigerant working pairs at commercial level include AC/ethanol, AC/methanol or AC/ammonia, silica gel/water, and zeolite/water pairs [5,6,93,220,221]. Despite its high latent heat of vaporization compared with ethanol, ammonia, and methanol, water has low saturation pressure than ethanol and that limits its evaporation [5,82]. On the other hand, methanol and ammonia have higher saturation pressure than water but are toxic [5,6]. In addition, ethanol is non-toxic and environmentally benign [8] and could easily be produced at small scale level using local knowledge, but with high water content [222]. A compatible adsorbent is required if the locally produced ethanol, with high water content (normally 60% ethanol) is to be used as a refrigerant. There are a number of adsorbents that could be used such as Zeolite. However, the high desorption temperature of adsorbents such as zeolite [6,79,82] implies high desorption energy, which can affect affordability. Unlike other adsorbents, AC can be produced from biomass including agricultural residues which

Stellenbosch University https://scholar.sun.ac.za

are readily available in many rural/poor communities. This can lead to the development of small-scale AC industries and which might make it easier to adopt the adsorption cooling technology in many rural communities.

The Ideal adsorbent is desired to be non-toxic and non-corrosive, have relatively low desorption temperature, adsorb large quantities of refrigerant, large latent heat of adsorption than sensible heat, low cost and readily available [7,223,224]. One of the commonly used adsorbents is the activated carbon which can be made commercially from many carbonaceous materials including agricultural residues such as mango kernel which are readily available in rural agricultural communities[225]. However, activated carbon used in many adsorption studies are commercially produced and are not affordable to many rural agricultural farmers. Therefore, there is a need to use locally available material for activated carbon production. The performance of these locally produced activated carbon needs to be evaluated and compared with the commercial activated carbon. In this study, mango seed husk was used to produce activated carbon for use in adsorption cooling. Mango seed has no economic value and is, therefore, a source of pollution when disposed of in the environment. The mango seed husk activated carbon was paired with both pure (99.7%) and impure (60%) ethanol as refrigerants.

As a result of the inherent heat and mass transfer limitations associated with the adsorbents and refrigerant working pairs used in ACS, a lot of energy is required to power this technology. Therefore, ACS targeted for areas with the absence of or limited electricity, high-grade ethanol and water supply could be powered either by direct biomass combustion or by waste heat from agro-processes [4,226]. However,

Stellenbosch University https://scholar.sun.ac.za

modifications of the AC to ensure improved heat and mass transfer would be required to use the low-grade ethanol as a refrigerant.

Table 6.1 Coefficient of performance (COP) and specific cooling power (SCP) for some adsorption working pairs.

Adsorption working pair	**COP**	**SCP (Wkg^{-1})**	**Reference**
AC/methanol	0.34		[227]
AC/R32	0.23	250	[228]
AC/ethanol	0.7-0.8		[81]
$CaCl_2$/graphite/ammonia	0.3	1000	[229]
Strontium chloride-expanded graphite/NH_3	0.24	291.5	[230]
Silica gel/water	0.16-0.496		[231–233]
AC/ammonia	0.35	520	[234]
Zeolite/foam aluminium/water	0.55	500	[82]
Zeolite/water	0.25	7	[235]
Zeolite/metal chips/water	0.56		[236]
AC fiber/$CaCl_2$/ammonia	0.6	330	[6]
AQSOA FAM-Z02/water	0.31	436	[237]

Note: Activated carbon = AC

Several studies have been done to improve the thermal performance of ACS by increasing the heat transfer area of the adsorbent beds using fins [99,238,239], reducing the thermal resistance between the adsorbent wall and the adsorbent material through consolidating adsorbent bed [240] and reducing thermal resistance through the formation of composite adsorbents [79,99,121,241]. These studies employed pure refrigerants paired with various adsorbents (Table 5.1). For instance,

Stellenbosch University https://scholar.sun.ac.za

Tso et al. [79,242] formed AC-silica gel-$CaCl_2$ composite adsorbent paired with pure water as the refrigerant while El-Sharkawy et al [81] paired AC with low-grade ethanol. However, studies involving the mixture of water and ethanol as the refrigerant (as is the case with the low-grade ethanol) have not been reported. Obviously, water/ethanol mixtures are miscible and cooling in the evaporator depends on the amount of refrigerant that is adsorbed by the adsorbent and the refrigerant latent heat of vaporization. Since the latent heat of evaporation of water is about 60% higher than that for ethanol, the presence of water in the low-grade ethanol would facilitate cooling rate if paired with a suitable adsorbent with high adsorption capacity. Furthermore, there are technological and cost issues involved to purify or dehydrate the water-ethanol mixture to the commercial ethanol grade (99% ethanol) normally used in conventional ACS [243,244]. Thermal performance of adsorbents has been enhanced through the composite formation. For example, Wang et al. [241] formed consolidated composite adsorbent with expanded graphite and $CaCl_2$ to improve thermal conductivity of $CaCl_2$. Tanashev et al. [160,161] formed composite silica gel-$CaCl_2$ adsorbent which increased the thermal conductivity of silica gel bed from 0.112 $Wm^{-1}K^{-1}$ to 0.153 $Wm^{-1}K^{-1}$. In a silica gel-$CaCl_2$-aluminum hydroxide composite bed, the thermal conductivity of silica gel increased from 0.12 $Wm^{-1}K^{-1}$ to 0.227 $Wm^{-1}K^{-1}$ [162]. Other chloride salts used include $MgCl_2$, $BaCl_2$, $SrCl_2$ [6], $MnCl_2$, $NiCl_2$ and $CoCl_2$ [93] and LiCl [94]. Notably, the thermal conductivity of $CaCl_2$ is 1.09 $Wm^{-1}K^{-1}$ [96] while the thermal conductivity of AC ranges from 0.15 $Wm^{-1}K^{-1}$ to 0.50 $Wm^{-1}K^{-1}$ [86–89]. Therefore, utilization of chloride salts with higher thermal conductivity in the composites leads to improved heat transfer but may have implications on the mass transfer during adsorption/desorption process leading to reduced COP due to clogging of pores as well as causing corrosion to the adsorber [245,246]. Sodium chloride

Stellenbosch University https://scholar.sun.ac.za

(NaCl) despite its higher thermal conductivity of 7 $Wm^{-1}K^{-1}$ [159], than $CaCl_2$, has not been used to improve the thermal and adsorption performance of AC. Use of NaCl would be advantageous to form the composite with AC because of the potential to improve both the heat and mass transfer properties when paired with ethanol/water mixture. The high water affinity of NaCl in the AC is expected to increase the mass transfer of the mixture in the adsorbent bed and simultaneously increase the thermal conductivity and heat of adsorption of the AC.

Furthermore, AC used in many adsorption studies are commercially produced and are not affordable to many rural agricultural farmers. Therefore, there is a need to use locally available material for activated carbon production. The performance of these locally produced activated carbon needs to be evaluated and compared with the commercial activated carbon. Therefore, the objective of this study is to determine the technical performance of using the mixture of ethanol and water (low-grade ethanol (60% ethanol and 40% water) as refrigerants(representing likely quality of ethanol produced in local small-scale distilleries [222]) combined with composite AC+NaCl and mango seed AC as an adsorbent in ACS powered by combustion of biomass. The potential energy savings of using AC+NaCl composite adsorbents in a biomass waste (mango seeds with heating values closer to woody biomass [117,247], generated from mango processing plant) powered ACS was also evaluated. The results of the study are relevant for promoting application ACS in resource-limited (pure water or pure ethanol) areas. As a whole, the study is a step towards making ACS cost effective and resource efficient. The technical performance of the ACS was measured based on three factors (1) temperature profiles in the adsorbent container during desorption, (2) the duration of adsorption and desorption, and (3) temperature changes in the evaporator [248].

Stellenbosch University https://scholar.sun.ac.za

6.2 Materials and methodology

6.2.1 Materials

Commercial AC was GC E612 of mesh size 12 and apparent density of 0.49 gram/cubic centimeter (Indocarb Corporation Inc). NaCl (99.5% in purity) was purchased from (Kimix chemical and laboratory suppliers' cc). Mango seed husk AC produced in Chapter 5 was also used. Ethanol (99.7% purity, Merck Millipore) was used as the pure refrigerant. Tommy Atkins mango seeds were obtained from Hoedspruit fruit processors (South Africa). Liquid nitrogen baseline 5.0 (Afrox Ltd) and benzophenone of 99% purity (Sigma-Aldrich) were used for BET analysis and as a sensor material during thermal conductivity measurement of the adsorbent samples, respectively.

6.2.2 Composite adsorbent preparation

Commercial AC + NaCl composites were prepared according to procedure presented in Figure 6.1.

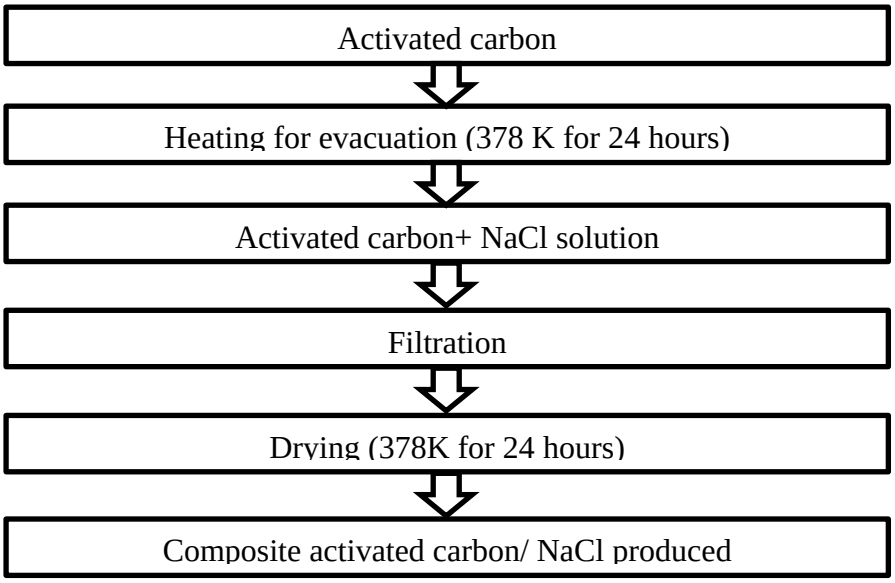

Figure 6.1 Impregnation of NaCl into activated carbon

Stellenbosch University https://scholar.sun.ac.za

Commercial AC (1 kg) was heated at 105 ˚C for 24 h to remove entrapped moisture. Commercial AC was subsequently impregnated with 2 L of NaCl solution at varying concentrations of 10 w/v %, 15 w/v %, 20 w/v %, 25 w/v %, 30 w/v % and 35.7 w/v %, for 24 h at room temperature (24 ˚C) and relative humidity of 65% and thereafter, dried at 105 ˚C for 24 h. The control (Commercial AC) and as well as mango seed AC were also soaked in demineralized water and dried under similar conditions.

6.2.3 Characterization of the adsorbents

About 0.3-0.6 g of each adsorbent was analyzed in a 3Flex instrument (Accelerated Surface Area and Porosimetry System, Micromeritics Instrument Corporation) for surface area. The samples were heated to remove moisture and vapour, and subsequently, cooled in liquid nitrogen at incremental dosages of 3.0 cm^3/g. Total nitrogen gas adsorbed and corresponding gas pressure at a given temperature was plotted to generate adsorption isotherms. Surface area, pore volume and pore area of the samples were calculated based on Brunauer–Emmett–Teller (BET) theory [209]. Furthermore, Scanning Electron Microscopy (SEM) was performed to confirm that the pores of the adsorbent were impregnated with the NaCl.

6.2.4 Determination of adsorption capacity, kinetics and isotherm of adsorbents

The objective of this experiment was to determine the equilibrium adsorption capacity of various adsorbent-refrigerant pairs at different temperatures and pressure. The adsorbents to be used in this experiment are the composite adsorbents produced in Section 6.2.2, as well as mango seed husk AC and commercial AC. The refrigerants are ethanol at 99.7%, and 60 % purity. The test rig for these experiments was designed and built as shown in Figure 6.2. It consists of a stainless steel vessel containing the adsorbent bed and refrigerant bottle. 60 mm and height 70mm containing 30 g of

Stellenbosch University https://scholar.sun.ac.za

adsorbents to be tested. The temperature changes in both the adsorption bed and the refrigerant bottle were monitored using CENTER 306 thermometer (Center Technology Corp.) equipped with data logger and dual input K- type thermocouples (temperature range -200 ˚C – 1370 ˚C, resolution 0.1 ˚C). The refrigerant bottle and the adsorption bed were connected by a non-return valve. Before the start of the experiment, the adsorbent bed was connected to a vacuum pump to evacuate the bed to about 0.01 kPa by opening valves V1 and V2 while valve V3 remained closed. The temperature of adsorbent bed was then gradually increased by application of heat up to 4 h while the evacuation process was still ongoing. This process was performed to get rid of all residual gases in the adsorption bed. The adsorption bed pressure reached at the end of the evacuation process was noted and valve V2 was closed. Valve V3 was then opened and the vacuum was created over the refrigerant until the changed into vapour. Valve 1 was then closed and valves V2 and V3 were open to allow the refrigerant vapour to move from the refrigerant bottle to the adsorbent to be adsorbed. During the adsorption runs, the temperature of the refrigerant bottle remained constant (24 ˚C) as the set-up is in the conditioned room, the same conditions that the actual constructed adsorption cooling system was operated. The accuracy of the weighing balance was ±0.01 g. The effect of the weight of the piping, valve, and others on the measurement would be minimal since their weight before and during the experimental runs was assumed to be unchanged. As the adsorption process continued, the valve V2 was closed every 120 seconds and the adsorbent bed was isolated and dismantled and weighed. The pressure and temperature changes in the adsorption bed and the refrigerant bottle was also recorded. This process continued until the bed reached its adsorption capacity and cannot adsorb

Stellenbosch University https://scholar.sun.ac.za

any more of the refrigerant. Finally, the vacuum was recreated in the adsorption bed to start a new adsorption run.

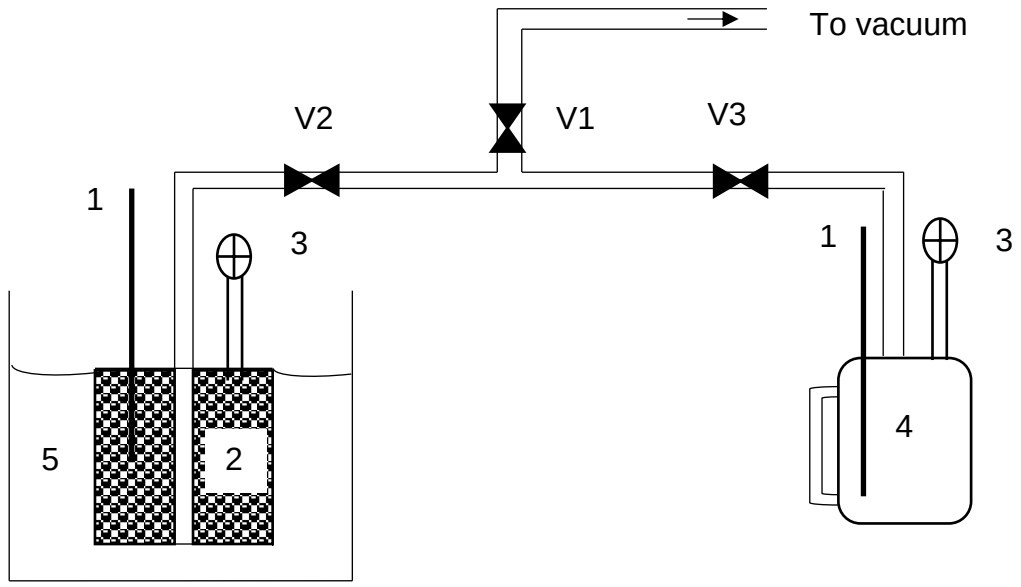

1. Thermocouple 2. Adsorbent bed 3. Vacuum gauge 4. Refrigerant bottle 5. Hot water bath; V1,V2,&V3 are valves

Figure 6.2 Experimental rig to study adsorption capacity of different adsorbent refrigerant pairs

Stellenbosch University https://scholar.sun.ac.za

This process was repeated at five different temperatures 25 ˚C, 30 ˚C, 35 ˚C, 40 ˚C and 45 ˚C. The data from this experiment was fitted using Dubinin–Astakhov (D–A) equation discussed in Section 2.2.2 because it is widely used for adsorption of gases onto microporous adsorbents[249].

$$W = W_0 \, exp\left[\left(-\frac{A}{E}\right)^n\right] \qquad 6.1$$

Where A is the adsorption potential (kJkg^{-1}) of the adsorbent/refrigerant pair that could be estimated using Equation 6.2

$$A = RT \, ln\left(\frac{P_s}{P}\right) \qquad 6.2$$

Substituting Equation 6.2 into Equation 6.1 and linearization gives

$$ln\, W = ln\, W_0 - \frac{1}{E^n}\left\{RT \, ln\frac{P_s}{P}\right\}^n \qquad 6.3$$

Where W stands for the equilibrium capacity of the adsorbent/refrigerant pair (kgkg^{-1}) W_0 is the maximum adsorption capacity of the adsorbent/refrigerant pair(kgkg^{-1}). E is the adsorption characteristic energy (kJkg^{-1}) which measures the adsorption strength between adsorbent and refrigerant. T is the adsorption temperature (K), Ps defines the saturation pressure of the refrigerant at the adsorption temperature (kPa) whilst P is the equilibrium pressure (kPa). The exponential parameter n gives the best fitting of ln(W) vs A^n. Refrigerant saturation pressure (Ps) was estimated for high-grade ethanol using Antoine Equation (Equation 6.4)

$$P_S = 10^{A-\frac{B}{C+T}} \qquad 6.4$$

The constants A, B, and C for the ethanol are 8.20417, 1642.89, and 230.03 respectively; P_S is in mmHg which could be converted to kPa. Since low-grade ethanol is a mixture where both water and ethanol contribute to the overall saturated pressure of the mixture, Raoult's Law [77] was used to estimate the values of saturated pressures using the equation

Stellenbosch University https://scholar.sun.ac.za

$$P_{water} = x_{water} P_{S,water} \quad 6.5$$

$$P_{ethanol} = x_{ethanol} P_{S,ethanol} \quad 6.6$$

$$P_S = P_{S,water} + P_{S,ethanol} \quad 6.7$$

P_{water} and $P_{ethanol}$ are the partial vapour pressures (kPa) of water and ethanol in the mixture, x_{water} and $x_{ethanol}$ are the mole fractions of water and ethanol; $P_{S,water}$ and $P_{S,ethanol}$ are the saturated pressure (kPa) values of component water and ethanol component if they were on their own as pure liquids and these could be estimated using Antoine equation. The constants A, B, and C for the water used for the Antoine equation are 8.07131, 1730.63 and 233.426, respectively.

6.2.5 Determination of mango seeds heating value

Mango seed heating value ($MJkg^{-1}$) was determined in Cal2k Eco bomb calorimeter (Digital Data Systems Pty Ltd). About 0.5 g of powdered whole mango seeds (250 µm) were combusted in the crucible of the Cal2k Eco bomb calorimeter.

6.2.6 Experimental set up of the adsorption cooling system

The adsorption cooler system was designed to run totally on bio-resources generated from waste streams. The ACS was designed and built as described in Section 4.1. The ACS consisted of two adsorbers (A and B), condenser, evaporator, valves and a combustion stove (Fig 6.3). The operation and thermodynamics of the systems are similar to that of a typical ACS described in Section 2.1.3. The entire set up was operated at 5 kPa and used commercial AC (GC E 612 Indocarb Corporation Inc) and the AC-NaCl composites produced following the procedure presented in Figure 6.1. The adsorbents were paired with pure ethanol (99.7%), Merck Millipore) and impure ethanol (60% by weight, as indicated earlier to mimic the quality of ethanol normally produced at a small-scale in many rural communities [222]) as the refrigerants.

Stellenbosch University https://scholar.sun.ac.za

a.

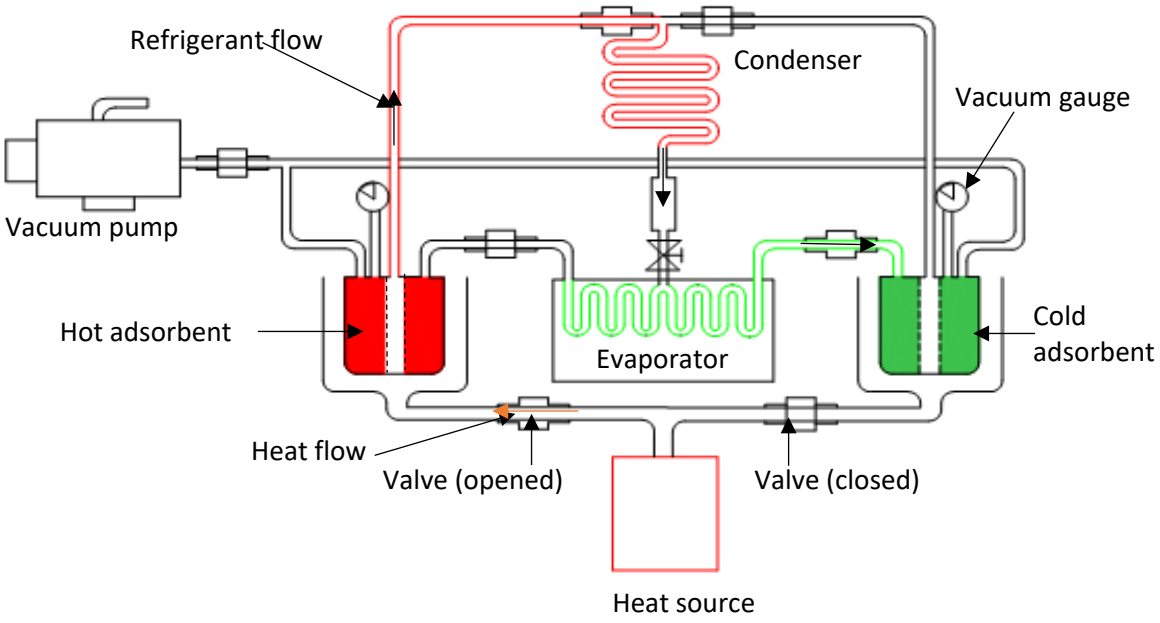

b.

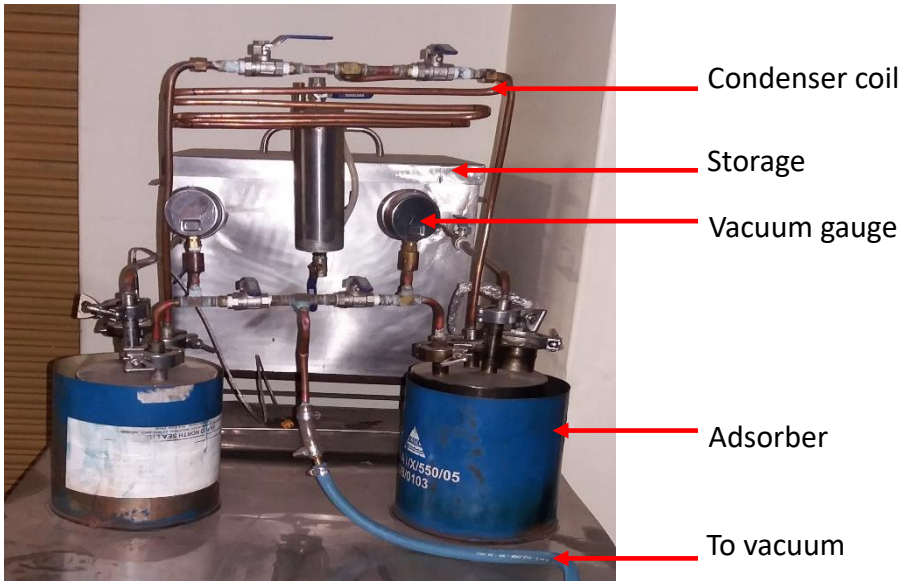

Figure 6.3 a. Schematic diagram of the adsorption refrigeration cycle b. ACS designed (volume of storage chamber is 0.0225 m³; condenser coil is 2.5m long; volume of adsorber 0.004m³)

The temperature profiles in both the adsorber and the cooler were monitored using CENTER 306 thermometer (Center Technology Corp.) equipped with data logger and dual input K- type thermocouples (temperature range -200 ^{0}C – 1370 ˚C, resolution

Stellenbosch University https://scholar.sun.ac.za

0.1 ˚C). The operation principle of an adsorption cooling cycle has been described in Section 2.3.

6.2.7 Thermodynamics of the adsorption cooling system

The operating energy of the adsorption system was generated from the combustion of mango seeds in the combustion stove (Fig 6.3). The energy supply to the system was accounted for based on the heating value of the mango seeds, determined experimentally using a bomb calorimeter. The total energy requirement of the system was determined from the total amount of mango seeds combusted during the desorption process, taking into consideration of the combustion efficiency of biomass. Among the many ways of assessing the technical performance of a cooling technology such as energy efficiency ratio (EER), the coefficient of performance (COP [63,64]) and the specific cooling power (SCP [65,66]). COP and SCP were used in this study because they are the common assessment criteria used for ACS. The energy and performance analysis of the ACS is as follows

$$Q_{eva} = m_{ref} h_{fg} \qquad 6.8$$

Where: h_{fg} is the specific latent heat of vaporization of either high-grade ethanol or the low-grade ethanol (Jkg^{-1}), Q_{eva} is the amount of heat removed from the storage chamber (Jkg^{-1}), m_{ref} is the mass of refrigerant adsorbed (kg).

$$h_{fg}(ethanol - water\ mixture) = 0.6h_{fg}(ethanol) + 0.4h_{fg}(water) \qquad 6.9$$

The value of specific latent heat of vaporization of high-grade ethanol used is 842 kJkg^{-1} while that for the low-grade ethanol was estimated using the relation

The total energy input during desorption could be expressed as

$$Q_{total} = Q_{sensible} + Q_{latent} \qquad 6.10$$

Stellenbosch University https://scholar.sun.ac.za

Where: Q_{total} is the total desorption energy (J). Since mango seed was combusted to serve as the source of energy in this study, the sensible energy supplied ($Q_{sensible}$) could be estimated as the useful energy supplied ($Q_{supplied}$) to the ACS during combustion. $Q_{sensible}$ and Q_{latent} are expressed as follows:

$$Q_{latent} = q_{st} \int_{W_o}^{W_{min}} dW \qquad 6.11$$

$$q_{st} = -R \frac{\partial \, ln \, P}{\partial \left(\frac{1}{T}\right)} \qquad 6.12$$

$$Q_{supplied} = \eta_1 \times \eta_2 \times m_{mango} \times LHV \qquad 6.13$$

Where q_{st} is the isosteric heat of adsorption (kJkg^{-1}), Q_{latent} is the latent heat released during desorption (kJkg^{-1}), W_{min} is the minimum adsorbent that remains after desorption (kgkg^{-1}), W_o is the maximum adsorption capacity of the refrigerant (kgkg^{-1}), R is the gas constant (8.314 $\mathrm{kJmol^{-1}K^{-1}}$) which can be converted to kJkg^{-1} using the molecular weight of the refrigerant, P and T are the adsorption equilibrium pressure (kPa) and temperature (K) respectively, m_{mango} is the mass of mango seed combusted, LHV is the lower heating value of mango seed estimated in the bomb calorimetry to be 17.80 MJkg^{-1}.

The assumptions for Equation 6.13 are as follows

1. The combustion of the mango seed was assumed to have occurred in excess oxygen
2. The combustion chamber was approximated to cookstoves operating in a natural convection mode driven by the chimney effect of buoyant fluid forces.
3. Wood conversion efficiency (η_1) of 90% in excess oxygen, [173].

Stellenbosch University https://scholar.sun.ac.za

4. The fraction of combustion energy from cookstoves into the cooking vessel (η_2) was 12.5% [174,175].
5. Steady feeding rate of the mango seeds into combustion stove

COP is the ratio of useful cooling to the energy supplied and could be estimated as

$$COP = \frac{Q_{eva}}{Q_{supplied}} \qquad 6.14$$

Where: Q_{eva} is the evaporator useful cooling (J), COP is the coefficient of performance.

$$Specific\ cooling\ power(SCP) = \frac{Q_{eva}}{m_{ads}\tau_{cycle}}(W/kg\ adsorbent) \qquad 6.15$$

Where: m_{ads} is the mass of the adsorbent (kg), τ_{cycle} is the cycle time (s)

6.2.8 Thermal conductivity and heating and cooling rate measurement of powdered adsorbents

The thermal conductivity of powdered commercial and composite AC was measured using differential scanning calorimetry method [250] at a heating rate of 10 °C/min with a nitrogen flow rate of 100 mL/min. Benzophenone with the melting point of 48 ˚C was used as the sensor material. The process involved placing a sensor material in pellet form (5 mm diameter) into a 5 mm aluminium container (calorimeter), which was heated until the sensor material melted. A slope of the graph obtained from melting of the sensor material (Equation 6.16) was used to determine the thermal resistance between the aluminium container and the sensor material.

$$\frac{\dot{Q}}{\Delta T} = \frac{1}{R} \qquad 6.16$$

Where: $\frac{\dot{Q}}{dT}$ is the slope of the melting region of the graph, R is thermal resistance between the aluminium container and the sensor material (KW^{-1}). Subsequently, about 0.05 g of each of the powdered commercial and composite ACs was spread uniformly into the aluminium container to a height of about 1 mm and the sensor material was

Stellenbosch University https://scholar.sun.ac.za

placed on top. The aluminium container and its contents were heated again until the sensor material melted. The slope of the graph obtained from melting of the sensor material was also calculated and the thermal resistance between the aluminum container and sensor material with the sample was calculated using Equation 6.17.

$$\frac{\dot{Q}}{\Delta T} = \frac{1}{R'} \qquad 6.17$$

where R' is the thermal resistance (KW^{-1}) between the aluminium container and sensor material with the sample. The results obtained from Equation 6.17 were used to determine the thermal conductivity of the AC by using Equation 6.18

$$k = \frac{L}{A(R' - R)} = \frac{L}{AR_s} \qquad 6.18$$

Where L is the height of the sample (m), A is the contact area between the sample and the sensor material (m^2), Rs is the resistance (KW^{-1}) of the sample material (powdered AC), k is its thermal conductivity ($Wm^{-1}K^{-1}$). To determine the extent of clogging of the pores and refrigerant affinity in performance improvement of the composite adsorbent paired with low-grade ethanol through a heat transfer and mass transfer, heating rate, and cooling rate were calculated using Equation 6.19 and 6.20.

$$Average\ cooling\ rate = \frac{T_{eva,initilal} - T_{eva,final}}{cycle\ time} \qquad 6.19$$

$$Average\ heating\ rate = \frac{T_{des,initial} - T_{des,final}}{cycle\ time} \qquad 6.20$$

Where $T_{eva,initilal}$ is the initial evaporator temperature (˚C), $T_{eva,final}$ is the initial evaporator temperature (˚C), $T_{des,initial}$ is the initial desorption temperature (˚C), $T_{des,final}$ is the final desorption temperature (˚C).

Stellenbosch University https://scholar.sun.ac.za

6.3 Results and discussion

6.3.1 Effect of NaCl on thermal conductivity of the adsorbents

Presence of NaCl in the pores of AC forming the AC + NaCl composites adsorbents had a significant effect ($p<0.05$) on the thermal conductivity of the AC + NaCl composite. The thermal conductivity increased with increase in the NaCl concentration (Table 6.2). For example, in Table 6.2 an increase of up to 2350% was achieved in AC composites with 25% NaCl compared to 500% with 10% NaCl. The thermal conductivity achieved with the mango seed husk AC was relatively higher than that for the untreated commercial AC (Table 6.2). This could be because the commercial AC was not treated. The granular form of the NaCl granule registered 5.12 $Wm^{-1}K^{-1}$ (Table 6.2), which is not too far from the 7 $Wm^{-1}K^{-1}$ reported in the literature for granular NaCl [159].

Table 6.2 Thermal conductivity of powdered adsorbents

Adsorbent	Thermal conductivity($Wm^{-1}k^{-1}$)	Improvements (%)
NaCl	5.12 ±0.6	N.A
Mango seed AC	$2.34 \times 10^{-4} \pm 1.12 \times 10^{-5}$ a	N.A
AC only	$2.15 \times 10^{-4} \pm 2.12 \times 10^{-5}$ a	N.A
AC +10 % NaCl	$1.19 \times 10^{-3} \pm 1.41 \times 10^{-5}$ b	500.0
AC +15 % NaCl	$1.42 \times 10^{-3} \pm 2.12 \times 10^{-5}$ c	600.0
AC +20 % NaCl	$2.25 \times 10^{-3} \pm 7.07 \times 10^{-5}$ d	1000.0
AC + 25% NaCl	$5.00 \times 10^{-3} \pm 1.41 \times 10^{-4}$ e	2350.0
AC + 30% NaCl	$5.40 \times 10^{-3} \pm 1.41 \times 10^{-4}$ f	2550.0
AC + 35.7 % NaCl	$5.95 \times 10^{-3} \pm 7.07 \times 10^{-5}$ g	2900.0

*Values with different superscripts are significantly different at $P<0.05$, Activated carbon = AC

Despite the differences in the actual value of the NaCl thermal conductivity, the trends for the thermal conductivity of the composite AC at different NaCl concentrations (Table 6.2) [65] were similar to what is reported in the literature [86–88] for other salts.

Stellenbosch University https://scholar.sun.ac.za

Notably, the NaCl filled up the pores in the composite AC (Figure 6.4), thus, decreasing the BET surface area, number of micropores and mesopores in comparison with commercial untreated AC (Table 6.3). During operation, as the NaCl concentration increases, the blockage of the pores increases, which initially limits the ethanol adsorption capacity of the composite adsorbents as temperature increases (Table 6.4).

Table 6.3 Adsorption characteristics of activated carbon before and after impregnation with NaCl

Adsorbent	**BET surface area (m^2g^{-1})**	**Micro pore volume (m^3g^{-1})**	**Mesopore+ macropore (cm^3g^{-1})**	**Total pore volume (cm^3g^{-1})**
AC only	1 237	0.4245	0.0104	0.4349
Mango seed AC	415	0.14	0.0	0.14
AC + 10% NaCl	1 129	0.3873	0.0058	0.3931
AC + 15% NaCl	1 120	0.3676	0.023	0.3906
AC + 20% NaCl	1 067	0.3653	0.0138	0.3791
AC + 25% NaCl	1 069	0.3552	0.0093	0.3645
AC + 30% NaCl	1 008	0.3078	0.0367	0.3445
AC + 35.7% NaCl	793	0.2902	0.0407	0.3309

Activated carbon = AC

Similar results have been obtained when silica gel and calcium chloride were impregnated into the pores of AC [79]. The clogging of the pores might be overcome by the affinity between the NaCl and the water in the mixture, thus facilitating the transfer of the ethanol through the pores. The implications of the NaCl impregnation on heat transfer and the transfer of the refrigerant are further discussed in the subsequent Sections.

Stellenbosch University https://scholar.sun.ac.za

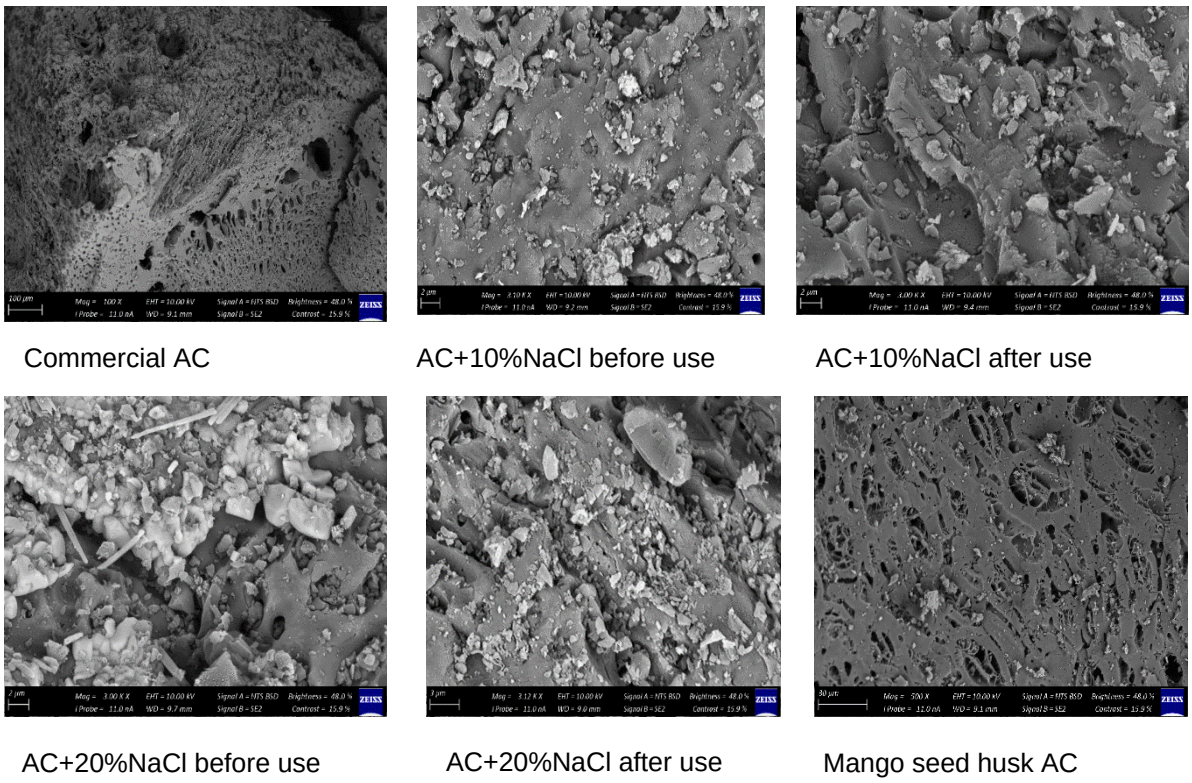

Commercial AC | AC+10%NaCl before use | AC+10%NaCl after use

AC+20%NaCl before use | AC+20%NaCl after use | Mango seed husk AC

Figure 6.4 SEM of some selected adsorbent. Note: AC= Activated carbon

6.3.2 Effect of NaCl impregnation on adsorption uptake, kinetics and heat of adsorption

The adsorption uptake for the various adsorbents paired with both high-grade and low-grade ethanol is shown in Figure 6.5. The adsorption uptake of the composite adsorbents decreased with increased NaCl concentration for both refrigerants as a result of the reduction in pore size as well as BET surface area (Fig 6.4, Table 6.3) when compared with commercial untreated AC. Mango seed husk AC, on the other hand, performed poorly in comparison with the composites adsorbents and commercial untreated AC due to less pore size and BET surface area. In addition, the adsorption uptake for all adsorbents tested paired with both low-grade and high-grade ethanol reduces with increase in temperature for both refrigerants.

Stellenbosch University https://scholar.sun.ac.za

Table 6.4 Adsorption uptake at different temperatures for both high-grade and low-grade ethanol

	Adsorption uptake ($kgkg^{-1}$) at different temperatures				
Adsorbent/refrigerant pairs	**25˚C**	**30 ˚C**	**35 ˚C**	**40 ˚C**	**45 ˚C**
AC/ethanol	0.7425	0.7332	0.6875	0.6689	0.6319
AC+10%NaCl/ethanol	0.6425	0.6352	0.6275	0.6139	0.6019
AC+15%NaCl/ethanol	0.6125	0.6032	0.5827	0.5689	0.5421
AC+20%NaCl/ethanol	0.6012	0.5832	0.5612	0.5471	0.5289
AC+25%NaCl/ethanol	0.5913	0.5762	0.5545	0.5349	0.5119
AC+30%NaCl/ethanol	0.5385	0.5187	0.4918	0.4731	0.4419
AC+35.7%NaCl/ethanol	0.5025	0.4912	0.4775	0.4639	0.4419
Mango seed AC/ethanol	0.2325	0.2132	0.2045	0.1809	0.1559
AC/impure ethanol	0.7225	0.7192	0.6975	0.6789	0.6569
AC+20%NaCl/impure ethanol	0.6213	0.6061	0.5895	0.5699	0.5509
AC+25%NaCl/impure ethanol	0.6075	0.5812	0.5625	0.5529	0.5209
AC+30%NaCl/impure ethanol	0.5465	0.5192	0.5086	0.4979	0.4619
Mango seed AC/impure ethanol	0.2375	0.2162	0.2045	0.1799	0.1579

Note: The low-grade ethanol was tested at three points: 0, 20, 25, 30% NaCl Concentration

This reduction is due to the increase in kinetic energy of the refrigerant molecules which weakens the van der Waals forces that attract the refrigerant to the adsorbent leading to the reduction in adsorption uptake [69,73]. Furthermore, comparison of the adsorption uptake for a particular adsorbent paired with both high-grade and low-grade ethanol reveals that the composite adsorbents performed slightly better when paired low-grade ethanol than when paired with high-grade ethanol. This is may be attributed to the presence of NaCl in the pores attracts the water component of the refrigerant

Stellenbosch University https://scholar.sun.ac.za

(chemisorption) which facilitates adsorption of more water component of the refrigerant until a critical temperature is reached [69,73]. This has led to an increase in adsorption rate and adsorption heat (Tables 6.5 & 6.7) of composite adsorbents paired with low-grade ethanol in comparison with high-grade ethanol and reduction in adsorption time.

Table 6.5 Adsorption rate of the adsorbents paired with high-grade and low-grade ethanol

Adsorbent/refrigerant pairs	**Adsorption rate (kgs^{-1})**
AC/ethanol	2.174×10^{-4}
AC+10% NaCl/ethanol	1.750×10^{-4}
AC+15% NaCl/ethanol	1.696×10^{-4}
AC+20% NaCl/ethanol	1.637×10^{-4}
AC+25% NaCl/ethanol	1.699×10^{-4}
AC+30% NaCl/ethanol	1.330×10^{-4}
AC+35.7% NaCl/ethanol	1.122×10^{-4}
Mango seed AC/ethanol	1.917×10^{-4}
AC/impure ethanol	1.840×10^{-4}
AC+20% NaCl/impure ethanol	2.967×10^{-4}
AC+25% NaCl/impure ethanol	2.500×10^{-4}
AC+30% NaCl/impure ethanol	3.144×10^{-4}
Mango seed AC/impure ethanol	1.920×10^{-4}

AC=Activated carbon

Note: The low-grade ethanol was tested at three points: 0, 20, 25, 30% NaCl Concentrations

The values in Table 6.4 were used to fit data for the adsorption capacity of the adsorbent paired with both high-grade and low-grade ethanol using Equations 6.1 to

Stellenbosch University https://scholar.sun.ac.za

6.7. The Dubinin-Astakhov (D-A) equation fitted parameters for the tested adsorbent paired with the refrigerants are shown in Table 6.6.

Table 6.6 Adsorption isotherm parameters of the adsorbents paired with both high-grade and low-grade ethanol

Adsorbent/refrigerant pairs	E (kJkg-^{1})	n	Predicted Equilibrium uptake (W_o) (kgkg^{-1})	Equilibrium uptake (W) (kgkg^{-1})	Uptake deviation %
AC/ethanol	205	1.60	0.7866	0.7425	5.9
AC+10% NaCl/ethanol	386	1.70	0.6548	0.6425	1.5
AC+15% NaCl/ethanol	260	1.72	0.6341	0.6125	3.5
AC+20% NaCl/ethanol	237	1.75	0.6185	0.6012	2.9
AC+25% NaCl/ethanol	222	1.80	0.6121	0.5913	3.5
AC+30% NaCl/ethanol	188	1.76	0.5651	0.5385	4.9
AC+35.7% NaCl/ethanol	224	2.00	0.5164	0.5025	2.8
Mango seed AC/ethanol	127	1.90	0.2644	0.2325	13.7
AC/impure ethanol	304	1.65	0.7308	0.7225	1.1
AC+20% NaCl/impure ethanol	316	1.60	0.6288	0.6213	1.2
AC+25%NaCl/impure ethanol	316	1.60	0.6106	0.6075	0.5
AC+30% NaCl/impure ethanol	266	1.65	0.5497	0.5465	0.6
Mango seed AC/impure ethanol	118	1.70	0.2477	0.2375	4.3

Note: The low-grade ethanol was tested at three points: 0, 20, 25, 30% NaCl Concentrations

From the results, the commercial AC has the maximum predicted adsorption capacity, which reduce with the decrease in BET surface area as well as pore size. Furthermore, the values of n fall within the range of 1.6-2.0 expected for Dubinin-Astakhov (D-A)

Stellenbosch University https://scholar.sun.ac.za

model [84]. The Clausius-Clapeyron equation (Equation 6.14) was used to estimate the heat of adsorption for the adsorbents paired with both the high-grade and low-grade ethanol. Using this equation (Equation 6.14), a graph of $\partial \ln P$ vs $\partial\left(\frac{1}{T}\right)$ were generated (Fig 6.5). The values of pressure and temperature were obtained from direct measurement during the adsorption process described in Section 6.2.4. By multiplying the slope of these graphs with the gas constant of the respective refrigerant, values of heat of adsorption were obtained as shown in Table 6.7. The results in Table 6.7 show that when the BET surface area and pore size reduced, the heat of adsorption increases. However, the heat of adsorption is higher for adsorbents paired with low-grade ethanol compared with high-grade ethanol. This could be due to a strong affinity for water in case of composite adsorbents paired with low-grade ethanol. Secondly, Uddin [84]suggested that reduction is pore size results in stronger interaction between the refrigerant and the adsorbent. Thus, adsorbents with narrower pore size produce higher heat of adsorption. In the case of adsorbents paired with high-grade ethanol, the values obtained are a bit less than those obtained in the literature (between 1026-1104 [81,84]) obtained for commercial AC paired with high-grade ethanol. Despite slightly higher literature values for the heat of adsorption of AC paired with high-grade ethanol than the results obtained in this study, it has been suggested that as the adsorption continues over time, the heat of adsorption approaches the latent heat vaporization of the refrigerant [84,251]. Thus, the closer the heat of adsorption values are to the latent heat vaporization value the better.

Stellenbosch University https://scholar.sun.ac.za

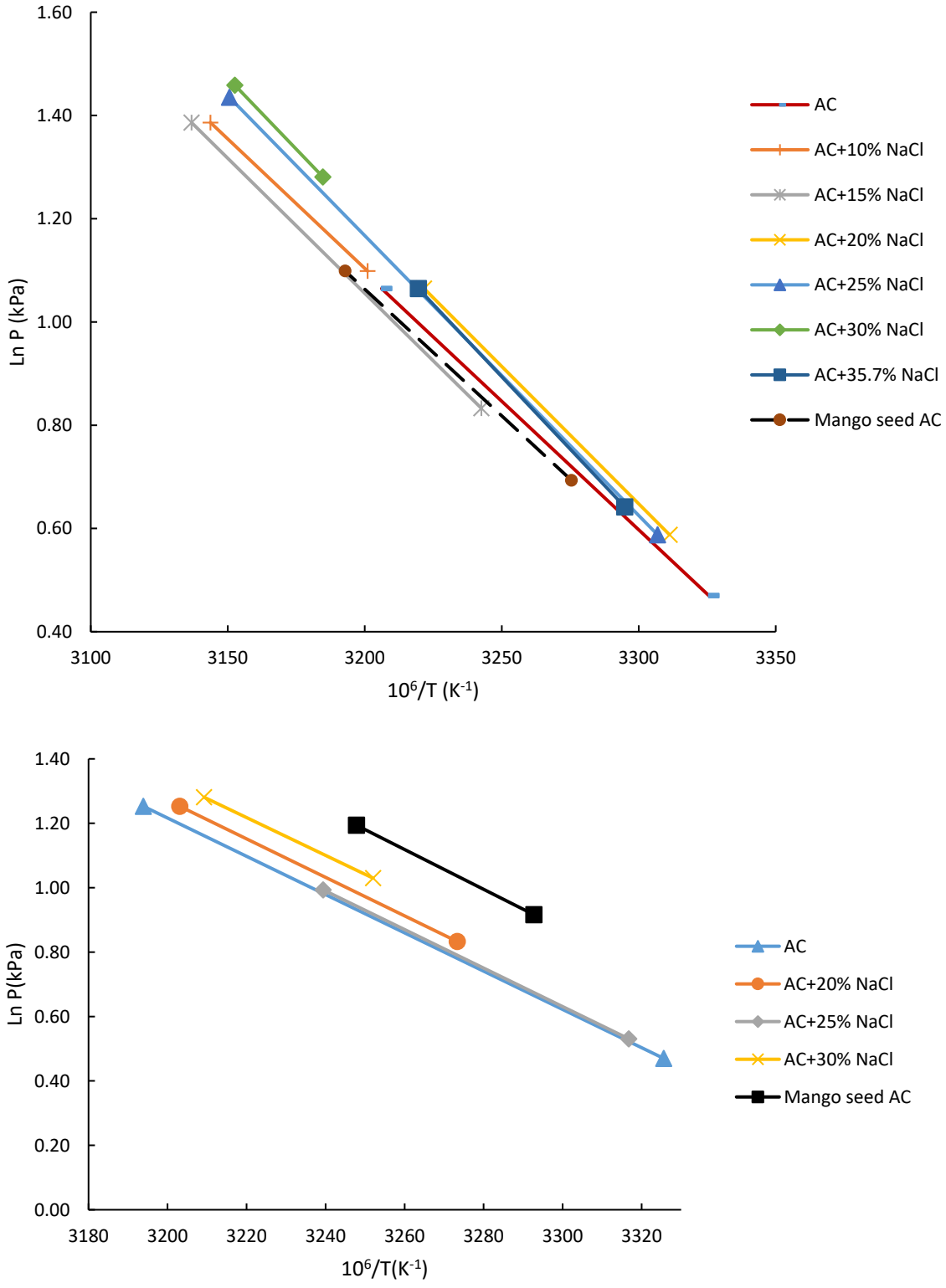

Figure 6.5 Plot of LnP vs I/T for adsorbents paired with (a) high-grade ethanol (b) low-grade ethanol. Note: The low-grade ethanol was tested at three points: 0, 20, 25, 30% NaCl Concentration

Stellenbosch University https://scholar.sun.ac.za

Table 6.7 Heat of adsorption of the adsorbents paired with both high-grade and low-grade ethanol

Adsorbent/refrigerant pairs	Heat of adsorption($kJkg^{-1}$)
AC/ethanol	900
AC+10% NaCl/ethanol	921
AC+15% NaCl/ethanol	943
AC+20% NaCl/ethanol	962
AC+25% NaCl/ethanol	980
AC+30% NaCl/ethanol	999
AC+35.7% NaCl/ethanol	1017
Mango seed AC/ethanol	886
AC/impure ethanol	1420
AC+20% NaCl/impure ethanol	1425
AC+25% NaCl/impure ethanol	1428
AC+30% NaCl/impure ethanol	1435
Mango seed AC/impure ethanol	1415

Note: The low-grade ethanol was tested at three points: 0, 20, 25, 30% NaCl Concentrations

6.3.3 Effect of NaCl on activated carbon/ethanol pair cycle time in the adsorption cooling system

Cycle time was measured as the sum of adsorption and desorption times. Comparison of the cycle times of untreated commercial AC and its composite paired with high-grade ethanol reveals that the cycle time of the adsorption cooler reduced from about 4000 seconds for untreated commercial AC to about 3200 seconds when AC + NaCl (35.7%) composite was used as adsorbents paired with high-grade ethanol as a

Stellenbosch University https://scholar.sun.ac.za

refrigerant (Fig 6.6). The reduction in the cycle time increased with increased NaCl concentration. Such an effect is a confirmation of increased heat transfer performance of the AC + NaCl composites adsorbents compared to pure AC (Fig 6.6). The results can be attributed to the possible reduction of intra-granular thermal resistance and pore size (Fig 6.4, Table 6.3) of the AC + NaCl composites formed which has led to the reduction in the adsorption uptake as NaCl increases (Table 6.4). Furthermore, the NaCl is sparingly soluble in ethanol [252] such that during the adsorption process, the NaCl inside the AC pores reacts with adsorbed ethanol vapour according to the gas-solid reaction (Equation 6.21):

$$NaCl_s + nC_2H_5OH_g \rightarrow NaCl.nC_2H_5OH \qquad 6.21$$

Equation 6.21 suggests the formation of a layer containing NaCl-ethanol on the surface of the grain [253] with increased heat transfer properties. The reduction in the cycle time is in agreement with similar studies by Askalany et al [254] where metal filings with high thermal conductivity (iron, copper, aluminium) were added to AC to form composite adsorbents paired with hydro-fluorocarbon (HFC-R407C) as a refrigerant. Notably, the cycle time followed a similar trend to studies by Askalany et al [254], despite the different high heat transfer material used (NaCl) in this study. In the study, the cycle time for pure AC of 3000 seconds reduced to about 1600 seconds when the percentage of the metal filings increased to about 30% [254]. The results follow similar trend achieved in an optimized prototype ACS employing pure AC paired with pure ethanol [255], suggesting the potential of obtaining even greater reduced time if the current system is optimized.

Stellenbosch University https://scholar.sun.ac.za

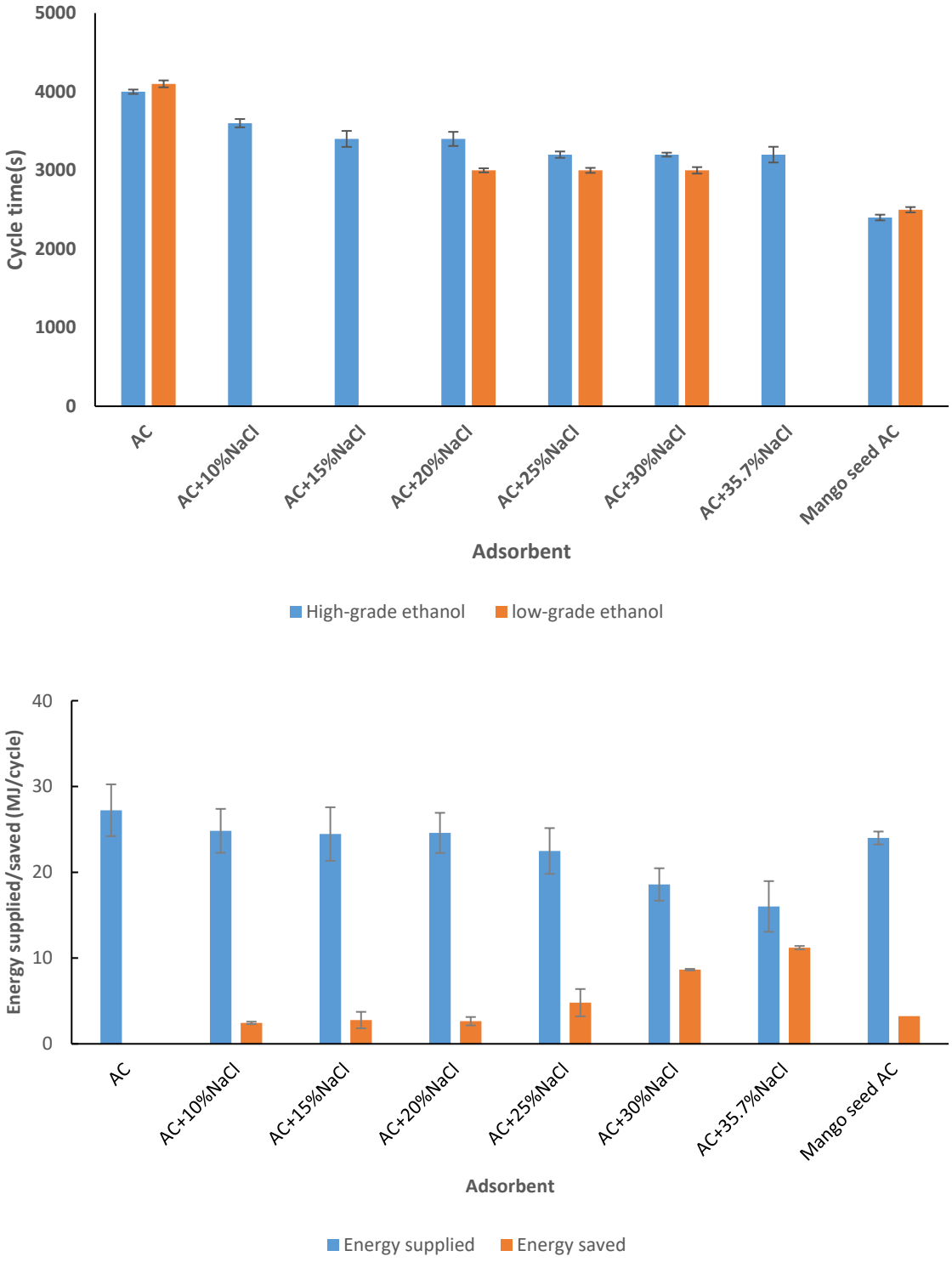

Figure 6.6 (a) Cycle time and (b) energy supplied when adsorbents are paired with both high-grade and low-grade ethanol. Note: The low-grade ethanol was tested at three points: 0, 20, 25, 30% NaCl Concentration

Stellenbosch University https://scholar.sun.ac.za

Corresponding to the reduced cycle time, the amount of energy input during the desorption process reduced significantly in comparison with the pure AC (Fig 6.6b). About 27 MJ/cycle of thermal energy was utilized during the desorption process when untreated commercial AC was used as the adsorbent while about 80% of that amount was utilized when AC composite with 35.7 % (w/v) NaCl was used (Fig 6.6b). Therefore, such reduced energy use can be due to improved heat transfer ability of the adsorbents attributed to the reduced intra-granular thermal resistance coupled with the high thermal conductivity of the adsorbent. Secondly, the reduction in energy supplied may also be attributed to the increase in adsorption heat as NaCl increases which reduces the amount of refrigerant adsorbed (Table 6.4), and subsequently decreased the energy supplied desorb the refrigerant (Fig 6.6).

Similar reasons could be used to explain the reduction in cycle time when untreated commercial AC and its composite were paired with low-grade ethanol. In the case of mango seed husk AC, its cycle time and energy supplied is lower when compared with the commercial untreated AC. This may be due to its lower pore size, surface area, and adsorption uptake.

6.3.4 The overall performance of adsorption cooling system using adsorbents paired with high-grade ethanol (99.7%)

Evidently, the formation of AC+NaCl composite as adsorbent paired with high-grade ethanol refrigerant, despite improving the thermal conductivity of the AC, thus, increasing the heat transfer, impeded the mass transfer of the refrigerant. The results show that the SCP of the adsorption cooler decreased from 84.5 Wkg^{-1} for untreated commercial AC to 39.5 Wkg^{-1} when the AC formed a composite with NaCl (35.7 % w/v) (Fig 6.7b). Similarly, the COP of the ACS decreased with increasing concentration

Stellenbosch University https://scholar.sun.ac.za

of the NaCl in the composite (Figure 6.6a). The higher value of COP and SCP recorded for untreated commercial AC may be due to the higher adsorption uptake rate of the untreated commercial AC compared with the other adsorbents (Table 6.4 & 6.5). A similar trend was reported for untreated commercial AC where the COP of the adsorption system decreased from 0.67 to 0.41 with the use of the AC in a composite with $CaCl_2$ [6] [6]. El-Sharkawy et al [81] also studied ACS with AC paired with ethanol and found out that the COP ranged between 0.7-0.8 [81]. Values of COP and SCP of other previous studies are shown in Table 6.1. The reduction in COP in this study is associated with the reduction in the number of available pores on the adsorption bed which lead to increase in adsorption heat (Table 6.7), consequently, reducing the amount of ethanol adsorbed. The presence of the NaCl most likely blocks the ethanol vapour from reaching the micropores of the AC or its leaching into the refrigerant negatively affects the amount of ethanol adsorbed. As a result, the ethanol vapour adsorbs onto the surface of the NaCl salt inside the micropore and condenses to form a layer containing NaCl and ethanol as expressed in Equation 6.21. Such a layer is may also contribute to reducing the transfer of ethanol to beneath the surface layer.

The reduction in mass transfer implies the reduced amount of ethanol vapour absorbed, thus, decreasing the temperature drop in the evaporator and the COP (Fig 6.7a and 6.7c). Gordeeva et al [253] found out that methanol adsorption by a LiCl-AC composite reduced as methanol solution began to form a layer close to the surface of the composite grains resulting in agglomerations [253]. Furthermore, the results from the experiments (Fig 6.6) showed that as the NaCl concentration increased, less ethanol was adsorbed. Thus, the results apply to areas where AC is easily accessible.

Stellenbosch University https://scholar.sun.ac.za

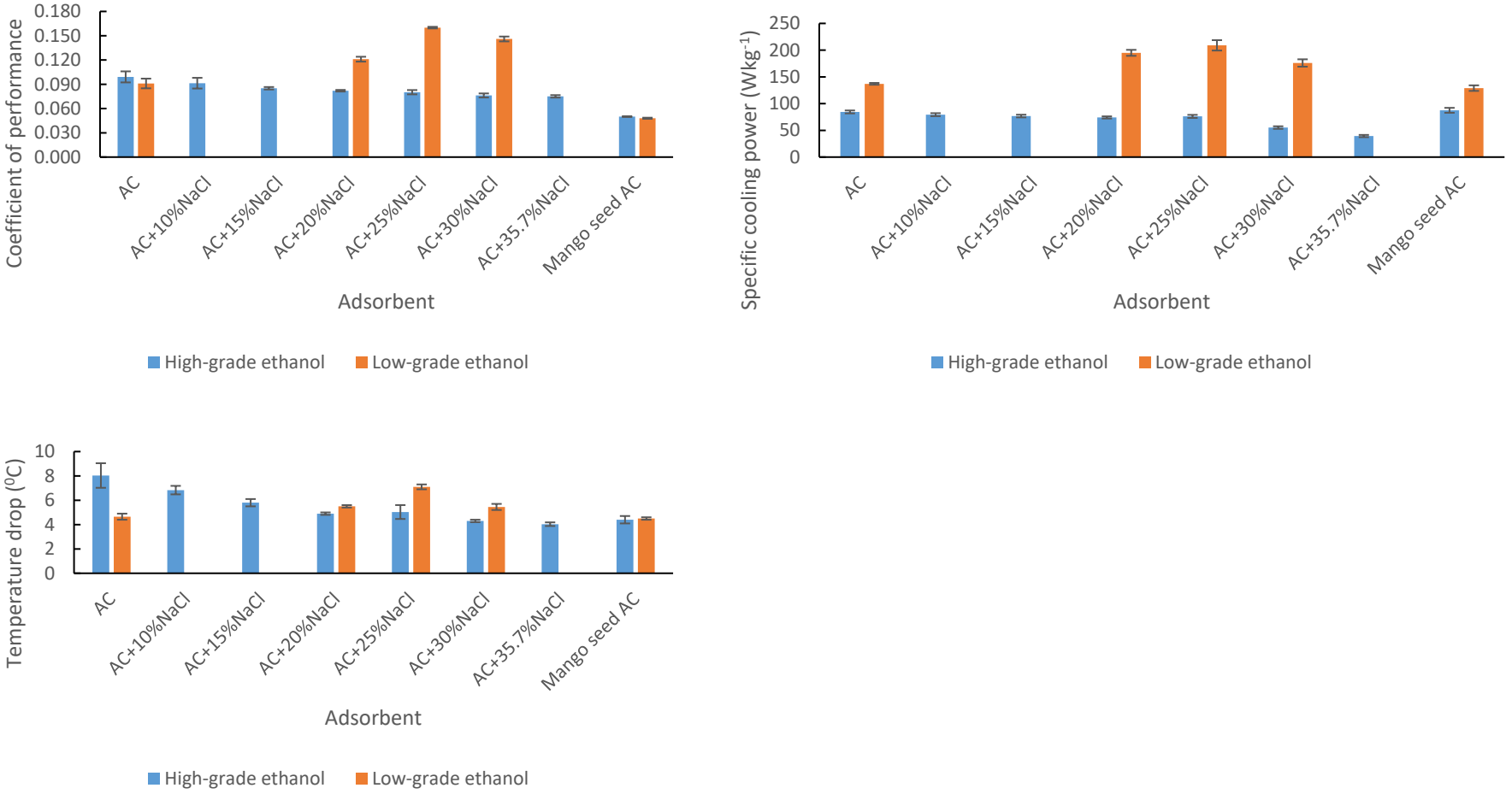

Figure 6.7 Comparison of performance of adsorption cooler using selected AC-sodium chloride (AC +NaCl) composite as adsorbent paired with high purity ethanol and low-grade ethanol as refrigerants (a) Coefficient of performance (b) Specific cooling power (c) Temperature drop. Note: The low-grade ethanol was tested at three points: 0, 20, 25, 30% NaCl Concentration

Stellenbosch University https://scholar.sun.ac.za

However, where AC is not accessible, but silica gel is readily available, using pure water as refrigerant paired with silica gel+ NaCl composite would eliminate the limitations of the AC +NaCl composites. In addition, Wang et al [241] observed the formation of the liquid layer on the surface of $CaCl_2$-expanded graphite adsorbent, which reduced the mass transfer of ammonia to the layer beneath [121]. Therefore, improvements in heat transfer performance of the adsorbents of the cooler do not necessarily translate into an improved mass transfer of the refrigerant. An integrated approach that considers both the thermal and mass transfer properties of the adsorbent and refrigerant is necessary to achieve better overall performance for both heat transfer and mass transfer in the system. In addition to enhancing heat transfer properties, the advantage of using the AC adsorbent in a composite with chlorides is realized from its attraction to water as discussed in the subsequent Section. The performance of mango seed husk AC, on the other hand, is inferior to both the untreated commercial AC and the composites. The SCP and COP recorded for mango seed husk AC was 0.048 and 87.5 Wkg^{-1} respectively. This inferior performance may be due to the low pore size and surface area of the mango seed husk AC.

6.3.5 Overall performance of adsorption cooling system using adsorbents paired with low-grade ethanol (60% ethanol and 40% water).

The use of composite AC and low-grade ethanol was characterized by improvements in both heat and mass transfer and rise in heat of adsorption. Composite AC with 20%, 25% and 30% NaCl concentration were the top three performing adsorbents with relatively high SCP when compared with AC with 35.7% NaCl paired with high-grade (99.7%) ethanol (Fig 6.7b). However, when these AC+NaCl composites were paired with low-grade ethanol (60% ethanol), which contained 40% water, the SCP was higher, 123 Wkg^{-1}, 150 Wkg^{-1}, and 113 Wkg^{-1}, respectively (Figure 6.7b) than when

Stellenbosch University https://scholar.sun.ac.za

paired with high-grade ethanol, 74 Wkg^{-1}, 76 Wkg^{-1} and 55 Wkg^{-1}, respectively(Fig 6.7b). Furthermore, the COP of the composite AC containing 20%, 25% and 30% NaCl paired with low-grade ethanol were 0.121, 0.160 and 0.146, respectively (Fig 6.7a), higher than when paired with high purity ethanol, thus 0.082, 0.080, and 0.076, respectively (Fig 6.7a).

The improved performance of the ACS with carbon+NaCl composites/low ethanol grade pair is attributed to the ability of the NaCl to attract the water fraction from the low-grade ethanol in its pores [79,256] through diffusion, thereby increasing the mass transfer, thus enhanced adsorption of the refrigerant. Since latent heat of vaporization of water is about 60% higher than that of water, the more water attracted from the low-grade ethanol the faster higher the mass transfer (see adsorption rate in Table 6.5) and the faster cooling effect is achieved. Consequently, higher temperature drops (Fig 6.7c) were achieved in the adsorption cooler with ethanol/water mixture as a refrigerant than when the composite adsorbent was paired with high purity ethanol as the refrigerant (Fig 6.7c). Besides, the type of adsorption that occurs between the water molecules and the NaCl is chemisorption, which is enhanced when the adsorption heat is increased until a critical temperature is reached [69]. Thus, increasing NaCl concentration resulted in a corresponding increase in water adsorption due to the rise in the heat of adsorption and blockage of pores as NaCl concentration increases (Table 6.7). Furthermore, when the untreated AC is paired with low-grade ethanol COP value of 0.091 (Fig 6.7a) is obtained which is comparable to the COP of 0.099 obtained when untreated AC was paired with high purity ethanol (Fig 6.7a). Similar behaviour could be observed when mango seed husk AC was paired with both high-grade and low-grade ethanol, though mango seed husk AC recorded low COP values. This behaviour may be due to the dual adsorption of water

Stellenbosch University https://scholar.sun.ac.za

and ethanol from the water-ethanol mixture, which is a typical phenomenon in such mixture [71]. A study by Dreisbach et al [71] indicated that at reduced pressure (1 kPa); water, although very little, is adsorbed by the AC, which condenses inside the micropores of the AC thus, blocking the adsorption of the ethanol. Such behaviour results in reduced SCP (75.5 Wkg^{-1}) and temperature drop (4.7 $^{\circ}C$) (Fig 6.7b&c) because of the longer time it takes to evaporate the refrigerant [71]. The COP values for the AC paired with pure ethanol is comparable to values of between 0.07 and 0.097 obtained by Frazzica et al [255] in a prototype ACS that employed similar adsorbent-pure ethanol refrigerant pair. Thus, low-grade ethanol could be paired with untreated AC where high purity ethanol is not accessible to obtained comparable COP and about 50% temperature drop.

The results have shown that AC+NaCl composites paired with low-grade ethanol outperform the non-composite adsorbents paired with both high-grade and low-grade ethanol, most probably because of the dual role the NaCl play in enhancing the diffusion of the water through the pore and increase in thermal conductivity of the water though the adsorbent and the increased heat transfer. The dynamics of such a dual system in the adsorption system are subject to further research. Otherwise, the pairing of the activated + NaCl composite with low-grade ethanol as a refrigerant is a potential alternative adsorption-refrigerant pair that can be employed in ACSs for off-grid communities that produce own low-grade ethanol without the need for expensive upgrading.

Stellenbosch University https://scholar.sun.ac.za

6.3.6 Heat and Mass transfer dynamics in adsorption cooling using AC+NaCl composite adsorbents paired with low-grade ethanol (60% ethanol and 40% water).

The results discussed earlier showed that the composite formation with NaCl resulted in performance improvement when paired with low-grade ethanol due to improvement in heat and mass transfer. The result in Figure 6.8 shows that the performance improvement of the composite paired with low-grade ethanol is largely due to the heat transfer improvement brought about by clogging of some of the pores with the NaCl, which resulted in high heating rate in the adsorber. Cooling rate, on the other hand, occurred due to the affinity of the composite adsorbents and the low-grade ethanol, resulting in lowering of temperature in the storage chamber. Thus, the clogging of the pores by the NaCl contributes more to performance improvement than the affinity between the composite adsorbents and the low-grade ethanol (Fig 6.8). Therefore, the combination of the heating rate and cooling rate provides the net performance of the ACS.

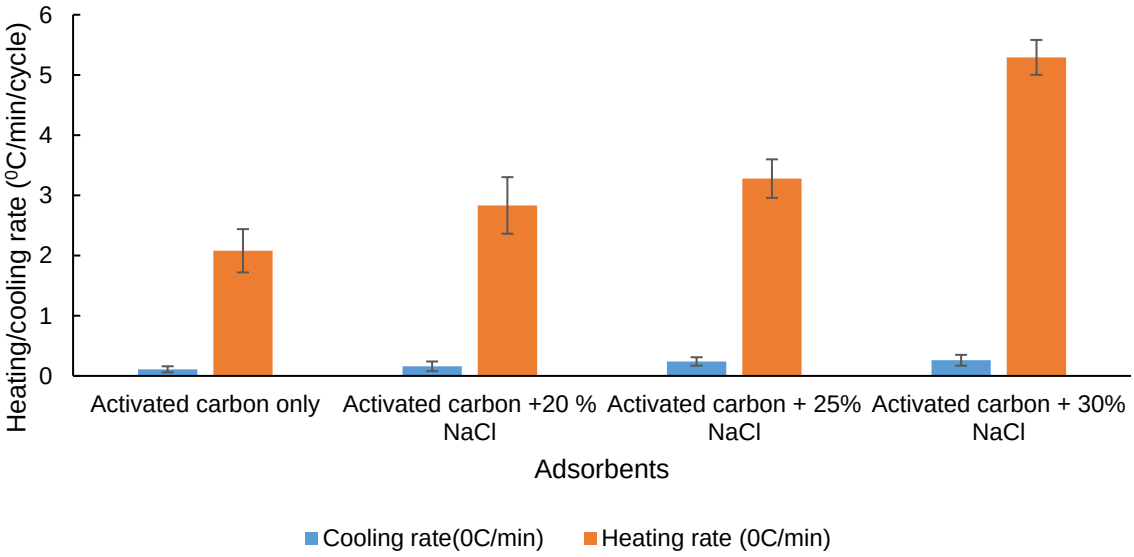

Figure 6.8 Cooling rate and heating rate of selected adsorbents paired with low-grade ethanol

Stellenbosch University https://scholar.sun.ac.za

6.4 Conclusion

The improved heat and mass transfer when AC + NaCl composite enabled low-grade ethanol to be used as an alternative refrigerant that is tailor-made for off-grid conditions with limited access to high-grade refrigerants. Furthermore, the use of impure ethanol as refrigerant provides a viable means of promoting micro scale distilleries factor that can facilitate the adoption and ownership of the technology. It is also evident that waste biomass such as mango seeds can provide adequate energy to run an adsorption cooler with AC + NaCl composite adsorbents paired with ethanol, thus a resource efficient ACS is possible.

Furthermore, the results experiments showed that as the NaCl concentration increased, less ethanol was adsorbed. Thus, the results apply to areas where AC is easily accessible. However, where AC is not accessible but silica gel is readily available, using pure water as refrigerant paired with silica gel+ NaCl composite would eliminate the limitations of the AC +NaCl composites.

6.5 Recommendations for improvement of the adsorption cooling system using AC-NaCl composite adsorbents paired with low-grade ethanol

The performance of the current systems and its practical use is subject to further improvements. The untreated AC/pure ethanol pair was used as the benchmark to assess the performance of composite adsorbents/refrigerant pairs, however, the system should be validated commercial chillers that use similar adsorbent/refrigerant pairs operating under the same conditions. In addition, the combustion chamber for the ACS should be enclosed to improve fuel conversion efficiency. Ultimately, configuring the ACS to use rejected heat from unit operations such as the drying process would make the system more efficient. The use of NaCl should be used with

Stellenbosch University https://scholar.sun.ac.za

caution considering that in high concentration may have adverse effects on the environment. Moreover, it has been observed that there was about 5-27% increase in weight of the AC after impregnation with NaCl. About 1-5% decrease in weight of the composite AC after the experiments due to leaching. The leached NaCl (which remains in the adsorber as NaCl evaporation temperature is not reached during desorption) may cause corrosion stainless steel adsorber unit after multiple cycles. Although the risk of using ethanol is limited because the ACS is a closed system operating under vacuum, thus the pressure within the system is less than the atmospheric pressure, it is important to avoid any external leakage as this could affect system efficiency.

Stellenbosch University https://scholar.sun.ac.za

Stellenbosch University https://scholar.sun.ac.za

Chapter 7 An integrated strategy targeting drying and cooling unit operations to improve economic viability and reduce environmental impacts in a mango processing plant

ABSTRACT

An Integrated strategy of replacing boiler fuel and vapour compression cooling technology in dried mango chips processing plant powered on-grid and off-grid was investigated. Three scenarios for each power setting were studied, on-grid: coal as boiler fuel and conventional vapour compression chiller (CVCC) for cooling (Scenario 1), mango seed as boiler fuel and CVCC for cooling (Scenario 2) and mango seed as boiler fuel and adsorption cooling system (ACS) for cooling (Scenario 3). Off-grid scenarios 4, 5 and 6 corresponded to on-grid scenarios 1, 2 and 3, respectively. Greenhouse gas (GHG) emissions and economic viability for each scenario were based on material and energy balances and South African economic conditions, respectively. On-grid scenario 3 showed the greatest potential for reducing emissions, emitting 7.10×10^5 $kgCO_2eq$ per annum and had the best internal rate of return (IRR) of 25.33% compared to scenarios 2 and 1 with 7.21×10^5 $kgCO_2eq$ and 7.89×10^5 $kgCO_2eq$ emissions per annum and IRR of 20.33% and 17.48%, respectively. In off-grid, scenario 6 emitted the least GHG of 6.90×10^5 $kgCO_2eq$ and had highest IRR of 24.84% compared to scenarios 5 & 4 with 6.98×10^5 $kgCO_2eq$ and 7.67×10^5 $kgCO_2eq$ emissions per annum and IRR of 18.88% and 16.09%, respectively. However, scenarios 3 and 6 had the highest energy demand due to mango seed drying. Nevertheless, the integrated intervention shows a great potential of reducing environmental impacts and improving the economic viability of a dried mango chips

Stellenbosch University https://scholar.sun.ac.za

processing plant by using renewable biomass fuel and ACS that utilizes boiler waste heat. Mango seed can be solar dried to reduce increased energy demand.

7.1 Introduction

Mango is one of the major tropical fruits produced worldwide [257] and a source of livelihood for many people [1]. The fruit provides nutrient such as Vitamins A and C, potassium and dietary fibre [258] and contributes towards reducing food and nutrition insecurity. Due to high perishability and seasonal availability, mango is processed into stable forms such as dried chips to extend shelf life and consumption period. Drying and cooling are the most energy-intensive unit operations in a dried mango chips processing plant. The energy may be derived from several sources such as fossil fuel and renewable sources. Some of the energy sources may not be readily available in many mango growing communities in the required form and quantities, resulting in both economic and environmental implications. In addition, utilization of grid electrical energy as well as off-grid fossil fuel sources like diesel and petrol, contribute to carbon dioxide emissions [180]. The level of environmental impacts for different energy sources differs depending on the type and source of fuel [259]. For example, the amount of CO_2 emitted from diesel and coal are 7.41×10^{-5} $kgkJ^{-1}$ and 9.46×10^{-5} $kgkJ^{-1}$ of energy produced, respectively [259]. Renewable energy options such as solar and wind although with a relatively lesser damaging effect on the environment than fossil fuels, their availability might not be reliable [114]. Other renewable energy sources such as geothermal have high capital costs (between US$ 1,500 to US$ 3,000 per kW) [115] whereas, hydro energy is dependent on the availability of sources of water such as rivers [114]. Therefore, biomass energy derived from waste streams of dry mango processing can be considered in the energy mix for the processing plant. Therefore, it is imperative to assess the potential impacts the use of biomass energy

Stellenbosch University https://scholar.sun.ac.za

would have on the sustainability of the mango processing in terms of economic, environmental and social impacts when used a fuel boiler.

Mango seed is a carbon-neutral energy source [260]. About 540×10^3 kg of seeds is generated as waste from processing 86.4×10^6 kg of mango fruits into dry chips. These mango seeds can be used to substitute or partially substitute coal or electricity to reduce the fossil fuel energy demand for the boiler and associated greenhouse gas emission. The mango seed has energy content (21.74 $MJkg^{-1}$) [117] that is comparable to coal (18.0-25.5 $MJkg^{-1}$) [117]. Besides, the utilization of mango seed waste as a heat source can be an economical way of reducing the problem of waste disposal [12]. Energy demand during the mango processing can further be reduced through heat recovery, which can be used in other unit operations such as cold storage, within the process. The boiler generating power for the drying section of the mango processing loses about 10-30% energy from the flue gas exiting at up to 250 ˚C (it is not advisable the decrease the temperature of flue gas below 140 ˚C, as this will result in the formation of water droplets and the corrosion of the boiler) in the form of waste heat [261], which can be recovered to power the cold storage, as a strategy to reduce total energy demand and cost and its associated negative environmental impacts. Therefore, cooling and drying are two critical unit operations that can be integrated to reduce negative environmental impacts and improve the economic benefits associated with mango processing. Considering that the conventional vapour compression chiller (CVCC) uses refrigerants, which contribute to the degradation of the environment [218], further reduction of negative environmental impacts is to use alternative cooling technology that does not rely on the fossil-based material to operate. Many studies have been done to find such alternative cooling technologies to replace the conventional cold storage technology [262]. One of such alternative

Stellenbosch University https://scholar.sun.ac.za

technology is the adsorption cooling system (ACS) that uses environmentally benign refrigerants [82] and can be powered by the waste heat generated from the boiler exhaust stream, thus making it a potential low-cost chiller. However, new environmental and social risks would emerge with such a transition. Therefore, this study investigates the economic and environmental benefits of replacing the CVCC with the low-cost adsorption cooling chiller (LCAC) as well as coal with mango seed as boiler fuel in the mango processing in both on-grid and off-grid power setting to ascertain their potential impacts on dry mango processing plant. In this study, on-grid power setting refers to the power situation where the electrical energy required to run the electrical equipment used in the processing of the mango is derived from the national grid while in the off-grid setting the electrical power required is provided by diesel electricity generator.

7.2 Methodology

7.2.1 Description of the dried mango chips production

A brief description of the dried mango chips processing is as follows: Fresh matured mangoes are sorted out and washed in hot water at a 50˚C temperature to destroy eggs and larvae of flies and to reduce bacteria load to help prolong the shelf life [258]. The treated mangoes are immediately cooled and stored at about 10-12˚C to prolong its shelf life of the mango and to regulate the demand for the processed final product [258]. Depending on the demand for the dried mango chips, the mangoes are taken from storage and ripened at room temperature (25˚C) to the level of ripening desired by the processor, washed to remove any dirt on the mango surface, peeled and cut into sizes rages 0.02-0.08 m [258], dried at 65˚C using steam (at 2-3 kPa) generated from combustion of coal. The final product of moisture content of about 20% (wet

Stellenbosch University https://scholar.sun.ac.za

basis) is packaged for onward distribution and selling. The process flow sheet to produce the dried mango chips under different energy and cooling scenarios is shown in Figure 7.1.

7.2.2 Scenarios description

The approach to economic and environmental analyses comprised process modelling of the production of dried mango chips in both on-grid and off-grid communities. From these two power settings, three scenarios each were created and analyzed. A brief description of each scenario is shown in Table 7.1. Analysis of each scenario was done by following the steps in Figure 7.2. Available information from literature was used to synthesize the process flow sheet, followed by material and energy balance (performed in Microsoft Excel 2010) for each scenario. The data generated from the material and energy balance, as well as information from equipment manufacturers, were used to select and size the equipment. Equipment price quotations from equipment suppliers were used to estimate the fixed capital cost of the various processing scenarios.

7.2.3 Material and energy balance

In performing materials and energy balance calculations, the composition of mango (weight %), process conditions and mass and energy conversion efficiencies were adopted from literature as referenced in the subsequent sections and additional information is available as supplementary data (Tables C1, C2, and C3 in the Appendix). Where information was not available, data were collected from a commercial dried mango chips processor (Table C2). Only energy utilized directly in each process was considered and estimated.

Stellenbosch University https://scholar.sun.ac.za

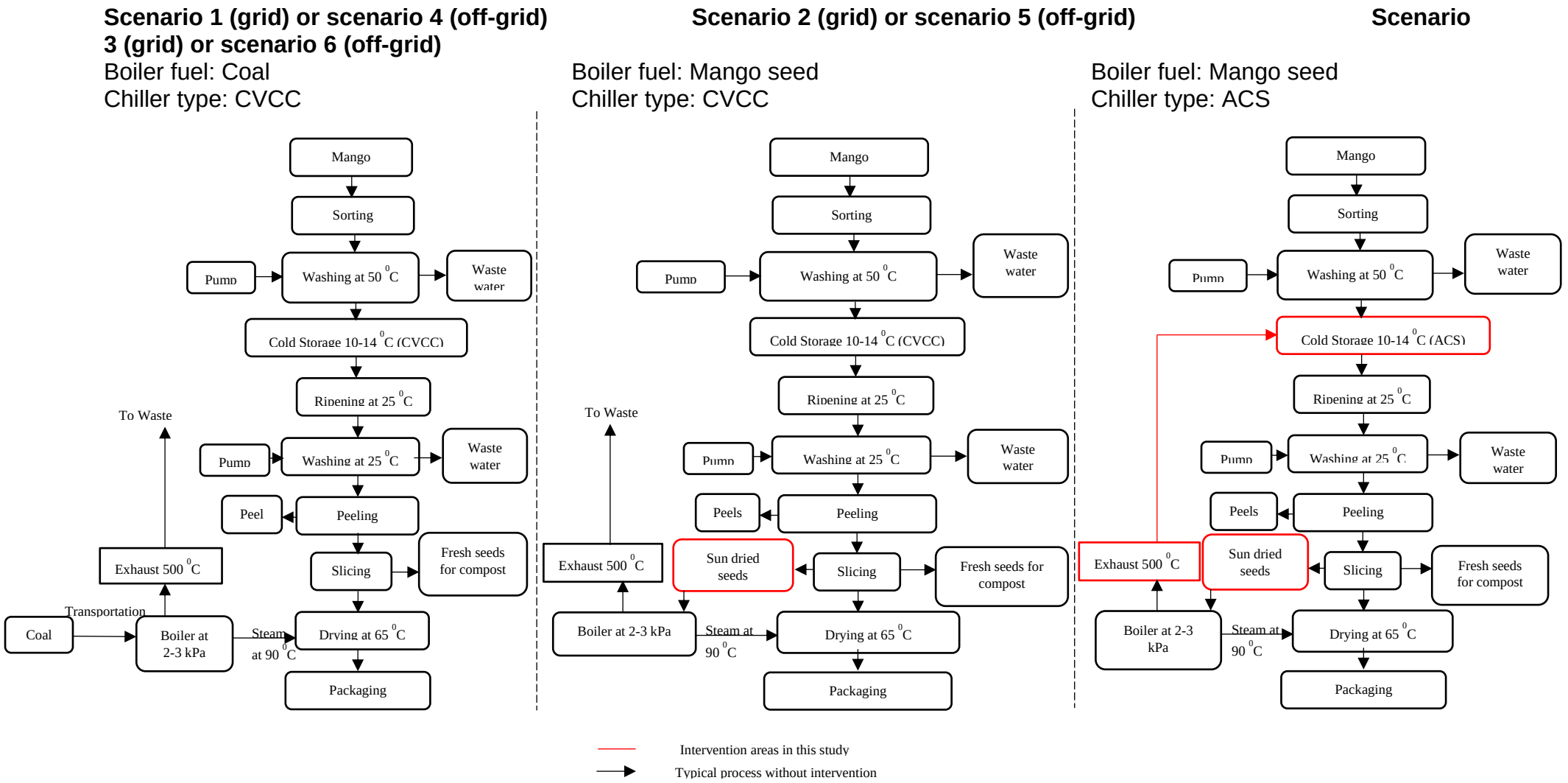

Note: CVCC is conventional vapour compression chiller; ACS is adsorption cooling system

Figure 7.1 Process diagrams for dried mango chips processing for both on-grid and off-grid scenarios

Stellenbosch University https://scholar.sun.ac.za

Table 7.1 Description of the scenarios for replacement of coal with mango seed as boiler fuel and integration of adsorption cooling system in a dried mango chips process

Scenarios	Power setting	Boiler fuel	Boiler waste heat utilization	Chiller type
1	On-grid	Coal	Rejected into environment	CVCC
2	On-grid	Mango seed	Rejected into environment	CVCC
3	On-grid	Mango seed	Recycled to the ACS	ACS
4	Off-grid	Coal	Rejected into environment	CVCC
5	Off-grid	Mango seed	Rejected into environment	CVCC
6	Off-grid	Mango seed	Recycled to ACS	ACS

Note: ACS is adsorption cooling system; CVCC is conventional vapour compression chiller

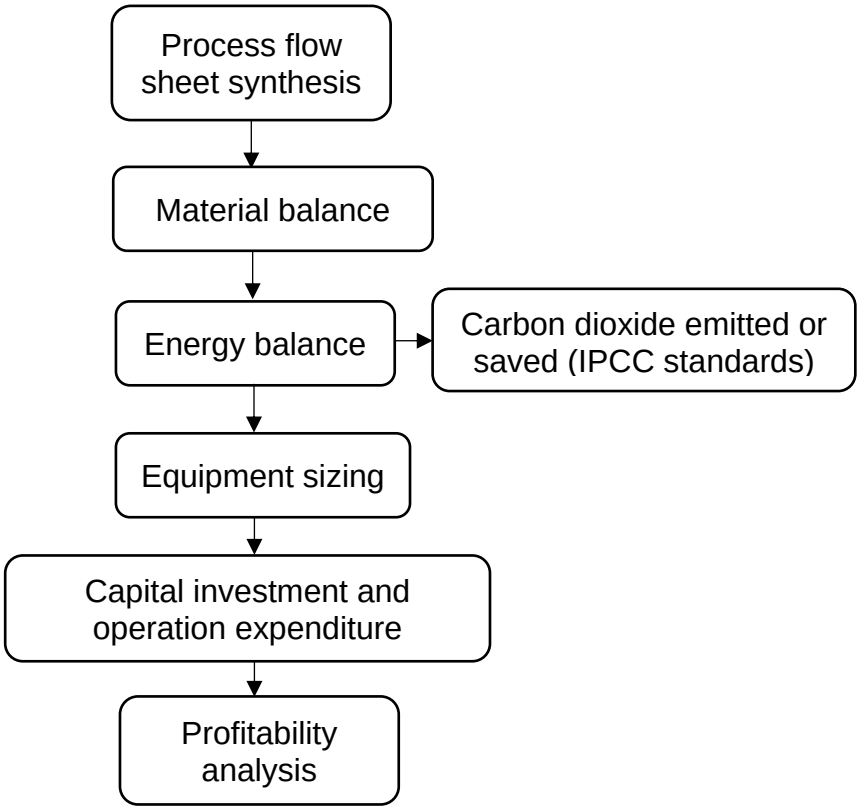

Figure 7.2 Procedure followed for the economic and environmental analysis of a process plant in which coal is replaced with mango seed as boiler fuel and cooling is provided with adsorption cooling system. Note: IPCC = Intergovernmental Panel on Climate Change.

Stellenbosch University https://scholar.sun.ac.za

Thus, kinetic and potential energy, which are already available in each unit operation and manual energy expenditure were not considered. The result from material and energy balance were used to perform the environmental and economic analyses of each scenario.

7.2.3.1 Combustion to thermal energy estimation

The conversion of mango seed or coal to thermal energy in boilers was based on Equation 7.1

$$\eta = \frac{Q_{useful}}{Q_{fuel}} \times 100 \qquad 7.1$$

Where Q_{useful} is the useful energy produced in the boiler at 3 kPa and 90˚C (2561 kJkg^{-1}), Q_{fuel} for coal was assumed to be 30.08 MJkg^{-1} [117] while that for mango seed was measured using bomb calorimetry to be 17.80 MJkg^{-1}, η is the combustion efficiency assumed to be 85% [263]. Since steam at 3 kPa is used to dry the mango chips, the total amount of coal or mango seed required to generate the steam was calculated using Equation 7.2

$$m_{fuel} = \frac{Q_{useful}}{\eta_{th} \times Q_{fuel}} \qquad 7.2$$

where m_{fuel} is the mass of the coal or mango seed needed to generate the steam (kg).

7.2.3.2 Electrical power conversion

Energy requirements for electrical equipment were estimated using the power requirement of the equipment and the working hours.

$$Q_{elect} = 3600 \times P_{elect} \times t \qquad 7.3$$

Stellenbosch University https://scholar.sun.ac.za

P_{elect} is the electrical power requirement of the equipment (kW), t is the working duration (hours), 3600 is the conversion factor from hours to seconds and Q_{elect} is the electrical heat generated (kJ).

7.2.3.3 Dryer energy balance

The estimation of thermal energy used during drying of mango chips was based on Equations 7.4 to 7.7.

$$Q_{drier} = Q_{solid} + Q_{sensible} + Q_{latent} \quad 7.4$$

$$Q_{solid} = m_{solid} \times C_{p,solid}(T_f - T_i) \quad 7.5$$

$$Q_{sensible} = m_{water} \times C_{p,water}(100 - T_i) \quad 7.6$$

$$Q_{latent} = m_{water} \times \lambda_{100} \quad 7.7$$

Q_{dryer} is the total energy required for drying (kJ), $Q_{solid}$is the energy required to raise the temperature of mango chips from room temperature to the final product drying temperature (kJ), $Q_{sensible}$ is the energy required to raise temperature of water in the mango chips to 100˚C (kJ), Q_{latent} is the latent heat of vaporization of water, (kJ), m_{solid} is the mass of final dried product (kg), $C_{p,solid}$ is the specific heat of dried product (2.18 kJkg^{-1}˚C $^{-1}$) (Ikegwu and Ekwu 2009), $C_{p,water}$ is the specific heat of water (4.18 kJkg^{-1}˚C $^{-1}$), m_{water} is the mass of water evaporated product (kg), T_f is the final product drying temperature (˚C), T_i is the initial drying temperature assumed to be 25˚C, and λ_{100} is the enthalpy of vaporization of water at 100˚C (2257 kJkg^{-1}). Similar equations (Equations 7.4-7.7) can be used to estimate the energy required for sun drying.

7.2.3.4 Cold storage refrigeration load

The total refrigeration load was calculated as the sum of heat leakage through the wall, air change heat gain, products heat load, respiratory heat load by workers in the storage room, heat produced by fans, and heat produced by an electric bulb in the room. The following assumptions were made to estimate the total refrigeration load.

Stellenbosch University https://scholar.sun.ac.za

1. Average mass and density of mango are 0.20 kg and 1068 kgm^{-3} [264] respectively.
2. Processing capacity was 30,000 kg of mangoes per day.
3. The dimension of storage space was assumed to be 20 x 9.5 x 5.5 m with the external surface area of the storeroom of 772 m^2.
4. The storage room has Insulation (polystyrene) of thickness 0.25 m and thermal conductivity of 3.84 $\times 10^{-5}$ $kWm^{-1}K^{-1}$.
5. The maximum ambient temperature and storage temperature was assumed to be 35˚C and10˚C, respectively.
6. Assuming two men working in the storage room and respiratory heat per person is 3163 kJh^{-1} and heat from the light bulb is 1000 W [265], and heat transfer from the fan is 250 W [265] and assuming three fans working in the storage room.

Heat leakage through the wall is

$$Heat\ leak\ (kJh^{-1}) =) = \frac{A \times \Delta T \times k}{\Delta x} \qquad 7.8$$

A is the storage room surface area (m^2), ΔT is the temperature difference between the ambient and storage temperature (˚C), Δx is the wall thickness (m), k is the wall thermal conductivity ($kWm^{-1}K^{-1}$).

$$Air\ change\ heat\ gain(kJh^{-1}) = \frac{storage\ volume\ \times Air\ change\ factor \times vometric\ heat\ gain}{24\ hours} \qquad 7.9$$

Volumetric heat gained as a result of air change at 35˚C is 82.7 kJm^{-3} and air change factor is 2.7 [266].

$$Product\ heat\ load\ (kJh^{-1}) = \frac{Processing\ capacity \times C_{p,mango}\ \times \Delta T}{24\ hours} \qquad 7.10$$

Stellenbosch University https://scholar.sun.ac.za

$C_{p,mango}$ is the specific heat of mango (3.74 kJkg^{-1}°C $^{-1}$), ΔT is the temperature difference between the ambient and storage temperature (°C)

$$Human\ respiratory\ heat(kJh^{-1}) = N_P \times 3163\ kJh^{-1} \quad 7.11$$

N_P is Number of persons working in the storage room, 3163 kJh^{-1} is the respiratory heat produced per person.

$$Heat\ produced\ by\ fan(kJh^{-1}) = N_{fan} \times 250\ W \times 3.6 \quad 7.12$$

Heat transfer from the fan is 250 W [265], 3.6 is the conversion factor to convert to per hour, N_{fan} is the number of fans used.

$$Heat\ produced\ by\ the\ light\ bulb(kJh^{-1}) = N_{bulb} \times 1000\ W \times 3.6 \quad 7.13$$

Heat from the light bulb is 1000 W [265], 3.6 is the conversion factor to convert to per hour, N_{bulb} is the number of electric bulbs used.

Thus the total cold storage energy consumption could be estimated using Equation 7.14

$$Cold\ storage\ energy\ consumtion = \frac{Refrigeration\ Storage\ heat\ load}{COP} \quad 7.14$$

Assuming the average COP (coefficient of performance) of the chiller is 3.5 [265].

7.2.3.5 Fuel transportation

The energy consumed to transport the boiler fuel to the mango processing plant was estimated by Equation 7.15.

$$Q_{trans} = \eta \times m_{fuel} \times Q_{fuel} \quad 7.15$$

η is the truck engine efficiency, m_{fuel} is the amount of diesel fuel used by the truck (kg), Q_{fuel} is the heating value of the diesel (MJkg^{-1}), and Q_{trans} is the energy consumed (MJ).

7.2.3.6 Specific energy demand

Stellenbosch University https://scholar.sun.ac.za

The specific energy demand is the energy consumed to produce a unit mass of the final product. It is the ratio of the total energy required for the mango processing to the amount of the final product per annum. This was determined using Equation 7.16.

$$Q_{specific} = \frac{Q_{Total}}{m_{product}} \qquad 7.16$$

$Q_{specific}$ is the specific energy demand (kJ/kg), Q_{Total} is the annual total energy consumed (kJ), $m_{product}$ is the amount of dried mango chips produced per annum. In this study, the total mass of the dried mango chips produced per annum is 6.51×10^5 kg.

7.2.4 Economic impact assessment parameters

Economic feasibility evaluation apprises the investors of the risks and benefits associated with financial investment. The economic evaluation of the scenarios was conducted based on the South African economic condition. The cost of equipment was obtained from equipment suppliers and technical reports (Tables C4 and C5 in the Appendix). Where necessary, some equipment costs were estimated based on cost data from different years using chemical engineering plant cost index (CEPCI) and the capacities adjusted using Equations 7.17 &7.18 [178].

$$C = C_O \left(\frac{M}{M_O}\right)^n \qquad 7.17$$

$C \text{ and } C_O \text{ are equipment costs at capacities } M \text{ and } M_O; n \text{ is the scale index}$

$$Present\ cost = Original\ cost \left(\frac{CEPCI\ \ at\ present\ time}{CEPCI\ at\ time\ original\ was\ obtained}\right) \qquad 7.18$$

The variable operating costs were calculated based on the raw material and flow rates of utilities resulted from material and energy balance calculations and their market prices (Tables S4 and S5 in the Appendix). The operating costs, the tax rate/ interest rate, insurance, and maintenance costs were based on the South African economic condition. Since profit is expected at the end of the project after initial investment has

Stellenbosch University https://scholar.sun.ac.za

been made, some economic indicators such as net present value (NPV) and internal rate of return (IRR) takes into account time value of money [178] were evaluated based the calculated capital costs and operating costs, on the basis of real values in the cumulative cash-flow calculation. NPV provides an indication of the returns on investment of a project over the project life in the present monetary value terms. A positive NPV signifies the project value increases by that amount over the capital investment in present monetary value at the discount rate considered. An NPV of zero denotes the investment has made no losses or gains over the period and at the discount rate considered. A negative NPV indicates the project is not viable at the discount rate considered [177]. IRR is the discount rate at which the project break-even with no losses or gains (the discount rate at which NPV equals zero). An IRR greater than the prevailing interest rate suggests positive NPV, and a viable project whereas an IRR less than the prevailing interest rate denote a negative NPV and unviable project. In addition, a sensitivity analysis of the economic performance of a representative scenario was carried out to study the robustness of the economic results in response to the fluctuation of some economic parameters. The applied parameters/method for the economic evaluation, are defined in Table 7.2.

7.2.5 Environmental impact assessments

Reduction in greenhouse gas (GHG) emissions is one of the goals of recent technological innovations due to the contribution of GHG emissions to climate change and global warming. Therefore, this study accessed the impact of intended interventions on carbon dioxide emissions from the dried mango processing plant.

Stellenbosch University https://scholar.sun.ac.za

Table 7.2 Economic impact assessment parameters for a mango process plant using mango seed as boiler fuel and adsorption cooling system

Parameters	Value	Parameters	Value
Annual operating hours	2880	Start-up duration	1 year
Loan interest (%)	8	Plant capacity (kg/day)	30000
Loan term (years)	8	Income tax rate (%)	28
Equity loan (%)	40:60	Inflation rate (%)	5.7
Working capital	25% fixed capital	Cost year for analysis	2018
Depreciation period (years)	12	Minimum acceptable IRR (real term) (%)	9.3
Salvage value	0	Plant service life (years)	12
Prices			
Currency conversion US$1	14.51	Electricity price(US$/kWh)	1.47773 [c]
Coal price(US$/kg)	0.080289 [a]	Diesel price(US$/L)	1.4261 [c]
Mango price(US$/kg)	0.758098 [b]	Water(US$/kg)	0.00148 [d]
Dried mango chips (US$/kg)	9.50		

[a] Available: www.indexmundi.com [2018, January 15]; [b] Research Markets and Economic Centre. 2016. *SA Fruit Trade Flow*. [Online], Available: https://www.namc.co.za/wp-content/uploads/2018/03/South-African-Fruit-flow-report-Mar-2018-Issue29.pdf.

[c] EIA. 2011. *Annual Energy Outlook with projections to 2035*.; [d] CoCT. 2017. Tariff structure from 1 July 2017. (July 2017). [Online], Available: https://resource.capetown.gov.za/cityassets/Files/Tariff_increases_from1July17.pdf.

The amount of energy expended by various unit operations, the fuel type used to supply energy under various scenarios and their respective emission factors were considered in the estimation of carbon dioxide (CO_2), methane (CH_4), and nitrous oxide (N_2O) emissions. Furthermore, the amount of CH_4 and N_2O emitted were converted to their equivalent CO_2 by using their respective global warming potential (GWP) values. The GWP for CO_2, CH_4, and N_2O are 1, 25, and 310, respectively [180]. To calculate the amount of GHG emitted, the following assumptions were made in the GHG emission estimation

1. Intergovernmental Panel on Climate Change (IPCC) standards were used
2. Distance from the coal source to the plant is 100 km (200 km round trip)

Stellenbosch University https://scholar.sun.ac.za

3. 25 ton-truck with a diesel consumption of 0.048 m^3 per 100 km was used to transport the coal [267]
4. The compost site is situated near the plant (distance from the plant to the compost site is assumed to be zero).
5. All other activities within the plant other than the scenarios being considered to remain the same.

7.2.5.1 Estimation of GHG emission from electrical equipment

CO_2, CH_4, and N_2O produced as a result of electrical energy produced using coal or diesel can be estimated using equations 7.19 to 7.21 [259].

$$CO_2\ (kgyr^{-1}) = P_{elect} \times t \times 3600 \times Emission\ factor_{CO2} \qquad 7.19$$

$$CH_4\ (kgyr^{-1}) = P_{elect} \times t \times 3600 \times Emission\ factor_{CH4} \qquad 7.20$$

$$N_2O\ (kgyr^{-1}) = P_{elect} \times t \times 3600 \times Emission\ factor_{N2O} \qquad 7.21$$

P_{elect} is the electrical power requirement of the equipment (kW), t is the working duration (hours) per annum, 3600 is the conversion factor from hours to seconds. The CO_2 emission factor for diesel and coal are 7.41×10^{-5} kgkJ^{-1} and 9.46×10^{-5}kgkJ^{-1} [259] respectively. The CH_4 emission factor for diesel and coal are 3.0×10^{-9}kgkJ^{-1} and 1.0×10^{-8}kgkJ^{-1} [259] respectively. The N_2O emission factor for diesel and coal are 6.0×10^{-10} kgkJ^{-1} and 1.5×10^{-9} kgkJ^{-1}[259] respectively.

7.2.5.2 Estimation of GHG emission from boiler fuel combustion

The amount of CO_2, CH_4 and N_2O produced by combustion of coal or biomass in the boiler can be estimated using Equations 7.22 to 7.24 [180].

$$CO_2\ (kgyr^{-1}) = m_{fuel} \times Q_{fuel} \times \eta_{th} \times Emission\ factor_{fuel} \times 2880 \qquad 7.22$$

$$CH_4\ (kgyr^{-1}) = m_{fuel} \times Q_{fuel} \times \eta_{th} \times Emission\ factor_{fuel} \times 2880 \qquad 7.23$$

$$N_2O\ (kgyr^{-1}) = m_{fuel} \times Q_{fuel} \times \eta_{th} \times Emission\ factor_{fuel} \times 2880 \qquad 7.24$$

Stellenbosch University https://scholar.sun.ac.za

η_{th} is the boiler combustion efficiency assumed to be 80% (Suntivarakorn and Treedet 2016), m_{fuel} is the amount of boiler fuel combusted (kg), Q_{fuel} is the heating value of the fuel (MJkg^{-1}). CO_2 emission factor for biomass combustion is 1.12×10^{-4} kgkJ^{-1}, CO_2 emission factor for coal combustion is 9.46×10^{-5} kgkJ^{-1} [259]. CH_4 emission factor for biomass combustion is 3.0×10^{-8} kgkJ^{-1}, CH_4 emission factor for coal combustion is 1.0×10^{-8} kgkJ^{-1}[259]; The N_2O emission factor for biomass combustion and coal are 4.0×10^{-9} kgkJ^{-1} and 1.5×10^{-9} kgkJ^{-1} [259] respectively; η is the boiler combustion efficiency assumed to be 85% (Suntivarakorn and Treedet 2016); 2880 is the total number of working hours the boiler operates.

7.2.5.3 Estimation of GHG emission from mango seed composting

During composting of the biomass, the amount of methane generated can be estimated using Equation 7.25.

$$CO_2\ (kgyr^{-1}) = Emission\ factor_{compost,CO2} \times M_{compost} \times TS \qquad 7.25$$

$$CH_4\ (kgyr^{-1}) = Emission\ factor_{compost,CH4} \times M_{compost} \qquad 7.26$$

$$N_2O\ (kgyr^{-1}) = Emission\ factor_{compost,N2O} \times M_{compost} \qquad 7.27$$

TS is the total solid assumed to be 30% [179], $M_{compost}$ is the mass of the composted material on wet basis (541440 kg mango seed in case of scenarios 1 &4, and 189160 kg mango seed in case of scenarios 2,3,5,& 6), $Emission\ factor_{compost,CO2}$ is the emission factor assumes to be 0.44 kg per dry matter [179]. $Emission\ factor_{compost,CH4}$ and $Emission\ factor_{compost,N2O}$ assumed to be 0.004 kg per waste treated and 0.0003 kg per wet waste treated [179].

Stellenbosch University https://scholar.sun.ac.za

7.2.5.4 Estimation of GHG emission from coal transport

Using equation 7.2, the total energy for drying is 5.33 TJ per year. The total amount of coal required per annum for the generation of steam for drying is 209 Mg. Assuming 25 ton truck is used to transport the coal, and the coal source is 100 km (200 km round trip) from the plant, then the truck would make about 8 trips. Therefore, the total GHG are emitted determined by equation 7.28 to 7.30 [180].

$$CH_4\ (kgyr^{-1}) = distance\ \times Emission\ factor_{CH4} \qquad 7.28$$

$$N_2O\ (kgyr^{-1}) = distance\ \times Emission\ factor_{N2O} \qquad 7.29$$

$$CO_2\ (kgyr^{-1}) = volume\ of\ Fuel\ \times Q_{fuel} \times Emission\ factor_{CO2} \qquad 7.30$$

Q_{fuel} is 38463MJm^{-3}, $Emission\ factor_{CO2}$ is 7.0×10^{-5} kgCO$_2$kJ^{-1}; $Emission\ factor_{CH4}$ is 2.069×10^{-5} kgCH$_4$ per kilometre, $Emission\ factor_{N2O}$ is 8.326×10^{-6} kgN$_2$O per kilometre [180].

7.2.5.5 Conversion of CH_4 and N_2O produced into equivalent CO_2

To convert the CH_4 and N_2O produced into equivalent CO_2, Equation 31 was used [180]

$$CO_2\ equivalent\ for\ CH_4/N_2O\ (kgyr^{-1}) = CH_4\ /N_2O(kgyr^{-1})\ \times GWP \qquad 7.31$$

The GWP for CH_4 and N_2O are 25 and 310, respectively [179,180]

7.2.5.6 Estimation of specific CO_2 emitted

Specific CO_2 emitted is the ratio of the total CO_2 emitted to the amount of final product (dried chips) per annum.

$$Specific\ CO_2\ emitted = \frac{Total\ CO_2\ emitted}{Total\ dried\ mango\ slice} \qquad 7.32$$

7.2.6 Sustainability analysis of dried mango chips processing

In this study, some aspects of the three pillars defining sustainability, thus, the economic, environmental and social impacts, were assessed to provide an indication

Stellenbosch University https://scholar.sun.ac.za

of the sustainability of the proposed scenarios. The sustainability indicators for the analysis are given in Table 7.3.

Table 7.3 Sustainability indicators for sustainability analysis of dried mango chips processing

Sustainability Criteria	**Sustainability Indicator**
Economic	Total capital Investment, internal rate of return
Environmental	Total Greenhouse gas emission
Society	Incidences of accidents, fire hazards

The indicators were ranked from 1 to 6, with 1 being the best scenario for the indicator and 6 worst for the indicator. This approach is similar to the sustainability index assessment method used by Evans et al. [268]. The ranking of the unquantifiable sustainability indicators such as the risk of fire and incidence of accidents were based on the main contributing factor of these indicators. For instance, since methane gas is produced during decomposition of the mango waste during composting or at landfills and the concentration of the methane gas depends on the quantity of the mango waste. Thus, the larger the quantity mango waste for composting, the higher the concentration of methane gas produced and higher the risk of fire (as a result of methane gas production as 5-15% [269]). Similarly, the higher the number of trips made to transport coal using trucks on national, regional and municipal roads the higher the accident risks.

Stellenbosch University https://scholar.sun.ac.za

7.3 Results and discussion

7.3.1 The impact of integrating adsorption cooling system on process energy demand

The integration of adsorption cooling technology powered by heat from the boiler exhaust as well as the use of mango seed as boiler fuel resulted in an increase in total energy demand and specific energy demand for both on-grid and off-grid scenarios (Fig. 7.3). The annual energy demand for the on-grid scenarios (scenarios 1, 2 & 3) was 6435 GJ, 6862 GJ, and 7424 GJ respectively, with the corresponding annual specific energy demand of 0.0099 $GJkg^{-1}$, 0.0105 $GJkg^{-1}$ and 0.0114 $GJkg^{-1}$ (Fig 7.3 a). Additional information is presented in Table C6 in the Appendix. Scenario 1 recorded the least annual energy demand and specific energy demand when compared with scenario 2 and 3 due to the type of cooling technology and boiler fuel investigated. Considering that both scenario 1 & 2 used CVCC for cooling, the difference in the energy demand can be attributed to the replacement of the boiler fuel (coal) with mango seeds. The energy was spent in drying the mango seeds generated on site prior to combustion in the boiler, which was less than the energy required to transport coal to the plant. The energy for drying the mango seed was about 441 GJ per year while the energy expended on coal transportation was about 15 GJ per year (Fig. 7.3 a). This led to about 7% increase in total energy demand by scenario 2 over scenario 1. Furthermore, the energy demand for scenario 3 was higher than that for scenario 2. Both scenarios used mango seeds as the boiler fuel, thus, the difference in energy demand between the two scenarios (2 & 3) is due to the replacement of the cooling technology, which increased the cooling energy requirement.

Stellenbosch University https://scholar.sun.ac.za

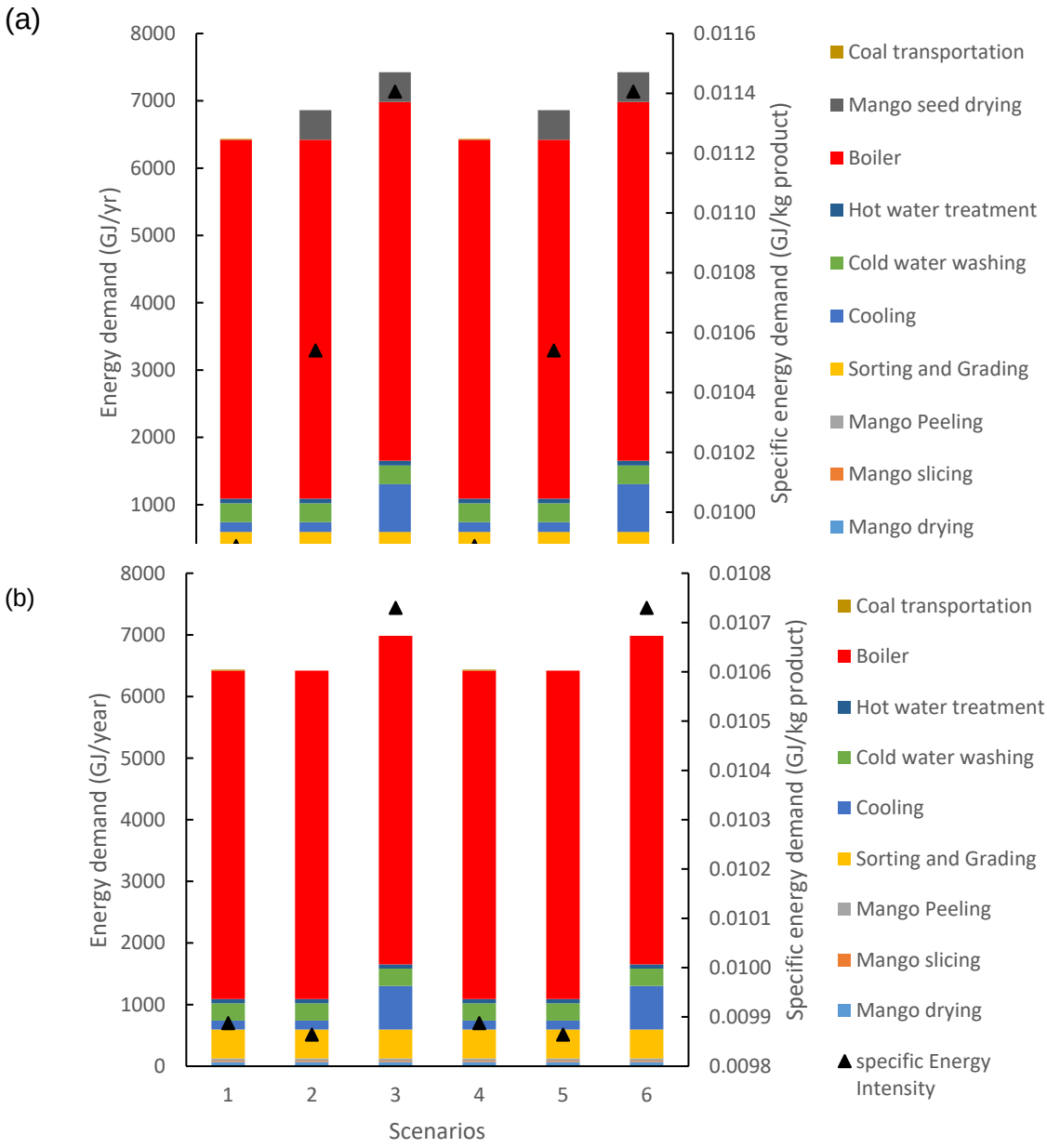

Figure 7.3 Energy demand for dried mango chips processing (a) including energy for mango seed drying (b) excluding energy for mango seed drying in an on-grid setting: scenario 1 (coal as boiler fuel and conventional vapour compression chiller(CVCC)), scenario 2 (mango seed as boiler fuel and CVCC) and scenario 3(adsorption cooling system (ACS) and mango seed as boiler fuel) and off-grid setting: scenario 4 (coal as boiler fuel and CVCC) scenario 5 (mango seed as boiler fuel and CVCC) and scenario 6 (ACS and mango seed as boiler fuel)

The energy consumption by ACS is usually higher than that of CVCC due to the low (COP) [101]. The coefficient of performance (COP) of ACS and CVCC is 0.1 and 2 -

Stellenbosch University https://scholar.sun.ac.za

4 respectively [26]. The energy consumption by CVCC was 708 GJ per year while energy demand by ACS was 145 GJ per year (Fig. 7.3a). Consequently, the energy demand by scenario 3 increased by about 8% over scenario 2. Therefore, a combined increase of 15% in energy consumption over scenario 1 was contributed by employing ACS and replacement of boiler fuel with mango seed (scenario 3). The energy demand can be reduced by sun drying the mango seeds. However, such mango seed processing would be possible in areas where solar energy is freely available. The sensitivity analysis showed that discounting the energy for mango seed drying, the energy demand for scenario 2 & 3 would reduce by 441 GJ, making the energy demand for scenario 2 to be 15 GJ (0.23%) less than that for scenario 1 since the energy expended on coal transportation was 15 GJ. However, the energy demand for scenario 3 would be 564 GJ (about 9%) still more than that of scenario 2 (Figs. 7.3a & b) because of the high-energy demand by ACS. Similar trends were observed for the off-grid scenarios (scenarios 4, 5 & 6). The annual energy consumption for the off-grid scenarios was 6435 GJ, 6861 GJ, and 7424 GJ respectively, with the corresponding annual specific energy demand of 0.0099 $GJkg^{-1}$, 0.0105 $GJkg^{-1}$ and 0.0114 $MJkg^{-1}$ (Fig. 7.3 a). Again, by sun-drying the mango seeds the energy demand for scenarios 5 & 6 would reduce by 441 GJ (Fig. 7.3b). Therefore, both the drying of the mango seed and the operation of the ACS cooling technology will require energy efficient power sources. Detailed amount of energy demand by each scenario can be found in the supplementary data in Tables C6 in the Appendix.

7.3.2 The impact of integrating adsorption cooling system on carbon dioxide emission

The integration of adsorption cooling technology into the dried mango chips processing and replacement of coal with mango seed as boiler fuel in both on-grid and

Stellenbosch University https://scholar.sun.ac.za

off-grid scenarios showed the potential to reduce GHG when compared with process scenarios that employ the conventional cooling technology. For the grid scenarios, the estimated annual GHG emission and specific GHG emission was highest for scenario 1 followed by scenarios 2 & 3 thus, 7.89×10^5 $kgCO_2eq$, 7.21×10^5 $kgCO_2eq$ and 7.10×10^5 $kgCO_2eq$, respectively and corresponding specific CO_2 emission of 1.21 $kgCO_2eq$ per kg, 1.11 kg CO_2eq per kg and 1.09 kg CO_2eq per kg, respectively (Fig. 7.4). This can be attributed to both the utilization of mango seed as boiler fuel and replacement of the CVCC with ACS. Evidently, the difference in emission between scenarios 1 & 2 is attributed to the replacement of coal with mango seed as boiler fuel because CVCC was used in both cases. The mango seed as the boiler fuel in scenario 2 increased the GHG emission by about 20% in comparison with coal as boiler fuel in scenario 1. The boiler annual GHG emitted by scenarios 1 & 2 is 5.07×10^5 $kgCO_2eq$, and 6.07×10^5 $kgCO_2eq$ respectively (Fig. 7.4). The increase in mango seed GHG emission may be due to higher emission factors in mango seed than in coal. The CO_2, CH_4 and N_2O emission factors for mango seed are 112000 kg/TJ, 30 kg/TJ, and 4 kg/TJ respectively, while that for coal is 96400 kg/TJ, 1 kg/TJ and 0.6 kg/TJ [270]. The utilization of mango seed as boiler fuel, however, led to the reduction in the quantity of mango seeds sent to the compost and its associated GHG emission. The annual compost GHG emitted by scenario 1 & 2 was 1.76×10^5 $kgCO_2eq$ and 9.44×10^3 $kgCO_2eq$, respectively. Therefore, the annual compost GHG emitted by scenario 1 was reduced by about 95% in scenarios 2 & 3 (Fig. 4).

Stellenbosch University https://scholar.sun.ac.za

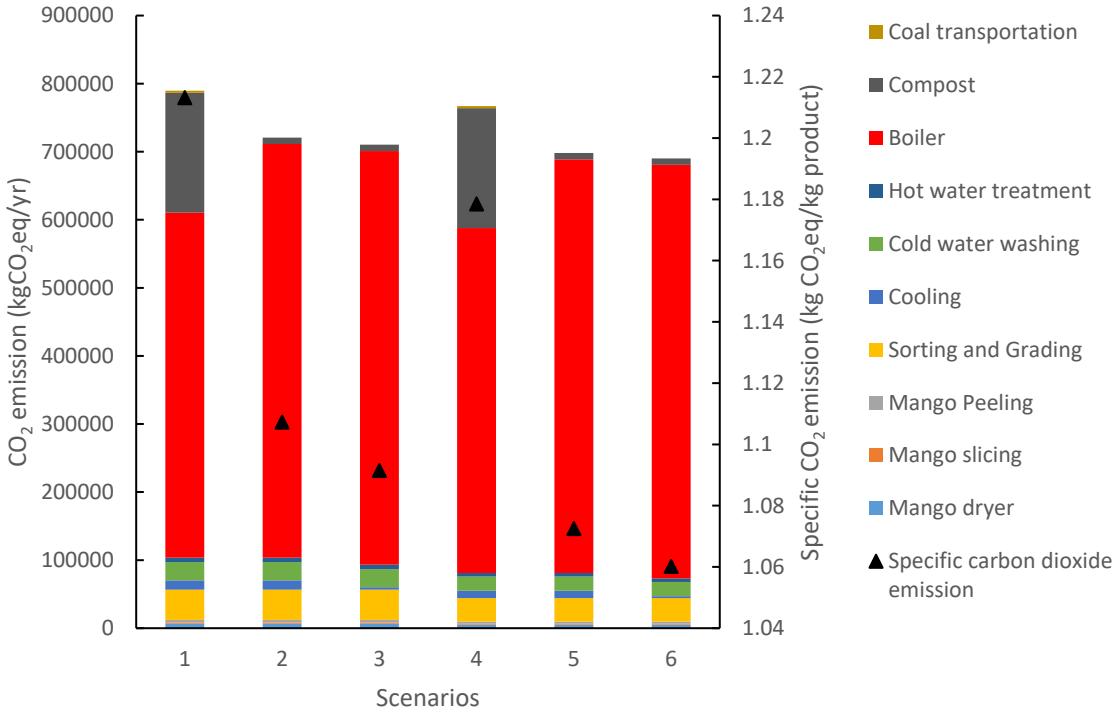

Figure 7.4 Greenhouse gas emission from dried mango chips processing in an on-grid setting: scenario 1 (coal as boiler fuel and conventional vapour compression chiller (CVCC)), scenario 2 (mango seed as boiler fuel and CVCC) and scenario 3 (adsorption cooling system (ACS) and mango seed as boiler fuel) and off-grid setting: scenario 4 (coal as boiler fuel and CVCC), scenario 5 (mango seed as boiler fuel and CVCC) and scenario 6 (ACS and mango seed as boiler fuel)

In addition, the mango seed as boiler fuel eliminated emission resulting from coal transportation because mango seeds are generated onsite. Transportation of coal emitted 3.18×10^3 $kgCO_2eq$ per annum which was eliminated as a result of coal replacement with mango seed as boiler fuel. Furthermore, the type of cooling technology used also contributed to the difference in GHG emitted by the grid scenarios. The CVCC was the cooling technology used in scenario 2, while ACS was employed in scenario 3. The estimated annual GHG emitted by scenarios 2 & 3 was 1.38×10^4 $kgCO_2eq$ and 3.55×10^3 $kgCO_2eq$, respectively (Fig. 7.4). As a result, about 74% reduction in GHG emission was estimated when the CVCC was replaced with ACS. Therefore, the replacement coal as the boiler (in scenario 1) with mango seed

Stellenbosch University https://scholar.sun.ac.za

(in scenario 2) led to the overall annual reduction of about 9% GHG emitted by scenario 1. Similarly, about 1% marginal annual reduction in GHG by scenario 2 was estimated when CVCC was replaced with ACS in scenario 3 (more details are presented in supplementary data Tables C7 & C8 in the Appendix).

Overall, a combined 10% reduction in annual GHG emission was estimated as a result of the replacement of both coal and CVCC in scenario 1 with mango seed and ACS in scenario 3. Similar trends were observed for the off-grid scenarios (scenarios 4, 5 & 6). However, the annual GHG were lower for off-grid scenarios than their on-grid counterparts. The estimated total annual CO_2 emission was 7.67×10^5 $kgCO_2eq$, 6.98×10^5 $kgCO_2eq$ and 6.90×10^5 $kgCO_2eq$ for scenarios 4, 5 & 6 respectively with specific CO_2 emissions of 1.19 kg CO_2eq per kg, 1.07 kg CO_2eq per kg and 1.06 $kgCO_2eq$ per kg (Fig. 7.4). The lower emissions estimated for the off-grid scenarios may be due to the type of fuels used for the electricity generation in both on-grid and off-grid setting scenarios and their different respective emission factors [271]. Electricity generation in the on-grid-scenarios was by coal combustion while in off-grid scenarios was by diesel. The CO_2, CH_4 and N_2O emission factors for diesel are 74100 kg per TJ, 3 kg per TJ and 0.6 kg per TJ respectively, while that for coal is 96400 kg per TJ, 1 kg per TJ and 0.6 kg per TJ [270].

Similar to the on-grid scenarios, the replacement coal as boiler fuel (in scenario 4) with mango seed (in scenario 5) resulted in the overall annual reduction of about 9% GHG emitted by scenario 4. Besides, when scenarios 5 and 6 were compared, emissions by scenario 6 was about 1% lower than scenario 5 while GHG emission by scenario 6 is about 10% lower than that of scenario 4 when both coal and CVCC in scenario 4 were replaced with mango seed and ACS in scenario 6 (Fig. 7.4). Detailed amount of GHG emitted by each scenario can be found in the supplementary data. In conclusion,

Stellenbosch University https://scholar.sun.ac.za

the replacement of coal with mango seed as boiler fuel and CVCC with ACS is beneficial in reducing the negative environmental impact associated with dried mango chips processing.

7.3.3 Economic impacts assessment

The Total capital investment cost is the sum of working capital and fixed capital investment. The replacement of CVCC with ACS increased the total capital investment for the scenarios that involved ACS by about 5% in both on-grid and off-grid scenarios. The TCI estimated for the on-grid scenarios is US$ 847900 for scenario 1 & 2 and US$ 895000 for scenario while TCI for off-grid scenarios is US$ 883000 for scenarios 4 & 5 and US$ 930000 for scenario 6 (Table 7.4). Additional information can be found in Table C9 in the Appendix. These differences can be attributed to the differences in the cost of cooling technology employed. Consequently, the purchased equipment cost for scenarios that employed CVCC is lower than from scenarios that employed ACS. As a result, the specific capital investment for scenarios that employed CCVC is lower than that for scenarios that employed ACS for both on-grid and off-grid settings. Specific capital investment is the ratio of total capital investment to the amount of final product (dried mango chips) produced annually. The specific capital investment for on-grid scenarios is 1.30 US$ per kg scenarios 1 & 2 and 1.37 US$ per kg for scenario 3.Similarly, the specific capital investment for off-grid scenarios is 1.36 US$ per kg for scenarios 4 & 5 and 1.43 US$ per kg for scenario 6 (Table 7.4).Using the estimated capital investment cost and operating cost, cumulative cash flow analysis was performed on the basis of real term monetary values.

Stellenbosch University https://scholar.sun.ac.za

Table 7.4 Breakdown of total capital investment (TCI) for dried mango chips processing

	Factor	Scenarios					
		1	2	3	4	5	6
Purchased equipment (k$)	25% FCI	169.6	169.6	179.0	176.6	176.6	186.0
Equipment installation (k$)	10% FCI	67.8	67.8	71.6	70.6	70.6	74.4
Installed piping (k$)	8% FCI	54.3	54.3	57.3	56.5	56.5	59.5
Instrumentation/Control (k$)	8% FCI	54.3	54.3	57.3	56.5	56.5	59.5
Electrical installed (k$)	5% FCI	33.9	33.9	35.8	35.3	35.3	37.2
Utilities installed (k$)	15% FCI	101.7	101.7	107.4	106.0	106.0	111.6
Building and construction (k$)	10% FCI	67.8	67.8	71.6	70.6	70.6	74.4
Engineering and supervision (k$)	10% FCI	67.8	67.8	71.6	70.6	70.6	74.4
Contractor's fee (k$)	3% FCI	20.3	20.3	21.5	21.2	21.2	22.3
Contingency (k$)	6% FCI	40.7	40.7	43.0	42.4	42.4	44.6
Total Fixed capital Investment(FCI) (k$)		678.3	678.3	716.0	706.0	706.0	744.0
Working Capital (k$)	25% FCI	169.6	169.6	179.0	176.6	176.6	186.0
Total Capital Investment (TCI) (k$)		847.9	847.9	895.0	883.0	883.0	930.0
Specific capital investment ($/kg)		1.30	1.30	1.37	1.36	1.36	1.43

Note: Scenario 1 (on-grid, coal as boiler fuel and conventional vapour compression chiller (CVCC)), scenario 2 (on-grid, mango seed as boiler fuel and CVCC) and scenario 3 (on-grid, adsorption cooling system (ACS) and mango seed as boiler fuel) scenario 4 (off-grid, coal as boiler fuel and CVCC), scenario 5 (off-grid, mango seed as boiler fuel and CVCC) and scenario 6 (off-grid, ACS and mango seed as boiler fuel).

Stellenbosch University https://scholar.sun.ac.za

It was found that the on-grid scenarios are marginally more profitable than their off-grid counterparts considering a discount rate of 9.3% for projecting cashflows on a real basis, i.e. no inflation adjustments for future project years [272]. The IRR is 17.48%, 20.33%, and 25.33% respectively for the on-grid scenarios, while 16.09%, 18.88 and 23.84% is the IRR estimated for the off-grid scenarios (Fig. 7.5). This suggests that the on-grid scenarios would break even at slightly higher interest rates when compared with their off-grid counterparts. In addition, the net cash flow (NPV) are evidently higher for the on-grid scenarios than their off-grid counterparts due to the lower IRR values for the off-grid scenarios. The lower IRR values for the off-grid scenarios may be due to the extra cost incurred to acquire electricity generators. Subsequently, the NPV for the on-grid scenarios is higher than the off-grid scenarios counterparts (Fig. 7.5). Furthermore, for the on-grid scenarios, the IRR and NPV for scenario 2 are higher than the IRR and NPV for scenario 1. This may be due to the elimination of the cost of coal and coal transportation cost. Similarly, the IRR and NPV for scenario 3 are higher than the IRR and NPV for scenario 2. This may be due to the reduction in electricity cost to run the CVCC since ACS employed in scenario 3 was powered by waste exhaust from the boiler. Similar observations could be made for the off-grid scenarios. This is evident in the differences in their respective variable operating costs (Fig. 7.5). Furthermore, the discounted payback periods (9.3% discount rate) for the on-grid scenarios were found to be 9.5 years, 8.0 years and 5.9 years respectively for scenarios 1, 2 & 3 (See supplementary data in Appendix Figs. C1 & C2 for more details).

Stellenbosch University https://scholar.sun.ac.za

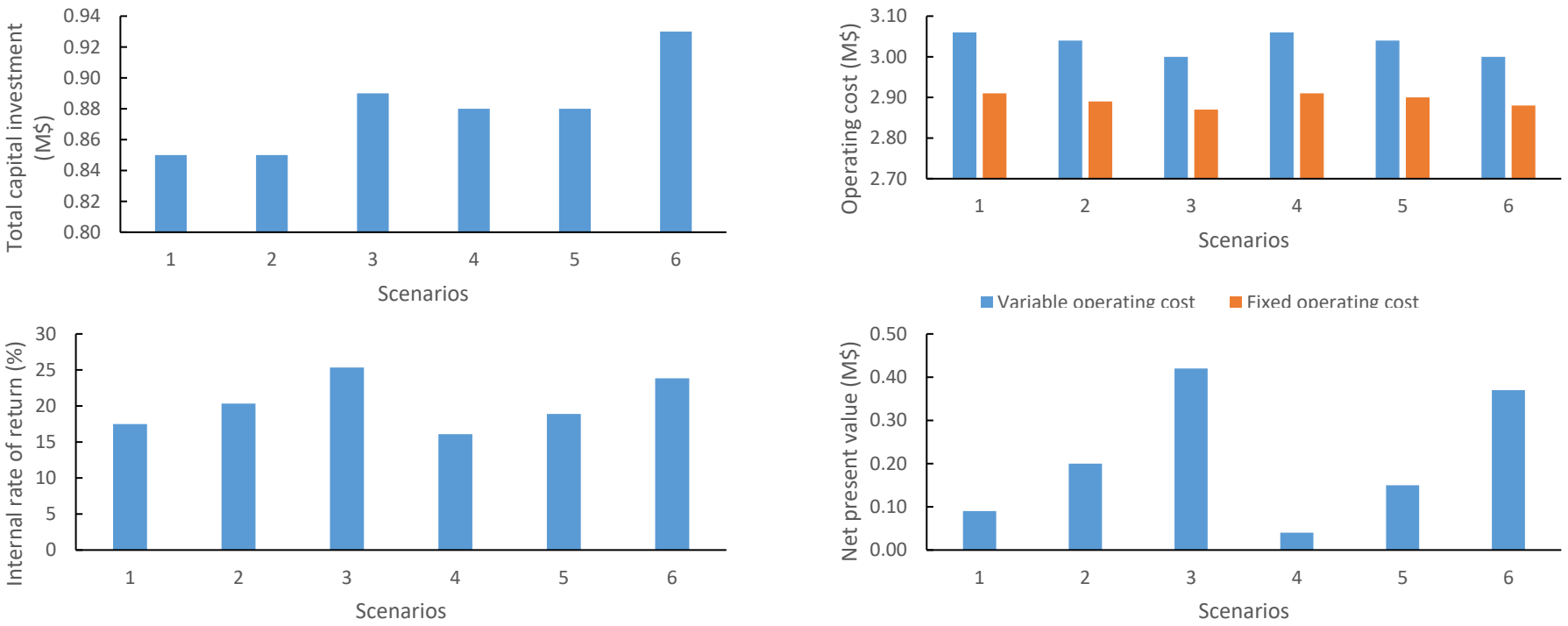

Figure 7.5 Results of economic analysis for dried mango chips production by scenarios in an on-grid setting: scenario 1 (coal as boiler fuel and conventional vapour compression chiller (CVCC)), scenario 2 (mango seed as boiler fuel and CVCC) and scenario 3 (adsorption cooling system (ACS) and mango seed as boiler fuel) and off-grid setting: scenario 4 (coal as boiler fuel and CVCC), scenario 5 (mango seed as boiler fuel and CVCC) and scenario 6 (ACS and mango seed as boiler fuel)

Stellenbosch University https://scholar.sun.ac.za

Similarly, the discounted payback periods (15% discount rate) for the off-grid scenarios were found to be 11.0 years, 8.8 years and 6 years respectively for scenarios 4, 5 & 6. (See supplementary data in Figs. C1 & C2 in the Appendix for details). The differences in the payback periods may be due to the reasons discussed above.

Sensitivity analysis was performed on the economic models to ascertain their robustness by varying the selling price of the dried mango chips (Table 7.5). Based on the sensitivity analysis results, the economic performance of all the scenarios for on-grid and off-grid settings are very sensitive to the changes in selling price of the dried mango chips. By reducing the selling price from 9.50 US$/kg to 9.0 US$/kg (about 5.3% reduction) resulted in negative NPV or IRR suggesting that the scenarios are not economically viable at 9.0 US$/kg selling price while increasing the selling price from 9.50 US$/kg to 10.0 US$/kg (about 5.3% increment) increased both NPV and IRR (Table 7.5). Thus, increasing the selling price would lead to higher net cash flow to the investor if the consumers are able to afford the high selling price. Therefore, the affordability of the product to the consumer must be taken into account when the selling price is being increased.

7.3.4 Sustainability analysis of dried mango chips processing

The sustainability of the dried mango chips processing is shown in Fig.7. 6. Scenario 1 & 2 (on-grid scenarios) ranked the best in terms of TCI followed by scenario 4 & 5 (off-grid scenarios), scenario 3 and then scenario 4. In terms of the GHG emission, scenario 1 ranked the worst while scenario 6 ranked the best. This is in conformity with the values of GHG emitted by each scenario in Fig. 7.4. Furthermore, scenario 2, 3, 5 & 6 ranked the best in terms of risk of fire and accident followed by both scenarios 1 & 4. Overall, scenario 1 is less sustainable when compared with scenarios 2 & 3 for

Stellenbosch University https://scholar.sun.ac.za

the grid setting while scenario 4 is less sustainable compared with scenarios 4 & 5 for the off-grid setting. These are in conformity with the results of the environmental and economic impacts discussed in Section 7.3, suggesting that replacement of coal with a renewable source like mango seed waste, as well as using cooling technology that uses the waste heat from the boiler would improve the sustainability of the mango processing plant.

Table 7.5 Effect of changing mango selling price on internal rate of return (IRR) and net present value (NPV) of dried mango chips processing

Selling Price (US$)	**Economic Indices**	**Scenarios**					
		1	2	3	4	5	6
10.00	NPV (M$)	1.36	1.47	1.69	1.31	1.42	1.64
	IRR (%)	47.63	50.06	53.00	45.34	47.69	50.65
9.50	NPV (M$)	0.09	2.01	0.42	0.04	0.15	0.37
	IRR (%)	17.48	20.33	25.33	16.09	18.88	23.84
9.00	NPV (M$)	-1.18	-1.07	-0.85	-1.23	-1.12	-0.90
	IRR (%)	-∞	-∞	-23.72	-∞	-∞	-27.04

Note: Scenario 1 (on-grid, coal as boiler fuel and conventional vapour compression chiller (CVCC)), scenario 2 (on-grid, mango seed as boiler fuel and CVCC) and scenario 3 (on-grid, adsorption cooling system (ACS) and mango seed as boiler fuel) scenario 4 (off-grid, coal as boiler fuel and CVCC), scenario 5 (off-grid, mango seed as boiler fuel and CVCC) and scenario 6 (off-grid, ACS and mango seed as boiler fuel).

Stellenbosch University https://scholar.sun.ac.za

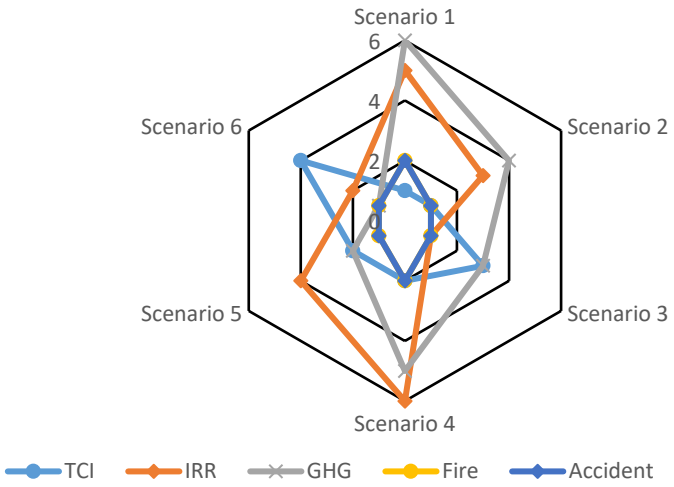

Figure 7.6 Results of sustainability analysis of dried mango chips processing in an on-grid setting: scenario 1 (coal as boiler fuel and conventional vapour compression chiller (CVCC)), scenario 2 (mango seed as boiler fuel and CVCC) and scenario 3 (adsorption cooling system (ACS) and mango seed as boiler fuel) and off-grid setting: scenario 4 (coal as boiler fuel and CVCC), scenario 5 (mango seed as boiler fuel and CVCC) and scenario 6 (ACS and mango seed as boiler fuel) 1 being the best scenario for that indicator and 6 worst for the indicator

7.4 Conclusion

The integration of adsorption chiller along with replacement of coal with mango seed as boiler fuel in dried mango chips processing plant increased the energy demand for the intervention scenarios (scenarios that involved utilization of mango seed as boiler fuel and ACS). Such high energy consumption could be reduced by sun-drying of the mango seeds prior to utilization as boiler fuel. In addition, the utilization of mango seed as boiler fuel and ACS as the cooling technology could result in less GHG emission into the environment and improve the economic performance of the dried mango processing plant. Thus, replacement of boiler fuel and cooling technology that run on renewable resources has shown the potential to improve the sustainability of the mango dry chip processing. The current analysis is targeting a new mango dry chip processing facility, thus, transition factors are not applicable. Implementing the suggested innovations into an existing mango processing plant would require

Stellenbosch University https://scholar.sun.ac.za

consideration of transitional costs and environmental and social impacts associated with retrofitting, modification and decommissioning existing technology, the establishment of new or cancellation of contracts with resource suppliers and establishment of new environmental and safety standards.

7.5 Limitations and transition considerations

The mango seed waste has a low bulk density, 375 kgm^{-3} [273] and low heating value compared to coal, bulk density 771 kgm^{-3} , [274]. Therefore, the current facilities for holding coal (which is the current practice) would have to be expanded almost two times in size to accommodate the handling of the mango seed to ensure enough supply for the same amount of thermal energy generation to power the boiler. Such a requirement would constitute additional costs and resource consumption. In addition, space would be required for constructing drying facilities for the mango seed prior to combustion in the boiler. The cost and legal fees associated with the acquisition of such resources warrant consideration. Furthermore, to make the switch from CVCC to ACS, the change in the refrigerant used by CVCC to one to be used by the ACS, would need to cancel old and establish new supply chains with new risks and constraints, which may result in additional legal costs. Furthermore, the disposal, decommissioning or reconfiguration of the current CVCC according to legislated standards and procedures and the associated social and environmental impacts would increase the cost of transitioning into the new technology.

Stellenbosch University https://scholar.sun.ac.za

Chapter 8 General discussion, conclusion and recommendation

8.1 General discussion

The study has shown the potential to produce AC from mango seed husk using NaCl as the activation chemical. However, the production process needs some technical improvements to improve the quality and performance of the AC. The results (Chapter 5) show that the AC had inferior properties compared with the commercial AC in terms of BET surface area and pore size and adsorption capacity for use in ACS as discussed in Chapters 5 and 6. The BET surface area and adsorption capacity of the mango seed husk AC produced in this study was 415 m^2g^{-1} and 0.23 $kgkg^{-1}$ which is lower than 1237 m^2g^{-1} and 0.74 $kgkg^{-1}$ for commercial AC paired with high-grade ethanol. The pyrolysis method used for the production of the AC from the mango seed husk might not be a suitable method. Pyrolysis equipment has high initial capital cost and it depends on the consumption of a huge amount of power that may not be available at the small-scale level considered in this study. Therefore, there is need to investigate more methods to improve the mango seed husk AC production process such as the use of NaOH or K_2CO_3 as the activation chemical and the microwave technology for the carbonization [132]. Such as investigations could be of economic and environmental benefit to the mango fruit producers, processors, and the environment.

Due to the poor functional properties of the mango AC, the study focused on how the use low-grade ethanol as a refrigerant in ACS paired with commercial AC. Low-grade ethanol is a resource that can be made readily available to resource-poor communities because the pre-existence of the technical know-how to produce it [222]. In the study, the modification of the commercial activated carbon (AC) by impregnating with NaCl

Stellenbosch University https://scholar.sun.ac.za

salts (Chapter 6) improved the performance when paired with low-grade ethanol (60% ethanol; 40% water) than high-grade (99.7%) as refrigerants in ACS. However, the amount of the refrigerant adsorbed and desorbed by the composite AC + NaCl for each cycle was reduced, which could be a result of the salts leaching out from the adsorbent, which with time can affect the performance of the ACS [59,79]. Therefore, the regeneration of the adsorbent bed may be required. Furthermore, the increase in concentration of NaCl in the composite adsorbent increased the 'compressor effect' (increase in temperature and pressure) thereby increasing the heat and mass transfer of the refrigerant (both low-grade and high-grade ethanol) from the composite adsorbent. Consequently, the performance of the ACS was also affected. However, due to the high latent heat of evaporation of low-grade ethanol as a result of the water fraction present, the performance of the composite adsorbent paired with low-grade ethanol was slightly higher than the composite adsorbent paired with grade-ethanol. Moreover, increase in compressor effect (pressure and temperature) also increased the amount of heat of adsorption released since heat of adsorption is dependent on the pressure and temperature attained in the adsorber.

The design for the ACS was made to suit off-grid users from the operation point of view. However, considerations should also be made on the selection of construction materials to ensure that the materials used, are compatible with the adsorbent and the refrigerant. In this study, the adsorbent vessel was made of stainless steel 304. Therefore, the use of AC impregnated with NaCl paired with oxygen-rich refrigerant (low-grade ethanol) could cause erosion of the vessel with time, consequently, affecting the performance of the ACS. As part of the ACS design, selection of suitable material to suit the adsorbent bed and the refrigerant and at the same time withstand the high desorption temperatures should be integral to ensure long shelf life and safe

Stellenbosch University https://scholar.sun.ac.za

operations. Moreover, the designed adsorption cooling system (ACS) was heated with dry heat from open combustion of mango seeds, which is not the most efficient (12.5% efficiency [174,175]) and safe process in case of leakage of the refrigerant (ethanol), which is highly flammable and volatile. Therefore, efficient processes for combusting the mango seed husks should be explored. Furthermore, such a method should be compatible with the operating refrigerant. The integration of the ACS to other processes that can use the mango seed as fuel, in the process releasing waste heat, as demonstrated in the dried mango chips processing (Chapter 7), could be a suitable model to use to avoid open combustion of the mango seed husks during the operation of the ACS.

The use of low-grade ethanol as refrigeration is on the assumption that dehydrating the ethanol to upgrade its quality is an expensive exercise. However, cheaper ways of dehydrating (scrubbing) the ethanol such as the use of bio-based sorbents, can be explored to improve the quality of the refrigerant [70,275]. Low-grade ethanol is widely produced in many small-scale distilleries and its use in the ACS could facilitate the adsorption of this technology while exploring methods for improving the ethanol quality. However, in areas where silica gel is accessible, forming composite with silica gel + NaCl paired with pure water as refrigerant would eliminate the heat and mass transfer challenges associated with using AC+NaCl composites paired with ethanol.

The study has shown that the mango seed husk as a waste can be used as a feedstock for energy production replacing expensive coal that is used in Mango processing plants. However, it should be recognized that the state of the mango seed husk can increase the energy demand for the plant because of the need to transport and dry them before use as demonstrated in the energy demand intervention scenarios

Stellenbosch University https://scholar.sun.ac.za

presented in Chapter 7. However, the energy demand arising from the pre-processing of the seed husks could be reduced through solar drying prior to combustion in the boiler. In this study, solar drying of the mango seed prior to combustion in the boiler has led to about 441 GJ reduction in annual energy demand [276]. Furthermore, the utilization of mango seed as boiler fuel and ACS as the cooling technology could reduce the waste generated during mango processing, reduce the degradation of the environment through GHG emission reduction and improve resource use efficiency.

The utilization of mango seed as boiler fuel, however, led to the reduction in the quantity of mango seed sent to the compost and its associated GHG emission. For instance, the annual compost GHG emitted by scenario 1 (coal as boiler fuel and CVCC the cooling technology) was reduced by 95% from 1.76×10^{5} $kgCO_2eq$ to 9.44×10^{3} $kgCO_2eq$ when mango seed was as boiler fuel and ACS as the cooling technology. Therefore, integrating ACS and biomass waste in fruit processing could have an immense benefit to the environment as well as the processor.

8.2 Overall Conclusion

It is possible to improve the heat and mass transfer of activated carbon paired with low-grade ethanol. The improvement in heat and mass transfer when AC + NaCl was paired with low-grade ethanol suggests that low-grade ethanol can be used as an alternative refrigerant. Moreover, the utilization of low-grade ethanol, which is characteristics of the ethanol produced in many small-scale distilleries, can be used in ACS without the need for upgrading. This would increase the demand for this low-grade ethanol and improve the economic benefits of this distilleries. Besides, the utilization of low-grade ethanol would reduce the operating cost of the ACS and promote small-scale distilleries which could influence the adoption of this technology.

Stellenbosch University https://scholar.sun.ac.za

Furthermore, mango seed which is a waste streams of mango processing could be used to produce the activated carbon needed for the adsorption cooling system as well as a source of renewable energy to power the cooling system. Thus, it is easy to adopt the adsorption cooling system in many fruit processing communities since low-grade ethanol could be produced in many fruit processing communities and there is readily available biomass waste for energy and adsorbent production. Furthermore, integration of the adsorption cooling system in fruit processing could reduce the negative environmental impacts and improve economic viability in both grid and off-grid power conditions.

8.3 Recommendation

The performance of the current systems and its practical use is subject to further improvements. The untreated AC/pure ethanol pair was used as the benchmark to assess the performance of composite adsorbents/refrigerant pairs. However, the system should be validated with other commercial chillers that use similar adsorbent/refrigerant pairs operating under the same conditions in areas where silica gel is accessible, forming a composite with silica gel + NaCl paired with pure water as refrigerant would eliminate the mass transfer challenges associated with using AC+NaCl composites paired with ethanol.

The combustion chamber for the ACS should be enclosed to improve fuel conversion efficiency. Ultimately, configuring the ACS to use rejected heat from unit operations such as the drying process would make the system more efficient. The use of NaCl should be used with caution considering that in high concentration it may have adverse effects on the environment. Moreover, NaCl may cause corrosion to stainless steel adsorber unit. Although the risk of using ethanol is limited because the ACS is a closed

Stellenbosch University https://scholar.sun.ac.za

system operating under vacuum, thus the pressure within the system is less than the atmospheric pressure, it is imperative to ensure that there are no external leakages which will reduce the efficiency of the system.

During adsorption of low-grade ethanol onto the composite adsorbent, some amount of leaching of NaCl from the composite adsorbent occurred during multiple adsorption cycles. The effect of this leaching on the overall system performance was not analyzed in this study. Therefore, it is recommended that a system-wide analysis is done to ascertain the impact of leaching on the on the overall performance of the system.

At the current production capacity of mango processing facility used as a case study, it is possible to generate enough energy to power the entire plant using technologies such as CHP (combustion, heat, and power) or turbine technology to generate power. However, since the mango processing period is just four months it is not economically wise to invest in such technology for it to be lying idle for two-thirds of the year. Therefore, it highly recommended that further studies be done to ascertain the possibility of import mangoes from other mango producing countries during the off-season for processing and then generate energy from the waste generated to power the plant, and how these affect the profitability of the plant. Alternatively, during off-season, other fruits could also be processed, and the waste generated from this fruit together with the mango waste can be used to generate the renewable energy to power the plant. The mango processors processed other fruits and use renewable.

Stellenbosch University https://scholar.sun.ac.za

References

[1] FAO, Climate change and food security, Food Agric. Organ. United Nations. (2008). http://rstb.royalsocietypublishing.org/content/360/1463/2139.short.

[2] R.J. Hodges, J.C. Buzby, B. Bennett, Postharvest losses and waste in developed and less developed countries: Opportunities to improve resource use, J. Agric. Sci. 149 (2011) 37–45. doi:10.1017/S0021859610000936.

[3] M.P. Islam, T. Morimoto, A new zero energy cool chamber with a solar-driven adsorption refrigerator, Renew. Energy. 72 (2014) 367–376. doi:10.1016/j.renene.2014.07.038.

[4] R.E. Critoph, Rapid cycling solar/biomass powered adsorption refrigeration system, Renew. Energy. 16 (1999) 673–678. doi:10.1016/S0960-1481(98)00250-X.

[5] J.S. Lewis, I. Chaer, S.A. Tassou, Reviews of Alternative Refrigeration Technologies, (2007). http://www.grimsby.ac.uk/documents/defra/tech-newrefrigetechs.pdf (accessed February 13, 2015).

[6] L.W. Wang, R.Z. Wang, R.G. Oliveira, A review on adsorption working pairs for refrigeration, Renew. Sustain. Energy Rev. 13 (2009) 518–534. doi:10.1016/j.rser.2007.12.002.

[7] M.A. Alghoul, M.Y. Sulaiman, B.Z. Azmi, M.A. Wahab, Advances on multi-purpose solar adsorption systems for domestic refrigeration and water heating, Appl. Therm. Eng. 27 (2007) 813–822. doi:10.1016/j.applthermaleng.2006.09.008.

[8] Q. Cui, G. Tao, H. Chen, X. Guo, H. Yao, Environmentally benign working pairs for adsorption refrigeration, Energy. 30 (2005) 261–271. doi:10.1016/j.energy.2004.05.005.

Stellenbosch University https://scholar.sun.ac.za

[9] A.N. Shmroukh, A. Hamza, H. Ali, S. Ookawara, Adsorption working pairs for adsorption cooling chillers : A review based on adsorption capacity and environmental impact, Renew. Sustain. Energy Rev. 50 (2015) 445–456. doi:10.1016/j.rser.2015.05.035.

[10] A. Kwaghger, E. Adejoh, Optimization of conditions for the preparation of activated carbon from mango nuts using ZnCl 2, Int. J. Eng. Res. Dev. 1 (2012) 1–7.

[11] A. Kwaghger, E.I.K.H.A. Iortyer, Experimental analysis on the use of mango nuts as adsorbents for solid adsorption refrigeration, Int. J. Sci. Eng. Res. 3 (2012).

[12] S. Kittiphoom, Utilization of Mango seed, Int. Food Res. J. 19 (2012) 1325–1335.

[13] T. Brosnan, D. Sun, Precooling techniques and applications for horticultural products- a review, Internatiional J. Refrig. 24 (2001) 154–170.

[14] H.Z. Hassan, A.A. Mohamad, Y. Alyousef, H.A. Al-Ansary, A review on the equations of state for the working pairs used in adsorption cooling systems, Renew. Sustain. Energy Rev. 45 (2015) 600–609. doi:10.1016/j.rser.2015.02.008.

[15] A.F.M.M. Rahman, Development of Advanced Multi Stage Adsorption Refrigeration Cycles Development of Advanced Multi Stage Adsorption Refrigeration Cycles, Tokyo Unversity of Agriculture and Technology, Japan, 2013.

[16] V. Murugavel, R. Saravanan, Life cycle cost analysis of waste heat operated absorption cooling systems for building hvac applications, in: Proc. Tenth Int. Conf. Enhanc. Build. Oper., Kuwait, 2010. http://oaktrust.library.tamu.edu/bitstream/handle/1969.1/94127/ESL-IC-10-10-77.pdf?sequence=1.

Stellenbosch University https://scholar.sun.ac.za

[17] S. Becken, K. Becken, Greenhouse gas emissions from refrigerants – information for hotels Contact, 2015. http://www.greenhotelier.org/wp-content/uploads/2016/03/Greenhouse-gas-emissions-from-refrigerantsfinal.pdf.

[18] F. Nsaful, Process Modelling of Sugar Mill Biomass to Energy Conversion Processes and Energy Integration of Pyrolysis, (2012) 1–171.

[19] P. Srikhirin, S. Aphornratana, S. Chungpaibulpatana, A review of absorption refrigeration technologies, Renew. Sustain. Energy Rev. 5 (2000) 343–372. doi:10.1016/S1364-0321(01)00003-X.

[20] B. Prasartkaew, S. Kumar, A low carbon cooling system using renewable energy resources and technologies, Energy Build. 42 (2010) 1453–1462. doi:10.1016/j.enbuild.2010.03.015.

[21] A. Paurine, G.G. Maidment, I.W. Eames, J. Missenden, A. Day, A review of " pumpless " absorption refrigeration cycles, VII Minsk Int. Semin. Heat Pipes, Heat Pumps, Refrig. Power Sources. (2011) 470–481.

[22] I.I. El-Sharkawy, K. Uddin, T. Miyazaki, B.B. Saha, S. Koyama, J. Miyawaki, S.H. Yoon, Adsorption of ethanol onto parent and surface treated activated carbon powders, Int. J. Heat Mass Transf. 73 (2014) 445–455. doi:10.1016/j.ijheatmasstransfer.2014.02.046.

[23] H.Z. Hassan, A.A. Mohamad, H.A. Al-Ansary, Development of a continuously operating solar-driven adsorption cooling system: Thermodynamic analysis and parametric study, Appl. Therm. Eng. 48 (2012) 332–341. doi:10.1016/j.applthermaleng.2012.04.040.

[24] R.E. Critoph, Performance Limitations of Adsorption Cycles for Solar Cooling, 41 (1988) 21–31. doi:10.1016/0038-092X(88)90111-9.

Stellenbosch University https://scholar.sun.ac.za

[25] R.Z. Wang, R.G. Oliveira, Adsorption refrigeration-An efficient way to make good use of waste heat and solar energy, Prog. Energy Combust. Sci. 32 (2006) 424–458. doi:10.1016/j.pecs.2006.01.002.

[26] O. Amer, R. Boukhanouf, H.G. Ibrahim, A Review of evaporative cooling technologies, Int. J. Environ. Sci. Dev. 6 (2015). doi:10.7763/IJESD.2015.V6.571.

[27] M. Aswaney, Forced-air precooling of fruits and vegetables, Air Cond. Refrig. J. (2007) 57–62. http://www.pre-coolers.net/documents/forced-air-precooling-of-fruits-and-vegetables.pdf.

[28] I. Alibas, N. Koksal, Forced-air, vacuum and hydro preccoling of cauliflower(Brassica oleracea L. v var.botrytis cv . Freemont): part I . Determination of precooling parameters, Food Sci. Technol. 34 (2014) 730–737.

[29] L. Kitinoja, J.F. Thompson, Pre-cooling systems for small-scale producers, Stewart Postharvest Rev. 6 (2010) 1–14. doi:10.2212/spr.2010.2.2.

[30] G. Thorpe, The design and operation of hydrocoolers A Smart Water Funded Project, (2008).

[31] H.M. Ozturk, A. Hepbasli, Experimental performance assessment of a vacuum cooling system through exergy analysis method, J. Clean. Prod. 161 (2017) 781–791. doi:10.1016/j.jclepro.2017.05.118.

[32] H.M. Ozturk, H.K. Ozturk, Effect of pressure on the vacuum cooling of iceberg lettuce, Int. J. Refrig. 32 (2009) 395–403. doi:10.1016/j.ijrefrig.2008.09.009.

[33] D.W. Sun, L. Zheng, Vacuum cooling technology for the agri-food industry: Past, present and future, J. Food Eng. 77 (2006) 203–214. doi:10.1016/j.jfoodeng.2005.06.023.

[34] K.. V. Vala, F. Saiyed, D.C. Joshi, Evaporative Cooled Storage Structures : An

Stellenbosch University https://scholar.sun.ac.za

Indian Scenario, Trends Postharvest Technol. 2 (2014) 22–32.

[35] International Institute of Refrigeration, 27th Informatory Note on Refrigeration Technologies / January 2015, 2015. doi:10.1063/1.449615.

[36] Energy.gov, Evaporative Coolers, (2012). https://www.energy.gov/energysaver/home-cooling-systems/evaporative-coolers (accessed June 20, 2018).

[37] R. Lazzarin, Technical note on evaporative cooling, 2012. http://www.iifiir.org/userfiles/file/webfiles/in-depth_files/Evaporative_cooling_Lazzarin_2014_EN.pdf.

[38] E.V. Gomez, F.C.R. Martínez, A.T. González, The phenomenon of evaporative cooling from a humid surface as an alternative method for air-conditioning, Int. J. Energy Enivironment. 1 (2010) 69–96.

[39] J. Camargo, C. Ebinuma, A mathematical model for direct and indirect evaporative cooling air conditioning systems, Brazilian Congr. Therm. …. (2002) 30–34. http://www.abcm.org.br/pt/wp-content/anais/encit/2002/Paper-title/09/CIT02-0855.PDF.

[40] S. Jain, P.. Dhar, S.. Kaushik, Evaluation of solid-desiccant-based evaporative cooling cycles for typical hot and humid climates, Int. J. Refrig. 18 (1995) 287–296. doi:10.1016/0140-7007(95)00016-5.

[41] E. Kozubal, J. Woods, J. Burch, A. Boranian, T. Merrigan, Desiccant Enhanced Evaporative Air-Conditioning (DEVap): Evaluation of a New Concept in Ultra Efficient Air Conditioning Desiccant Enhanced Evaporative Air-Conditioning (DEVap): Evaluation of a New Concept in Ultra Efficient Air Conditioning, (2011). doi:Contract, 303, 275-3000.

[42] A. Montecucco, J. Siviter, A.R. Knox, The effect of temperature mismatch on

Stellenbosch University https://scholar.sun.ac.za

thermoelectric generators electrically connected in series and parallel, Appl. Energy. 123 (2014) 47–54. doi:10.1016/j.apenergy.2014.02.030.

[43] S.. . Wani, A.P. Shrotri, S.P. Mane, S.M. Gheji, Review of Experimental Evaluation of Adsorption Cooling System Powered By Exhaust Heat of an Automobile, Int. J. Innov. Res. Sci. Eng. Technol. 4 (2015) 4437–4441. doi:10.15680/IJIRSET.2015.0406052.

[44] B.B. Saha, A. Akisawa, T. Kashiwagi, Solar/waste heat driven two-stage adsorption chiller: The prototype, Renew. Energy. 23 (2001) 93–101. doi:10.1016/S0960-1481(00)00107-5.

[45] B.B. Saha, S. Koyama, I.I. El-sharkawy, K. Kariya, K.C. Ng, B. Baran, S. Koyama, I.I. El-sharkawy, B.B. Saha, K. Kuwahara, I.I. El-sharkawy, K.C. Ng, Saha et al. - 2006 - Experiments for measuring adsorption characteristics of an activated carbon fiber, ethanol pair using a plate-fin heat exchanger.pdf, 9669 (2011).

[46] M.Z.I. Khan, K.C.A. Alam, B.B. Saha, A. Akisawa, T. Kashiwagi, Study on a re-heat two-stage adsorption chiller - The influence of thermal capacitance ratio, overall thermal conductance ratio and adsorbent mass on system performance, Appl. Therm. Eng. 27 (2007) 1677–1685. doi:10.1016/j.applthermaleng.2006.07.005.

[47] R. Wang, R. Oliveira, Adsorption refrigeration—An efficient way to make good use of waste heat and solar energy☆, Prog. Energy Combust. Sci. 32 (2006) 424–458. doi:10.1016/j.pecs.2006.01.002.

[48] F. Meunier, Second law analysis of a solid adsorption heat pump operating on reversible cascade cycles: Application to the Zeolite-water pair, J. Heat Recover. Syst. 5 (1985) 133–141. doi:10.1016/0198-7593(85)90045-1.

Stellenbosch University https://scholar.sun.ac.za

[49] S. V. Shelton, W.J. Wepfer, D.J. Miles, Square wave analysis of the solid-vapor adsorption heat pump, Heat Recover. Syst. CHP. 9 (1989) 233–247. doi:10.1016/0890-4332(89)90007-0.

[50] R.E. Critoph, Forced convection adsorption cycle with packed bed heat regeneration, 22 (1999) 38–46. doi:10.1016/S0140-7007(97)00036-4.

[51] A. Akahira, K.C.A. Alam, Y. Hamamoto, A. Akisawa, T. Kashiwagi, Mass recovery adsorption refrigeration cycle—improving cooling capacity, Int. J. Refrig. 27 (2004) 225–234. doi:10.1016/j.ijrefrig.2003.10.004.

[52] K.C.A. Alam, B.B. Saha, A. Akisawa, T. Kashiwagi, Influence of design and operating conditions on the system performance of a two-stage adsorption chiller, Chem. Eng. Commun. 191 (2004) 981–997. doi:10.1080/00986440490276182.

[53] B.B. Saha, S. Koyama, J.B. Lee, K. Kuwahara, K.C. a Alam, Y. Hamamoto, a. Akisawa, T. Kashiwagi, Performance evaluation of a low-temperature waste heat driven multi-bed adsorption chiller, Int. J. Multiph. Flow. 29 (2003) 1249–1263. doi:10.1016/S0301-9322(03)00103-4.

[54] B.B. Saha, S. Koyama, T. Kashiwagi, a. Akisawa, K.C. Ng, H.T. Chua, Waste heat driven dual-mode, multi-stage, multi-bed regenerative adsorption system, Int. J. Refrig. 26 (2003) 749–757. doi:10.1016/S0140-7007(03)00074-4.

[55] A.S. Uyun, A. Akisawa, T. Miyazaki, Y. Ueda, T. Kashiwagi, Numerical analysis of an advanced three-bed mass recovery adsorption refrigeration cycle, Appl. Therm. Eng. 29 (2009) 2876–2884. doi:10.1016/j.applthermaleng.2009.02.008.

[56] M.Z.I. Khan, B.B. Saha, K.C.A. Alam, A. Akisawa, T. Kashiwagi, ICME05-TH-03 PERFORMANCE INVESTIGATION ON MASS RECOVERY THREE-BED ADSORPTION CYCLE, 2005 (2005) 28–30.

Stellenbosch University https://scholar.sun.ac.za

[57] H.T. Chua, K.C. Ng, A. Malek, T. Kashiwagi, A. Akisawa, B.B. Saha, Multi-bed regenerative adsorption chiller - improving the utilization of waste heat and reducing the chilled water outlet temperature fluctuation, Int. J. Refrig. 24 (2001) 124–136. doi:10.1016/S0140-7007(99)00078-X.

[58] K.C. Ng, X. Wang, Y.S. Lim, B.B. Saha, A. Chakarborty, S. Koyama, A. Akisawa, T. Kashiwagi, Experimental study on performance improvement of a four-bed adsorption chiller by using heat and mass recovery, Int. J. Heat Mass Transf. 49 (2006) 3343–3348. doi:10.1016/j.ijheatmasstransfer.2006.01.053.

[59] D.C. Wang, Y.H. Li, D. Li, Y.Z. Xia, J.P. Zhang, A review on adsorption refrigeration technology and adsorption deterioration in physical adsorption systems, Renew. Sustain. Energy Rev. 14 (2010) 344–353. doi:10.1016/j.rser.2009.08.001.

[60] M.Z.I. Khan, K.C. a Alam, B.B. Saha, a. Akisawa, T. Kashiwagi, Performance evaluation of multi-stage, multi-bed adsorption chiller employing re-heat scheme, Renew. Energy. 33 (2008) 88–98. doi:10.1016/j.renene.2007.01.012.

[61] K. Habib, M.A.B.A. Majid, S.A.B. Sulaiman, Study on two stage activated carbon/HFC-134a based adsorption chiller, IOP Conf. Ser. Earth Environ. Sci. 16 (2013) 012084. doi:10.1088/1755-1315/16/1/012084.

[62] K.C.A. Alam, A. Akahira, Y. Hamamoto, A. Akisawa, T. Kashiwagi, A four-bed mass recovery adsorption refrigeration cycle driven by low temperature waste/renewable heat source, Renew. Energy. 29 (2004) 1461–1475. doi:10.1016/j.renene.2004.01.011.

[63] M. Li, C.J. Sun, R.Z. Wang, W.D. Cai, Development of no valve solar ice maker, Appl. Therm. Eng. 24 (2004) 865–872. doi:10.1016/j.applthermaleng.2003.10.002.

Stellenbosch University https://scholar.sun.ac.za

[64] G. Maggio, L.G. Gordeeva, a. Freni, Y.I. Aristov, G. Santori, F. Polonara, G. Restuccia, Simulation of a solid sorption ice-maker based on the novel composite sorbent “lithium chloride in silica gel pores,” Appl. Therm. Eng. 29 (2009) 1714–1720. doi:10.1016/j.applthermaleng.2008.07.026.

[65] A. Dzigbor, A. Chimphango, Evaluating the potential of using ethanol/water mixture as a refrigerant in adsorption cooling system by using activated carbon - sodium chloride composite adsorbent, Int. J. Refrig. 97 (2019) 132–142. doi:10.1016/j.ijrefrig.2018.09.025.

[66] B.B. Saha, K. Habib, I.I. El-Sharkawy, S. Koyama, Adsorption characteristics and heat of adsorption measurements of R-134a on activated carbon, Int. J. Refrig. 32 (2009) 1563–1569. doi:10.1016/j.ijrefrig.2009.03.010.

[67] S. Elmetenani, M.L. Yousfi, L. Merabeti, Z. Belgroun, A. Chikouche, Investigation of an evaporative air cooler using solar energy under Algerian climate, Energy Procedia. 6 (2011) 573–582. doi:10.1016/j.egypro.2011.05.066.

[68] B.J. Condon, Surface area and porosity determination by physiosorption, n.d.

[69] A.H. Berger, A.S. Bhown, Comparing Physisorption and Chemisorption Solid Sorbents for use Separating CO 2 from Flue Gas using Temperature Swing Adsorption, Energy Procedia. 4 (2011) 562–567. doi:10.1016/j.egypro.2011.01.089.

[70] J.A. Delgado, V.I. Águeda, M.A. Uguina, J.L. Sotelo, A. García-Sanz, A. García, Separation of ethanol–water liquid mixtures by adsorption on BPL activated carbon with air regeneration, Sep. Purif. Technol. 149 (2015) 370–380. doi:10.1016/j.seppur.2015.06.011.

[71] B.F. Dreisbach, H.W. Lösch, Adsorption measurement of water / ethanol mixtures on activated carbon fiber, Chem. Eng. Technol. 24 (2001) 1001–1005.

Stellenbosch University https://scholar.sun.ac.za

[72] L.G. Gordeeva, G. Restuccia, a. Freni, Y.I. Aristov, Water sorption on composites “LiBr in a porous carbon,” Fuel Process. Technol. 79 (2002) 225–231. doi:10.1016/S0378-3820(02)00186-8.

[73] V.J. Inglezakis, A.A. Zorpas, Heat of adsorption, adsorption energy and activation energy in adsorption and ion exchange systems, Desalin. Water Treat. 39 (2012) 149–157. doi:10.1080/19443994.2012.669169.

[74] K. Knaebel, A “How to” guide for adsorber design, (2007). http://www.adsorption.com/wp-content/uploads/2016/04/AdsorberDes2.pdf (accessed October 15, 2015).

[75] N. Ayawei, A.N. Ebelegi, D. Wankasi, Modelling and Interpretation of Adsorption Isotherms, J. Chem. 2017 (2017) 1–11. doi:10.1155/2017/3039817.

[76] K.Y. Foo, B.H. Hameed, Insights into the modeling of adsorption isotherm systems, Chem. Eng. J. 156 (2010) 2–10. doi:10.1016/j.cej.2009.09.013.

[77] J.M. ;Richardso. J.F. Coulson, Particle Technology and Separation Proceses, Butterworth-Heinemann, Oxford, 2002.

[78] Q. Chen, Y. Tian, P. Li, C. Yan, Y. Pang, L. Zheng, H. Deng, W. Zhou, X. Meng, Study on Shale Adsorption Equation Based on Monolayer Adsorption, Multilayer Adsorption, and Capillary Condensation, J. Chem. 2017 (2017) 1–11. doi:10.1155/2017/1496463.

[79] C.Y. Tso, C.Y.H. Chao, Activated carbon , silica-gel and calcium chloride composite adsorbents for energy efficient solar adsorption cooling and dehumidification systems Adsorbants composites au gel de silice / chlorure de calcium ` mes de refroidissement et de de ´ shumidifica, Int. J. Refrig. 35 (2012) 1626–1638. doi:10.1016/j.ijrefrig.2012.05.007.

[80] C. Nguyen, D.D. Do, The Dubinin-Radushkevich equation and the underlying

Stellenbosch University https://scholar.sun.ac.za

microscopic adsorption description, Carbon N. Y. 39 (2001) 1327–1336. doi:10.1016/S0008-6223(00)00265-7.

[81] I.I. El-Sharkawy, B.B. Saha, S. Koyama, J. He, K.C. Ng, C. Yap, Experimental investigation on activated carbon-ethanol pair for solar powered adsorption cooling applications, Int. J. Refrig. 31 (2008) 1407–1413. doi:10.1016/j.ijrefrig.2008.03.012.

[82] A.A. Askalany, M. Salem, I.M. Ismael, A.H.H. Ali, M.G. Morsy, B.B. Saha, An overview on adsorption pairs for cooling, Renew. Sustain. Energy Rev. 19 (2013) 565–572. doi:10.1016/j.rser.2012.11.037.

[83] C.W. Chan, J. Ling-Chin, A.P. Roskilly, A review of chemical heat pumps, thermodynamic cycles and thermal energy storage technologies for low grade heat utilisation, Appl. Therm. Eng. 50 (2013) 1257–1273. doi:10.1016/j.applthermaleng.2012.06.041.

[84] MD Kutub Uddin, Study on Adsorption Characteristics of Ethanol onto Activated Carbons - Effect of Surface Treatment, Kyushu University, Japan, 2014. doi:10.1021/je100973t.

[85] H. Demir, M. Mobedi, S. Ülkü, A review on adsorption heat pump: Problems and solutions, Renew. Sustain. Energy Rev. 12 (2008) 2381–2403. doi:10.1016/j.rser.2007.06.005.

[86] H. Kuwagaki, T. Meguro, J. Tatami, K. Komeya, K. Tamura, An improvement of thermal conduction of activated carbon by adding graphite, J. Mater. Sci. 38 (2003) 3279–3284. doi:10.1023/A:1025138005230.

[87] Z. Jin, B. Tian, L. Wang, R. Wang, Comparison on thermal conductivity and permeability of granular and consolidated activated carbon for refrigeration, Chinese J. Chem. Eng. 21 (2013) 676–682. doi:10.1016/S1004-9541(13)60525-

Stellenbosch University https://scholar.sun.ac.za

X.

[88] D. Menard, X. Py, N. Mazet, Activated carbon monolith of high thermal conductivity for adsorption processes improvement. Part B. Thermal regeneration, Chem. Eng. Process. Process Intensif. 46 (2007) 565–572. doi:10.1016/j.cep.2006.07.013.

[89] D. Menard, X. Py, N. Mazet, Activated carbon monolith of high thermal conductivity for adsorption processes improvement: Part A: Adsorption step, Chem. Eng. Process. Process Intensif. 44 (2005) 1029–1038. doi:10.1016/j.cep.2005.02.002.

[90] Z. Tamainot-Telto, S.J. Metcalf, R.E. Critoph, Y. Zhong, R. Thorpe, Carbon-ammonia pairs for adsorption refrigeration applications: ice making, air conditioning and heat pumping, Int. J. Refrig. 32 (2009) 1212–1229. doi:10.1016/j.ijrefrig.2009.01.008.

[91] I.I. El-Sharkawy, M. Hassan, B.B. Saha, S. Koyama, M.M. Nasr, Study on adsorption of methanol onto carbon based adsorbents, Int. J. Refrig. 32 (2009) 1579–1586. doi:10.1016/j.ijrefrig.2009.06.011.

[92] T. Gunhan, V. Demir, a. K. Yagcioglu, Evaluation of the Suitability of Some Local Materials as Cooling Pads, Biosyst. Eng. 96 (2007) 369–377. doi:10.1016/j.biosystemseng.2006.12.001.

[93] A.N. Shmroukh, A. Ali, A. Abel-Rahman, Adsorption refrigeration working pairs: The state-of-the-art in the application, Int. J. Chem. Mater. Sci. Eng. 7 (2013) 25–37. http://www.waset.org/Publications/adsorption-refrigeration-working-pairs-the-state-of-the-art-in-the-application/17246.

[94] L.G. Gordeeva, A. Freni, T.A. Krieger, G. Restuccia, Y.I. Aristov, Composites “lithium halides in silica gel pores”: Methanol sorption equilibrium, Microporous

Stellenbosch University https://scholar.sun.ac.za

Mesoporous Mater. 112 (2008) 254–261. doi:10.1016/j.micromeso.2007.09.040.

[95] S.D. Sharma, H. Kitano, K. Sagara, Phase Change Materials for Low Temperature Solar Thermal Applications, Res. Rep. Fac. Eng. Mie Univ. 29 (2004) 31–64.

[96] V. V Tyagi, S.C. Kaushik, A. Pandey, S.K. Tyagi, Experimental study of supercooling and pH behaviour of a typical phase change material for thermal energy storage, Indian J. Pure Appl. Phys. 49 (2011) 117–125.

[97] J.J. Guilleminot, a. Choisier, J.B. Chalfen, S. Nicolas, J.L. Reymoney, Heat transfer intensification in fixed bed adsorbers, Heat Recover. Syst. CHP. 13 (1993) 297–300. doi:10.1016/0890-4332(93)90052-W.

[98] A.N. Shmroukh, A.H.H. Ali, A.K. Abel-Rahman, Experimental Study on Adsorption Capacity of Activated Carbon Pairs with Different Refrigerants, Int. J. Chem. Mol. Nucl. Mater. Metall. Eng. Vol7,. 7 (2013) 25–31.

[99] X.H. Li, X.H. Hou, X. Zhang, Z.X. Yuan, A review on development of adsorption cooling—Novel beds and advanced cycles, Energy Convers. Manag. 94 (2015) 221–232. doi:10.1016/j.enconman.2015.01.076.

[100] A.N. Shmroukh, A.H.H. Ali, A.K. Abel-rahman, Experimental Study on Adsorption Capacity of Activated Carbon Pairs with Different Refrigerants, 7 (2013) 461–467.

[101] A.A. Askalany, M. Salem, I.M. Ismail, A.H.H. Ali, M.G. Morsy, A review on adsorption cooling systems with adsorbent carbon, Renew. Sustain. Energy Rev. 16 (2012) 493–500. doi:10.1016/j.rser.2011.08.013.

[102] T. Kawano, M. Kubota, M.S. Onyango, F. Watanabe, H. Matsuda, Preparation of activated carbon from petroleum coke by KOH chemical activation for

Stellenbosch University https://scholar.sun.ac.za

adsorption heat pump, Appl. Therm. Eng. 28 (2008) 865–871. doi:10.1016/j.applthermaleng.2007.07.009.

[103] Z. AlOthman, M. Habila, R. Ali, Preparation of activated carbon using the copyrolysis of agricultural and municipal solid wastes at a low carbonization temperature, in: 2011 Int. Conf. Biol. Environ. Chem., Singapore, 2011: pp. 67–72. http://www.ipcbee.com/vol24/14-ICBEC2011-C00040.pdf.

[104] Argus Media Inc., Energy Argus, (2015).

[105] The Colorado River commision of Nevada, World Fossil Fuels Reserves and Expected Consumtion, (2002) 1–3.

[106] L. Stockman, Petroleum Coke : the coal hiding in the Tar Sands, (2013). http://priceofoil.org/content/uploads/2013/01/OCI.Petcoke.FINALSCREEN.pdf.

[107] I.A.W. Tan, A.L. Ahmad, B.H. Hameed, Preparation of activated carbon from coconut husk: Optimization study on removal of 2,4,6-trichlorophenol using response surface methodology, J. Hazard. Mater. 153 (2008) 709–717. doi:10.1016/j.jhazmat.2007.09.014.

[108] U.J. Etim, S.A. Umoren, U.M. Eduok, Coconut coir dust as a low cost adsorbent for the removal of cationic dye from aqueous solution, J. Saudi Chem. Soc. (2012) S67–S76. doi:10.1016/j.jscs.2012.09.014.

[109] K. Oertel, M. Fischer, Adsorption cooling system for cold storage using methanol/silicagel, Appl. Therm. Eng. 18 (1998) 773–786. doi:10.1016/S1359-4311(97)00107-5.

[110] C.N. Hamelinck, A.P.C. Faaij, Future prospects for production of methanol and hydrogen from biomass, 2002. doi:10.1016/S0378-7753(02)00220-3.

[111] S. Bernesson, D. Nilsson, P.A. Hansson, A limited LCA comparing large- and small-scale production of ethanol for heavy engines under Swedish conditions,

Stellenbosch University https://scholar.sun.ac.za

Biomass and Bioenergy. 30 (2006) 46–57. doi:10.1016/j.biombioe.2005.10.002.

[112] M. Saifuddin, M. Saifuddin, M.M. Khandaker, A. Hossain, S. Jahan, N.B. Mat, N. Boyce, Bioethanol Production from Mango Waste (Mangifera indica L . cv chokanan): Biomass as Renewable Energy, (2014).

[113] L.V. Reddy, O. Vijaya, S. Reddy, Y. Wee, Production of ethanol from mango (Mangifera indica L .) peel by Saccharomyces cerevisiae CFTRI101, 10 (2011) 4183–4189. doi:10.5897/AJB10.2286.

[114] G. Riva, Utilization of renewable energy sources and energy- saving echnologies by small-scale milk plants and collection centres, 2011.

[115] K. Rafferty, Geothermal Power Generation, Geo-Heat Cent. (2000) 1–12. https://geoheat.oit.edu/pdf/powergen.pdf.

[116] F.A. Ola, S.O. Jekayinfa, Ref : C0605 Pyrolysis of mango stone shell:effect of heating temperature and residence time on product yields, (2014) 1–8.

[117] V. Mendu, T. Shearin, J.E. Campbell, J. Stork, J. Jae, M. Crocker, G. Huber, S. DeBolt, Global bioenergy potential from high-lignin agricultural residue, Proc. Natl. Acad. Sci. 109 (2012) 4014–4019. doi:10.1073/pnas.1112757109.

[118] L.W. Wang, R.Z. Wang, J.Y. Wu, Y.X. Xu, S.G. Wang, Design, simulation and performance of a waste heat driven adsorption ice maker for fishing boat, Energy. 31 (2006) 244–259. doi:10.1016/j.energy.2005.03.006.

[119] L.W. Wang, R.Z. Wang, J.Y. Wu, K. Wang, Compound absorbent for adsorption ice maker on fishing boats, Int. J. Refrig. 27 (2004) 401–408. doi:10.1016/j.ijrefrig.2003.11.010.

[120] L.W. Wang, R.Z. Wang, J.Y. Wu, Z.Z. Xia, K. Wang, A new type adsorber for adsorption ice maker on fishing boats, Energy Convers. Manag. 46 (2005) 2301–2316. doi:10.1016/j.enconman.2004.09.010.

Stellenbosch University https://scholar.sun.ac.za

[121] K. Wang, J.Y. Wu, R.Z. Wang, L.W. Wang, Composite adsorbent of CaCl2 and expanded graphite for adsorption ice maker on fishing boats, Int. J. Refrig. 29 (2006) 199–210. doi:10.1016/j.ijrefrig.2005.06.004.

[122] L.W. Wang, R.Z. Wang, J.Y. Wu, K. Wang, S.G. Wang, Adsorption ice makers for fishing boats driven by the exhaust heat from diesel engine: Choice of adsorption pair, Energy Convers. Manag. 45 (2004) 2043–2057. doi:10.1016/j.enconman.2003.10.021.

[123] L.W. Wang, J.Y. Wu, R.Z. Wang, Y.X. Xu, S.G. Wang, Experimental study of a solidified activated carbon-methanol adsorption ice maker, Appl. Therm. Eng. 23 (2003) 1453–1462. doi:10.1016/S1359-4311(03)00103-0.

[124] L. Wang, Energy efficiency and management in food processing facilities, (2009).

[125] S. Vasta, V. Palomba, A. Frazzica, G. Di Bella, A. Freni, Techno-Economic Analysis of Solar Cooling Systems for Residential Buildings in Italy, J. Sol. Energy Eng. 138 (2016) 031005. doi:10.1115/1.4032772.

[126] J.M. Calm, Emissions and environmental impacts from air-conditioning and refrigeration systems, Int. J. Refrig. 25 (2002) 293–305. doi:10.1016/S0140-7007(01)00067-6.

[127] Mayekawa Mfg. Co. Ltd, Adsorption Chiller Operating Manual, (2015) 1–150. http://www.mayekawa.co.id/pic/AdRef-Noa---English-828.pdf (accessed June 21, 2018).

[128] S. Oberweis, T. Al-Shemmeri, Performance Evaluation of a Lithium-Chloride Absorption Refrigeration and an Assessment of Its Suitability for Biomass Waste Heat, Appl. Sci. 2 (2012) 709–725. doi:10.3390/app2040709.

[129] B. Doshi, M. Sillanpää, S. Kalliola, A review of bio-based materials for oil spill

Stellenbosch University https://scholar.sun.ac.za

treatment, Water Res. 135 (2018) 262–277. doi:10.1016/j.watres.2018.02.034.

[130] J.C. Moreno-Piraján, L. Giraldo, Study of activated carbons by pyrolysis of Mangifera Indica seed (mango) in presence of sodium and potassium hydroxide, E-Journal Chem. 9 (2012) 780–785. doi:10.1155/2012/909747.

[131] M.P. Elizalde-González, V. Hernández-Montoya, Characterization of mango pit as raw material in the preparation of activated carbon for wastewater treatment, Biochem. Eng. J. 36 (2007) 230–238. doi:10.1016/j.bej.2007.02.025.

[132] N.A. Rashidi, S. Yusup, A review on recent technological advancement in the activated carbon production from oil palm wastes, Chem. Eng. J. 314 (2017) 277–290. doi:10.1016/j.cej.2016.11.059.

[133] N. Abdullah, F. Sulaiman, The properties of the washed empty fruit bunches of oil palm, J. Phys. Sci. 24 (2013) 117–137. doi:10.1016/j.compositesb.2015.02.023.

[134] M. Soleimani, T. Kaghazchi, Agricultural waste conversion to activated carbon by chemical activation with phosphoric acid, Chem. Eng. Technol. 30 (2007) 649–654. doi:10.1002/ceat.200600325.

[135] F. Sulaiman, N. Abdullah, A.A. Rahman, Basic Properties of Washed and Unwashed Oil Palm Wastes, Proc. 3rd CUTSE Int. Conf. (2011) 8–9. doi:10.1021/jp407438j.

[136] N. Abdullah, H. Gerhauser, Bio-oil derived from empty fruit bunches, Fuel. 87 (2008) 2606–2613. doi:10.1016/j.fuel.2008.02.011.

[137] B.S. Grigis, A.A.-N. El-Hendawy, Porosity development in activated carbons obtained from date pits under chemical activation with phosphoric acid, Microporous Mesoporous Mater. 52 (2002) 105–117. doi:10.1016/S1387-1811(01)00481-4.

Stellenbosch University https://scholar.sun.ac.za

[138] S.O. Bamaga, M.W. Hussin, M.A. Ismail, Palm Oil Fuel Ash: Promising supplementary cementing materials, KSCE J. Civ. Eng. 17 (2013) 1708–1713. doi:10.1007/s12205-013-1241-9.

[139] A. Cobb, M. Warms, E.P. Maurer, S. Chiesa, Low-Tech Coconut Shell Activated Charcoal Production, Int. J. Serv. Learn. Eng. 7 (2012) 93–104.

[140] M.K.B. Gratuito, T. Panyathanmaporn, R.A. Chumnanklang, N. Sirinuntawittaya, A. Dutta, Production of activated carbon from coconut shell: Optimization using response surface methodology, Bioresour. Technol. 99 (2008) 4887–4895. doi:10.1016/j.biortech.2007.09.042.

[141] R. Hoseinzadeh Hesas, A. Arami-Niya, W.M.A. Wan Daud, J.N. Sahu, Preparation of granular activated carbon from oil palm shell by microwave-induced chemical activation: Optimisation using surface response methodology, Chem. Eng. Res. Des. 91 (2013) 2447–2456. doi:10.1016/j.cherd.2013.06.004.

[142] R. Pietrzak, P. Nowicki, J. Kaźmierczak, I. Kuszyńska, J. Goscianska, J. Przepiórski, Comparison of the effects of different chemical activation methods on properties of carbonaceous adsorbents obtained from cherry stones, Chem. Eng. Res. Des. 92 (2014) 1187–1191. doi:10.1016/j.cherd.2013.10.005.

[143] A. Arami-Niya, W.M.A. Wan Daud, F. S. Mjalli, F. Abnisa, M.S. Shafeeyan, Production of microporous palm shell based activated carbon for methane adsorption: Modeling and optimization using response surface methodology, Chem. Eng. Res. Des. 90 (2012) 776–784. doi:10.1016/j.cherd.2011.10.001.

[144] Z.Z. Chowdhury, S.B.A. Hamid, R. Das, M.R. Hasan, S.M. Zain, K. Khalid, M.N. Uddin, Preparation of carbonaceous adsorbents from lignocellulosic biomass and their use in removal of contaminants from aqueous solution, BioResources. 8 (2013) 6523–6555. doi:10.15376/biores.8.4.6523-6555.

Stellenbosch University https://scholar.sun.ac.za

[145] M.F. Alkhatib, S.A. Muyibi, J.O. Amode, Optimization of activated carbon production from empty fruit bunch fibers in one-step steam pyrolysis for cadmium removal from aqueous solution, Environmentalist. 31 (2011) 349–357. doi:10.1007/s10669-011-9342-9.

[146] I.I. Gurten, M. Ozmak, E. Yagmur, Z. Aktas, Preparation and characterisation of activated carbon from waste tea using K2CO3, Biomass and Bioenergy. 37 (2012) 73–81. doi:10.1016/j.biombioe.2011.12.030.

[147] M. Oghbaei, O. Mirzaee, Microwave versus conventional sintering: A review of fundamentals, advantages and applications, J. Alloys Compd. 494 (2010) 175–189. doi:10.1016/j.jallcom.2010.01.068.

[148] T. Kim, J. Lee, K.-H. Lee, Microwave heating of carbon-based solid materials, Carbon Lett. 15 (2014) 15–24. doi:10.5714/CL.2014.15.1.015.

[149] W. Sangchoom, R. Mokaya, Valorization of Lignin Waste: Carbons from Hydrothermal Carbonization of Renewable Lignin as Superior Sorbents for CO<inf>2</inf> and Hydrogen Storage, ACS Sustain. Chem. Eng. 3 (2015) 1658–1667. doi:10.1021/acssuschemeng.5b00351.

[150] A. Funke, F. Ziegler, Hydrothermal carbonization of biomass: A summary and discussion of chemical mechanisms for process engineering, Biofuels, Bioprod. Biorefining. 4 (2010) 160–177. doi:10.1002/bbb.198.

[151] E. Yagmur, M. Ozmak, Z. Aktas, A novel method for production of activated carbon from waste tea by chemical activation with microwave energy, Fuel. 87 (2008) 3278–3285. doi:10.1016/j.fuel.2008.05.005.

[152] R. Wirasnita, T. Hadibarata, A.R.M. Yusoff, Z. Yusop, Removal of Bisphenol A from Aqueous Solution by Activated Carbon Derived from Oil Palm Empty Fruit Bunch, Water, Air, Soil Pollut. 225 (2014) 2148. doi:10.1007/s11270-014-2148-

Stellenbosch University https://scholar.sun.ac.za

x.

[153] H. a Ruiz, M. a Zambrano, L. Giraldo, Production and characterisation of activated carbon from oil-palm shell for carboxylic acid, Orient. J. Chem. 31 (2015) 753–762. doi:10.13005/ojc/310217.

[154] M.A. Islam, I.A.W. Tan, A. Benhouria, M. Asif, B.H. Hameed, Mesoporous and adsorptive properties of palm date seed activated carbon prepared via sequential hydrothermal carbonization and sodium hydroxide activation, Chem. Eng. J. 270 (2015) 187–195. doi:10.1016/j.cej.2015.01.058.

[155] M.A. Islam, M.J. Ahmed, W.A. Khanday, M. Asif, B.H. Hameed, Mesoporous activated coconut shell-derived hydrochar prepared via hydrothermal carbonization-NaOH activation for methylene blue adsorption, J. Environ. Manage. 203 (2017) 237–244. doi:10.1016/j.jenvman.2017.07.029.

[156] D. Kalderis, M.S. Kotti, A. Méndez, G. Gascó, Characterization of hydrochars produced by hydrothermal carbonization of rice husk, Solid Earth. 5 (2014) 477–483. doi:10.5194/se-5-477-2014.

[157] S. Román, J.M. Valente Nabais, B. Ledesma, J.F. González, C. Laginhas, M.M. Titirici, Production of low-cost adsorbents with tunable surface chemistry by conjunction of hydrothermal carbonization and activation processes, Microporous Mesoporous Mater. 165 (2013) 127–133. doi:10.1016/j.micromeso.2012.08.006.

[158] H.Z. Hassan, A Solar Powered Adsorption Freezer: A Case Study for Egypt's Climate, Int. J. Energy Eng. 3 (2013) 21–29. doi:10.5923/j.ijee.20130301.04.

[159] P. Tooklang, S. Vaivudh, S. Sukchai, W. Rakwichian, Thermal Distribution Performance of NPCM : NaCl , NaNO3 and KNO3 in the Thermal Storage System, Energy Power Eng. 6 (2014) 174–185.

Stellenbosch University https://scholar.sun.ac.za

[160] Y.Y. Tanashev, Y.I. Aristov, Thermal conductivity of a silica gel + calcium chloride system: The effect of adsorbed water, J. Eng. Phys. Thermophys. 73 (2000) 876–883. doi:10.1017/CBO9781107415324.004.

[161] Y.Y. Tanashev, A. V. Krainov, Y.I. Aristov, Thermal conductivity of composite sorbents “salt in porous matrix” for heat storage and transformation, Appl. Therm. Eng. 61 (2013) 401–407. doi:10.1016/j.applthermaleng.2013.08.022.

[162] A. Freni, M.M. Tokarev, G. Restuccia, A.G. Okunev, Y.I. Aristov, Thermal conductivity of selective water sorbents under the working conditions of a sorption chiller, Appl. Therm. Eng. 22 (2002) 1631–1642. doi:10.1016/S1359-4311(02)00076-5.

[163] M.H.A. Jahurul, I.S.M. Zaidul, K. Ghafoor, F.Y. Al-Juhaimi, K.L. Nyam, N.A.N. Norulaini, F. Sahena, A.K. Mohd Omar, Mango (Mangifera indica L.) by-products and their valuable components: A review, Food Chem. 183 (2015) 173–180. doi:10.1016/j.foodchem.2015.03.046.

[164] Walter K. Tang, Effect of Inorganic Salts on Pyrolysis of Wood, Cellulose, and Lignin Determined by Differential Thermal Analysis, US For. Serv. Res. Pap. 82 (1968) 1–37.

[165] J.E. Lozano, ASHRAE Handbook-Refrigeration (SI), in: Therm. Propierties Foods, 2006: pp. 9.1-9.31.

[166] S. Shahir, R. Visvananthan, Maturity measurement of mango and banana as related to ripening, Trends Biosci. 7 (2014) 741–744.

[167] Y.A. Cengel, A.J. Ghajar, Heat and Mass Transfer Fundamentals and Applications, 4th ed., McGraw Hill,Inc., New York, USA, 2011.

[168] O. Laguerre, Heat Transfer and Air Flow in a Domestic Refrigerator, in: M.M. Farid (Ed.), Math. Model. Food Process., CRC Press, 2010: pp. 445–474.

Stellenbosch University https://scholar.sun.ac.za

doi:10.1201/9781420053548-c16.

[169] GBH Enterprises Ltd, Process Egineering Guide: Air cooled heat exchanger design, (n.d.). GBHEterprises.com.

[170] R.K. Sinnott, Chemical Engineering Design, 4th ed., Elsevier, Oxford, 2005. doi:10.1016/S1385-8497(00)00184-4.

[171] I.I.T. Kharagpur, Lesson 22, Comp. A J. Comp. Educ. (n.d.) 1–37. https://nptel.ac.in/courses/112105129/pdf/R&AC Lecture 22.pdf.

[172] D.M. Admiraal, C.W. Bullard, Heat transfer in refrigerator- condensers and evaporators, (1993). https://www.ideals.illinois.edu/bitstream/handle/2142/9750/TR048.pdf?sequence=2 (accessed October 3, 2015).

[173] M. Bryden, D. Still, P. Scott, G. Hoffa, D. Ogle, R. Balis, K. Goyer, Design Principles for Wood Burning Cook Stoves, Technical Report 80574, Hazelton road, Cottage Groove, Oregon 97424, 2005.

[174] O. Adria, J. Bethge, The overall worldwide saving potential from domestic cooking stoves and ovens Authors, (2013) 1–15. http://www.bigee.net/media/filer_public/2014/03/17/appliance__residential_cookingstoves__worldwide_potential__20140220__8.pdf (accessed June 1, 2016).

[175] O. Adria, J. Bethge, What users can save with stoves and ovens cooking stoves and ovens, Bigee.Net. (2013) 1–30. http://www.bigee.net/media/filer_public/2014/03/17/appliance__residential_cookingstoves__user_savings__20140220__8.pdf.

[176] H. Yang, R. Yan, H. Chen, D.H. Lee, C. Zheng, Characteristics of hemicellulose, cellulose and lignin pyrolysis, Fuel. 86 (2007) 1781–1788. doi:10.1016/j.fuel.2006.12.013.

Stellenbosch University https://scholar.sun.ac.za

[177] M.S. Peters, K.D. Timmerahus, Plant Design and Economics for Chemical Engineers, 4th ed., McGraw Hill,Inc., New York, 1991.

[178] M.B. Zacharias, S.D. George, Food Process Design, Marcel Dekker Inc., New York, 2003.

[179] Research Triangle Institute (RTI), Greenhouse Gas Emissions Estimation Methodologies for Biogenic Emissions from Selected Source Categories : Solid Waste Disposal Wastewater Treatment Ethanol Fermentation, 2010.

[180] EPA, Direct Emissions from Mobile Combustion Sources, Energy Econ. 34 (2008) 1580–1588. doi:10.1016/j.eneco.2011.11.013.

[181] C. Torres-Leon, R. Rojas, J.C. Contreras-Esquivel, L. Serna-Cock, R.E. Belmares-Cerda, C.N. Aguilar, Mango seed: Functional and nutritional properties, Trends Food Sci. Technol. 55 (2016) 109–117. doi:10.1016/j.tifs.2016.06.009.

[182] S. Chakraborty, S. De, S. DasGupta, J.K. Basu, Adsorption study for the removal of a basic dye: Experimental and modeling, Chemosphere. 58 (2005) 1079–1086. doi:10.1016/j.chemosphere.2004.09.066.

[183] S.M. Yakout, G. Sharaf El-Deen, Characterization of activated carbon prepared by phosphoric acid activation of olive stones, Arab. J. Chem. 9 (2016) S1155–S1162. doi:10.1016/j.arabjc.2011.12.002.

[184] M. Matos, M.F. Barreiro, A. Gandini, Olive stone as a renewable source of biopolyols, Ind. Crops Prod. 32 (2010) 7–12. doi:10.1016/j.indcrop.2010.02.010.

[185] O. Ioannidou, a. Zabaniotou, Agricultural residues as precursors for activated carbon production-A review, Renew. Sustain. Energy Rev. 11 (2007) 1966–2005. doi:10.1016/j.rser.2006.03.013.

[186] C. Nieto-Delgado, M. Terrones, J.R. Rangel-Mendez, Development of highly

Stellenbosch University https://scholar.sun.ac.za

microporous activated carbon from the alcoholic beverage industry organic by-products, Biomass and Bioenergy. 35 (2011) 103–112. doi:10.1016/j.biombioe.2010.08.025.

[187] C. Nieto-Delgado, J.R. Rangel-Mendez, Production of activated carbon from organic by-products from the alcoholic beverage industry: Surface area and hardness optimization by using the response surface methodology, Ind. Crops Prod. 34 (2011) 1528–1537. doi:10.1016/j.indcrop.2011.05.014.

[188] B.G. Salas-Enrıquez, A.M. Torres-Huerta, E. Conde-Barajas, M.A. Domınguez-Crespo, L. Dıaz-Garcia, M.L.X. de la Negrete-Rodrıguez, Activated carbon production from the Guadua amplexifolia using a combination of physical and chemical activation, J. Therm. Anal. Calorim. 124 (2016) 1383–1398. doi:10.1007/s10973-016-5238-8.

[189] Suhas, P.J.M. Carrott, M.M.L. Ribeiro Carrott, Lignin - from natural adsorbent to activated carbon: A review, Bioresour. Technol. 98 (2007) 2301–2312. doi:10.1016/j.biortech.2006.08.008.

[190] D. Adinata, W.M.A. Wan Daud, M.K. Aroua, Preparation and characterization of activated carbon from palm shell by chemical activation with K2CO3, Bioresour. Technol. 98 (2007) 145–149. doi:10.1016/j.biortech.2005.11.006.

[191] D.C. Cruz, Production of Bio-coal and Activated Carbon From Biomass, The University of Western Ontario London, Ontario, Canada, 2013. https://ir.lib.uwo.ca/cgi/viewcontent.cgi?article=2382&context=etd.

[192] W.T. Tsai, C.Y. Chang, S.L. Lee, A low cost adsorbent from agricultural waste corn cob by zinc chloride activation, Bioresour. Technol. 64 (1998) 211–217. doi:10.1016/S0960-8524(97)00168-5.

[193] I. Yakub, M. Mohammad, Z. Yaakob, Effects of Zinc Chloride Impregnation on

Stellenbosch University https://scholar.sun.ac.za

the Characteristics of Activated Carbon Produced from Physic Nut Seed Hull, Adv. Mater. Res. 626 (2013) 751–755. doi:10.4028/www.scientific.net/AMR.626.751.

[194] The National Institute for Occupational Safety and Health (NIOSH), Phosphoric acid, (2018). https://www.cdc.gov/niosh/npg/npgd0506.html (accessed November 25, 2018).

[195] The National Institute for Occupational Safety and Health (NIOSH), Zinc Chloride, (2015). https://www.cdc.gov/niosh/ipcsneng/neng1064.html (accessed November 25, 2018).

[196] Anonymous, Sodium Chloride Material safety data sheet, (2010). http://mpf.aap.cornell.edu/mpf/msds/printmaking/Intaglio/SodiumChloride.pdf (accessed November 26, 2018).

[197] S. Mise, T.N. Patil, Adsorption Studies of Chromium(VI) on Activated Carbon Derived from Mangifera indica (Mango) Seed Shell, J. Inst. Eng. Ser. A. 96 (2015) 237–247. doi:10.1007/s40030-015-0124-0.

[198] Calgon Carbon Coporation, Product Bulletin, 2013. http://www.calgoncarbon.com/wp-content/uploads/product-literature/WPX.pdf.

[199] D.C. Montgomery, Design and Analysis of Experiments, Eighth, John Wiley & Sons. Inc., New Jersey, 2012. doi:10.1198/tech.2006.s372.

[200] ASTM International, Standard test methods for moisture in activated carbon, 14 (1999) 1–4. doi:10.1520/D2867-09.2.

[201] ASTM International, Standard test method for total ash content of activated carbon, ASTM Stand. 15 (2004) 1–2. doi:10.1520/D2866-11.2.

[202] ASTM International, Standard test method for volatile matter content of activated carbon samples, ASTM Stand. 15 (2004) 3–4. doi:10.1520/D5832-98R08.2.

Stellenbosch University https://scholar.sun.ac.za

[203] A. Sluiter, B. Hames, R.O. Ruiz, C. Scarlata, J. Sluiter, D. Templeton, D. of Energy, Determination of Structural Carbohydrates and Lignin in Biomass, 2008. doi:NREL/TP-510-42618.

[204] M. Molina-Sabio, F. RodRíguez-Reinoso, F. Caturla, M.J. Sellés, Porosity in granular carbons activated with phosphoric acid, Carbon N. Y. 33 (1995) 1105–1113. doi:10.1016/0008-6223(95)00059-M.

[205] A. Mianowski, M. Owczarek, A. Marecka, Surface Area of Activated Carbon Determined by the Iodine Adsorption Number, 2007. doi:10.1080/00908310500430901.

[206] N. Setoyama, K. Kaneko, F. Rodriguez-Reinoso, Ultramicropore Characterization of Microporous Carbons by Low-Temperature Helium Adsorption, J. Phys. Chem. 100 (1996) 10331–10336. doi:10.1021/jp960467p.

[207] A.. Linares-Solano, C. de L. Salinas-Maritnez, J. Alcafiiz-Monge, D. Cazorla-Amoros, Further Microporous Advances Carbons in the Characterization by Physical Adsorption of of Gases, Tanso. 185 (1998) 316–325.

[208] D. Lozano-Castello, D. Cazorla-Amoros, A. Linares-Solano, Usefulness of CO2 adsorption at 273 K for the characterization of porous carbons, Carbon N. Y. 42 (2004) 1231–1236. doi:10.1016/j.carbon.2004.01.037.

[209] H. de Jonge, M.C. Mittelmeijer-Hazeleger, Adsorption of CO 2 and N 2 on Soil Organic Matter: Nature of Porosity, Surface Area, and Diffusion Mechanisms, Environ. Sci. Technol. 30 (1996) 408–413. doi:10.1021/es950043t.

[210] K. Gergova, N. Petrov, S. Eser, Adsorption properties and microstructure of activated carbons produced from agricultural by-products by steam pyrolysis, Carbon N. Y. 32 (1994) 693–702. doi:10.1016/0008-6223(94)90091-4.

[211] K.J. Silgado, G.D. Marrugo, J. Puello, Adsorption of chromium (VI) by activated

Stellenbosch University https://scholar.sun.ac.za

carbon produced from oil palm endocarp, Chem. Eng. Trans. 37 (2014) 721–726. doi:10.3303/CET1437121.

[212] Z. Qiao, Y. Wang, Y. Gao, H. Li, T. Dai, Y. Liu, Commercial Activated Carbons as the Sources for Produding Multicolor Photoluminescent Carbon Dots by Chemical Oxidation, Chem. Commun. (2010) 8812–8814. doi:10.1039/C0CC02724C.

[213] A. Dzigbor, A. Chimphango, Production and optimization of NaCl-activated carbon from mango seed using surface response methodology, Biomass Convers. Biorefrinery. (2019) 16–18. doi:https://doi.org/10.1007/s13399-018-0361-3.

[214] Q.P. Campbell, J.R. Bunt, H. Kasaini, D.J. Kruger, The preparation of activated carbon from South African coal, J. South African Inst. Min. Metall. 112 (2012) 37–44.

[215] M. Pakuła, M. Walczyk, S. Biniak, A. Świątkowski, Electrochemical and FTIR studies of the mutual influence of lead(II) or iron(III) and phenol on their adsorption from aqueous acid solution by modified activated carbons, Chemosphere. 69 (2007) 209–219. doi:10.1016/j.chemosphere.2007.04.028.

[216] H. Peng, N. Wang, Z. Hu, Z. Yu, Y. Liu, J. Zhang, R. Ruan, Physicochemical characterization of hemicelluloses from bamboo (Phyllostachys pubescens Mazel) stem, Ind. Crops Prod. 37 (2012) 41–50. doi:10.1016/j.indcrop.2011.11.031.

[217] M.A. Henrique, H.A. Silverio, W.P. Flauzino Neto, D. Pasquini, Valorization of an agro-industrial waste, mango seed, by the extraction and characterization of its cellulose nanocrystals, J. Environ. Manage. 121 (2013) 202–209. doi:10.1016/j.jenvman.2013.02.054.

Stellenbosch University https://scholar.sun.ac.za

[218] M.S. Fernandes, G.J.V.N. Brites, J.J. Costa, A.R. Gaspar, V.A.F. Costa, Review and future trends of solar adsorption refrigeration systems, Renew. Sustain. Energy Rev. 39 (2014) 102–123. doi:10.1016/j.rser.2014.07.081.

[219] B. Choudhury, B.B. Saha, P.K. Chatterjee, J.P. Sarkar, An overview of developments in adsorption refrigeration systems towards a sustainable way of cooling, Appl. Energy. 104 (2013) 554–567. doi:10.1016/j.apenergy.2012.11.042.

[220] B.B. Saha, A. Akisawa, T. Kashiwagi, Silica gel water advanced adsorption refrigeration cycle, Energy. 22 (1997) 437–447. doi:10.1016/S0360-5442(96)00102-8.

[221] K.C. Ng, H.T. Chua, C.Y. Chung, C.H. Loke, T. Kashiwagi, a. Akisawa, B.B. Saha, Experimental investigation of the silica gel-water adsorption isotherm characteristics, Appl. Therm. Eng. 21 (2001) 1631–1642. doi:10.1016/S1359-4311(01)00039-4.

[222] E.I. Ohimain, P.E. Tuwon, E.A. Ayibaebi, Traditional Fermentation and Distillation of Raffia Palm Sap for the Production of Bioethanol in Bayelsa State , Nigeria, (2012) 131–141.

[223] D. Attan, M.A. Alghoul, B.B. Saha, J. Assadeq, K. Sopian, The role of activated carbon fiber in adsorption cooling cycles, Renew. Sustain. Energy Rev. 15 (2011) 1708–1721. doi:10.1016/j.rser.2010.10.017.

[224] M.A. Alghoul, M.Y. Sulaiman, B.Z. Azmi, K. Sopian, M.A. Wahab, Review of materials for adsorption refrigeration technology, Anti-Corrosion Methods Mater. 54 (2007) 225–229. doi:10.1108/00035590710762366.

[225] R.E. Critoph, Forced convection adsorption cycles, 18 (1998) 799–807. doi:10.1016/S1359-4311(97)00110-5.

Stellenbosch University https://scholar.sun.ac.za

[226] M. Berdja, B. Abbad, F. Yahi, F. Bouzefour, M. Ouali, Design and realization of a solar adsorption refrigeration machine powered by solar energy, Energy Procedia. 48 (2014) 1226–1235. doi:10.1016/j.egypro.2014.02.139.

[227] B. Dinesh, M. Sai Manikanta, T. Dishal Kumar, D. Sahu, A Case Study of a Low Power Vapour Adsorption Refrigeration System, in: IOP Conf. Ser. Mater. Sci. Eng., 2016. doi:10.1088/1757-899X/149/1/012227.

[228] A.A. Askalany, B.B. Saha, K. Habib, Adsorption Cooling System Carbon / R32 Adsorption Pair Employing Activated, MATEC Web Conf. 13 (2014) 1–6.

[229] R.G. Oliveira, R.Z. Wang, C. Wang, Evaluation of the cooling performance of a consolidated expanded graphite-calcium chloride reactive bed for chemisorption icemaker, Int. J. Refrig. 30 (2007) 103–112. doi:10.1016/j.ijrefrig.2006.08.003.

[230] S. Wu, T.X. Li, T. Yan, R.Z. Wang, Experimental study on a solar-powered thermochemical sorption refrigeration system using strontium chloride / EG-ammonia working pair, in: Int. Refrig. Air Cond. Conf., University of Purdue, Purdue, 2016: pp. 1–10.

[231] Z.S. Lu, R.Z. Wang, Z.Z. Xia, X.R. Lu, C.B. Yang, Y.C. Ma, G.B. Ma, Study of a novel solar adsorption cooling system and a solar absorption cooling system with new CPC collectors, 50 (2013). doi:10.1016/j.renene.2012.07.001.

[232] A. Alahmer, X. Wang, R. Al-Rbaihat, K.C. Amanul Alam, B.B. Saha, Performance evaluation of a solar adsorption chiller under different climatic conditions, Appl. Energy. 175 (2016) 293–304. doi:10.1016/j.apenergy.2016.05.041.

[233] W. Li, C. Joshi, P. Xu, F.P. Schmidt, Experimental Study on Adsorption Refrigeration System with Stratified Storage - Analysis of Storage Discharge Operation, in: 8th Int. Cold Clim. HVAC 2015 Conf. CCHVAC 2015, Elsevier

Stellenbosch University https://scholar.sun.ac.za

B.V., 2016: pp. 625–631. doi:10.1016/j.proeng.2016.06.416.

[234] T. Zeng, H. Huang, N. Kobayashi, J. Li, Performance of an Activated Carbon-Ammonia Adsorption Refrigeration System, Nat. Resour. 08 (2017) 611–631. doi:10.4236/nr.2017.810039.

[235] I. Solmuş, B. Kaftanoğlu, C. Yamali, D. Baker, Experimental investigation of a natural zeolite-water adsorption cooling unit, Appl. Energy. 88 (2011) 4206–4213. doi:10.1016/j.apenergy.2011.04.057.

[236] S. Trisupakitti, J. Jamradloedluk, S. Wiriyaumpaiwong, Adsorption cooling system using metal-impregnated zeolite-4A, Adv. Mater. Sci. Eng. 2016 (2016). doi:10.1155/2016/4283271.

[237] Z. He, Y. Bai, H. Huang, J. Li, Huhetaoli, N. Kobayashi, Y. Osaka, L. Deng, Study on the performance of compact adsorption chiller with vapor valves, Appl. Therm. Eng. 126 (2017) 37–42. doi:10.1016/j.applthermaleng.2017.07.130.

[238] T.X. Li, R.Z. Wang, L.W. Wang, J.K. Kiplagat, Study on the heat transfer and sorption characteristics of a consolidated composite sorbent for solar-powered thermochemical cooling systems, Sol. Energy. 83 (2009) 1742–1755. doi:10.1016/j.solener.2009.06.013.

[239] B.B. Saha, S. Koyama, I.I. El-Sharkawy, K. Kuwahara, K. Kariya, K.C. Ng, Experiments for measuring adsorption characteristics of an activated carbon fiber/ethanol pair using a plate-fin heat exchanger, HVAC R Res. 12 (2006) 767–782. doi:10.1080/10789669.2006.10391206.

[240] G. Restuccia, A. Freni, F. Russo, S. Vasta, Experimental investigation of a solid adsorption chiller based on a heat exchanger coated with hydrophobic zeolite, Appl. Therm. Eng. 25 (2005) 1419–1428. doi:10.1016/j.applthermaleng.2004.09.012.

Stellenbosch University https://scholar.sun.ac.za

[241] K. Wang, J.Y. Wu, R.Z. Wang, L.W. Wang, Effective thermal conductivity of expanded graphite-CaCl2 composite adsorbent for chemical adsorption chillers, Energy Convers. Manag. 47 (2006) 1902–1912. doi:10.1016/j.enconman.2005.09.005.

[242] C.Y. Tso, C.Y.H. Chao, S.C. Fu, International Journal of Heat and Mass Transfer Performance analysis of a waste heat driven activated carbon based composite adsorbent – Water adsorption chiller using simulation model, 55 (2012) 7596–7610. doi:10.1016/j.ijheatmasstransfer.2012.07.064.

[243] S. Al-Asheh, F. Banat, A.A. Fara, Dehydration of Ethanol-Water Azeotropic Mixture by Adsorption Through Phillipsite Packed-Column, Sep. Sci. Technol. 44 (2009) 3170–3188. doi:10.1080/01496390903182479.

[244] J.A. Delgado, V.I. Águeda, M.A. Uguina, J.L. Sotelo, A. García, P. Brea, A. García-Sanz, Separation of ethanol-water liquid mixtures by adsorption on a polymeric resin Sepabeads 207®, Chem. Eng. J. 220 (2013) 89–97. doi:10.1016/j.cej.2013.01.057.

[245] S.H. Mameng, A. Bergquist, E. Johansson, Corrosion of Stainless Steel in Sodium Chloride Brine Solutions, in: Corros. 2014, NACE International, San Antonio, TX, 2014: pp. 1–12. https://www.onepetro.org/conference-paper/NACE-2014-4077.

[246] M.D. Asaduzzaman, C. Mohammad, I. Mayeedul, Effects of concentration of sodium chloride solution on the pitting corrosion behavior of AISI 304L austenitic stainless steel, Chem. Ind. Chem. Eng. Q. 17 (2011) 477–483. doi:10.2298/CICEQ110406032A.

[247] C. Telmo, J. Lousada, Heating values of wood pellets from different species, Biomass and Bioenergy. 35 (2011) 2634–2639.

Stellenbosch University https://scholar.sun.ac.za

doi:10.1016/j.biombioe.2011.02.043.

[248] A. Sharafian, M. Bahrami, Assessment of adsorber bed designs in waste-heat driven adsorption cooling systems for vehicle air conditioning and refrigeration, Renew. Sustain. Energy Rev. 30 (2014) 440–451. doi:10.1016/j.rser.2013.10.031.

[249] K. Uddin, I.I. El-sharkawy, Thermodynamic analysis of adsorption refrigeration cycles using parent and surface treated maxsorb III / ethanol pairs, in: 15th Int. Refrig. Air Cond. Conf., Purdue, 2014.

[250] I. Tavman, Y. Aydogdu, M. Kök, a Turgut, a Ezan, Measurement of heat capacity and thermal conductivity of HDPE / expanded graphite nanocomposites by differential scanning calorimetry, Arch. Mater. Sci. Eng. 50 (2011) 56–60. http://www.archivesmse.org/vol50_1/5016.pdf.

[251] S.J. Peters, G.E. Ewing, Water on Salt: An Infrared Study of Adsorbed H 2 O on NaCl(100) under Ambient Conditions , J. Phys. Chem. B. 101 (2002) 10880–10886. doi:10.1021/jp972810b.

[252] S.P. Pinho, E. a. Macedo, Solubility of NaCl, NaBr, and KCl in water, methanol, ethanol, and their mixed solvents, J. Chem. Eng. Data. 50 (2005) 29–32. doi:10.1021/je049922y.

[253] L.G. Gordeeva, Y.I. Aristov, Composite sorbent of methanol “ LiCl in mesoporous silica gel” for adsorption cooling: Dynamic optimization, Energy. 36 (2011) 1273–1279. doi:10.1016/j.energy.2010.11.016.

[254] A.A. Askalany, S.K. Henninger, M. Ghazy, B.B. Saha, Effect of improving thermal conductivity of the adsorbent on performance of adsorption cooling system, Appl. Therm. Eng. 110 (2017) 695–702. doi:10.1016/j.applthermaleng.2016.08.075.

Stellenbosch University https://scholar.sun.ac.za

[255] A. Frazzica, V. Palomba, B. Dawoud, G. Gullì, V. Brancato, A. Sapienza, S. Vasta, A. Freni, F. Costa, G. Restuccia, Design , realization and testing of an adsorption refrigerator based on activated carbon / ethanol working pair, Appl. Energy. 174 (2016) 15–24. doi:10.1016/j.apenergy.2016.04.080.

[256] S. Al-Asheh, F. Banat, N. Al-Lagtah, Separation of ethanol–water mixtures using molecular sieves and biobased adsorbents, Chem. Eng. Res. Des. 82 (2004) 855–864. doi:10.1205/0263876041596779.

[257] K. Chang, G. Vaagt, S. Domingo, Mango-its current world-market situation, 2013.

[258] J. De la Cruz, H.. García, Mango: Post-harvest Operations, 2002.

[259] A. Garg, K. Kazunari, T. Pulles, 2006 IPCC Guidelines for National Greenhouse Gas Inventories, Volume 2: Energy, 2006. doi:10.1111/j.1440-1843.2006.00937_1.x.

[260] F. Cherubini, G.P. Peters, T. Berntsen, A.H. Strømman, E. Hertwich, CO2 emissions from biomass combustion for bioenergy: Atmospheric decay and contribution to global warming, GCB Bioenergy. 3 (2011) 413–426. doi:10.1111/j.1757-1707.2011.01102.x.

[261] M.C. Barma, R. Saidur, S.M.A. Rahman, A. Allouhi, B.A. Akash, S.M. Sait, A review on boilers energy use, energy savings, and emissions reductions, Renew. Sustain. Energy Rev. 79 (2017) 970–983. doi:10.1016/j.rser.2017.05.187.

[262] S.G. Wang, R.Z. Wang, Recent developments of refrigeration technology in fishing vessels, Renew. Energy. 30 (2005) 589–600. doi:10.1016/j.renene.2004.03.020.

[263] R. Suntivarakorn, W. Treedet, Improvement of Boiler’s Efficiency Using Heat

Stellenbosch University https://scholar.sun.ac.za

Recovery and Automatic Combustion Control System, Energy Procedia. 100 (2016) 193–197. doi:10.1016/j.egypro.2016.10.164.

[264] O.J. Ikegwu, F.C. Ekwu, Thermal and physical properties of some tropical fruits and their juices in Nigeria, J. Food Technol. 7 (2009) 38–42.

[265] W.A. Johnston, F.J. Nicholson, A. Roger, G.D. Stroud, Freezing and refrigerated storage in fisheries, 1994. http://www.fao.org/3/a-v3630e/V3630E00.htm#Contents.

[266] H. Ubabuike, E. Alfred, Design and Adaptation of a Commercial Cold Storage Room for Umudike Community and Environs, IOSR J. Eng. 2 (2012) 1234–1250.

[267] 2015 - 2016 Guide To Machinery Costs Trucks, (2016).

[268] A. Evans, V. Strezov, T.J. Evans, Assessment of sustainability indicators for renewable energy technologies, Renew. Sustain. Energy Rev. 13 (2009) 1082–1088. doi:10.1016/j.rser.2008.03.008.

[269] Matheson Gas Products, Gas Data Book, 7th Editio, 2001. doi:10.1016/j.physe.2012.03.016.

[270] D.R. Gómez, J.D. Watterson, B.B. Americanohia, C. Ha, G. Marland, E. Matsika, L.N. Namayanga, B. Osman-Elasha, J.D.K. Saka, K. Treanton, 2006 IPCC Guidelines for National Greenhouse Gas Inventories.Chapter 2: Stationary Combustion, 2006. doi:10.1016/S0166-526X(06)47021-5.

[271] F. Cherubini, GHG balances of bioenergy systems - Overview of key steps in the production chain and methodological concerns, Renew. Energy. 35 (2010) 1565–1573. doi:10.1016/j.renene.2009.11.035.

[272] A. Gezae, J.F. Görgens, Techno-economic analysis and environmental impact assessment of lignocellulosic lactic acid production, Chem. Eng. Sci. 162 (2017)

Stellenbosch University https://scholar.sun.ac.za

53–65. doi:10.1016/j.ces.2016.12.054.

[273] S.P. Divekar, R.D. Bisen, Engineering Properties of Locally Available Mango Stone, Int. J. Appl. Pure Sci. Agric. 415712 (2016) 121–130.

[274] J. Bai, C. Yang, Z. Zhao, X. Zhong, Y. Zhang, J. Xu, B. Xi, H. Liu, Effect of bulk density of coking coal on swelling pressure, J. Environ. Sci. (China). 25 (2013) S205–S209. doi:10.1016/S1001-0742(14)60657-4.

[275] J.A. Delgado, V.I. Águeda, M.A. Uguina, J.L. Sotelo, A. García, P. Brea, A. García-Sanz, Separation of ethanol-water liquid mixtures by adsorption on a polymeric resin Sepabeads 207®, Chem. Eng. J. 220 (2013) 89–97. doi:10.1016/j.cej.2013.01.057.

[276] A. Dzigbor, A. Chimphango, An integrated strategy targeting drying and cooling unit operations to improve economic viability and reduce environmental impacts in a mango processing plant, Clean Technol. Environ. Policy. 21 (2019) 139–153. doi:10.1007/s10098-018-1623-2.

[277] F.D. Romelle, A. Rani, R.S. Manohar, Chemical composition of some selected fruit peels, Eur. J. Food Sci. Technol. 4 (2016) 12–21.

[278] C.M. Ajila, S.G. Bhat, U.J.S. Prasada Rao, Valuable components of raw and ripe peels from two Indian mango varieties, Food Chem. 102 (2007) 1006–1011. doi:10.1016/j.foodchem.2006.06.036.

[279] R.N. Tharanathan, H.M. Yashoda, T.N. Prabha, Mango (Mangifera indica L.), “the king of fruits” - An overview, 2006. doi:10.1080/87559120600574493.

Stellenbosch University https://scholar.sun.ac.za

Stellenbosch University https://scholar.sun.ac.za

APPENDIX

Appendix A1

ELSEVIER LICENSE
TERMS AND CONDITIONS

Feb 27, 2019

This Agreement between Mr. Aaron Dzigbor ("You") and Elsevier ("Elsevier") consists of your license details and the terms and conditions provided by Elsevier and Copyright Clearance Center.

License Number	4536930865052
License date	Feb 27, 2019
Licensed Content Publisher	Elsevier
Licensed Content Publication	International Journal of Refrigeration
Licensed Content Title	Evaluating the potential of using ethanol/water mixture as a refrigerant in adsorption cooling system by using activated carbon - sodium chloride composite adsorbent
Licensed Content Author	Aaron Dzigbor,Annie Chimphango
Licensed Content Date	Jan 1, 2019
Licensed Content Volume	97
Licensed Content Issue	n/a
Licensed Content Pages	11
Start Page	132
End Page	142
Type of Use	reuse in a thesis/dissertation

Stellenbosch University https://scholar.sun.ac.za

Intended publisher of new work	other
Portion	full article
Circulation	500
Format	both print and electronic
Are you the author of this Elsevier article?	No
Will you be translating?	No
Title of your thesis/dissertation	Designing and evaluating the technical, economic and environmental performance of an adsorption cooling system operating using bioresources from waste streams of mango processing
Publisher of new work	Stellenbosch University
Expected completion date	Jun 2019
Estimated size (number of pages)	1
Requestor Location	Mr. Aaron Dzigbor Department of Process Engineering Stellenbosch University Stellenbosch, Western Cape 7602 South Africa Attn: Mr. Aaron Dzigbor
Publisher Tax ID	ZA 4110266048
Billing Type	Invoice
Billing Address	Mr. Aaron Dzigbor Department of Process Engineering Stellenbosch University

Stellenbosch University https://scholar.sun.ac.za

Stellenbosch, South Africa 7602

Attn: Mr. Aaron Dzigbor

Total 0.00 USD

Terms and Conditions

INTRODUCTION

1. The publisher for this copyrighted material is Elsevier. By clicking "accept" in connection with completing this licensing transaction, you agree that the following terms and conditions apply to this transaction (along with the Billing and Payment terms and conditions established by Copyright Clearance Center, Inc. ("CCC"), at the time that you opened your Rightslink account and that are available at any time at http://myaccount.copyright.com).

GENERAL TERMS

2. Elsevier hereby grants you permission to reproduce the aforementioned material subject to the terms and conditions indicated.

3. Acknowledgement: If any part of the material to be used (for example, figures) has appeared in our publication with credit or acknowledgement to another source, permission must also be sought from that source. If such permission is not obtained then that material may not be included in your publication/copies. Suitable acknowledgement to the source must be made, either as a footnote or in a reference list at the end of your publication, as follows:

"Reprinted from Publication title, Vol /edition number, Author(s), Title of article / title of chapter, Pages No., Copyright (Year), with permission from Elsevier [OR APPLICABLE SOCIETY COPYRIGHT OWNER]." Also Lancet special credit - "Reprinted from The Lancet, Vol. number, Author(s), Title of article, Pages No., Copyright (Year), with permission from Elsevier."

4. Reproduction of this material is confined to the purpose and/or media for which permission is hereby given.

5. Altering/Modifying Material: Not Permitted. However figures and illustrations may be altered/adapted minimally to serve your work. Any other abbreviations, additions, deletions and/or any other alterations shall be made only with prior written authorization of Elsevier Ltd. (Please contact Elsevier

Stellenbosch University https://scholar.sun.ac.za

at permissions@elsevier.com). No modifications can be made to any Lancet figures/tables and they must be reproduced in full.

6. If the permission fee for the requested use of our material is waived in this instance, please be advised that your future requests for Elsevier materials may attract a fee.

7. Reservation of Rights: Publisher reserves all rights not specifically granted in the combination of (i) the license details provided by you and accepted in the course of this licensing transaction, (ii) these terms and conditions and (iii) CCC's Billing and Payment terms and conditions.

8. License Contingent Upon Payment: While you may exercise the rights licensed immediately upon issuance of the license at the end of the licensing process for the transaction, provided that you have disclosed complete and accurate details of your proposed use, no license is finally effective unless and until full payment is received from you (either by publisher or by CCC) as provided in CCC's Billing and Payment terms and conditions. If full payment is not received on a timely basis, then any license preliminarily granted shall be deemed automatically revoked and shall be void as if never granted. Further, in the event that you breach any of these terms and conditions or any of CCC's Billing and Payment terms and conditions, the license is automatically revoked and shall be void as if never granted. Use of materials as described in a revoked license, as well as any use of the materials beyond the scope of an unrevoked license, may constitute copyright infringement and publisher reserves the right to take any and all action to protect its copyright in the materials.

9. Warranties: Publisher makes no representations or warranties with respect to the licensed material.

10. Indemnity: You hereby indemnify and agree to hold harmless publisher and CCC, and their respective officers, directors, employees and agents, from and against any and all claims arising out of your use of the licensed material other than as specifically authorized pursuant to this license.

11. No Transfer of License: This license is personal to you and may not be sublicensed, assigned, or transferred by you to any other person without publisher's written permission.

Stellenbosch University https://scholar.sun.ac.za

12. No Amendment Except in Writing: This license may not be amended except in a writing signed by both parties (or, in the case of publisher, by CCC on publisher's behalf).

13. Objection to Contrary Terms: Publisher hereby objects to any terms contained in any purchase order, acknowledgment, check endorsement or other writing prepared by you, which terms are inconsistent with these terms and conditions or CCC's Billing and Payment terms and conditions. These terms and conditions, together with CCC's Billing and Payment terms and conditions (which are incorporated herein), comprise the entire agreement between you and publisher (and CCC) concerning this licensing transaction. In the event of any conflict between your obligations established by these terms and conditions and those established by CCC's Billing and Payment terms and conditions, these terms and conditions shall control.

14. Revocation: Elsevier or Copyright Clearance Center may deny the permissions described in this License at their sole discretion, for any reason or no reason, with a full refund payable to you. Notice of such denial will be made using the contact information provided by you. Failure to receive such notice will not alter or invalidate the denial. In no event will Elsevier or Copyright Clearance Center be responsible or liable for any costs, expenses or damage incurred by you as a result of a denial of your permission request, other than a refund of the amount(s) paid by you to Elsevier and/or Copyright Clearance Center for denied permissions.

LIMITED LICENSE

The following terms and conditions apply only to specific license types:

15. **Translation**: This permission is granted for non-exclusive world **English** rights only unless your license was granted for translation rights. If you licensed translation rights you may only translate this content into the languages you requested. A professional translator must perform all translations and reproduce the content word for word preserving the integrity of the article.

16. **Posting licensed content on any Website**: The following terms and conditions apply as follows: Licensing material from an Elsevier journal: All content posted to the web site must maintain the copyright information line on the bottom of each image; A hyper-text must be included to the Homepage of the journal from which you are licensing at http://www.sciencedirect.com/science/journal/xxxxx or

Stellenbosch University https://scholar.sun.ac.za

the Elsevier homepage for books at http://www.elsevier.com; Central Storage: This license does not include permission for a scanned version of the material to be stored in a central repository such as that provided by Heron/XanEdu.
Licensing material from an Elsevier book: A hyper-text link must be included to the Elsevier homepage at http://www.elsevier.com . All content posted to the web site must maintain the copyright information line on the bottom of each image.

Posting licensed content on Electronic reserve: In addition to the above the following clauses are applicable: The web site must be password-protected and made available only to bona fide students registered on a relevant course. This permission is granted for 1 year only. You may obtain a new license for future website posting.
17. **For journal authors:** the following clauses are applicable in addition to the above:
Preprints:
A preprint is an author's own write-up of research results and analysis, it has not been peer-reviewed, nor has it had any other value added to it by a publisher (such as formatting, copyright, technical enhancement etc.).
Authors can share their preprints anywhere at any time. Preprints should not be added to or enhanced in any way in order to appear more like, or to substitute for, the final versions of articles however authors can update their preprints on arXiv or RePEc with their Accepted Author Manuscript (see below).
If accepted for publication, we encourage authors to link from the preprint to their formal publication via its DOI. Millions of researchers have access to the formal publications on ScienceDirect, and so links will help users to find, access, cite and use the best available version. Please note that Cell Press, The Lancet and some society-owned have different preprint policies. Information on these policies is available on the journal homepage.
Accepted Author Manuscripts: An accepted author manuscript is the manuscript of an article that has been accepted for publication and which typically includes author-incorporated changes suggested during submission, peer review and editor-author communications.
Authors can share their accepted author manuscript:

Stellenbosch University https://scholar.sun.ac.za

- immediately
    - via their non-commercial person homepage or blog
    - by updating a preprint in arXiv or RePEc with the accepted manuscript
    - via their research institute or institutional repository for internal institutional uses or as part of an invitation-only research collaboration work-group
    - directly by providing copies to their students or to research collaborators for their personal use
    - for private scholarly sharing as part of an invitation-only work group on commercial sites with which Elsevier has an agreement
- After the embargo period
    - via non-commercial hosting platforms such as their institutional repository
    - via commercial sites with which Elsevier has an agreement

In all cases accepted manuscripts should:

- link to the formal publication via its DOI
- bear a CC-BY-NC-ND license - this is easy to do
- if aggregated with other manuscripts, for example in a repository or other site, be shared in alignment with our hosting policy not be added to or enhanced in any way to appear more like, or to substitute for, the published journal article.

Published journal article (JPA): A published journal article (PJA) is the definitive final record of published research that appears or will appear in the journal and embodies all value-adding publishing activities including peer review co-ordination, copy-editing, formatting, (if relevant) pagination and online enrichment.

Stellenbosch University https://scholar.sun.ac.za

Policies for sharing publishing journal articles differ for subscription and gold open access articles:

Subscription Articles: If you are an author, please share a link to your article rather than the full-text. Millions of researchers have access to the formal publications on ScienceDirect, and so links will help your users to find, access, cite, and use the best available version.

Theses and dissertations which contain embedded PJAs as part of the formal submission can be posted publicly by the awarding institution with DOI links back to the formal publications on ScienceDirect.

If you are affiliated with a library that subscribes to ScienceDirect you have additional private sharing rights for others' research accessed under that agreement. This includes use for classroom teaching and internal training at the institution (including use in course packs and courseware programs), and inclusion of the article for grant funding purposes.

Gold Open Access Articles: May be shared according to the author-selected end-user license and should contain a CrossMark logo, the end user license, and a DOI link to the formal publication on ScienceDirect.

Please refer to Elsevier's posting policy for further information.

18. **For book authors** the following clauses are applicable in addition to the above: Authors are permitted to place a brief summary of their work online only. You are not allowed to download and post the published electronic version of your chapter, nor may you scan the printed edition to create an electronic version. **Posting to a repository:** Authors are permitted to post a summary of their chapter only in their institution's repository.

19. **Thesis/Dissertation**: If your license is for use in a thesis/dissertation your thesis may be submitted to your institution in either print or electronic form. Should your thesis be published commercially, please reapply for permission. These requirements include permission for the Library and Archives of Canada to supply single copies, on demand, of the complete thesis and include permission for Proquest/UMI to supply single copies, on demand, of the complete thesis. Should your thesis be published commercially, please reapply for permission. Theses and dissertations which contain embedded PJAs as part of the formal submission can

Stellenbosch University https://scholar.sun.ac.za

be posted publicly by the awarding institution with DOI links back to the formal publications on ScienceDirect.

Elsevier Open Access Terms and Conditions

You can publish open access with Elsevier in hundreds of open access journals or in nearly 2000 established subscription journals that support open access publishing. Permitted third party re-use of these open access articles is defined by the author's choice of Creative Commons user license. See our open access license policy for more information.

Terms & Conditions applicable to all Open Access articles published with Elsevier:

Any reuse of the article must not represent the author as endorsing the adaptation of the article nor should the article be modified in such a way as to damage the author's honour or reputation. If any changes have been made, such changes must be clearly indicated.

The author(s) must be appropriately credited and we ask that you include the end user license and a DOI link to the formal publication on ScienceDirect.

If any part of the material to be used (for example, figures) has appeared in our publication with credit or acknowledgement to another source it is the responsibility of the user to ensure their reuse complies with the terms and conditions determined by the rights holder.

Additional Terms & Conditions applicable to each Creative Commons user license:

CC BY: The CC-BY license allows users to copy, to create extracts, abstracts and new works from the Article, to alter and revise the Article and to make commercial use of the Article (including reuse and/or resale of the Article by commercial entities), provided the user gives appropriate credit (with a link to the formal publication through the relevant DOI), provides a link to the license, indicates if changes were made and the licensor is not represented as endorsing the use made of the work. The full details of the license are available at http://creativecommons.org/licenses/by/4.0.

CC BY NC SA: The CC BY-NC-SA license allows users to copy, to create extracts, abstracts and new works from the Article, to alter and revise the Article, provided

Stellenbosch University https://scholar.sun.ac.za

this is not done for commercial purposes, and that the user gives appropriate credit (with a link to the formal publication through the relevant DOI), provides a link to the license, indicates if changes were made and the licensor is not represented as endorsing the use made of the work. Further, any new works must be made available on the same conditions. The full details of the license are available at http://creativecommons.org/licenses/by-nc-sa/4.0.

CC BY NC ND: The CC BY-NC-ND license allows users to copy and distribute the Article, provided this is not done for commercial purposes and further does not permit distribution of the Article if it is changed or edited in any way, and provided the user gives appropriate credit (with a link to the formal publication through the relevant DOI), provides a link to the license, and that the licensor is not represented as endorsing the use made of the work. The full details of the license are available at http://creativecommons.org/licenses/by-nc-nd/4.0. Any commercial reuse of Open Access articles published with a CC BY NC SA or CC BY NC ND license requires permission from Elsevier and will be subject to a fee.

Commercial reuse includes:

- Associating advertising with the full text of the Article
- Charging fees for document delivery or access
- Article aggregation
- Systematic distribution via e-mail lists or share buttons

Posting or linking by commercial companies for use by customers of those companies.

20. **Other Conditions**:

v1.9

Questions? customercare@copyright.com or +1-855-239-3415 (toll free in the US) or +1-978-646-2777.

Stellenbosch University https://scholar.sun.ac.za

Appendix A2

SPRINGER NATURE LICENSE
TERMS AND CONDITIONS

Feb 06, 2019

This Agreement between Mr. Aaron Dzigbor ("You") and Springer Nature ("Springer Nature") consists of your license details and the terms and conditions provided by Springer Nature and Copyright Clearance Center.

License Number	4518070459721
License date	Jan 29, 2019
Licensed Content Publisher	Springer Nature
Licensed Content Publication	Biomass Conversion and Biorefinery
Licensed Content Title	Production and optimization of NaCl-activated carbon from mango seed using response surface methodology
Licensed Content Author	Aaron Dzigbor, Annie Chimphango
Licensed Content Date	Jan 1, 2019
Type of Use	Thesis/Dissertation
Requestor type	non-commercial (non-profit)
Format	print and electronic
Portion	full article/chapter
Will you be translating?	no
Circulation/distribution	>50,000
Author of this Springer Nature content	yes

Stellenbosch University https://scholar.sun.ac.za

Title	Designing and evaluating the technical, economic and environmental performance of an adsorption cooling system operating using bioresources from waste streams of mango processing
Institution name	Stellenbosch University
Expected presentation date	Jun 2019
Requestor Location	Mr. Aaron Dzigbor Department of Process Engineering Stellenbosch University Stellenbosch, Western Cape 7602 South Africa Attn: Mr. Aaron Dzigbor
Billing Type	Invoice
Billing Address	Mr. Aaron Dzigbor Department of Process Engineering Stellenbosch University Stellenbosch, South Africa 7602 Attn: Mr. Aaron Dzigbor
Total	0.00 USD

Terms and Conditions

Springer Nature Terms and Conditions for RightsLink Permissions

Springer Nature Customer Service Centre GmbH (the Licensor) hereby grants you a non-exclusive, world-wide licence to reproduce the material and for the purpose and requirements specified in the attached copy of your order form, and for no other use, subject to the conditions below:

1. The Licensor warrants that it has, to the best of its knowledge, the rights to license reuse of this material. However, you should ensure that the material you are requesting is original to the Licensor and does not carry the copyright

Stellenbosch University https://scholar.sun.ac.za

of another entity (as credited in the published version).

If the credit line on any part of the material you have requested indicates that it was reprinted or adapted with permission from another source, then you should also seek permission from that source to reuse the material.

2. Where **print only** permission has been granted for a fee, separate permission must be obtained for any additional electronic re-use.

3. Permission granted **free of charge** for material in print is also usually granted for any electronic version of that work, provided that the material is incidental to your work as a whole and that the electronic version is essentially equivalent to, or substitutes for, the print version.

4. A licence for 'post on a website' is valid for 12 months from the licence date. This licence does not cover use of full text articles on websites.

5. Where **'reuse in a dissertation/thesis'** has been selected the following terms apply: Print rights of the final author's accepted manuscript (for clarity, NOT the published version) for up to 100 copies, electronic rights for use only on a personal website or institutional repository as defined by the Sherpa guideline (www.sherpa.ac.uk/romeo/).

6. Permission granted for books and journals is granted for the lifetime of the first edition and does not apply to second and subsequent editions (except where the first edition permission was granted free of charge or for signatories to the STM Permissions Guidelines http://www.stm-assoc.org/copyright-legal-affairs/permissions/permissions-guidelines/), and does not apply for editions in other languages unless additional translation rights have been granted separately in the licence.

7. Rights for additional components such as custom editions and derivatives require additional permission and may be subject to an additional fee. Please apply to

Stellenbosch University https://scholar.sun.ac.za

Journalpermissions@springernature.com/bookpermissions@springernature.com for these rights.

8. The Licensor's permission must be acknowledged next to the licensed material in print. In electronic form, this acknowledgement must be visible at the same time as the figures/tables/illustrations or abstract, and must be hyperlinked to the journal/book's homepage. Our required acknowledgement format is in the Appendix below.

9. Use of the material for incidental promotional use, minor editing privileges (this does not include cropping, adapting, omitting material or any other changes that affect the meaning, intention or moral rights of the author) and copies for the disabled are permitted under this licence.

10. Minor adaptations of single figures (changes of format, colour and style) do not require the Licensor's approval. However, the adaptation should be credited as shown in Appendix below.

Stellenbosch University https://scholar.sun.ac.za

Appendix A3

SPRINGER NATURE LICENSE
TERMS AND CONDITIONS

Feb 06, 2019

This Agreement between Mr. Aaron Dzigbor ("You") and Springer Nature ("Springer Nature") consists of your license details and the terms and conditions provided by Springer Nature and Copyright Clearance Center.

License Number	4518070297888
License date	Jan 29, 2019
Licensed Content Publisher	Springer Nature
Licensed Content Publication	Clean Technologies and Environmental Policy
Licensed Content Title	An integrated strategy targeting drying and cooling unit operations to improve economic viability and reduce environmental impacts in a mango processing plant
Licensed Content Author	Aaron Dzigbor, Annie Chimphango
Licensed Content Date	Jan 1, 2018
Licensed Content Volume	21
Licensed Content Issue	1
Type of Use	Thesis/Dissertation
Requestor type	non-commercial (non-profit)
Format	print and electronic
Portion	full article/chapter
Will you be translating?	no

Stellenbosch University https://scholar.sun.ac.za

Circulation/distribution	>50,000
Author of this Springer Nature content	yes
Title	Designing and evaluating the technical, economic and environmental performance of an adsorption cooling system operating using bioresources from waste streams of mango processing
Institution name	Stellenbosch University
Expected presentation date	Jun 2019
Requestor Location	Mr. Aaron Dzigbor Department of Process Engineering Stellenbosch University Stellenbosch, Western Cape 7602 South Africa Attn: Mr. Aaron Dzigbor
Billing Type	Invoice
Billing Address	Mr. Aaron Dzigbor Department of Process Engineering Stellenbosch University Stellenbosch, South Africa 7602 Attn: Mr. Aaron Dzigbor
Total	0.00 USD

Terms and Conditions

Springer Nature Terms and Conditions for RightsLink Permissions

Springer Nature Customer Service Centre GmbH (the Licensor) hereby grants you a non-exclusive, world-wide licence to reproduce the material and for the purpose and requirements specified in the attached copy of your order form, and for no other use, subject to the conditions below:

Stellenbosch University https://scholar.sun.ac.za

1. The Licensor warrants that it has, to the best of its knowledge, the rights to license reuse of this material. However, you should ensure that the material you are requesting is original to the Licensor and does not carry the copyright of another entity (as credited in the published version).

   If the credit line on any part of the material you have requested indicates that it was reprinted or adapted with permission from another source, then you should also seek permission from that source to reuse the material.

2. Where **print only** permission has been granted for a fee, separate permission must be obtained for any additional electronic re-use.

3. Permission granted **free of charge** for material in print is also usually granted for any electronic version of that work, provided that the material is incidental to your work as a whole and that the electronic version is essentially equivalent to, or substitutes for, the print version.

4. A licence for 'post on a website' is valid for 12 months from the licence date. This licence does not cover use of full text articles on websites.

5. Where **'reuse in a dissertation/thesis'** has been selected the following terms apply: Print rights of the final author's accepted manuscript (for clarity, NOT the published version) for up to 100 copies, electronic rights for use only on a personal website or institutional repository as defined by the Sherpa guideline (www.sherpa.ac.uk/romeo/).

6. Permission granted for books and journals is granted for the lifetime of the first edition and does not apply to second and subsequent editions (except where the first edition permission was granted free of charge or for signatories to the STM Permissions Guidelines http://www.stm-assoc.org/copyright-legal-affairs/permissions/permissions-guidelines/), and does not apply for editions in other languages unless additional translation rights have been granted separately in the licence.

Stellenbosch University https://scholar.sun.ac.za

7. Rights for additional components such as custom editions and derivatives require additional permission and may be subject to an additional fee. Please apply to Journalpermissions@springernature.com/bookpermissions@springernature.com for these rights.

8. The Licensor's permission must be acknowledged next to the licensed material in print. In electronic form, this acknowledgement must be visible at the same time as the figures/tables/illustrations or abstract, and must be hyperlinked to the journal/book's homepage. Our required acknowledgement format is in the Appendix below.

9. Use of the material for incidental promotional use, minor editing privileges (this does not include cropping, adapting, omitting material or any other changes that affect the meaning, intention or moral rights of the author) and copies for the disabled are permitted under this licence.

10. Minor adaptations of single figures (changes of format, colour and style) do not require the Licensor's approval. However, the adaptation should be credited as shown in Appendix below.

Stellenbosch University https://scholar.sun.ac.za

Appendix B: Heat load calculation

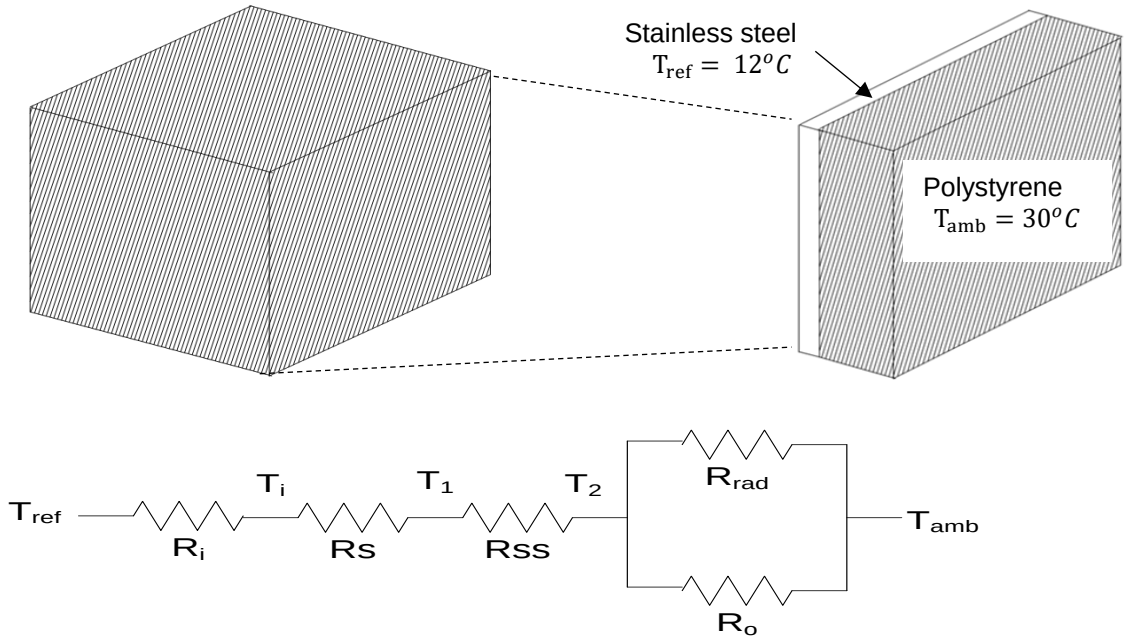

Figure B.1 Thermal resistance network

The following equations were used to model the heat transfer into the refrigerator cabinet.

$$\dot{Q} = \frac{T_{amb} - T_{ref}}{R_{total}} \qquad B.1$$

$$R_{total} = R_i + R_s + R_{ss} + R_{equiv} \qquad B.2$$

$$R_{equiv} = \frac{1}{R_o} + \frac{1}{R_{rad}} \qquad B.3$$

$$R_i = \frac{1}{Ah_i} \qquad B.4$$

$$R_s = \frac{X_s}{Ak_s} \qquad B.5$$

$$R_{ss} = \frac{X_{ss}}{Ak_{ss}} \qquad B.6$$

$$R_o = \frac{1}{Ah_o} \qquad B.7$$

Stellenbosch University https://scholar.sun.ac.za

$$R_{rad} = \frac{1}{Ah_{rad}} \qquad B.8$$

Where k_s and k_{ss} are thermal conductivity of the Styrofoam and stainless steel respectively $(Wm^{-1}K^{-1})$; X_{ss} is the thickness of the stainless steel wall (m); A is the heat transfer area (m^2); R_{total} is the total thermal resistance (KW^{-1}); h_i is the convective heat transfer coefficient between ambient air and the outer wall $(Wm^{-2}K^{-1})$; h_o is the convective heat transfer coefficient between refrigerator air and the inner wall $(Wm^{-2}K^{-1})$. Since the wall storage chamber has four vertical walls and two horizontal walls and heat transfer is by natural convection, the following expression could be used to determine the heat transfer coefficient of air, h_o, on the outside of the storage chamber.

$$Ra_L = \frac{g\beta(T_2 - T_{amb})L^3}{\nu^2} Pr \qquad B.9$$

$$Nu = 0.59 {Ra_L}^{1/4} \qquad (vertical\ wall) \qquad B.10$$

$$Nu = 0.54\ {Ra_L}^{1/4} \qquad (horizontal\ wall) \qquad B.11$$

$$h_o = \frac{k}{L} Nu \qquad B.12$$

$$T_f = \frac{T_2 + T_{amb}}{2} \qquad B.13$$

$$\beta = \frac{1}{T_f} \qquad B.14$$

Where ν is the kinematic viscosity (m^2s^{-1}), Pr is Prandtl number, β is the volume expansion coefficient (K^{-1}) and k is the thermal conductivity ($Wm^{-1}K^{-1}$) which can all be obtained from property tables. L is the characteristic length (m), Nu is Nusselt number, Ra_L is Rayleigh number, T_f is the absolute temperature (K).

Stellenbosch University https://scholar.sun.ac.za

The temperature of the outer surface of the storage chamber, T_2 in Equation B.9 is not known but could be calculated by the trial-and-error method. However,T_2 would be very close to ambient temperature, T_{amb}. Therefore, T_2 was assumed to be T_{amb}. A similar analysis could be made for the h_i calculation. Therefore, Equation B.2 above reduces to

$$R_{total} = R_s + R_{ss} + \frac{1}{R_{rad}} \qquad B.15$$

The value of h_{rad} in Equation B.8 was calculated using Equation B.15

$$h_{rad} = \varepsilon\sigma\left({T_2}^2 + {T_{amb}}^2\right)(T_2 + T_{amb}) \qquad B.16$$

Emissivity ε of stainless steel (polished) was assumed to be 0.075, Stefan-Boltzmann's constant σ is 5.670×10^{-8} $JK^{-4}m^{-2}s^{-1}$. By substituting the values of thickness and thermal conductivity of both stainless steel and polystyrene foam into their respective equations, the overall heat transfer coefficient was calculated. The refrigerator cabinet has six heat transfer areas: the floor area, ceiling area, and 4 side wall areas. The heat through each heat transfer area was calculated using Equation B.1.

Using the above information, heat transfer through the wall could be calculated as

$$A = 4(0.3 \times 0.4) + 2(0.4 \times 0.4) = 0.8\ m^2$$

$$R_s = \frac{0.05m}{(3.84 \times 10^{-5}\ W/mK) \times 0.8m^2} = 1.63\ K/W$$

$$R_{ss} = \frac{0.002m}{(17\ W/mK) \times 0.8m^2} = 1.47 \times 10^{-4}\ K/W$$

$$h_{rad} = 0.075 \times 5.670 \times 10^{-8}(303^2 + 303^2)(303 + 303) = 0.47\ W/m^2K$$

$$R_{rad} = \frac{1}{0.8 \times 0.47\ W/m^2K} = 2.66\ K/W$$

Stellenbosch University https://scholar.sun.ac.za

$$R_{total} = 1.63 + 1.47 \times 10^{-4} + \frac{1}{2.66} = 2\ K/W$$

$$\dot{Q}_{wall} = \frac{30 - 12}{2} = 9\ W$$

Product heat load

$$T_f = \frac{T_{amb} + T_{eva}}{2} = \frac{30 + 12}{2} = 21\ ℃$$

$$\beta = \frac{1}{T_f} = \frac{1}{294K} = 3.40 \times 10^{-3} K^{-1}$$

$$Gr_L = \frac{g\beta\left(T_{field} - T_{ref}\right) {L_c}^3}{\nu^2}$$

$Properties\ of\ air\ at\ 21\ ^0C\ \ are$

$$\rho = 1.20\ kg/m^3$$

$$k = 0.02514\ W/mK$$

$$\nu = 1.516 \times\ 10^{-5}\ m^2/s$$

$$Pr = 0.7309$$

Assuming mango to spherical, the following condition must hold.

$$Ra_D \leq\ 10^{\ 11}\ \ and\ \ Pr \geq 0.7$$

Thus Grashof number is evaluated

$$Gr_L = \frac{g\beta\left(T_{field} - T_{ref}\right) {L_c}^3}{\nu^2}$$

$$where\ L_c\ is\ the\ diameter\ of\ the\ mango$$

$$Gr_L = \frac{9.81(1/294)(30 - 12)(8.61\ \times\ 10^{\ -2})^3}{(1.516 \times\ 10^{-5}\ )^2}$$

$$Gr_L = 1\ 668\ 035.287$$

$$Ra_D = Gr_L\ Pr = \ 1\ 668\ 035.287\ \times\ 0.7309\ \approx 1.22\ \times 10^{\ 6}\ \leq\ 10^{\ 11}$$

$$Nu = 2 + \frac{0.589\ {Ra_D}^{1/4}}{[1 + \ (0.469/Pr)^{9/16}]^{4/9}}$$

Stellenbosch University https://scholar.sun.ac.za

$$Nu = 2 + \frac{0.589\ (1.22\ \times 10^{\ 6})^{1/4}}{[1 +\ (0.469/0.7309)^{9/16}]^{4/9}}$$

$$Nu = 17.1531$$

$$Nu = \frac{h\ L_c}{k}$$

$$h = \frac{Nu\ \times k}{L_c} = \frac{17.1531\ \times\ 0.02514}{8.61\ \times\ 10^{\ -2}}$$

$$h \approx 5\ W/m^2K$$

$$\dot{Q}_{product} =\ 5\ W/m^2K\ \times 1.64\ \times\ 10^{-2}\ m^2\ \times (30 - 12)K$$

$$\dot{Q}_{product} = 1.476\ W$$

Therefore for 111 mangoes,

$$\dot{Q} =\ 1.476\ W/mango\ \times 111\ mangoes$$

$$\dot{Q}_{product} = 163.836\ W$$

Total respiration heat $= 133.4\ \times 10^{-3}\ \mathrm{W/kg} \times 38\ \mathrm{kg} = 5.0692\ \mathrm{W}$

Table B1: Summary of refrigerator heat load

Component	**Values**
Heat transfer through walls	9 W
Product field heat load	163.836 W
Respiratory heat load	5.0692 W
Total	**177.9052 W**

Adding* 10% *for safety, total heat load becomes* 195.6957 *W

Evaporator design calculation

$$\dot{Q}_{total} = hA(T_{amb} - T_{eva})$$

$$T_f = \frac{T_{amb} + T_{eva}}{2} = \frac{30 + 12}{2} = 21\ ℃$$

Stellenbosch University https://scholar.sun.ac.za

$$\beta = \frac{1}{T_f} = \frac{1}{294K} = 3.40 \times 10^{-3} K^{-1}$$

$$Ra_L = \frac{g\beta(T_{amb} - T_{eva}){L_c}^3}{v^2} Pr = \frac{9.81 \times 3.40 \times 10^{-3}(30-12)0.3^3}{(1.516 \times 10^{-5})^2} \times 0.7309$$

$$= 51.572 \times 10^6$$

$$Nu = 0.59 \times {Ra_L}^{1/4} = 0.59 \times (51.572 \times 10^6)^{1/4} = 50$$

$$Nu = \frac{hL_c}{k}$$

$$h = \frac{k \times Nu}{L_c} = \frac{0.02514 \times 50}{0.3} = 4.189\ W/m^2K$$

$$665.6428$$

$$A = \frac{\dot{Q}_{total}}{h(T_{amb} - T_{eva})} = \frac{195.6957\ W}{4.189\ W/m^2K\ (30-12)} = 2.6\ m^2$$

Condenser design calculation

Heat rejected by the condenser

$$\dot{Q_{con}} = \dot{m_{ref}}\ h_{fg} + \dot{m_{ref}} C_{p,ref}\ (T_{sat} - T_{con}) \qquad (14)$$

$$\dot{Q_{con}} = (2.174 \times 10^{-4}\ kg/s)[(840 \times 10^3 J/kg) + (3.03 \times 10^3 J/kg\,K)(80-35)K]$$

$$\dot{Q_{con}} \approx 212.3\ W$$

$$\Delta T_{lm} = \frac{(T_1 - t_2) - (T_2 - t_1)}{\ln\left(\frac{T_1 - t_2}{T_2 - t_1}\right)}$$

$$\Delta T_{lm} = \frac{(80-35) - (35-30)}{\ln \frac{80-35}{35-30}} = 18.2\ ℃$$

$$h_i = 0.555 \left[g\rho_l \frac{(\rho_l - \rho_v)\ {k_l}^3\ h_{fg}}{\mu_l \times (T_{sat} - T_s) \times d} \right]^{1/4}$$

T_s is the pipe wall temperature taken to be equal to the final condenser air temperature

Stellenbosch University https://scholar.sun.ac.za

$$h_i = 0.555\left[\frac{9.81\ \times 797.25\ (797.25 - 1.430) \times (0.179)^3\ \times (840\ \times 10^{\ 3})}{1.1980\ \times (6.25\ \times\ 10^{-3})(80 - 35)}\right]^{1/4}$$

$$h_i = 546.1876\ W/m^2K$$

$$h_i = 0.77h_o$$

$$h_o = \frac{h_i}{0.77} = \frac{546.1876\ W/m^2K}{0.77} = 709.3345\ W/m^2K$$

The overall heat transfer coefficient could also be calculated using Equation 4.16

$$\frac{1}{U_O} = \frac{1}{h_o} + \frac{1}{h_{od}} + \frac{d_o \ln(d_o/d_i)}{2k_w} + \frac{d_o}{d_i} \times \frac{1}{h_{id}} + \frac{d_o}{d_i} \times \frac{1}{h_i}$$

$$\frac{1}{U_o} = \frac{1}{709.3345} + \frac{1}{5000} + \frac{9.375 \times 10^{-3} \ln(9.375 \times 10^{-3}/6.25 \times 10^{-3})}{2 \times 378}$$

$$+ \left(\frac{9.375 \times 10^{-3}}{6.25 \times 10^{-3} \times 5000}\right) + \left(\frac{9.375 \times 10^{-3}}{6.25 \times 10^{-3} \times 546.1876}\right)$$

$$U_o = 214.54\ W/m^2K$$

$$\dot{Q}_{con} = U_o A \Delta T_{lm}$$

$$A = \frac{212.3\ W}{(214.54\ W/m^2K) \times 18.2\ ℃} = 0.054\ m^2$$

$$A = 2\pi rL$$

$$L = \frac{0.054}{2\pi \times (6.25 \times 10^{\ -3})} \approx 1.38\ m$$

Therefore the condenser pipe should be about 1.38 m long.

Stellenbosch University https://scholar.sun.ac.za

Appendix C

Table C1 Values of mango composition used in material and energy balance of the dried mango processing

Component	Value	Source
Mango seed	15% of peeled mango weight	[12]
Mango seed moisture content	45% of mango seed weight	[12]
Mango peel	9.94% of mango weight	[277]
Mango peel moisture	72.5% of mango peel weight	[278]
Ripe mango pulp moisture	80.85% of mango weight	[279]

Stellenbosch University https://scholar.sun.ac.za

Table C2 Values of parameters used in material and energy balance during dried mango processing

Parameter	Values	Source
Dried mango moisture	20.5%	(I. Fourie, Personal communication, October 12, 2017)
Steam properties	3 kPa, 90^0C	(I. Fourie, Personal communication, October 12, 2017)
Boiler efficiency	80%	[263]
Conventional chiller Coefficient of performance	3.0	[26]
Adsorption chiller Coefficient of performance	0.6	[101]
Drying temperature	65^0C	(I. Fourie, Personal communication, October 12, 2017)
Hot water (50^0C) volume	20000 liters/30000 kg of mango	(I. Fourie, Personal communication, October 12, 2017)
Cold water volume	1600 liters/20000 kg of mango	(I. Fourie, Personal communication, October 12, 2017)
Storage temperature	10-14^0C	(I. Fourie, Personal communication, October 12, 2017)
Storage duration	4 weeks	(I. Fourie, Personal communication, October 12, 2017)

Stellenbosch University https://scholar.sun.ac.za

Table C3 Estimation of capital expenditure for dried mango chips processing in an on-grid setting: scenario 1 (coal as boiler fuel and conventional vapour compression chiller (CVCC)), scenario 2 (mango seed as boiler fuel and CVCC) and scenario 3 (adsorption cooling system (ACS) and mango seed as boiler fuel) and off-grid setting: scenario 4 (coal as boiler fuel and CVCC), scenario 5 (mango seed as boiler fuel and CVCC) and scenario 6 (ACS and mango seed as boiler fuel).

	Scenarios					
	1	**2**	**3**	**4**	**5**	**6**
Fixed capital ($)	678314	678314	715939	706394	706394	744019
Working capital ($)	169578	169578	178985	176598	176598	186005
Total capital($)	847892	847892	894924	882996	882992	930024
Product (kg)	650880	650880	650880	650880	650880	650880
Specific capital Investment ($/kg)	1.30	1.30	1.37	1.36	1.36	1.43

Stellenbosch University https://scholar.sun.ac.za

Table C4 Breakdown of operating cost for dried mango chips processing in an on-grid setting: scenario 1 (coal as boiler fuel and conventional vapour compression chiller (CVCC)), scenario 2 (mango seed as boiler fuel and CVCC) and scenario 3 (adsorption cooling system (ACS) and mango seed as boiler fuel) and off-grid setting: scenario 4 (coal as boiler fuel and CVCC), scenario 5 (mango seed as boiler fuel and CVCC) and scenario 6 (ACS and mango seed as boiler fuel).

	Scenarios					
	1	**2**	**3**	**4**	**5**	**6**
Utilities ($)	313234	313234	268973	313234	313234	268973
Raw materials ($)	2745917	2729152	2729152	2745917	2729152	2729152
Labour ($)	451907	451907	451907	451907	451907	451907
Maintenance ($)	47482	47482	50116	49448	49448	52081
Insurance and Tax ($)	6783	6783	7159	7064	7064	7440
General overhead ($)	13566	13566	14319	14128	14128	14880
Packaging ($)	1789444	1781062	1760813	1790848	1782466	1762217
Sales expenses ($)	298241	296844	293469	298475	297078	293703
Research and development ($)	298241	296844	293469	298475	297078	293703
Total ($)	5964814	5936874	5869376	5969494	5941554	5874056
Product (kg)	650880	650880	650880	650880	650880	650880
Specific operating cost ($/kg)	9.16	9.12	9.02	9.17	9.13	9.02

Stellenbosch University https://scholar.sun.ac.za

Table C5 Amount of boiler fuel combusted and mango seed composted per annum

Scenarios	Amount of boiler fuel	Amount of mango seed send to compost
1	209 Mg of coal	541Mg
2	352 Mg dried mango dried (512 fresh seed)	29 Mg
3	352 Mg dried mango seed (512 fresh seed)	29 Mg
4	209 Mg of coal	541Mg
5	352 Mg dried mango seed (512 fresh seed)	29 Mg
6	352 Mg dried mango seed (512 fresh seed)	29 Mg

Stellenbosch University https://scholar.sun.ac.za

Table C6: Energy demand for dried mango chips processing in an on-grid setting: scenario 1 (coal as boiler fuel and conventional vapour compression chiller (CVCC)), scenario 2 (mango seed as boiler fuel and CVCC) and scenario 3 (adsorption cooling system (ACS) and mango seed as boiler fuel) and off-grid setting: scenario 4 (coal as boiler fuel and CVCC), scenario 5 (mango seed as boiler fuel and CVCC) and scenario 6 (ACS and mango seed as boiler fuel).

Unit operations	**Scenarios**					
	1	**2**	**3**	**4**	**5**	**6**
Mango drying (GJ)	70	70	70	70	70	70
Mango slicing(GJ)	19	19	19	19	19	19
Mango Peeling (GJ)	39	39	39	39	39	39
Sorting and Grading (GJ)	467	467	467	467	467	467
Cooling (GJ)	145	145	708	145	145	708
Cold water washing (GJ)	280	280	280	280	280	280
Hot water treatment(GJ)	70	70	70	70	70	70
Boiler (GJ)	5330	5330	5330	5330	5330	5330
Sun drying (GJ)	0	441	441	0	441	441
Coal transportation (GJ)	15	0	0	15	0	0
Total (GJ)	6435	6861	7424	6435	6861	7424
Product (kg)	650880	650880	650880	650880	650880	650880
Specific Energy Intensity (GJ/kg)	0.0099	0.0105	0.0114	0.0099	0.0105	0.0114

Stellenbosch University https://scholar.sun.ac.za

Table C7 Greenhouse gas (GHG) emission dried mango chips processing dried in an on-grid setting: scenario 1 (coal as boiler fuel and conventional vapour compression chiller (CVCC)), scenario 2 (mango seed as boiler fuel and CVCC) and scenario 3 (adsorption cooling system (ACS) and mango seed as boiler fuel)

	On-grid scenarios											
	1				2				3			
	CO_2 (kg)	CH_4 (kg CO_{2e})	N_2O ($kgCO_{2e}$)	Total ($kgCO_{2e}$)	CO_2 (kg)	CH_4 (kg CO_{2e})	N_2O ($kgCO_{2e}$)	Total (kg CO_{2e})	CO_2 (kg)	CH_4 (kg CO_{2e})	N_2O ($kgCO_{2e}$)	Total (kg CO_{2e})
Mango dryer	6620	2	33	6655	6620	2	33	6655	6620	2	33	6655
Mango slicing	1839	0	9	1849	1839	0	9	1849	1839	0	9	1849
Mango Peeling	3678	1	18	3697	3678	1	18	3697	3678	1	18	3697
Sorting and Grading	44137	12	217	44365	44137	12	217	44365	44137	12	217	44365
Cooling	13731	4	67	13803	13731	4	67	13803	3531	1	17	3549
Cold water washing	26482	7	130	26619	26482	7	130	26619	26482	7	130	26619
Hot water treatment	6620	2	33	6655	6620	2	33	6655	6620	2	33	6655
Boiler	504251	133	2479	506863	59700	3998	6610	607607	597000	3998	6610	607607
Compost	71470	54144	50354	175968	3832	2903	2700	9436	3832	2903	2700	9436
Coal transportation	3174	1	6	3174	0	0	0	0	0	0	0	0
Total	682004	54306	53346	789655	703940	2928	9817	720685	693739	6926	9766	710431

Stellenbosch University https://scholar.sun.ac.za

Table C8: Greenhouse gas (GHG) emission from dried mango chips processing in an off-grid setting: scenario 4 (coal as boiler fuel and conventional vapour compression chiller (CVCC)), scenario 5 (mango seed as boiler fuel and CVCC) and scenario 6 (ACS and mango seed as boiler fuel).

	Off-grid scenarios											
	4				**5**				**6**			
	CO_2 (kg)	CH_4 (kg CO_{2e})	N_2O ($kgCO_{2e}$)	Total (kg CO_{2e})	CO_2 (kg)	CH_4 (kg CO_{2e})	N_2O ($kgCO_{2e}$)	Total (kg CO_{2e})	CO_2 (kg)	CH_4 (kg CO_{2e})	N_2O ($kgCO_{2e}$)	Total (kg CO_{2e})
Mango dryer	5186	5	13	5204	5186	5	13	5204	5186	5	13	5204
Mango slicing	1441	1	4	1446	1441	1	4	1446	1441	1	4	1446
Mango Peeling	2881	3	7	2891	2881	3	7	2891	2881	3	7	2891
Sorting and Grading	34572	35	87	34694	34572	35	87	34694	34572	35	87	34694
Cooling	10756	11	27	10794	10756	11	27	10794	2766	3	7	2776
Cold water washing	20743	21	52	20816	20743	21	52	20816	20743	21	52	20816
Hot water treatment	5186	5	13	5204	5186	5	13	5204	5186	5	13	5204
Boiler	504251	133	2479	506863	597000	3998	6610	607607	597000	3998	6610	607607
Compost	71470	54144	50354	175968	3832	2903	2700	9436	3832	2903	2700	9436
Coal transportation	3174	1	6	3182	0	0	0	0	0	0	0	0
Total	659660	54360	53042	767062	681596	6983	9512	698091	673606	6975	9492	690073

Stellenbosch University https://scholar.sun.ac.za

Table C9: Results of economic analysis of the dried mango chips processing in an on-grid setting: scenario 1 (coal as boiler fuel and conventional vapour compression chiller (CVCC)), scenario 2 (mango seed as boiler fuel and CVCC) and scenario 3 (adsorption cooling system (ACS) and mango seed as boiler fuel) and off-grid setting: scenario 4 (coal as boiler fuel and CVCC), scenario 5 (mango seed as boiler fuel and CVCC) and scenario 6 (ACS and mango seed as boiler fuel).

Parameter	**Scenarios**					
	1	**2**	**3**	**4**	**5**	**6**
TCI(M$)	0.85	0.85	0.89	0.88	0.88	0.93
Variable operating cost(M$)	3.06	3.04	3.00	3.06	3.04	3.00
Fixed operating cost(M$)	2.91	2.89	2.87	2.91	2.90	2.88
Mango sales Revenue (M$)	6.18	6.18	6.18	6.18	6.18	6.18
IRR (%)	17.48	20.33	25.33	16.09	18.88	23.84
NPV (M$)	0.09	2.01	0.42	0.04	0.15	0.37

Stellenbosch University https://scholar.sun.ac.za

Scenario 1

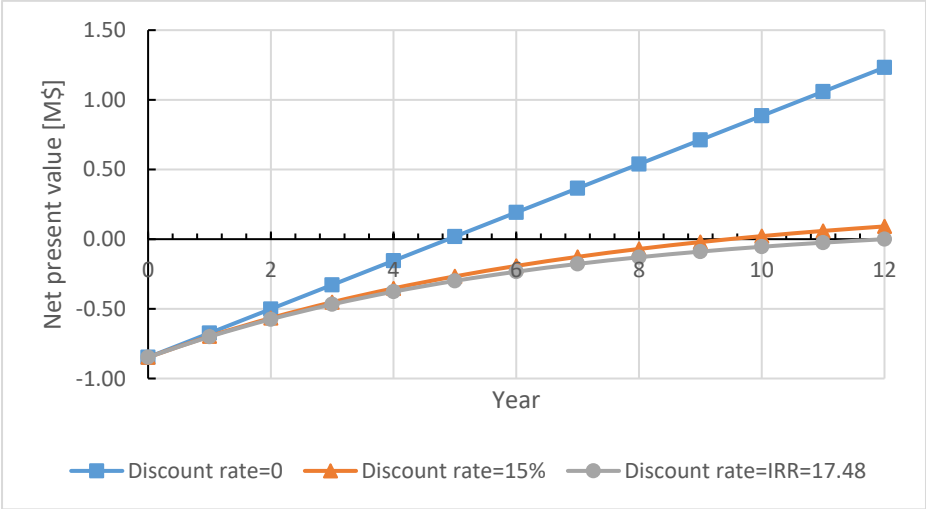

Scenario 2

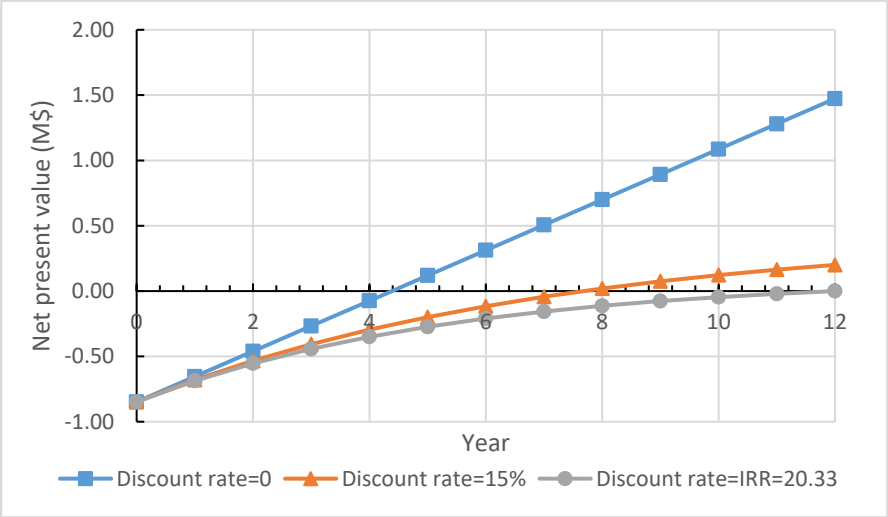

Scenario 3

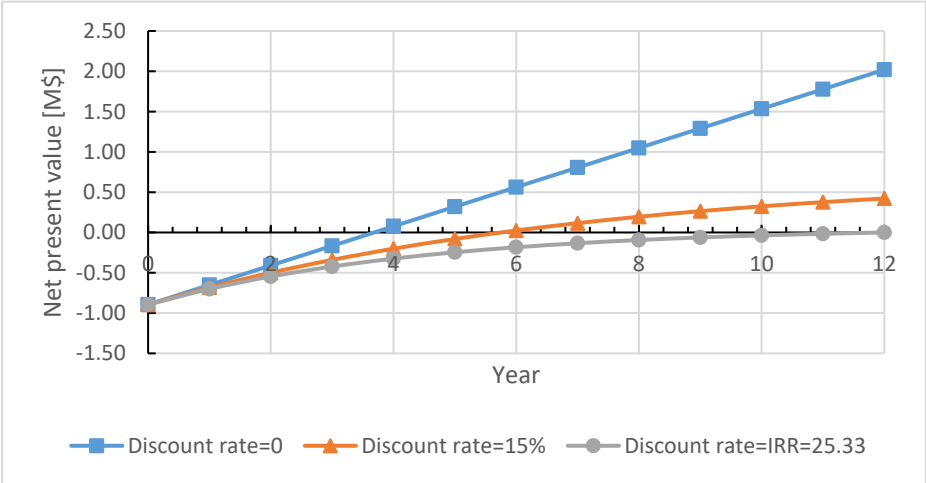

Figure C1: Simple payback and discounted payback periods dried mango chips processing in an on-grid setting: scenario 1 (coal as boiler fuel and conventional vapour compression chiller (CVCC)), scenario 2 (mango seed as boiler fuel and CVCC) and scenario 3 (adsorption cooling system (ACS) and mango seed as boiler fuel)

Stellenbosch University https://scholar.sun.ac.za

Scenario 4

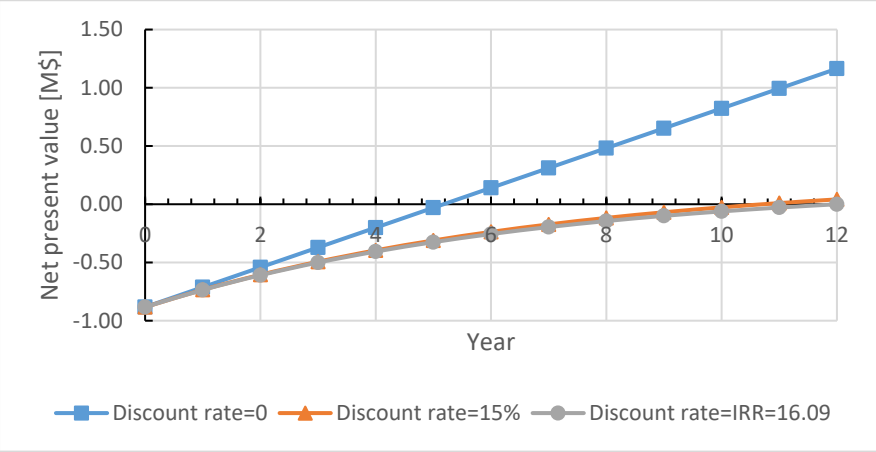

Scenario 5

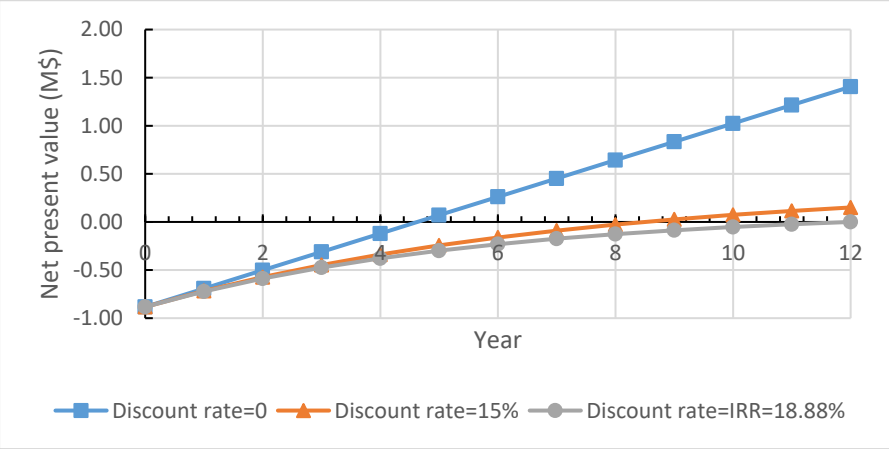

Scenario 6

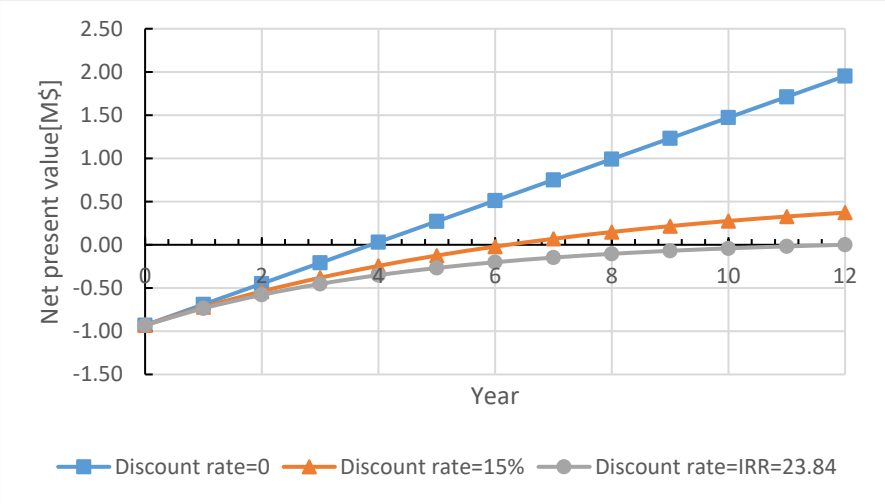

Figure C2: Simple payback and discounted payback periods dried mango chips processing in an off-grid setting: scenario 4 (coal as boiler fuel and conventional vapour compression chiller (CVCC)), scenario 5 (mango seed as boiler fuel and CVCC) and scenario 6 (ACS and mango seed as boiler fuel).